ESL-TR-91-06

GRANULAR BASES FOR HEAVILY LOADED PAVEMENTS

W.K.F. CHAN, S.F. BROWN

UNIVERSITY OF NOTTINGHAM
UNIVERSITY PARK
NOTTINGHAM UK NG72RD

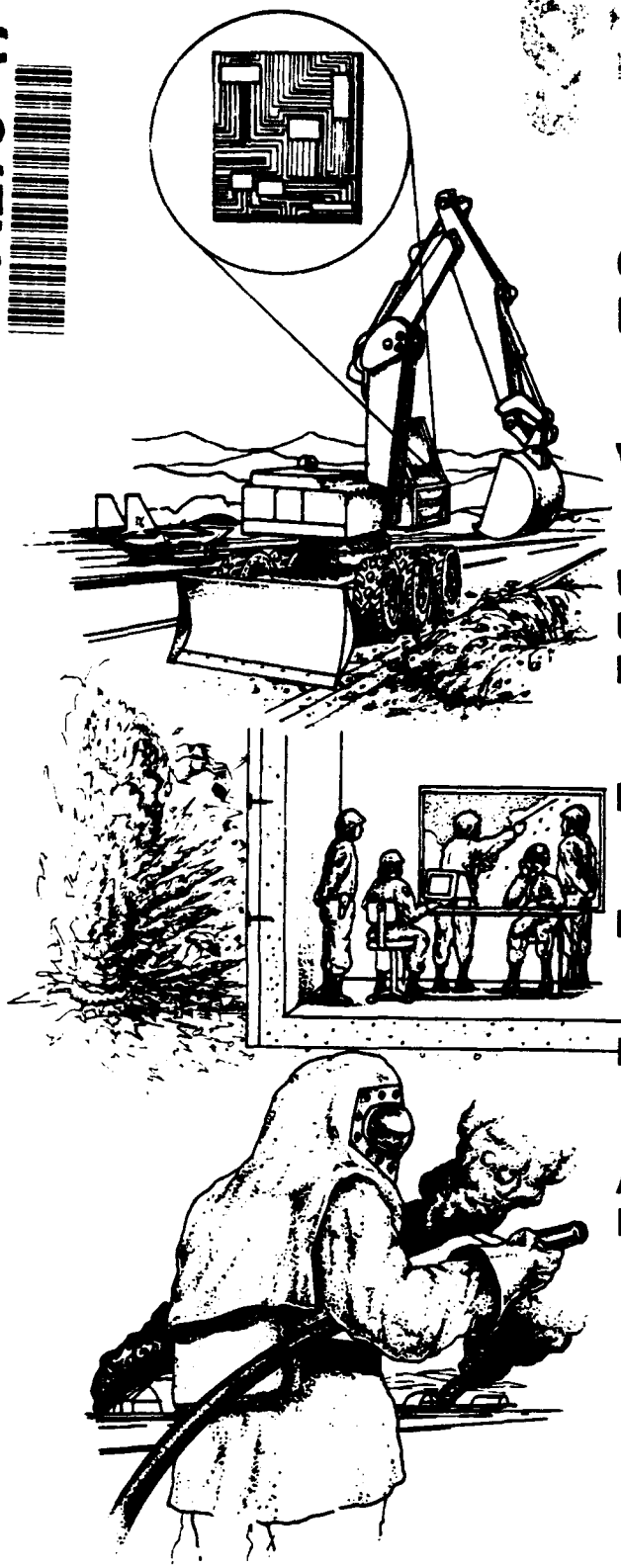

MARCH 1993

FINAL REPORT

FEBRUARY 1988 - DECEMBER 1990

ENGINEERING RESEARCH DIVISION
Air Force Civil Engineering Support Agency
Civil Engineering Laboratory
Tyndall Air Force Base, Florida 32403

NOTICE

PLEASE DO NOT REQUEST COPIES OF THIS REPORT FROM HQ AFESC/RD (ENGINEERING AND SERVICES LABORATORY). ADDITIONAL COPIES MAY BE PURCHASED FROM:

NATIONAL TECHNICAL INFORMATION SERVICE
5285 PORT ROYAL ROAD
SPRINGFIELD, VIRGINIA 22161

FEDERAL GOVERNMENT AGENCIES AND THEIR CONTRACTORS REGISTERED WITH DEFENSE TECHNICAL INFORMATION CENTER SHOULD DIRECT REQUESTS FOR COPIES OF THIS REPORT TO:

DEFENSE TECHNICAL INFORMATION CENTER
CAMERON STATION
ALEXANDRIA, VIRGINIA 22314

REPORT DOCUMENTATION PAGE

Form Approved
OMB No 0704-0188

1 AGENCY USE ONLY (Leave blank)	2. REPORT DATE	3 REPORT TYPE AND DATES COVERED
	March 1993	FINAL FEB 88 - DEC 90

4. TITLE AND SUBTITLE

GRANULAR BASES FOR HEAVILY LOADED PAVEMENTS

5. FUNDING NUMBERS

PE62206F
PR2673
TA00
WU84

6. AUTHOR(S)

W. K. F. CHAN AND S. F. BROWN

7. PERFORMING ORGANIZATION NAME(S) AND ADDRESS(ES)

UNIVERSITY OF NOTTINGHAM
UNIVERSITY PARK
NOTTINGHAM UK NG72RD

8. PERFORMING ORGANIZATION REPORT NUMBER

9 SPONSORING MONITORING AGENCY NAME(S) AND ADDRESS(ES)

AIR FORCE CIVIL ENGINEERING SUPPORT AGENCY
TYNDALL AFB FL 32403-5319
AIR FORCE OFFICE OF SCIENTIFIC RESEARCH
BOLLING AFB DC 20332-6448

10 SPONSORING MONITORING AGENCY REPORT NUMBER

ESL-TR-91-06

11 SUPPLEMENTARY NOTES

12a DISTRIBUTION AVAILABILITY STATEMENT

APPROVED FOR PUBLIC RELEASE
DISTRIBUTION UNLIMITED
AVAILABILITY SPECIFIED ON REVERSE OF FRONT COVER

12b DISTRIBUTION CODE

13 ABSTRACT (Maximum 200 words)

THIS RESEARCH IMPROVES THE UNDERSTANDING OF THE PERMANENT DEFORMATION CHARACTERISTICS OF GRANULAR MATERIALS UNDER REPEATED, REVERSED SHEAR LOADINGS IN FLEXIBLE PAVEMENTS. IN THE LABORATORY, TRIAXIAL TESTS PROVIDED VERTICAL REPEATED LOADINGS, AND A HOLLOW CYLINDER APPARATUS WAS USED TO APPLY REVERSING SHEAR STRESSES AND ASSOCIATED ROTATING PRINCIPAL PLANES. THE LABORATORY TESTS WERE ANALOGOUS TO LARGER SCALE TESTS THAT WERE RUN, USING VERTICAL PLATE AND TIRE LOADINGS. IT WAS FOUND THAT HIGHER MATERIAL DENSITIES LEAD TO LARGE IMPROVEMENTS IN PERMANENT DEFORMATION RESISTANCE, AND PERMANENT DEFORMATION IS SIGNIFICANTLY MORE WHEN STRESSES ARE REVERSED IN BOTH THE LABORATORY AND IN THE FIELD. THE FINDINGS WERE VALIDATED, USING TWO FULLY-INSTRUMENTED PILOT SCALE TRAFFICKING TESTS.

14 SUBJECT TERMS		15 NUMBER OF PAGES
FLEXIBLE PAVEMENT DESIGN	HOLLOW CYLINDER APPARATUS	151
SHEAR STRESSES	RUTTING	16. PRICE CODE

17 SECURITY CLASSIFICATION OF REPORT	18 SECURITY CLASSIFICATION OF THIS PAGE	19. SECURITY CLASSIFICATION OF ABSTRACT	20. LIMITATION OF ABSTRACT
UNCL	UNCL	UNCL	

NSN 7540-01-280-5500

Standard Form 298 (Rev. 2-89)
Prescribed by ANSI Std. 239-18
298-102

(The reverse of this page is blank.)

EXECUTIVE SUMMARY

Research was carried out to improve understanding of the complex properties relating to the resilient and, particularly, the permanent deformation characteristics of granular materials under repeated load and to determine how these properties could be improved by allowing the material to achieve maximum compacted density. The latter condition is believed to result in better mechanical performance of the granular material needed for heavy loading situations. Emphasis was also placed on understanding the role of reversed shear stresses and the associated rotating principal planes, which result from loading by a moving wheel load. To this end, a substantially modified repeated-load Hollow Cylinder Test Apparatus (HCA) was developed and used.

A grading design procedure which allowed convenient characterization of continuous gradings and offered a simple and repeatable means of carrying out the design tests for maximum density was proposed. The mechanical properties of a dry dolomitic limestone with a designed high-density grading and those with a standard British Department of Transport Type 1 grading were studied under various laboratory simulated stress conditions. Results of the study indicated that high density leads to slight improvement in resilient properties but a large improvement in permanent deformation resistance under repeated load.

The effect of reversed shear stress caused by a moving wheel load was studied in large-scale experiments using two wheel tracking facilities. The Slab Test Facility was adapted to allow optional repeated vertical plate loading without shear stress reversal, whilst in the larger Pavement Test Facility (PTF), experiments were carried out with both unidirectional and bidirectional wheel loadings. The effect of shear reversal was further studied in laboratory element tests by means of the repeated-load HCA and triaxial tests .

Results of the study indicated that the resilient behavior is not significantly affected by shear stress reversal and that the resilient shear strain model developed from triaxial testing is sufficiently accurate for pavement analysis. However, both the magnitude and rate of development of permanent strain increase when reversed shear stresses are applied. Bidirectional reversed shear stresses were shown to result in higher permanent strain than unidirectional ones.

To provide validation for the findings from the HCA tests, a pilot scale experiment involving two fully instrumented flexible pavement sections was performed in the Nottingham PTF. The objectives of the experiment were limited by the complex stress conditions existing in the granular

base and the number of instruments which could be installed in the test sections. Nevertheless, the results of the experiment were generally satisfactory and provided strong support for the use of the repeated-load HCA in future research.

The use of an HCA in the current research necessitated a major effort on the development of both laboratory equipment and testing technique. As a result, a versatile piece of testing apparatus which offers valuable opportunities for study of the fundamental behavior for soil and granular materials is now available.

PREFACE

This report, entitled "Granular Bases for Heavily Loaded Pavements" was prepared by the University of Nottingham, funded under Contract Number F49620-87-C-0085 by the Air Force Civil Engineering Support Agency, Civil Engineering Laboratory, Tyndall Air Force Base, Florida 32403-5319 through the Air Force Office of Scientific Research, Bolling Air Force Base, DC 20332-6448; the US Army Corps of Engineers, Waterways Experiment Station, Vicksburg, MS; and the Science and Engineering Research Council of Britain.

This report covers work performed between February 1988 and December 1990. The AFCESA/RD project officer was Jim Murfee.

This report has been reviewed by the Public Affairs Office and is releasable to the National Technical Information Service (NTIS). At NTIS, it will be available to the general public, including foreign nationals.

This technical report has been reviewed and is approved for publication.

JIM MURFEE, GS-13
Project Officer

FELIX T. UHLIK III, Lt Col, USAF
Chief, Air Base Systems Branch

EDGAR F. ALEXANDER, GM-14
Chief, Air Base Operability and
Repair Section

(The reverse of this page is blank)

TABLE OF CONTENTS

TABLE OF CONTENTS (continued)

TABLE OF CONTENTS (continued)

TABLE OF CONTENTS (continued)

LIST OF FIGURES

LIST OF FIGURES (continued)

LIST OF FIGURES (continued)

LIST OF FIGURES (continued)

LIST OF FIGURES (continued)

LIST OF FIGURES (continued)

LIST OF TABLES

LIST OF ABBREVIATIONS

A/D	Analoge to Digital
CBR	California Bearing Ratio
CIV	Clegg Impact Value
DCP	Dynamic Cone Penetrometer
HCA	Hollow Cylinder Apparatus
NDM	Nuclear Density Meter
PTF	Pavement Test Facility
RAM	Random Access Memory
STF	Slab Test Facility
LVDT	Linear Variable Differential Transformer

LIST OF SYMBOLS

G	Shear modulus
G1	Coefficient for shear modulus in Contour model
H	Height of hollow cylinder specimen
K	Bulk modulus
K1	Coefficient for bulk modulus in Contour model
L	Gauge length for LVDTs on hollow cylinder specimen
M_T	Torque on hollow cylinder specimen
R^2	Coefficient of correlation
W	Axial load on hollow cylinder specimen
a,b	Internal, external radius of hollow cylinder specimen
b	Intermediate principal stress parameter
d	Averaged diameter of hollow cylinder specimen
l	Displacement over the gauge length L, defined above
m	Coefficient for shear modulus in Contour model
n	Coefficient for bulk modulus in Contour model
p, p_m	Bulk, mean bulk stress
p_i, p_o	Inner and outer cell pressure in HCA
q	Deviator stress

q_{oct}	Octahedral shear stress
t	Thickness of the wall of hollow cylinder specimen
u	suction
w	water content
α	Angle of rotation of major principal stress from vertical
α	Coefficient used in Loach's resilient stress-strain model for soil
α_ε	Angle of rotation of major principal strain from vertical
β	Coefficient for bulk modulus in Contour model
γ	Engineering shear strain
δ	Prefix - meaning "change in"
$\varepsilon_r,\varepsilon_z,\varepsilon_\theta,\varepsilon_{45}$	Normal strains in hollow cylinder specimen
$\varepsilon_{\theta z}$	Pure shear strain in θ-z plane
$\varepsilon_1,\varepsilon_2,\varepsilon_3$	Principal strains
ε_h	Horizontal strain = $\varepsilon_r + \varepsilon_z$ in hollow cylinder specimen = $2\,\varepsilon_r$ in triaxial specimen
ε_s	Octahedral shear strain
ε_v	Volumetric strain
ε_{max}	Maximum shear strain in the θ-z plane
η_m	Mean shear stress ratio, $(q_{oct})_m/p_m$
$\sigma_r,\sigma_z,\sigma_\theta$	Normal stresses in hollow cylinder specimen
$\sigma_1,\sigma_2,\sigma_3$	Principal stresses
σ_c	Confining stress in triaxial specimen
σ_{oct}	Octahedral normal stress
$\tau_{\theta z}$	Torsional shear stress in θ-z plane

Suffices

m	mean
p	Permanent (strain)
r	in the radial direction
r	repeated (stress) or resilient (strain)
z	in the axial direction
θ	in the circumferential direction
max	maximum
failure	at failure

(The reverse of this page is blank.)

SECTION I

INTRODUCTION

A. OBJECTIVES

The objectives of this project were to understand the complex properties relating to the resilient and, particularly, the permanent deformation characteristics of granular materials under repeated loading and to determine how these properties could be improved by allowing the material to achieve maximum compacted density. The latter condition is believed to result in better mechanical performance of the granular material needed for heavy loading situations. An important emphasis of the project was placed on understanding the role of reversed shear stresses and the associated rotating principal planes, which result from loading by a moving wheel. A significant part of this investigation concentrated on the use of a substantially modified repeated-load Hollow Cylinder Apparatus (HCA). The performance of this testing device and its ability to simulate wheel traffic also formed an important part of the research.

B. BACKGROUND

The idea of using a mechanistic, rather than an empirical, approach to flexible pavement design has resulted in the need for better knowledge of the behavior of all materials used in pavement construction. When thin or low-stiffness bituminous layers are combined with heavy wheel loads, the behavior of granular bases and their role in providing structural support and contributing to the long-term serviceability of the pavement become important.

Research into the behavior of granular material in pavements has attracted a great deal of world-wide attention. Great progress has been made during the past 20 years in the understanding and mathematical modelling of the resilient stress-strain behavior of granular materials (1). This has led to some successes in the analysis of the elastic behavior of pavements with granular bases (2,3). However, characterization of the permanent deformation behavior which is related to rut formation remains as a difficult challenge.

The most commonly used laboratory device has been the repeated-load triaxial test apparatus. A cylinder of material is subjected to two stress components; a confining stress through a surrounding compressed medium and a vertical stress. Despite its relative simplicity, the limitations of stress conditions that can be applied to the cylindrical specimen are rather severe.

Figure 1 shows the stress conditions imposed on a vertically orientated element of granular material by a moving wheel load. It indicates that for each passage of the wheel, there is a corresponding reversal in the direction of the shear stress on the vertical and horizontal planes. An opposite sense of shear reversal will occur if the wheel travels in the other direction. The combination of vertical and horizontal stress can be reproduced in the repeated-load triaxial test when both the deviator and confining stresses are cycled. However, the reversal of shear stress requires an apparatus which can apply this mode of stress directly to the boundaries of the specimen. Various devices, such as the Cyclic Simple Shear Apparatus (4) and the Directional Shear Cell (5) emerged over the years. Nonetheless, one of the most promising methods is believed to be the Hollow Cylinder Apparatus. With it, a repeated torsion can be applied to a hollow thin-walled cylinder. If the hollow cylinder is at the same time subjected to an axial stress and a lateral stress over both the inner and outer cylinder face, then the stress conditions imposed on an element of material along the wall of the cylinder will be similar to those shown in Figure 1.

Because of the added ability to apply the reversed shear stress, an HCA can allow tests to be carried out within a much wider and more flexible stress regime. More importantly, it can simulate the in situ stress conditions. Hence, it will provide much stronger support for the longer-term objective of modelling the behavior of granular material with respect to its response to wheel loading in a pavement.

Despite shortcomings in understanding of the complex stress-strain behavior of granular bases, when properly specified and carefully constructed they have been successfully used under a wide variety of conditions to give both good performance and excellent economic benefits. One example can be found in the use of high-density crushed stone layers in road construction in South Africa (6) where stiff pavements able to carry heavy traffic have resulted.

The effect of density on granular material behavior has been studied by many researchers. The general conclusions were that high density led to both increase in resilient stiffness (7,8,9) and permanent deformation resistance (10,11). These findings further highlight the potential of using one of the many versions of granular materials in roadbase construction. However, to avoid the pitfalls and problems which can be associated with granular materials, it is essential to obtain a better understanding of their behavior under various conditions.

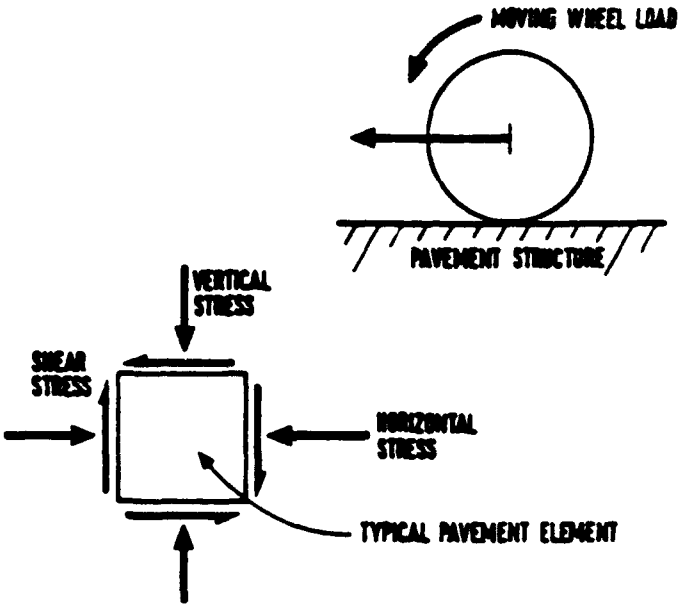

a. Stresses on Pavement Element.

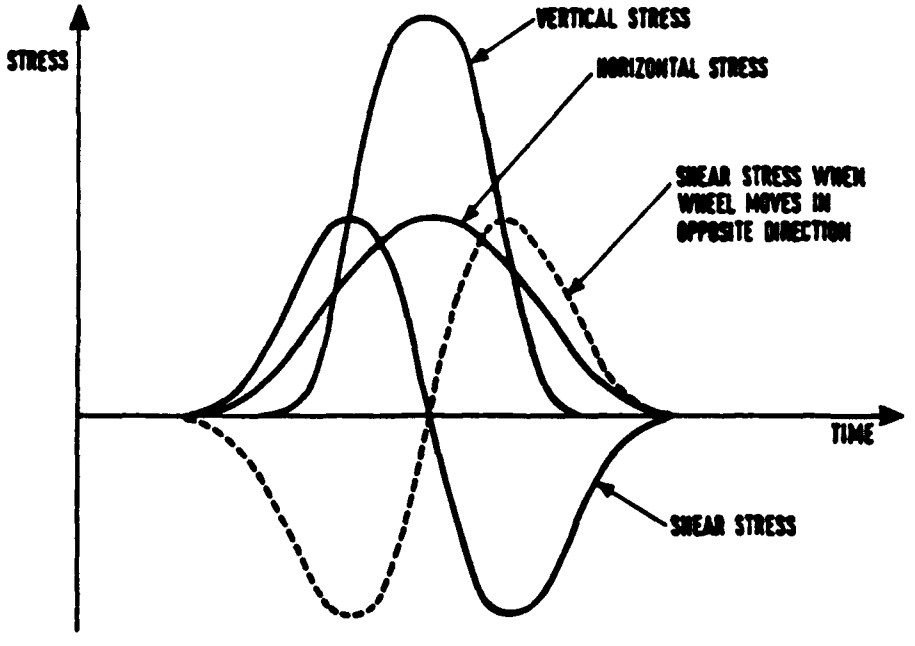

b. Variation of Stresses with Time.

Figure 1. Stresses Induced by a Moving Wheel Load on a Vertically Oriented Element of Granular Material.

C. APPROACH AND SCOPE

The compactibility of granular materials is strongly influenced by the aggregate grading. Therefore, to obtain high density, the densest grading for a particular source of aggregate was identified by means of a proposed grading design procedure. The behavior of the densely graded granular material was then studied under various laboratory simulated stress conditions. These conditions were separated into those which involved rotation of principal stress planes, such as those from a moving wheel load, and those which did not, such as those from a repeated vertical load applied on a stationary wheel or the repeated-load triaxial test apparatus. The effect of reversed shear stresses, principal plane rotation and intermediate principal stresses were further studied by means of a repeated-load HCA on a scaled down version of the same granular material. In order to provide validation for the findings from the HCA tests, a pilot scale experiment involving two fully-instrumented flexible pavement sections was performed in the Nottingham Pavement Test Facility (PTF).

The use of an HCA necessitated major effort on the development of both laboratory equipment and testing technique. Furthermore, improvement to the data acquisition system was carried out on both the repeated-load triaxial test apparatus and the PTF.

This report is divided into nine sections. Section II reports the findings of the grading investigation and the results of the performance tests on the high density granular materials. Section III describes the program and results of the large-scale rutting tests. Sections IV to VI describe, in detail, the modified repeated-load HCA, the test program and the results respectively. Section VII reports on the validation tests carried out in the PTF. Section VIII summarizes the accomplishments and the conclusions from the project and, finally, Section IX recommends further research.

SECTION II

GRADING INVESTIGATION AND PERFORMANCE OF HIGH-DENSITY GRANULAR MATERIAL

A. INTRODUCTION

The purpose of the gradation design in this project was mainly to achieve a maximum compacted density for the granular material concerned which, in turn, is believed to result in better mechanical properties. This approach assumes that the drainage capacity of the granular base, which may be reduced as a result of high density can be supplemented, in practice, by the provision of adequate drainage at layer boundaries and a good road surface maintenance program to prevent build-up of moisture within the layer. Various empirical and analytical grading design methods were reviewed during this project (12). The more theoretical and probably more accurate method used by Lees (13) was considered too complex and impractical. A balance was struck between the use of complex test methods, such as Lee's and the degree of accuracy of the design (i.e. the closeness to the grading which produces the theoretical maximum density). More emphasis was placed on the repeatability and simplicity of the method which would allow potentially large numbers of tests to be carried out efficiently. To this end, a procedure involving the use of the British Standard BS5835 (14) method for the standard vibrating hammer test and Fuller's grading curves (15) was adopted.

A high-quality dolomitic limestone, widely used in British highway construction, was chosen as the main testing material. A maximum particle size of 38 mm was used both in the grading investigation and the subsequent performance tests.

B. GRADING INVESTIGATION

The design parameter was "n" used in the Fuller's equation shown as follows:-

$$P = 100\left(\frac{d}{D}\right)^n \qquad (1)$$

where P = percentage finer than sieve size d
D = maximum particle size

n = real positive number less than one

Four gradings with "n" equal to 0.35, 0.4, 0.45 and 0.5 were used in the grading investigation. In addition, three gradings which represent the fine, middle and coarse side of the grading envelope for the British Standard Type 1 (16) subbase material were included. Despite their continuous shape, these gradings generally did not satisfy Equation (1), hence, their characterization could only be made by means of an approximated "n" value. The seven gradings used are plotted in Figure 2. All the samples used in the investigation were reconstituted from seven size fractions to ensure that the target gradings were achieved.

1. Compaction Tests for Grading Design

The compaction apparatus and the test method used are specified in the British Standard BS5835 (14) for the standard vibrating hammer test. Details of the compaction mold are illustrated in Figure 3. Compaction on the 2.5 kg specimens, which were dry, was provided by a 900 Watt vibrating hammer. For each of the Fuller's gradings, three tests were performed for each of the two compactive efforts, namely 180 and 360 seconds of compaction time. For the three gradings from the British Standard, only one compactive effort (180 seconds) was used.

2. Results of Compaction Tests

The average compacted densities for samples of the various gradings are plotted in Figure 4 against their "n" values. The results indicate that a peak density for the two compactive efforts can be obtained within the range of "n" value studied. Figure 4 shows that as compactive effort increases, there is a shift of the high density grading towards the coarse side (i.e., higher "n"). Based on the results from the higher compactive effort, it appears that the grading corresponding to the highest density for the dolomitic limestone has a Fuller's "n" value of about 0.39. The coefficient of uniformity corresponding to this grading is about 100. The test results for the lower compactive effort indicated that as much as 7 percent increase in dry density could be obtained when a designed grading, compared with a standard grading, was used.

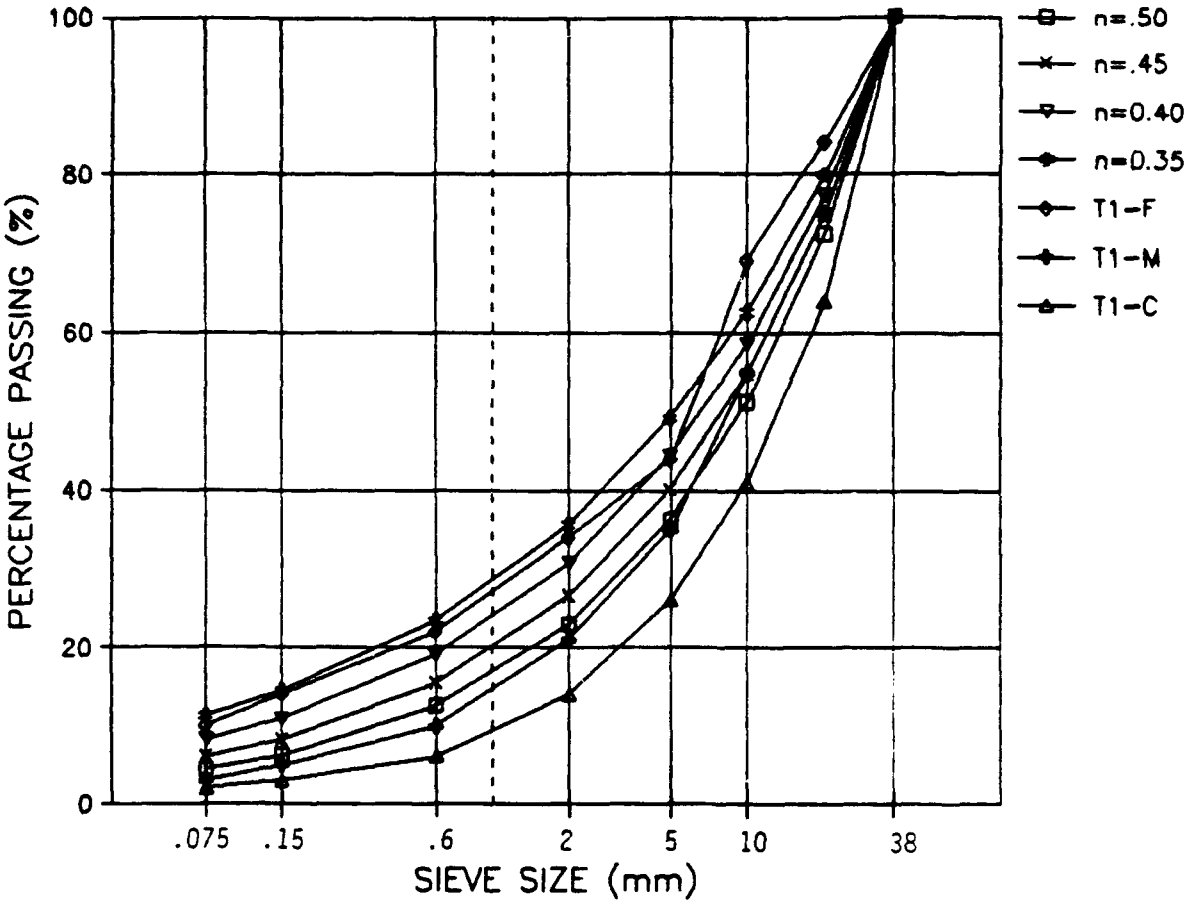

Note: T1-F, T1-M and T1-C represent the Fine, Middle and Coarse parts respectively, of the grading envelop for the British Type 1.

Figure 2. Gradings used in the Investigation of High-Density Grading.

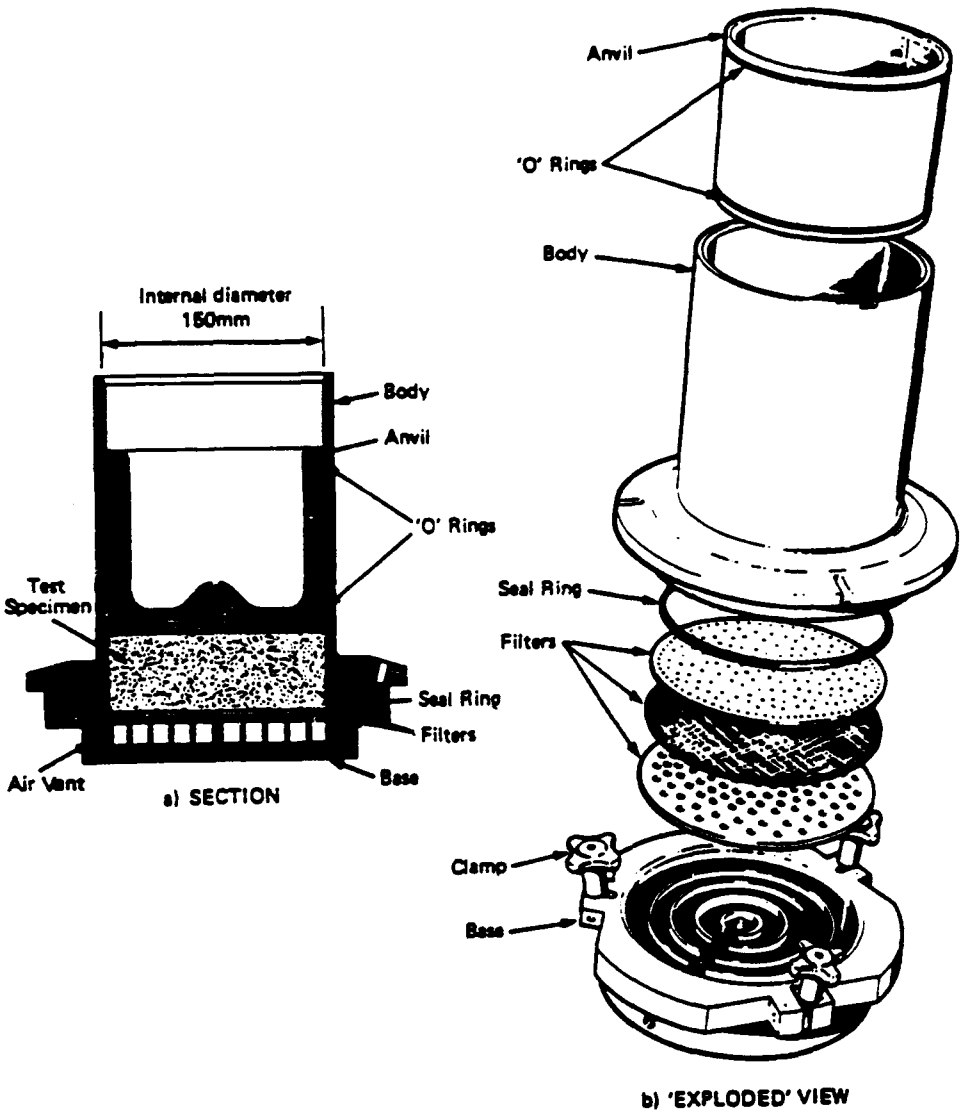

Figure 3. Details of Compaction Mold used in Grading Investigation.

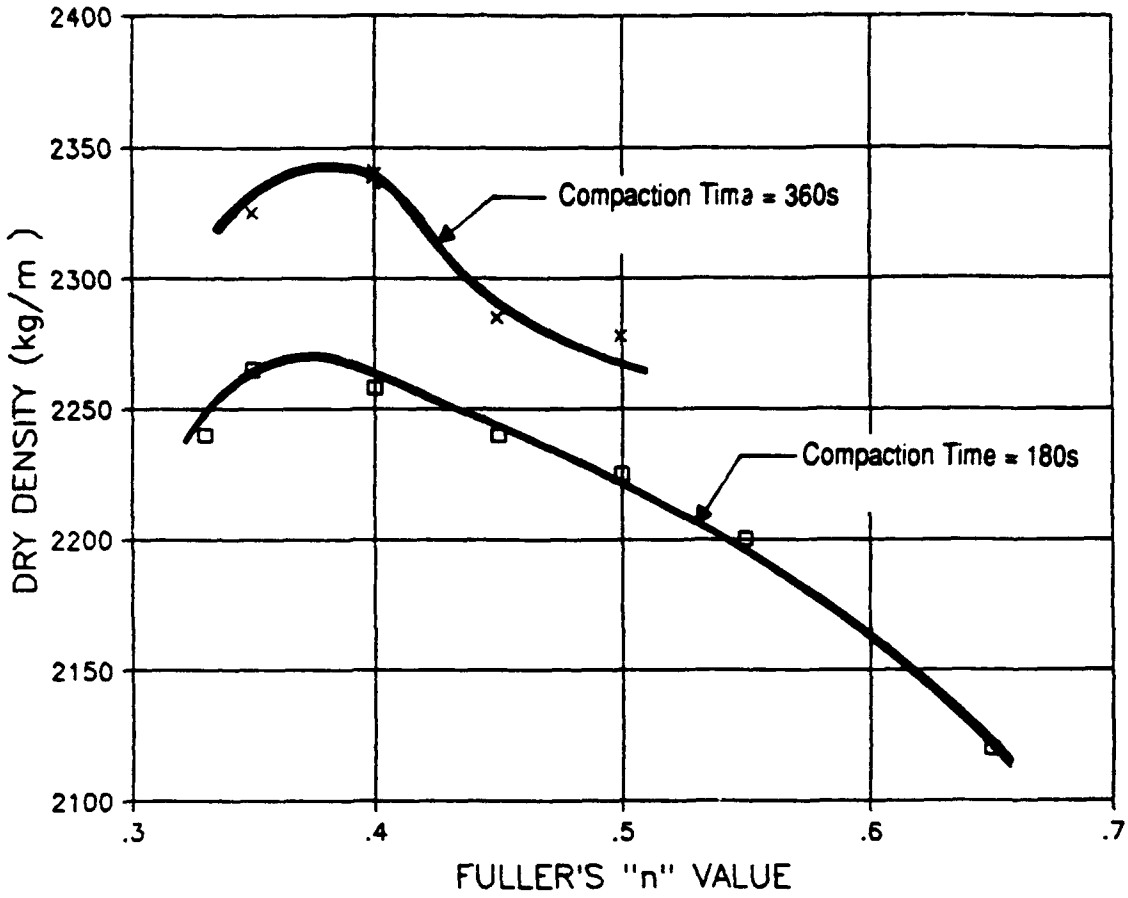

Figure 4. Variation of Compacted Dry Density with Fuller's Grading Parameter "n."

C. PERFORMANCE OF HIGH DENSITY GRANULAR MATERIAL

It appears useful to determine if there are benefits in using a specially designed high-density grading, such as the one obtained in this project, against one which is readily available, perhaps as "crusher run." To this end, the mechanical properties of two differently graded materials, one with a Fuller's "n" of 0.4 (identified as "optimum ", and the other a standard "as supplied" British Type 1 subbase grading, were studied. The investigation on insitu properties was performed with large containers and in test pits with granular materials compacted by heavy industrial type compactors. Two subgrade conditions, one stiff and one soft, were used to enhance the scope of the investigation. The mechanical properties that were determined in this project included the dry density obtained from the Nuclear Density Meter (NDM), the California Bearing Ratio (CBR) obtained from plate bearing tests, the Clegg Impact Value (CIV) from the Clegg hammer tests, the penetration resistance from the dynamic cone penetrometer tests. A description of these pieces of apparatus is reported elsewhere (17).

Response of the two granular materials to repeated load was further investigated by means of a repeated-load triaxial test apparatus, which was capable of testing specimen of 150 mm diameter. The apparatus is described in Appendix A.

1. Results of Insitu Performance Tests

A comparison of the performance data for the compacted materials is shown in Figure 5. On average, despite the scatter of data, the optimum-graded material is shown to have better properties. The most obvious improvement due to the dense grading comes from the DCP tests which generally involve the entire thickness of the compacted layer. An average of about 30 percent increase in penetration resistance was recorded. For the Plate Bearing and NDM tests which were carried out on the surface of the material, average improvements of 9 and 2 percent were recorded respectively. Most results indicate that stiff subgrade conditions generally lead to better performance because of the increase in dry density due to the stiffer support conditions during compaction.

2. Results of Repeated-load Triaxial Tests

Two series of tests, one on the optimum-graded and the other on the standard Type 1 graded dolomitic limestone were carried out. In each series , two sets of elastic stiffness tests, which involved 20 stress paths, and two permanent strain tests at an identical stress level were

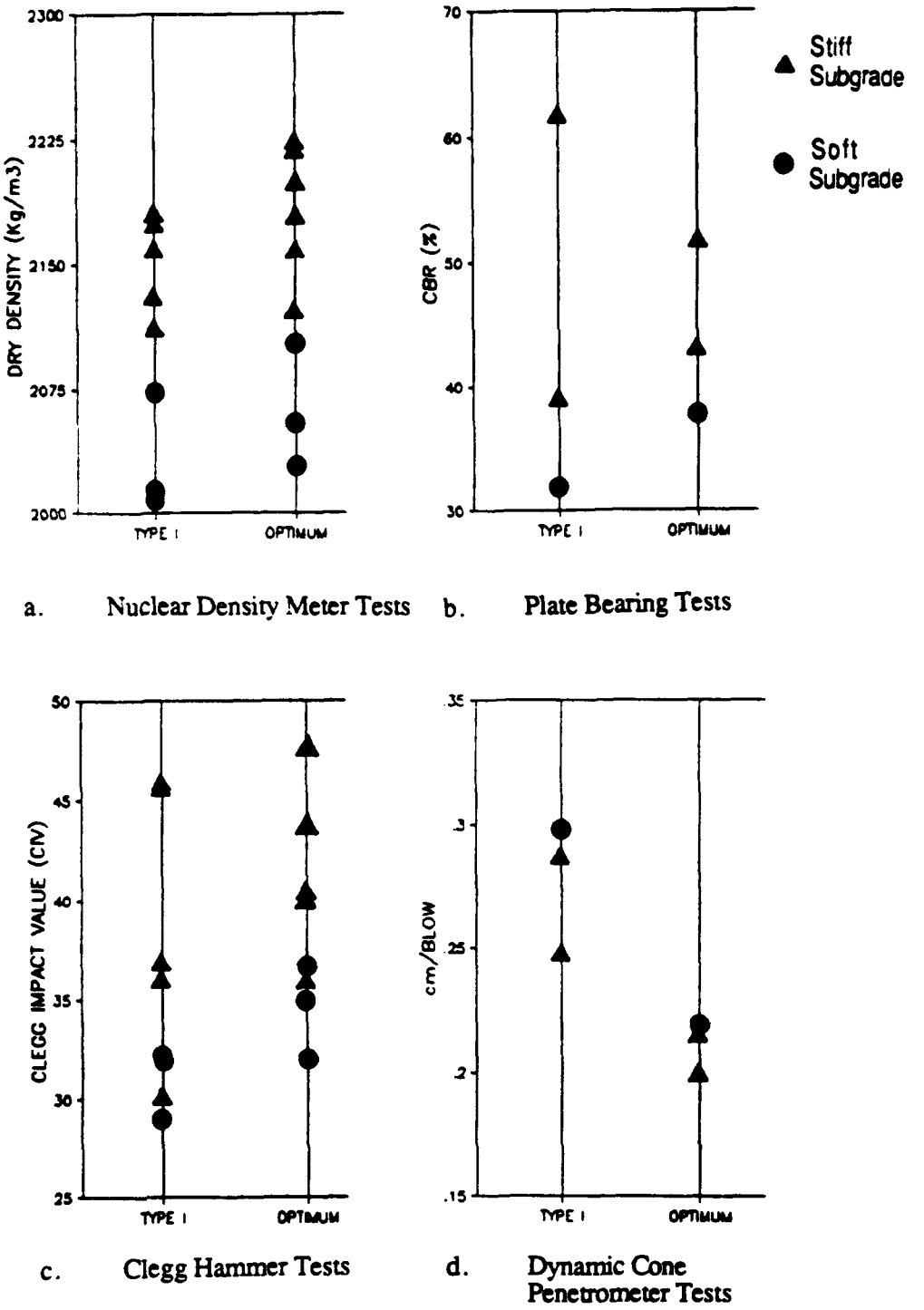

a. Nuclear Density Meter Tests

b. Plate Bearing Tests

c. Clegg Hammer Tests

d. Dynamic Cone Penetrometer Tests

Figure 5. Comparison of Results of In Situ Performance Tests carried out on Optimum Graded and Standard British Type 1 Graded Dolomitic Limestone.

performed. The stress paths used are shown in Figure 6. For the permanent strain tests, up to 10,000 stress cycles at a frequency of 1 Hz were applied to the test samples.

Both the average resilient and permanent axial and radial strains were measured during the tests. However, strains are more appropriately expressed in terms of the shear and volumetric invariants, ε_s and ε_v, which in triaxial conditions are defined as:-

$$\varepsilon_s = \frac{2}{3}(\varepsilon_1 - \varepsilon_3) \tag{2}$$

$$\varepsilon_v = \varepsilon_1 + 2\varepsilon_3 \tag{3}$$

where ε_1 and ε_3 are principal strains.

The corresponding stress invariants for ε_s and ε_v are q and p' respectively where:

$$q = \sigma_1' - \sigma_3' \tag{4}$$

$$p' = \frac{1}{3}(\sigma_1' + 2\sigma_3') \tag{5}$$

where σ_1' and σ_3' are principal effective stresses.

To summarize the stress-strain relationships of the granular materials tested, the mathematical contour model proposed by Pappin (18) and modified by Jouve et al. (19) was used. The model involves use of the following equations:-

$$G = \frac{q}{3(\varepsilon_s)_r} \tag{6}$$

$$G = G_1 p'^{(1-m)} \tag{7}$$

$$K = \frac{p'}{(\varepsilon_v)_r} \tag{8}$$

$$K = \frac{K_1 p'^{(1-n)}}{\left\{1 - \beta\left(\frac{q}{p'}\right)^2\right\}} \tag{9}$$

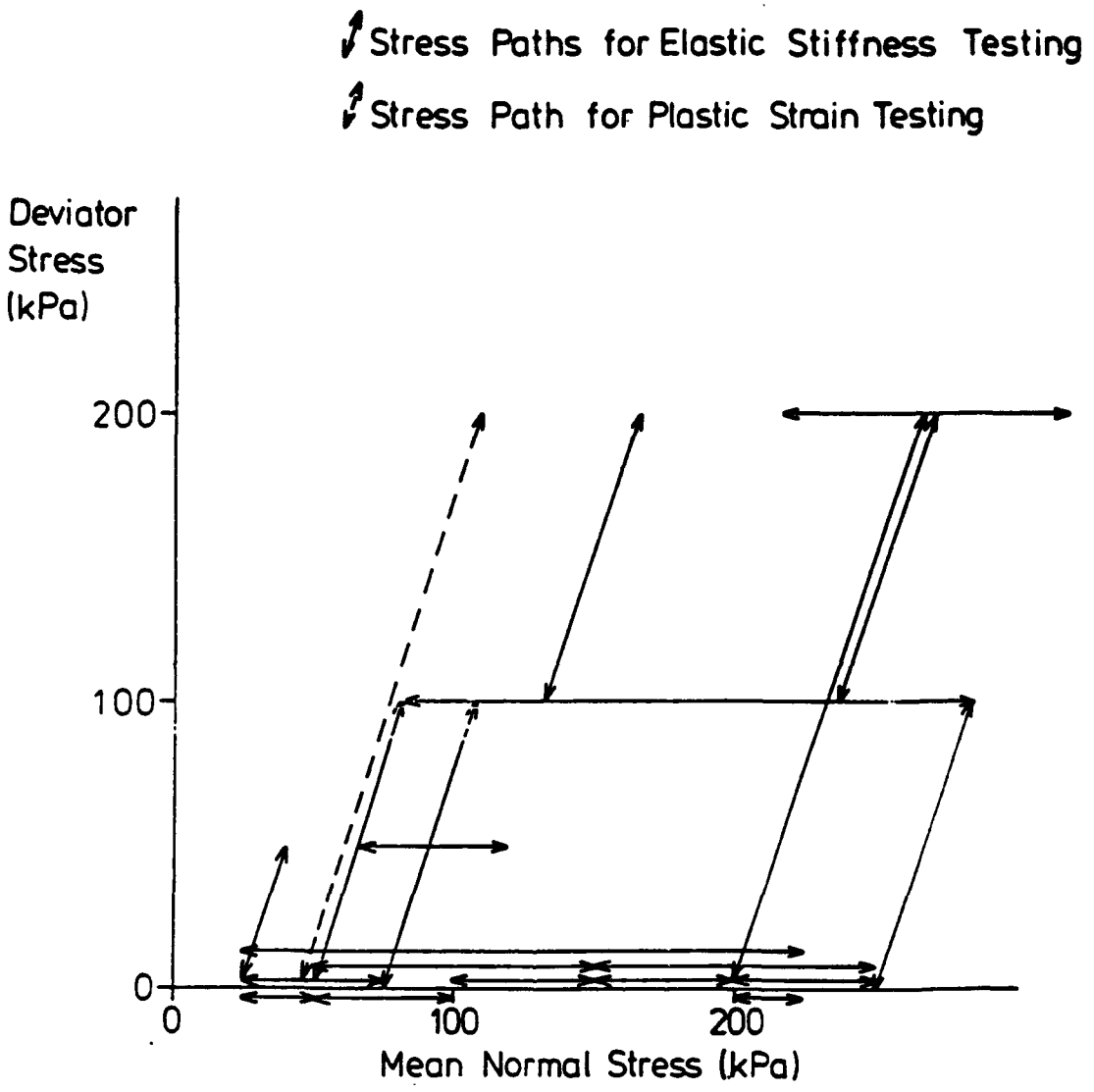

Figure 6. Stress Paths used in Repeated Load Triaxial Tests on Optimum Graded and Standard British Type 1 Graded Dolomitic Limestone.

where p', q, ε_s and ε_v are as defined earlier.

G is the resilient shear modulus

G_1 and m are the shear strain coefficients

K is the resilient bulk modulus

K_1, n and β are the volumetric strain coefficients

Since m,n and β are parameters mainly related to the material type, the same values can be used for both the Type 1 and optimum-graded material. As a result, the comparison between the two differently graded materials depends only on the values G_1 and K_1. Higher values indicate a stiffer material. The comparison is shown in Table 1, which indicates that the coefficients for both materials are similar in magnitude with the optimum graded material having a slightly higher stiffness than the Type 1 material.

The average permanent shear and volumetric strains for the two materials are shown in Figure 7. The results indicate that much less permanent strain, both shear and volumetric, was obtained from the denser samples. The improvement in the permanent deformation behavior for the denser optimum grading is more apparent than that from the resilient strain tests. Figure 7 also indicates that the permanent volumetric strain for both materials is of the dilatant type which is predicted for high-density material.

D. DISCUSSION

Despite the general improvement in density and other mechanical properties, no claim to superiority should be made for the optimum grading if conditions are outside those used in the tests. These conditions can include changes in material, moisture content or maximum particle size. Under these changes, new design tests have to be performed. In design tests for typical pavement materials with a maximum particle size of 38 mm, the use of Fuller's "n" value between 0.35 and 0.5, a coefficient of uniformity of 80 to 100 and a fines content (percent passing the 75 μm sieve) of less than 10 percent should provide a good starting point for determination of the optimum grading.

The observed improvement may be partly due to the use of a dense grading in a relatively dry condition where suction or negative pore pressure will develop, hence effectively increasing strength, stiffness and resistance to repeated load. Conversely, in situations where the moisture

TABLE 1

SUMMARY OF RESILIENT STRAIN COEFFICIENTS USED IN THE CONTOUR MODEL FOR GRANULAR MATERIAL

			Volumetric Strain Coefficients			Shear Strain Coefficients	
Test No.	Grading	Dry Density (kg/m^3)	K_1	n	β	G_1	n
1	Type I	2183	4188	0.33	0.12	4953	0.33
2	Type I	2130	3609	0.33	0.12	3785	0.33
Average of 1 & 2	Type I	2157	3877	0.33	0.12	4291	0.33
3	Optimum	2226	4383	0.33	0.12	4995	0.33
4	Optimum	2190	4129	0.33	0.12	4628	0.33
Average of 3 & 4	Optimum	2208	4252	0.33	0.12	4804	0.33

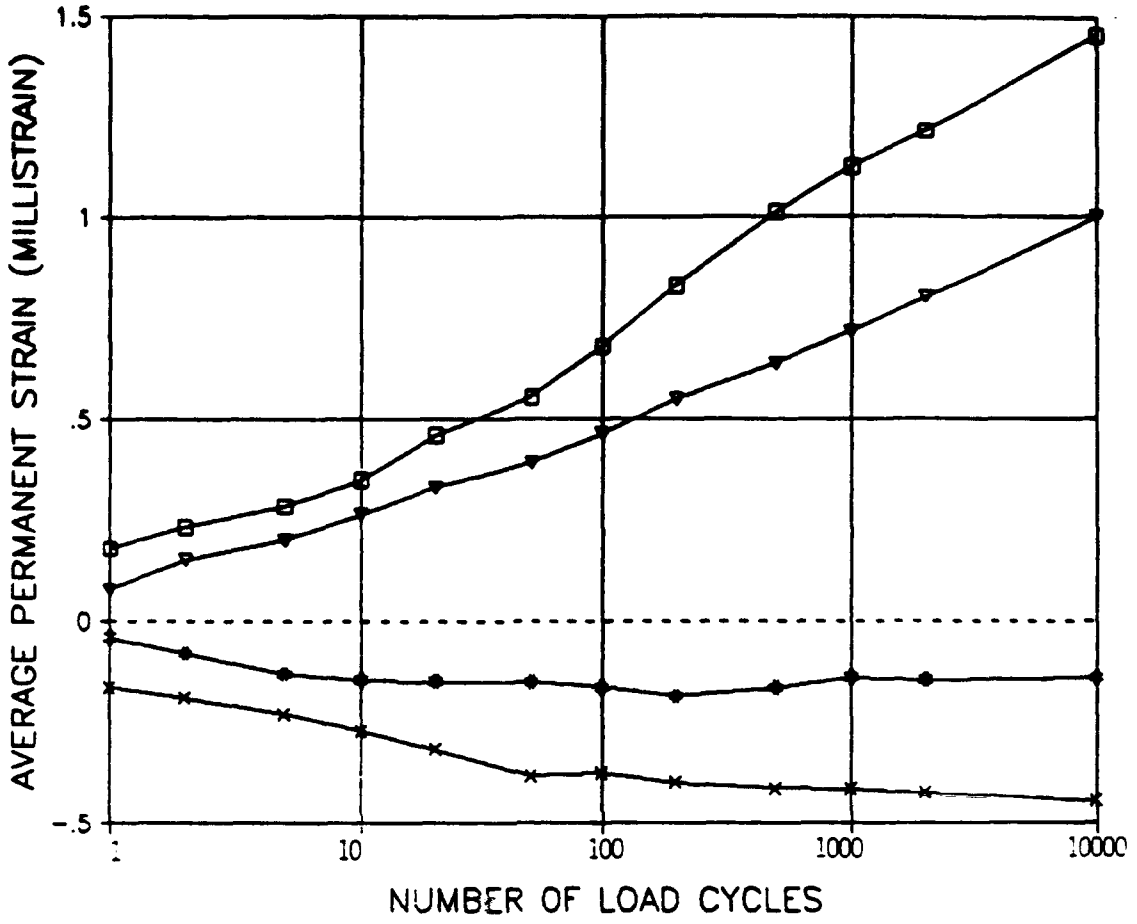

Ave. Permanent Shear Strain, Type I Grading.
Ave. Permanent Volumetric Strain, Type I Grading.
Ave. Permanent Shear Strain, Optimum Grading.
Ave. Permanent Volumetric Strain, Optimum Grading.

Figure 7. Variation of average Permanent Strains with Number of Loading Cycles in Repeated Load Triaxial Tests on Optimum Graded and Standard British Type 1 Graded Dolomitic Limestone.

condition approaches saturation, the relatively poorer drainage characteristic of the densely graded materials may neutralize or even have an opposite effect on the improvement gained. Therefore, it appears necessary to reiterate the fact that if high-density granular material is to be used with success, effective drainage and good surface maintenance of the pavement are essential.

SECTION III

LARGE-SCALE RUTTING TESTS

A. INTRODUCTION

As shown in Figure 1 of Section one, the stress conditions imposed on an element of granular material by a moving wheel load are extremely complex. For each passage of the wheel, principal plane rotation occurs as a result of the reversed shear stresses. At the present time, there are very few pieces of equipment capable of simultaneously applying the stress patterns shown in Figure 1 onto a test specimen. Although large amounts of data were obtained from the repeated-load triaxial tests (10,11,18,20), the latter only correctly simulates the in situ stress conditions underneath a circular plate which is repeatedly loaded vertically. Examination of this mode of loading in large scale, which does not involve the application of reversed shear stresses is needed to establish the difference in behavior, particularly in the development of permanent strains, compared with that due to wheel loading.

Examination of the difference in the permanent deformation behavior of granular material due to unidirectional and bidirectional wheel loading also appears to be desirable. In practice, all traffic travels in the same direction over the pavement (i.e. unidirectional). However, bidirectional loading is usually adopted for wheel tracking experiments to bring about failure of the test pavement in a reasonable period of time. Since the shear stress reversal conditions differ, an understanding of the different response of the material is needed.

This chapter describes an investigation which is aimed at highlighting the effect of reversed shear stresses on permanent deformation of granular materials. To tackle the problem caused by the difference between repeated vertical and moving wheel loading, the Nottingham Slab Test Facility (STF) was used. For the problem involving uni- and bidirectional wheel loading, the Nottingham PTF was employed.

The same dolomitic limestone and gradings used in the tests described in Section II was used. An open-graded carboniferous limestone was also used in the PTF tests. The grading envelopes of these materials are shown in Figure 8. The three materials enabled a range of compacted densities to be achieved.

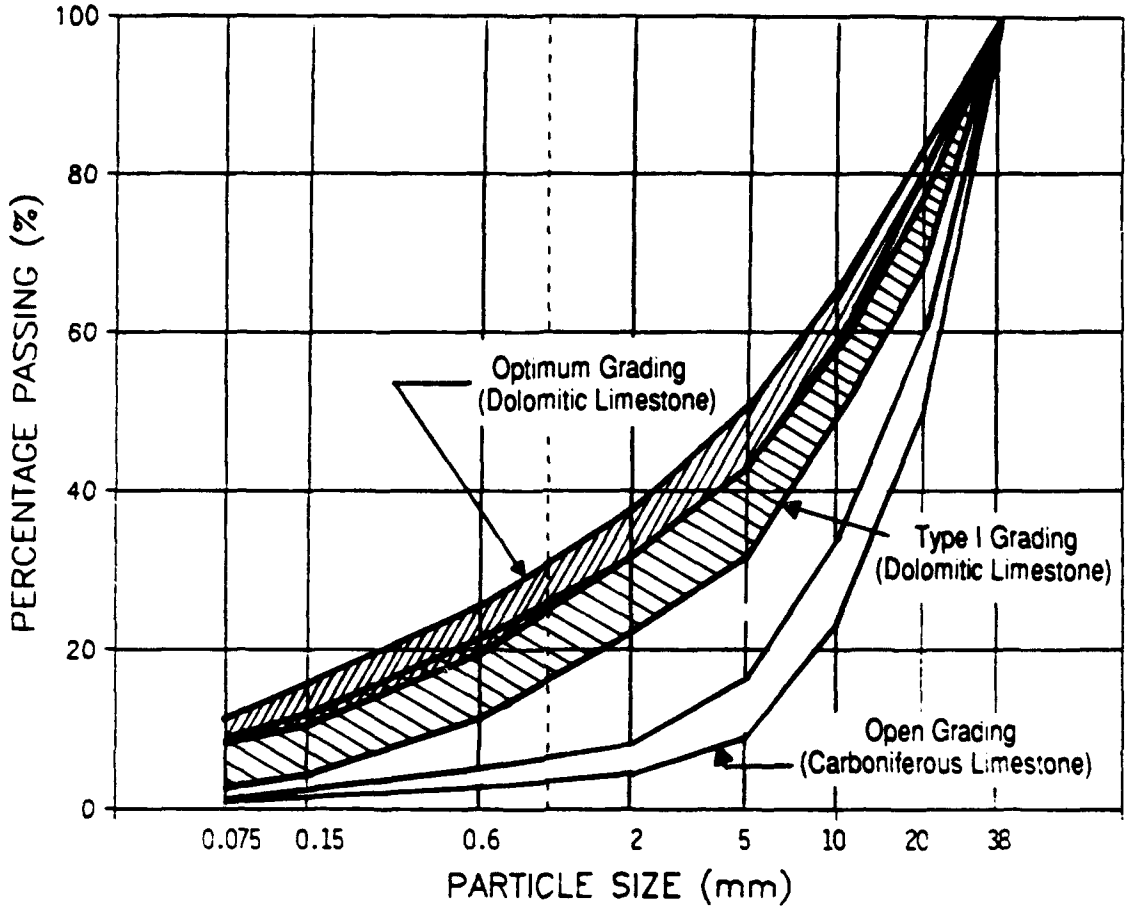

Figure 8. Grading Envelopes of Granular Materials used in Large-Scale Rutting Tests.

B. TEST FACILITIES AND EXPERIMENT PROGRAM

1. Slab Test Facility

The Nottingham STF was originally used to evaluate the deformation resistance of a slab of bituminous material. However, by confining a layer of compacted granular material in a mold, the facility can also be used to study the same characteristic of this material.

A side view of the STF is shown in Figure 9. The carriage is mounted onto a pair of beams and is driven by means of a wire rope tensioned around a drum which is axially coupled to the motor. Loading is provided via a hydraulic actuator located at one end of the facility. A feedback mechanism involving the use of four load cells located under the corners of the steel pallet is used. Constant wheel load over the slab can only be achieved by applying an increasing actuator load of the correct gradient as the wheel approaches the actuator. Alternatively, the wheel can be fixed at a position directly above the compacted granular material. Repeated vertical loading, which is regulated by means of a signal generator can then be applied via the hydraulic actuator onto the specimen.

A 75 mm wide hard rubber tire was used in both the repeated vertical and wheel-loading conditions to ensure that the same contact area was achieved. A sinusoidal waveform with frequency of 0.5 Hz (or one cycle of load every two seconds) was used for the repeated vertical loading condition. For the travelling wheel load, an average speed of approximately 2 km/hr was used. Loading in this case was bidirectional. An element of granular material loaded under the moving wheel had a rest period of approximately two seconds while that for the repeated vertical load was zero.

The samples tested in the STF were compacted in a specially manufactured steel mold as shown in Figure 10. The thickness of the granular layer was 180 mm. A 60 mm thick concrete slab with a rough surface was placed at the bottom of the steel mold to provide a rigid foundation for compaction. The entire mold was then placed on top of a piece of 25 mm thick soft rubber which simulated a medium-stiff subgrade condition. The rubber, in turn, was located on top of a steel platform with cross bracing at the bottom face to provide additional reinforcement. The weight of granular material used per sample was about 325 kg. Total weight of the assembly shown in Figure 10 was about 750 kg .

Compaction of the material was carried out by a heavy vibrating plate with a working area of 475x508 mm, weight of 1.25 kN and maximum centrifugal force of 10 kN.

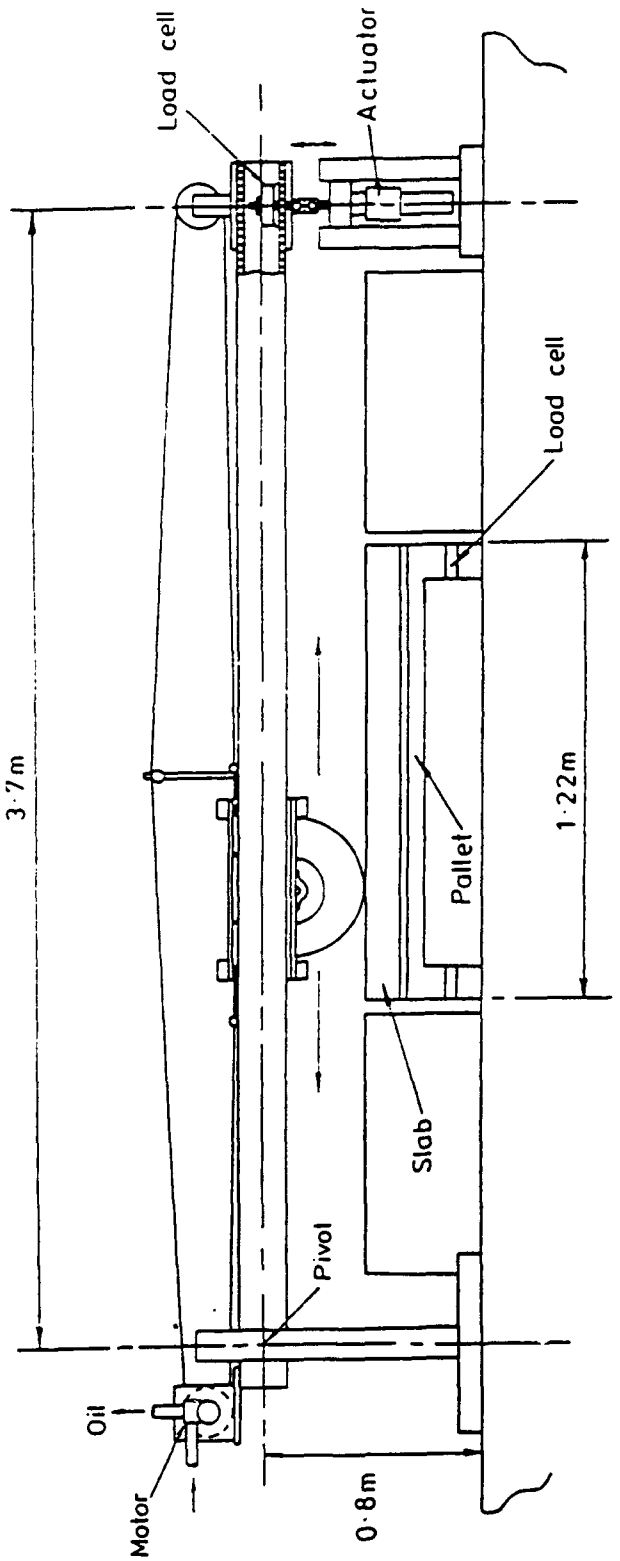

Figure 9. Side View of the Nottingham Slab Test Facility.

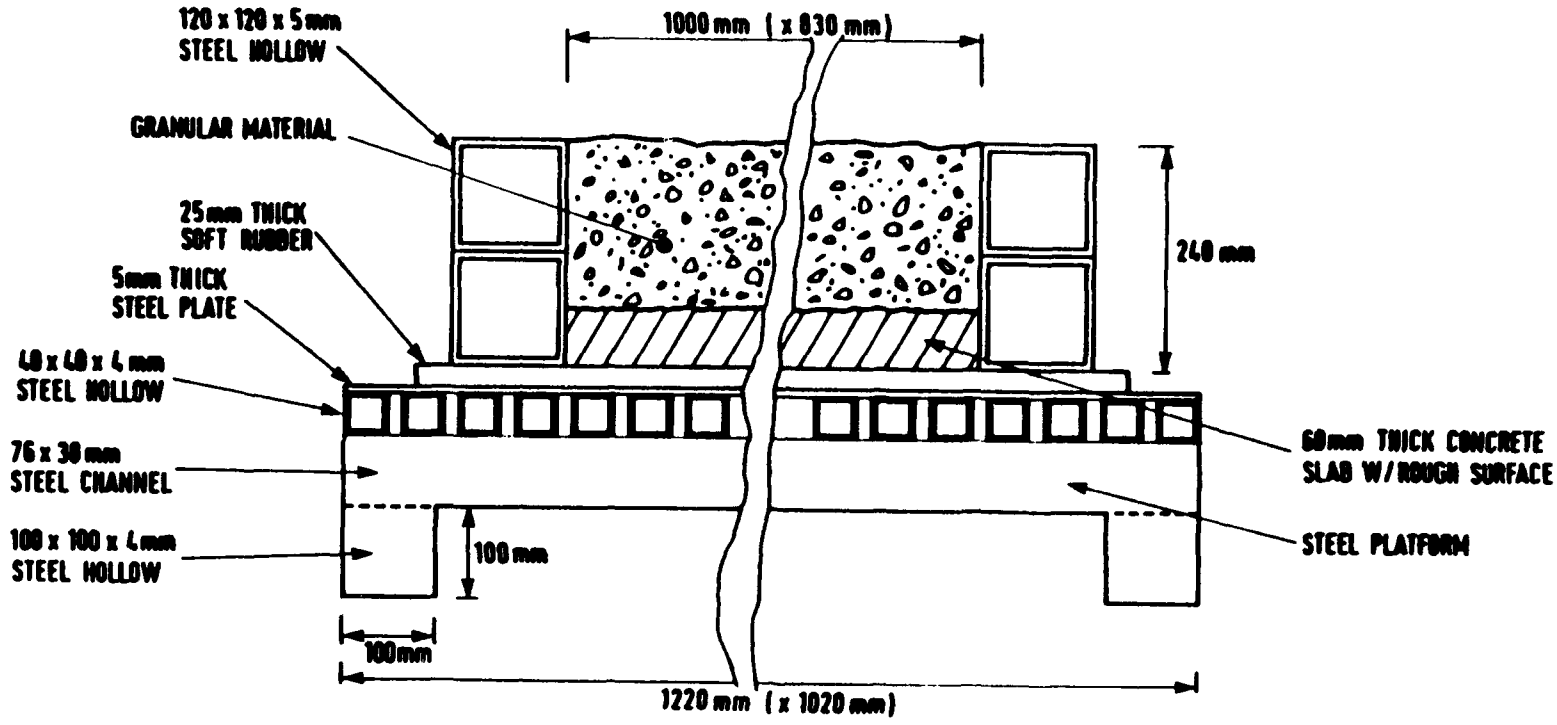

Figure 10. Details of Large Steel Mold used in Tests carried out in the Slab Test Facility.

Compaction was carried out in two layers with a thickness of 60 mm for the bottom and 120 mm for the top layer. Compaction was continued until refusal or no increase in density was detected in successive density measurements. In order to avoid segregation, the finest fraction of aggregates, (5 mm nominal size) was placed last and allowed to fill the void of the matrix formed by the larger size materials during compaction.

A 10 mm thick sand sheet asphalt mix with 10 percent by weight of a Grade 100 Pen bitumen was added to provide a smooth surface for the wheel. No instrumentation was installed in the sample because of great disturbance which could be caused by the necessary excavation and recompaction of the relatively small sample. Therefore, only the wheel load, the surface profile and the permanent vertical deformation of the granular layer underneath the center-line of the wheel were monitored.

Details of the test program and some material properties of the granular materials are shown in Table 2. A total of seven tests were carried out. These tests involved two levels of contact stress, (750 and 1100 kPa), two gradings and two types of loading (a moving wheel load and a repeated vertical load).

2. Pavement Test Facility

The Nottingham Pavement Test Facility (PTF) shown in Figure 11 was described in detail by Brown and Brodrick (22). In brief, it consists of a 560 mm diameter and 150 mm wide loading wheel fitted to a carriage, which runs on bearings between two beams spanning the long side of a rectangular laboratory. The beams are, in turn, mounted on end bogies which allow the whole assembly to traverse across the pavement. Lifting and lowering of the wheel, which determines the magnitude of the applied load, is controlled via two ultra-low friction rams by a servo-hydraulic system. A load feedback mechanism is incorporated to maintain constant load. The maximum load that can be achieved by the PTF is about 15 kN with a speed range of up to 16 km/hr. The whole assembly is housed in an insulated area where temperature could be controlled via heaters or cooling fans. Maximum dimensions of the pavement section that can be constructed are 4.8m long, 2.4m wide and 1.3m deep.

A cross-section of the pavement structure used for this experiment is shown in Figure 12. The thickness of the granular layer was 240 mm. The subgrade at the time of the tests consisted of an inorganic low plasticity silty clay . The CBR at the surface of the top 450 mm of material was found to be about 5 percent. Underneath this layer the material became much drier and stiffer with CBR of about 10 percent. The compaction of the granular materials was provided

TABLE 2

DETAILS OF RUTTING TESTS CARRIED OUT IN THE SLAB TEST FACILITY

Test No.	Grading	Means of Loading	Contact Pressure (kPa)	Dry Density (kg/m^3)	Average In-situ Properties		
					CBR (%)	CIV	DCP (cm/blow)
1	Type I	Plate	750	2182	62	46	0.25
2	Type I	Wheel	750	2180	-	46	-
3	Optimum	Plate	750	2225	52	35	0.20
4	Optimum	Plate	1100	2200	-	44	-
5	Optimum	Wheel	750	2220	-	40	-
6	Type I	Plate	1100	2160	39	37	0.22
7	Type I	Wheel	1100	2131	-	36	-

Note: "-" means no tests were performed.

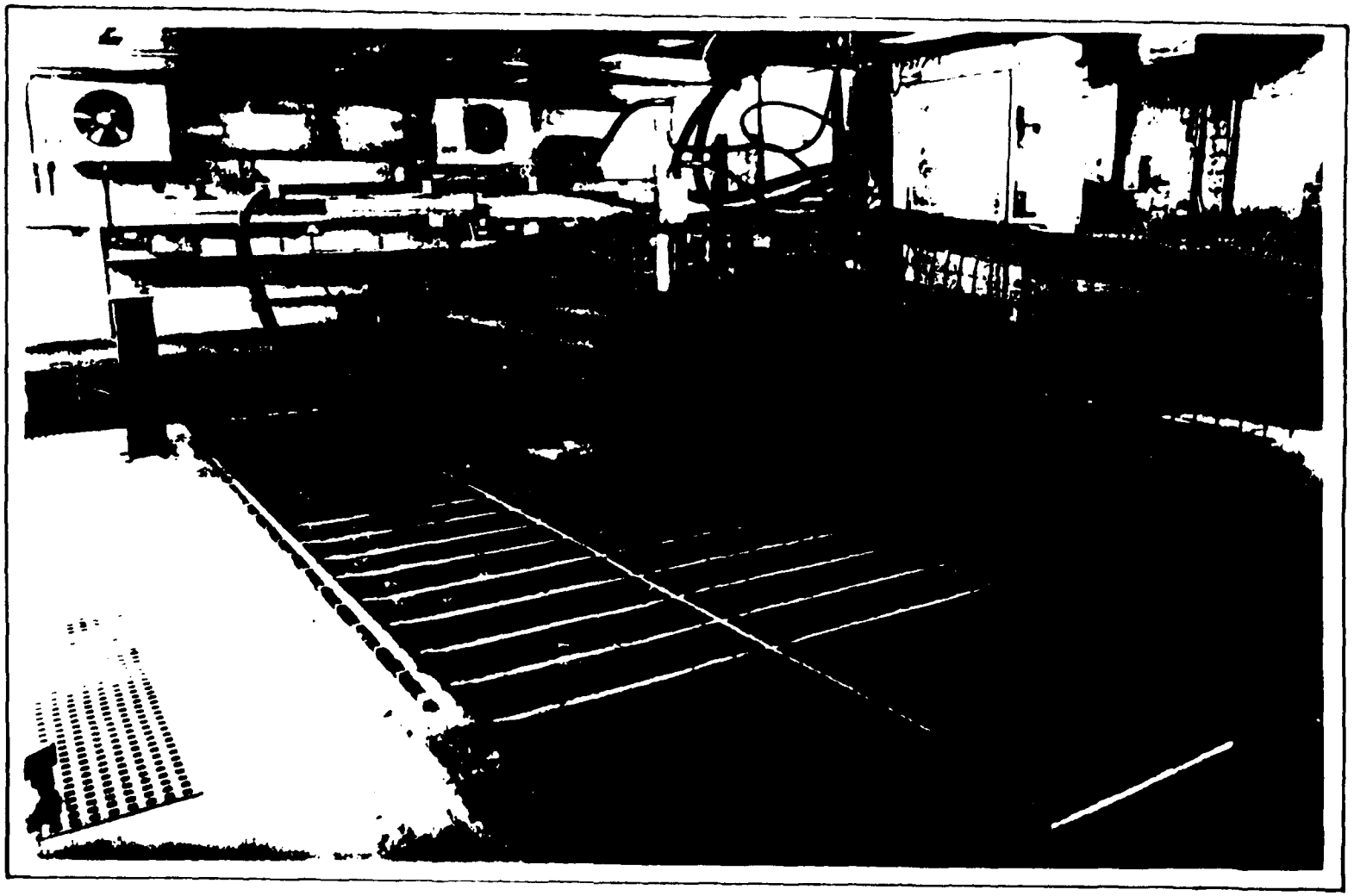

Figure 11. Nottingham Pavement Test Facility.

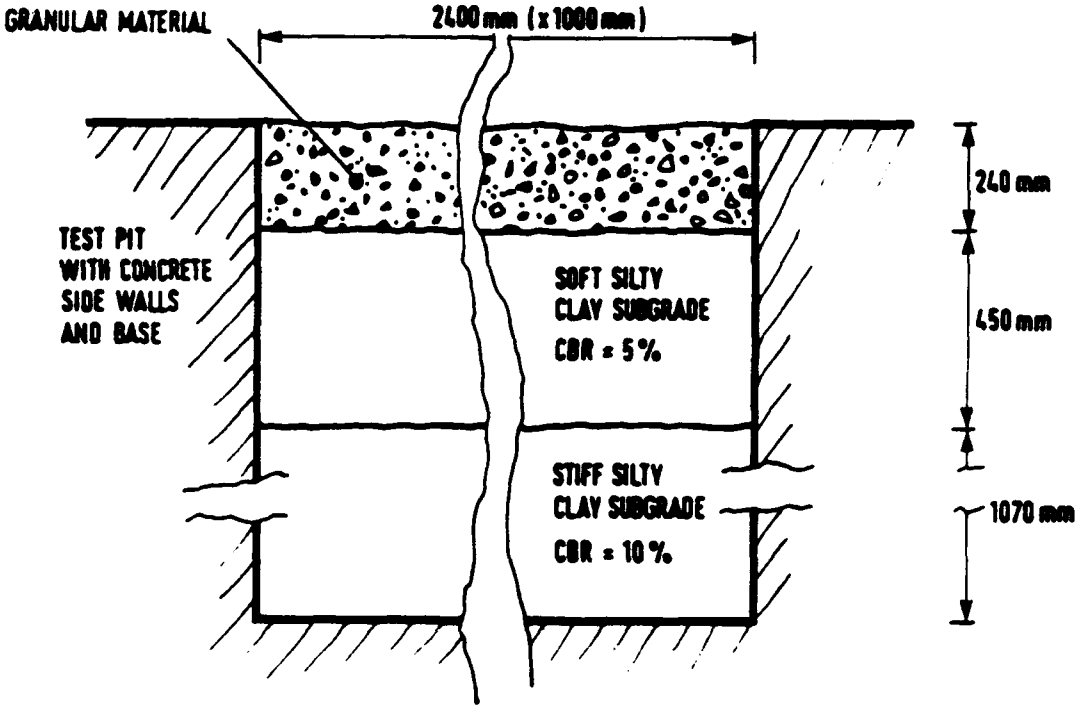

Figure 12. Cross-section of Pavement Structure used in Tests carried out in the Pavement Test Facility.

by a pedestrian operated single-drum vibrating roller which could generate a total centrifugal force of 22 kN. Compaction was carried out in two layers, each 120 mm in thickness and until refusal. A 10 mm thick sand sheet surface (as used in the STF tests) was again used.

For this part of the project, two wheel tracks, each running across the three pavement sections consisting of the three different granular materials were used. In one track, a unidirectional wheel load was applied and in the other, the loading was bidirectional.The movement of the wheel was channelized, hence allowing accelerated deformation of the sections to occur. Details of the sections and the material properties are shown in Table 3. A 150 mm wide wheel, with tyre pressure of 550 kPa and contact stress of about 500 kPa was used. Speed of the wheel was about 3 km/hr. The temperature inside the PTF during the tests was 24 to 27°C.

C. RESULTS OF RUTTING TESTS

1. Slab Test Facility Experiments

Figure 13 shows the profiles of the various sections at the end of the tests carried out in the STF and Figure 14 shows the variation of permanent vertical deformation with the number of load applications for all the tests.

Figure 13 indicates that a significant amount of heaving took place along the shoulder of the rut for those sections subjected to a moving wheel load. This occurred as a result of lateral spreading of the granular material. For these sections, the permanent vertical deformations were found to be at least three times higher than those subjected to a repeated vertical load. Whilst the increase in stress level caused a great deal of increase in permanent deformation in the wheel loading case, the permanent deformation due to repeated vertical load was not significantly affected by this factor. As far as rate of deformation is concerned, Figure 14 indicates that most deformation occurs within the first 1000 cycles of load. For sections subjected to wheel loading, deformation does not stabilise even after 6000 cycles of load. However, for sections subjected to repeated vertical load, very little additional deformation was observed after about 2000 cycles. Furthermore, the results show that sections with the "optimum" grading have less permanent deformation under both the moving wheel and repeated vertical loads.

The results of the tests performed in the Slab Test Facility indicated that, under the particular test conditions, far more permanent deformation was caused by a moving wheel load than a repeated vertical load. The primary reasons for the results are probably due to the additional

TABLE 3

DETAILS OF RUTTING TESTS CARRIED OUT IN THE PAVEMENT TEST FACILITY

Section No.	Grading	Material	Direction of Loading	Average Section Properties							
				Granular Base					Subgrade		
				Dry Density (kg/m^3)	Moisture Content (%)	CBR (%)	CIV	DCP (cm/blow)	Moisture Content (%)	CBR (%)	DCP (cm/blow)
1	Type I	Dolomitic Limestone	Unidirectional	2050	3.3	32	32	0.30	15.2	4.7	1.22
2	Optimum	Dolomitic Limestone	Unidirectional	2105	4.0	38	37	0.22	14.8	4.9	1.15
3	Open	Carboniferous Limestone	Unidirectional	1995	3.6	28	46	0.22	15.5	4.2	1.31
4	Type I	Dolomitic Limestone	Bidirectional	2011	4.2	-	29	-	15.2	4.5	-
5	Optimum	Dolomitic Limestone	Bidirectional	2056	3.2	-	32	-	15.6	4.7	-
6	Open	Carboniferous Limestone	Bidirectional	1966	3.5	-	40	-	15.0	5.0	-

Note: "-" means no tests were performed.

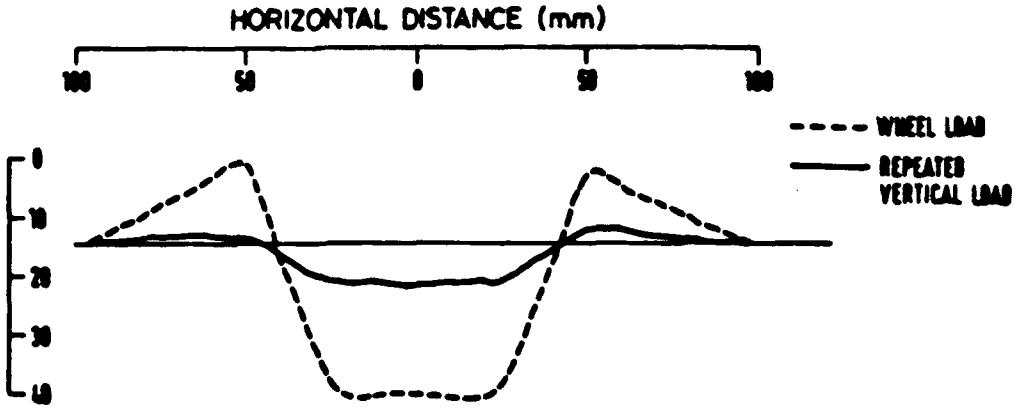

a. Type I Grading; Contact Pressure = 750 kPa.

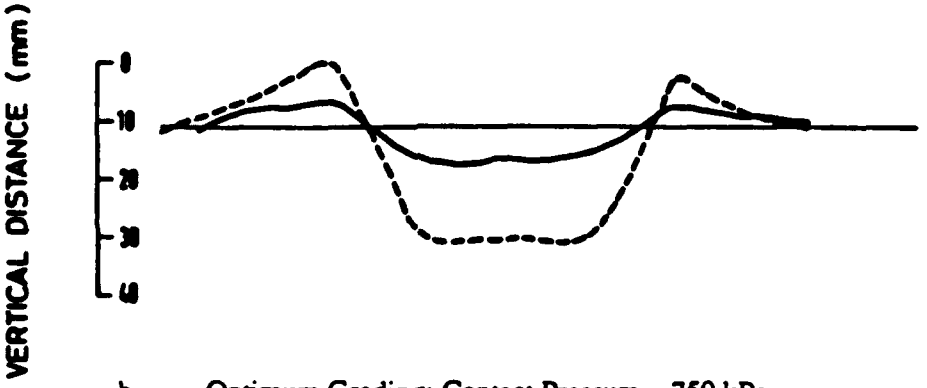

b. Optimum Grading; Contact Pressure = 750 kPa.

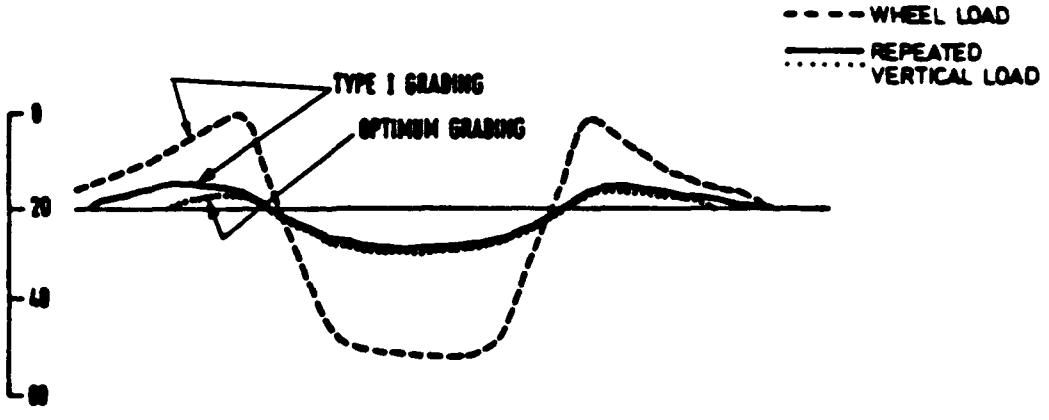

c. Contact Pressure = 1100 kPa.

Figure 13. Section Profiles at the End of the Rutting Tests carried out in the Slab Test Facility.

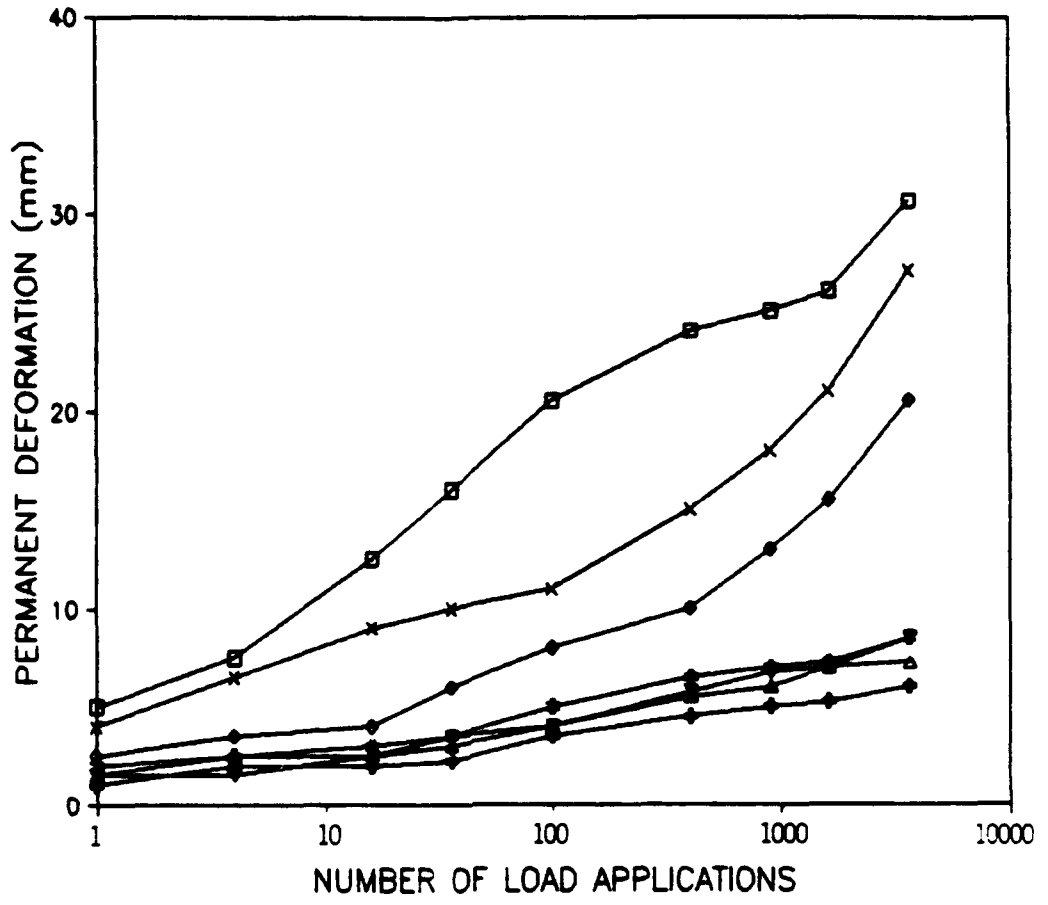

Symbol	Grading of Granular Base	Type of Loading	Contact Pressure (kPa)
	Type I	Wheel	750
	Type I	Repeated Plate	750
	Type I	Wheel	1100
	Type I	Repeated Plate	1100
	Optimum	Wheel	750
	Optimum	Repeated Plate	750
	Optimum	Repeated Plate	1100

Figure 14. Variation of Permanent Vertical Deformation with Number of Load Applications for the Rutting Tests carried out in the Slab Test Facility.

reversed shear stresses caused by the moving wheel and the lack of confining pressure at the surface of the granular material. The combined effect caused the material immediately in front of the wheel to dilate and weaken, and when the wheel moved over the weakened material, large deformation occurred. In the case of the repeated vertical load, the wheel contacts the pavement over a fixed area, effectively providing the confining pressure required for higher strength. This may account for the observation that the permanent deformation was not sensitive to the applied stress level.

2 Pavement Test Facility Experiments

Figures 15 and 16 show the results of the two series of tests carried out in the PTF. The profiles shown in Figure 15 indicate that in the two sections where dolomitic limestone was used, bidirectional loading caused 18 and 60 percent higher rut than those under unidirectional loading. However, the opposite effect was obtained for the section with an open-graded carboniferous limestone, where much higher deformation developed under both types of loading. The overall high deformation in these sections, which were generally less well compacted, might override any trend in the development of permanent deformation caused by the different modes of loading.

If the results from the carboniferous limestone sections can be discarded, then the tests from the PTF indicate that higher permanent deformation may be obtained from bidirectional than unidirectional wheel loading. The results apparently agreed with those obtained by Brown et al (23) who observed an increase of rut depth of 19 to 40 percent due to bidirectional loading. In bidirectional loading, the structure of the granular material, which is basically formed by the interparticle contacts, may be subjected to more disruption from the two opposite senses of reversed shear stress. As a results, the structure will be weakened and more deformation will occur. Again, the optimum graded dolomitic limestone was found to have less permanent vertical deformation.

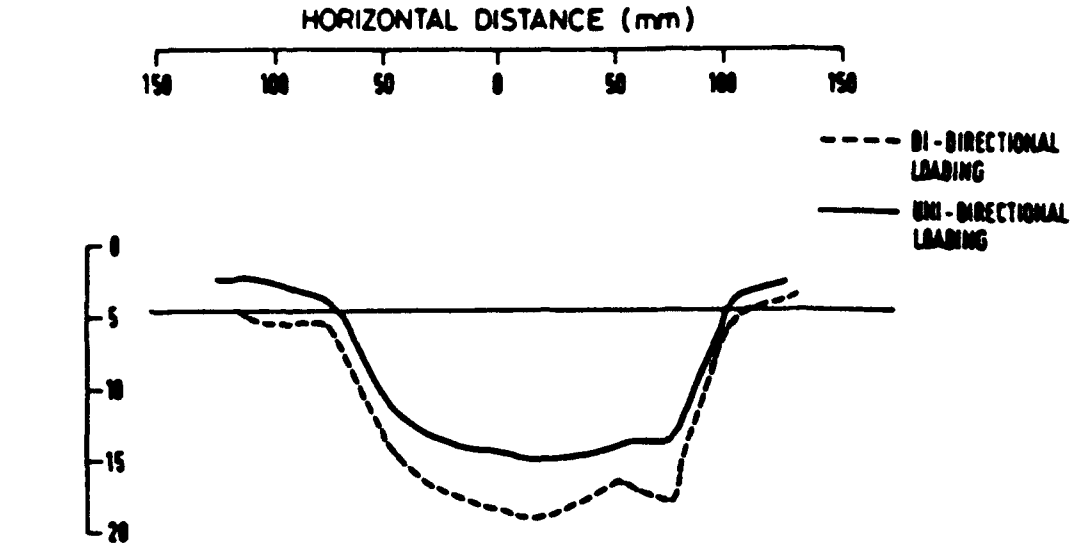

a. Type I Grading; Dolomitic Limestone.

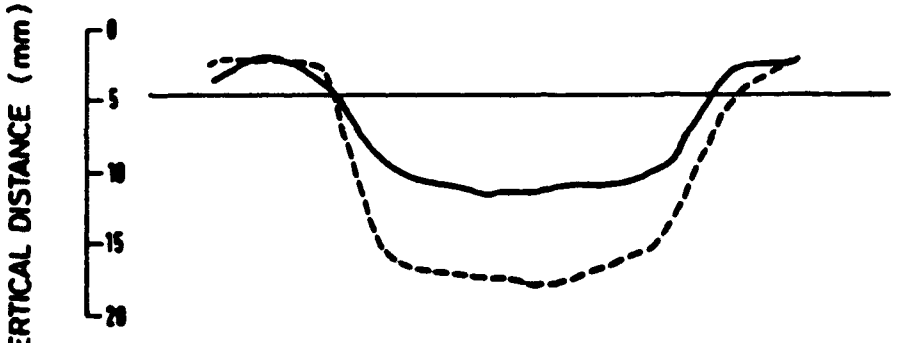

b. Optimum Grading; Dolomitic Limestone.

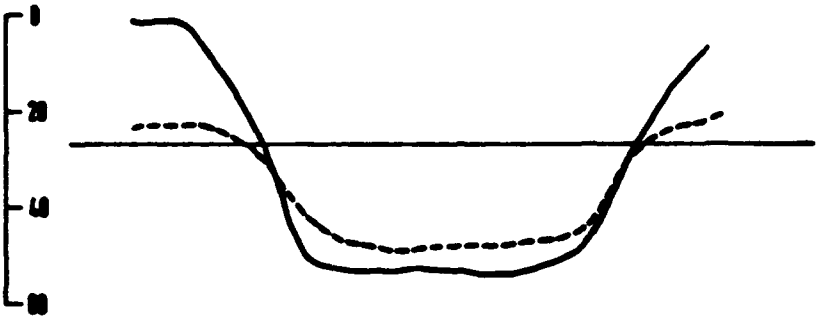

c. Open Grading; Carboniferous Limestone.

Figure 15. Section Profiles at the End of the Rutting Tests carried out in Pavement Test Facility.

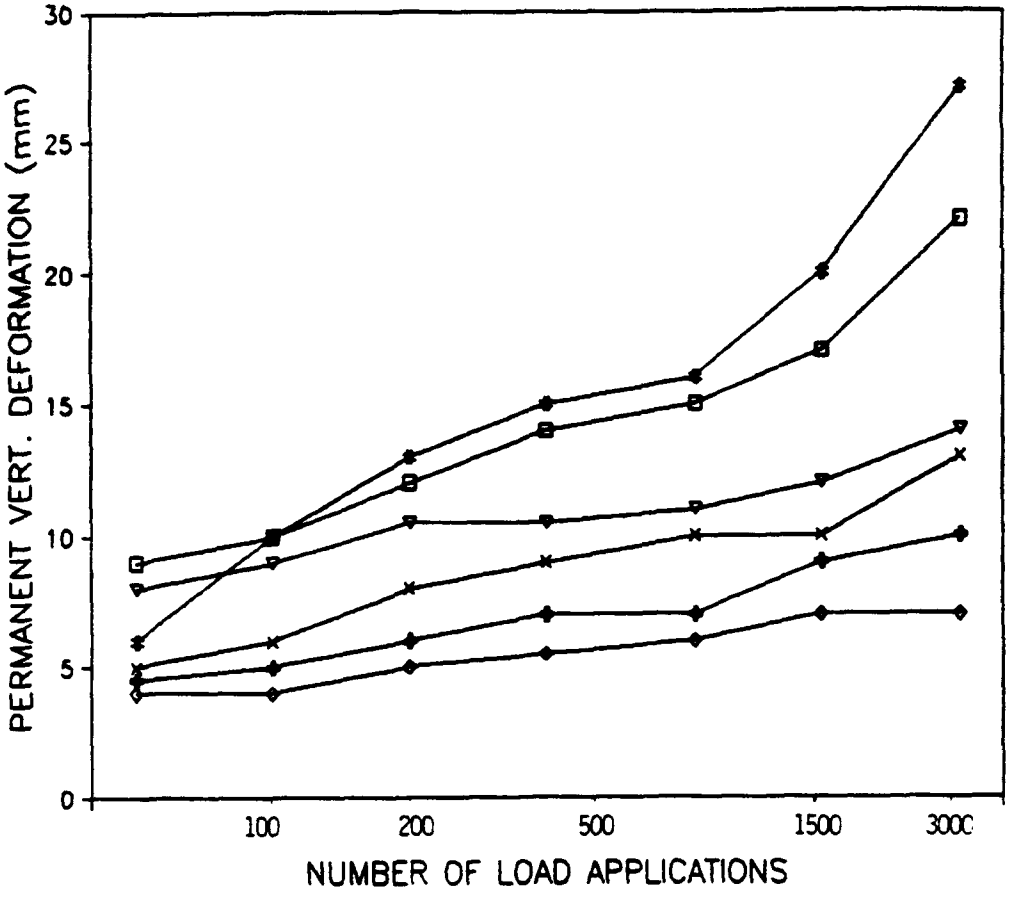

Symbol	Type of Granular Base	Grading of Granular Base	Type of Loading
	Dolomitic Limestone	Type I	Uni-directional
	Dolomitic Limestone	Type I	Bi-directional
	Dolomitic Limestone	Optimum	Uni-directional
	Dolomitic Limestone	Optimum	Bi-directional
	Carboniferous Limestone	Open	Uni-directional
	Carboniferous Limestone	Open	Bi-directional

Figure 16. Variation of Permanent Vertical Deformation with Number of Passes of Wheel Load for the Rutting Tests carried out in Pavement Test Facility.

SECTION IV

repeated-load HOLLOW CYLINDER TESTS

A. INTRODUCTION

The last section has shown that full-scale pavement testing is an essential component of road pavement research. However, because of the large amount of raw materials, instrumentation and human effort involved in each test, this type of experiment may only be cost-effective for the investigation or validation of an idea which has been shown to have potential. For background research or study of more fundamental principles, smaller scale accelerated testing on elements of material is clearly more desirable. In the study of granular material behavior in pavements, the repeated-load hollow cylinder test apparatus (HCA) appears to be a promising device. Its capability to apply reversed shear stresses to the test specimen has meant that realistic in situ stress conditions caused by a moving wheel loading can be simulated. The importance of close and correct simulation of this condition has already been highlighted by the results presented in Section III. Furthermore, studies of material anisotropy, principal stress rotation effects and the influence of different intermediate principal stresses are made possible using the HCA.

B. NOTTINGHAM REPEATED-LOAD HOLLOW CYLINDER TEST APPARATUS

The Nottingham HCA was first constructed in 1985 and the history of its development was reported by O'Reilly (24). Since then, some modifications have been performed.The basic configuration of the HCA is shown in Figure 17. For this project, further improvement modifications were made. These included:

1. Addition of an external pressure chamber and the associated pressurising system.

2. Redesign of the top cap and base to accommodate the new pressure chamber.

3. Upgrading of the electronic controls for the loading system.

4. Addition of a new data acquisition system.

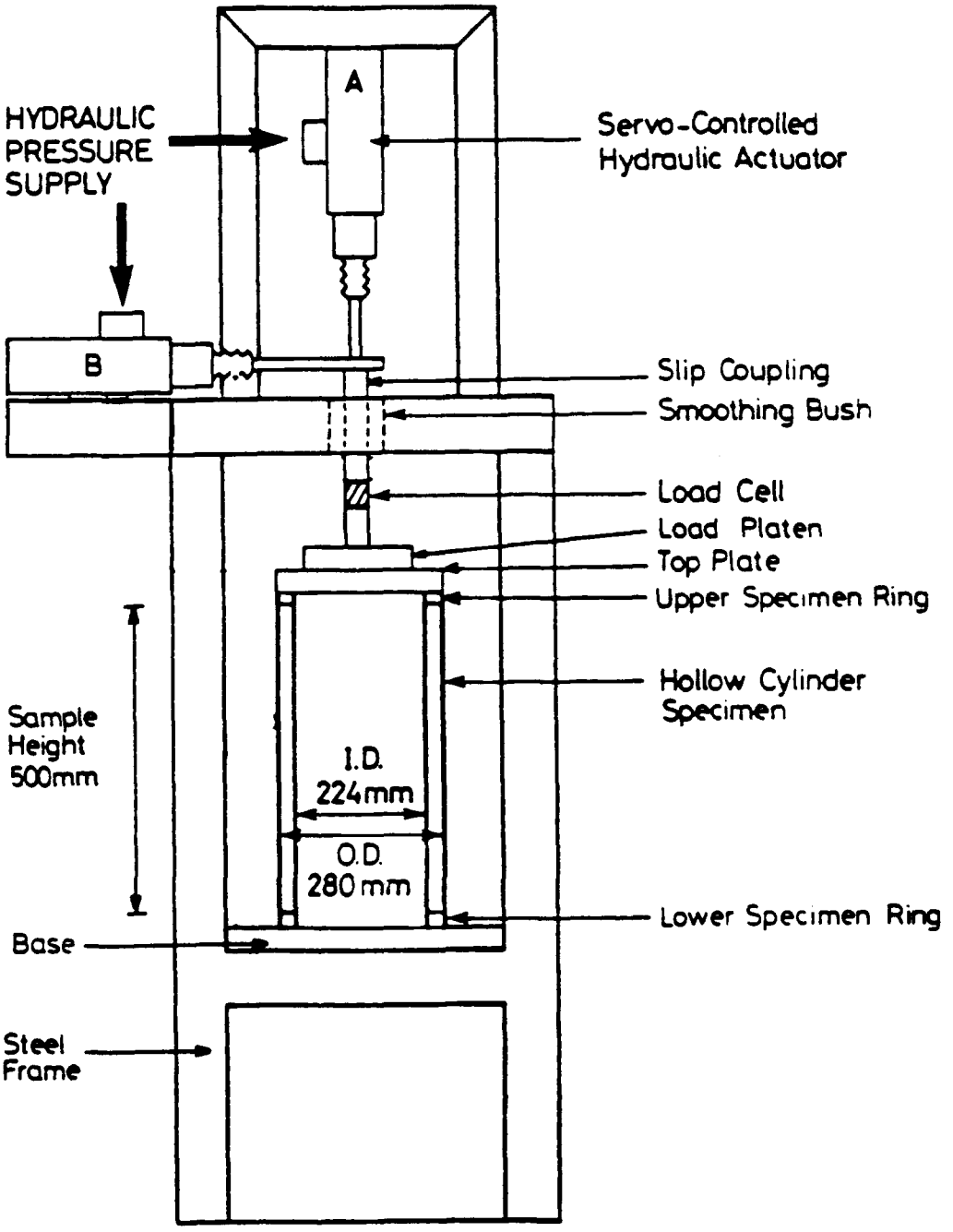

Figure 17. Basic Configuration of the Nottingham Repeated-Load Hollow Cylinder Apparatus.

A photograph of the laboratory setup of the modified apparatus is shown in Figure 18 and a flow diagram showing the interconnections between the various components of the system is presented in Figure 19.

1. Size of Test Apparatus and Specimen

The designed dimensions of the repeated-load HCA are mainly influenced by the size of the test specimen. One of the main inherent disadvantages of using a hollow cylinder specimen is the nonuniformity of stress and strain across the specimen wall due to curvature. Furthermore, because of the need to transfer shear stresses from the loading system to the specimen, a more severe end restraint effect normally results when compared with the triaxial tests. In order to reduce stress nonuniformity caused by specimen curvature, it is necessary to increase the external diameter and reduce the wall thickness of the specimen. As a result of these considerations, an external diameter of 280 mm and a wall thickness of 28 mm were adopted for the Nottingham hollow cylinder specimen. This produces a ratio of external diameter to wall thickness of 10, a value which finite-element calculations (25) showed to be satisfactory.

In determining the height of the specimen, both the presence of end restraints and the need to provide a sufficiently long gauge length for deformation measurements were considered. A study carried out by Wright et al (26) proposed that the height of the specimen should satisfy the following equation:-

$$H \geq 5.44 \sqrt{(b^2 - a^2)} \qquad (10)$$

where H is the height of hollow cylinder specimen
b is the external radius
a is the internal radius

Using this equation, a minimum height of 457 mm is required. Based on this criterion and other practical considerations, such as weight of the specimen and the dimensions of the loading frame, a height for the Nottingham hollow cylinder specimen of 500 mm was used.

2. Loading System

Both the vertical and torsional loads are applied by servo-controlled hydraulic actuators as shown in Figure 20. The vertically mounted actuator can provide a maximum load on

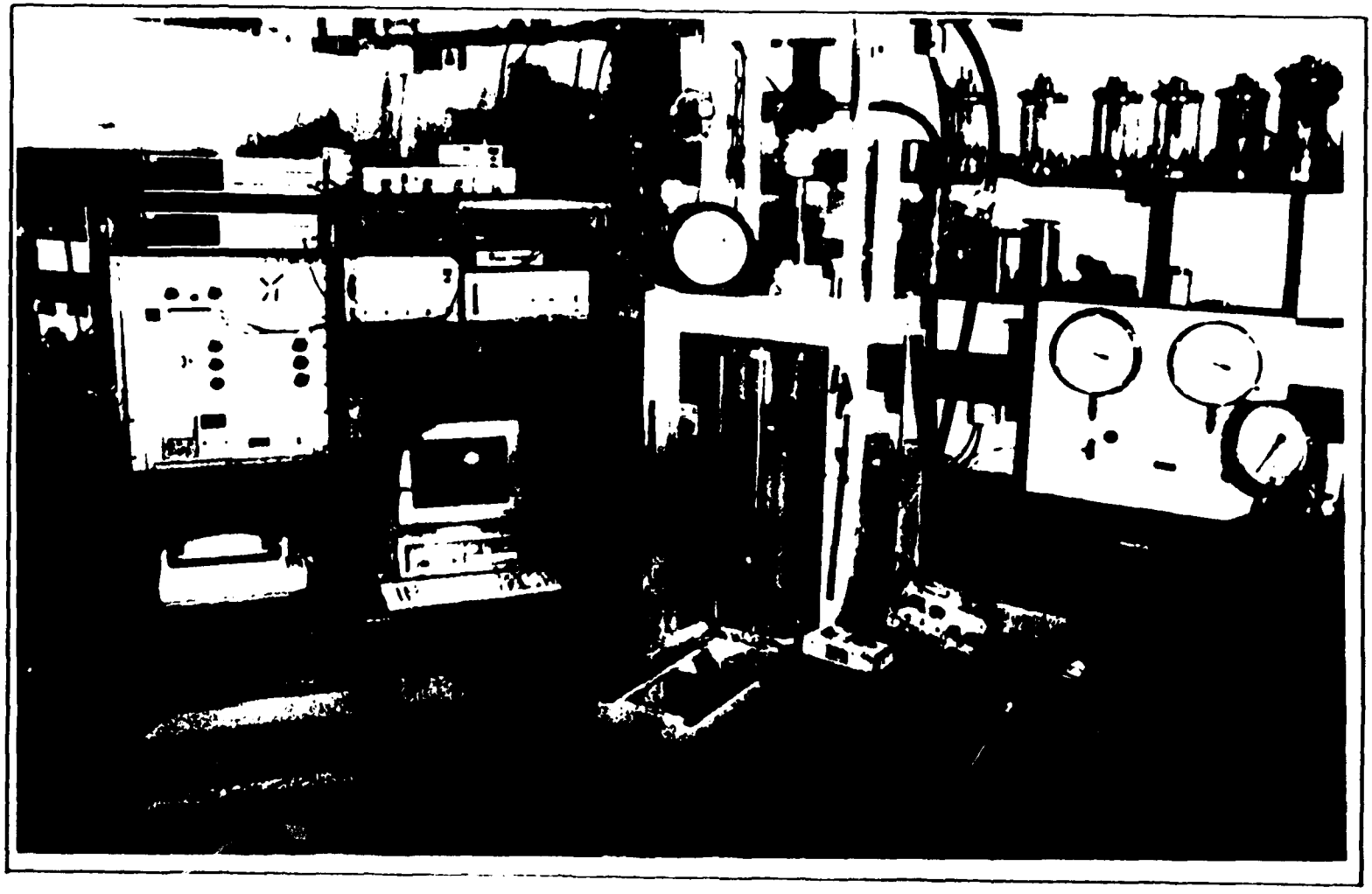

Figure 18. Laboratory Set-up of the Modified Nottingham Repeated-Load Hollow Cylinder Apparatus.

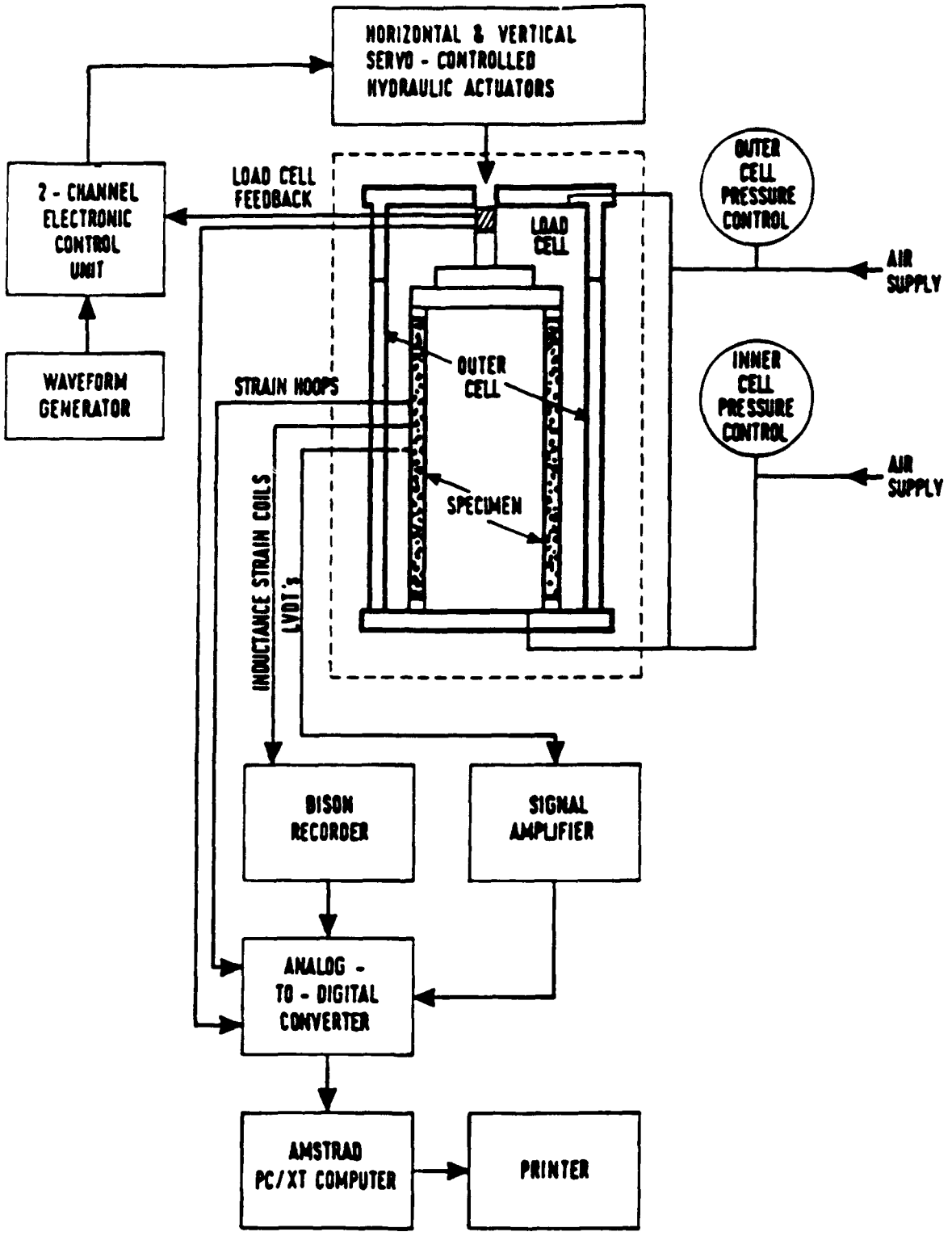

Figure 19. Inter-Relationship Between Different Components of the Repeated-Load Hollow Cylinder Test Apparatus.

Figure 20. Vertical and Horizontal Servo-controlled Hydraulic Actuators and Slip Coupling of the Repeated Load Hollow Cylinder Apparatus.

the specimen of 20 kN with a 150 mm stroke. The horizontally mounted actuator, with its stroke of 100 mm, can provide a torsional moment of up to 4.6 kNm to the centre shaft through the 230 mm long torque arm. A slip coupling device allows both the axial load and torque to be applied down the same shaft. It also enables both loads to be measured by a simple purpose-made, combined strain-gauged load cell (Figure 21) which is located immediately above the specimen. The axial load is transferred to the specimen via the top platen and the upper specimen ring. For the transfer of shear load, six shear vanes located at the bottom of the upper specimen ring and 16 interlocking castellations at the lower specimen ring (Figure 22) were used.

To carry out repeated loading, a waveform generator, capable of providing sinusoidal, square or triangular waveforms at frequencies between 0.001 and 100 Hz for two channels at variable phase angles shift was used. The command signal from the waveform generator is fed into the electronic control unit where it is compared with the feedback signal obtained from the load cell. An error signal is then sent to the two servo-valves so that they may make the necessary adjustments. The time required by this feedback closed loop control is generally very short, in the order of milliseconds, and can be adjusted by means of the gain setting to suit different test materials.

Confining pressure can be applied through the medium of silicone oil or compressed air in both the inner and outer cell chambers. The former medium is more desirable in repeated loading situations (due to the quicker response caused by the incompressibility of the fluid) while for constant pressures, the use of compressed air is found to be satisfactory. Maximum pressure of up to 400 kPa can be achieved for both the inner and outer cells. Both pressures can be controlled simultaneously by a single valve, hence allowing an isotropic condition during the pressure build up. Alternatively, pressures for the inner and outer cell can be controlled individually to allow pressure differences across the specimen wall. These pressures are monitored by pressure gauges located outside the HCA.

3 Sealing System

To maintain a good hollow cylindrical shape for the specimen of granular material during sample preparation and testing, a tight seal condition must be achieved. Furthermore, if different inner and outer cell pressures are to be used, a good sealing system becomes even more essential.

A section of the HCA with the specimen showing all the major sealing units is presented in Figure 23. The hollow cylinder specimen is basically enclosed by two 0.635 mm

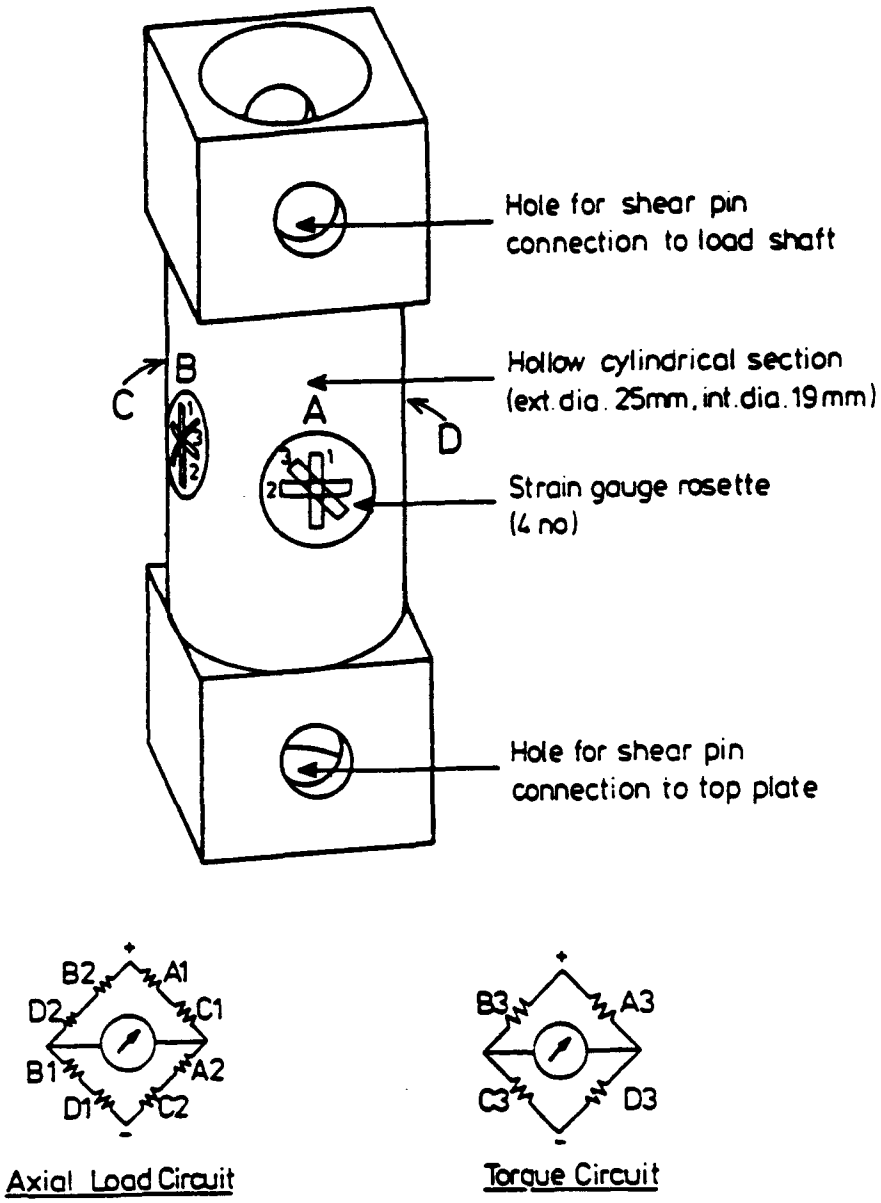

Figure 21. Combined Axial and Torsional Load Cell for the Repeated-Load Hollow Cylinder Test Apparatus.

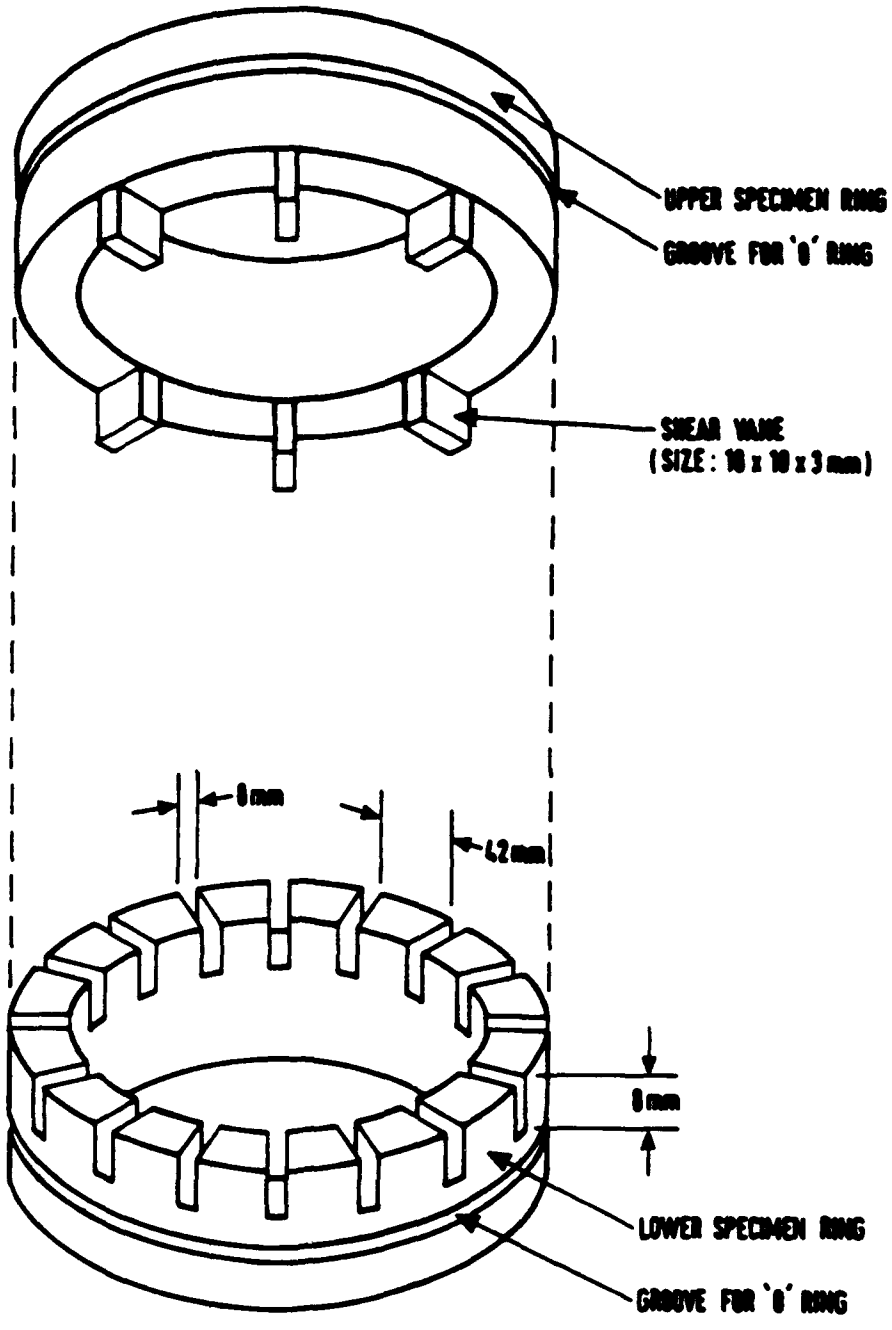

Figure 22. Details of Upper and Lower Specimen Rings for the Repeated-Load Hollow Cylinder Test Apparatus.

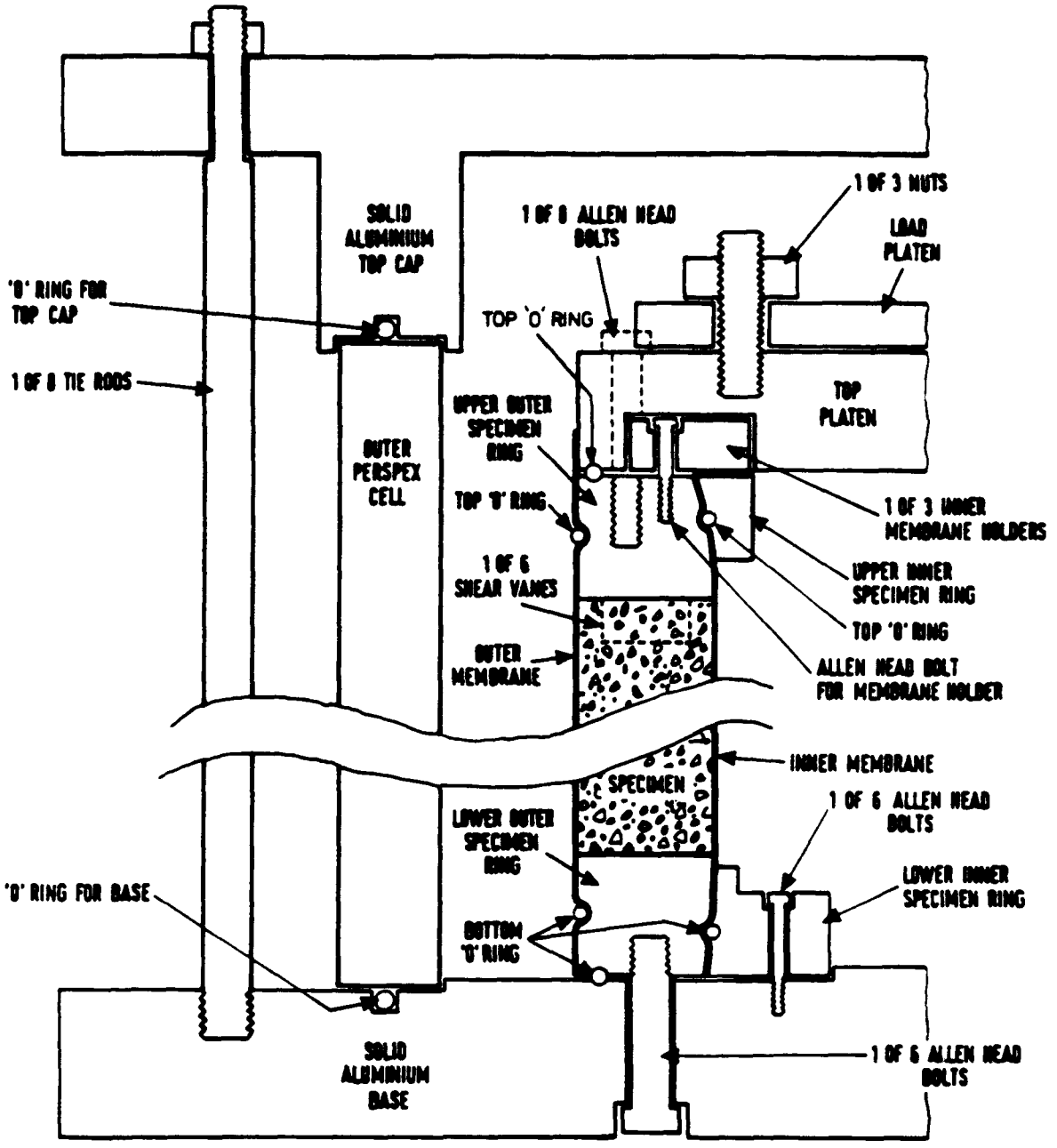

Figure 23. Details of Major Sealing Units for the Repeated-Load Hollow Cylinder Test Apparatus.

thick cylindrical latex membranes with different diameters (280 and 224 mm) and two pairs of specimen rings (upper and lower). The lower inner specimen ring, with its built-in rubber "O" ring is fastened to the base with six 3 mm diameter Allen head bolts. After the inner membrane is placed over this ring, the lower outer ring on which the specimen is made, slides in , trapping the inner membrane between the two tapered surfaces of the rings. The lower outer specimen ring is then fastened onto the base by six 8 mm Allen head bolts from the bottom of the base upward. A further "O" ring located at the bottom of this specimen ring provides a seal between the inner and outer pressure chambers. The outer membrane is simply secured by another "O" ring along the outside of the specimen ring.

A similar sealing method is adopted at the top of the specimen where the inner membrane is trapped between the tapered surfaces of the upper specimen rings. However, in order to tighten the two rings together, three membrane holder blocks with 3 mm Allen head bolts are used. After the outer membrane is secured by an "O" ring the top platen is placed and fastened with 8 mm Allen head bolts to the upper outer specimen ring which contains an "O" ring around the edge of its top face.

The outside pressure chamber consists of a hollow cylindrical perspex cell with 385 mm outside diameter and a wall thickness of 20 mm, a top cap and a base cast out of hard anodized aluminium. The three units are held together by eight 15 mm diameter tie rods. A thick rubber "O" ring is provided at each of the joints between the cell, cap and base. Two rubber seals are provided at the centre hole of the cap through which the driving shaft transfers the loads from the servo-rams to the specimen. Outside electrical, vacuum and pressure connections are made through holes provided in the cap and base. Each of these holes within the pressurised chamber are individually sealed with expansion "O" rings.

4. Deformation Measurements

Four independent deformation measurements are required to determine the complete strain pattern. These are the change in specimen wall thickness, the overall change in sample diameter, the axial deformation and the torsional deformation.

To measure the change in specimen wall thickness or the radial deformation, two pairs of 25 mm inductance coils attached to opposite sides of the specimen wall are used. A known alternating current flows in one coil and the current induced in the other, which is a function of their distance of separation, is recorded. Changes in specimen diameter are measured using two strain-gauged epoxy hoops attached to the inner chamber of the hollow cylinder

specimen using embedded studs. These devices, as shown in Figure 24, have been used extensively at Nottingham (27).

Axial deformation is measured by two LVDTs mounted vertically on the specimen by means of embedded studs. Deformation in a direction at 45 degrees to the vertical is also measured by means of LVDTs. This latter measurement, together with those from the axial and circumferential directions are used in the following equation to calculate the torsional deformation. A photograph of the arrangement of the instruments is shown in Figure 25.

$$\gamma = 2\varepsilon_{45} - \varepsilon_z - \varepsilon_\theta \qquad (11)$$

where γ = engineering shear strain
ε_{45} = normal strain at 45 degrees to vertical direction
ε_z = axial strain
ε_θ = circumferential strain

All the instrumentations were located at the middle one third of the specimen to minimize the end effects. Calibrations of the instrumentation were carried out regularly during the project. A description of the calibration methods, procedure used and results obtained are presented in Appendix B.

5. Data Acquisition System

The data acquisition system for this project consists basically of the following four components:-

a. A microcomputer with a single disk drive, a 20 Mb hard disk, an expanded 640 kb RAM (Random Access Memory), a colour monitor and option slots that support feature cards for additional devices.

b. An analogue-to-digital convertor with eight differential input channels, four output channels and four relays. The A/D conversion time is approximately 1.8 ms and up to 2048 readings can be stored at each execution.

c. An IEEE 488 interface card which organizes and manages information flow between 1 and 2.

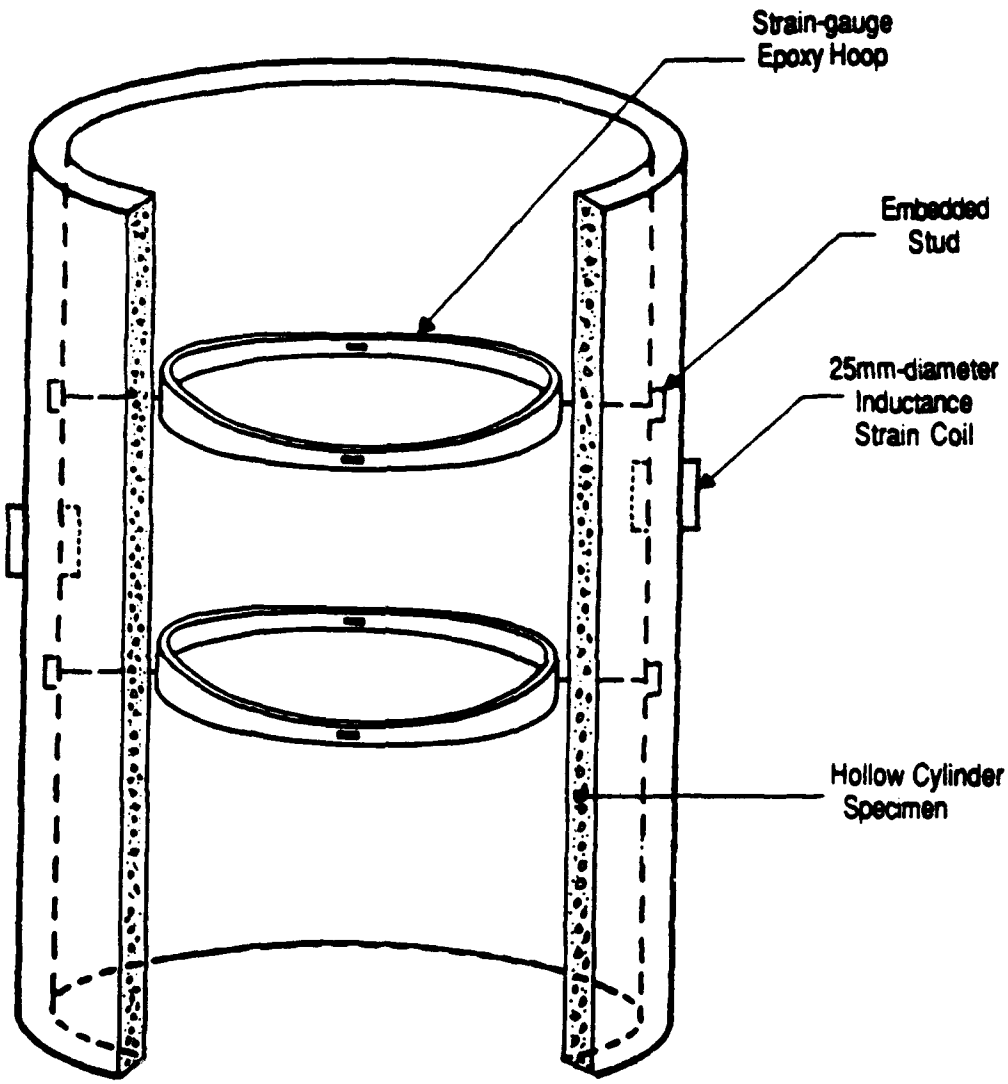

Figure 24. Strain -gauged Epoxy Hoops and 25mm-diameter Inductance Strain Coils mounted on the Hollow Cylinder Apparatus.

Figure 25. Arrangement of Vertical and 45-degree oriented LVDTs.

d. A line printer which provides hard copies of graphics and text.

Several soft ware programs have been developed to retrieve, store and analyze the data from the load cells, strain gauged hoops, inductance strain coils and LVDTs. Some of these programs use existing packages for plotting and managing of data. The main program for the data acquisition of the repeated-load HCA tests is called HCA. Details of this program, written in BASIC language are shown in Appendix C.

C. STRESS CONDITIONS IN A HOLLOW CYLINDER

Figure 26 shows a hollow cylinder sample under the action of axial load W, torque M_T, internal pressure p_i and external pressure p_o. Despite the use of a high ratio of external diameter to wall thickness and a tall specimen, stress non-uniformity cannot be completely eliminated. Therefore, it is necessary to assume that the stresses are uniform and hence allowing their average values to be defined. The stresses acting on an element of material along the wall of the hollow cylinder, shown in Figure 26, are defined as follows:-

$$\sigma_z = \frac{W}{\pi (b^2 - a^2)} + \frac{(p_o b^2 - p_i a^2)}{(b^2 - a^2)} \tag{12}$$

$$\sigma_r = \frac{(p_o b + p_i a)}{(b + a)} \tag{13}$$

$$\sigma_\theta = \frac{(p_o b - p_i a)}{(b - a)} \tag{14}$$

$$\tau_{\theta z} = \frac{3M_T}{2\pi (b^3 - a^3)} \tag{15}$$

where σ_z = average vertical stress

σ_r = average radial stress

σ_θ = average circumferential stress

$\tau_{\theta z}$ = average shear stress in the θ-z plane

a, b = internal and external radius of the specimen

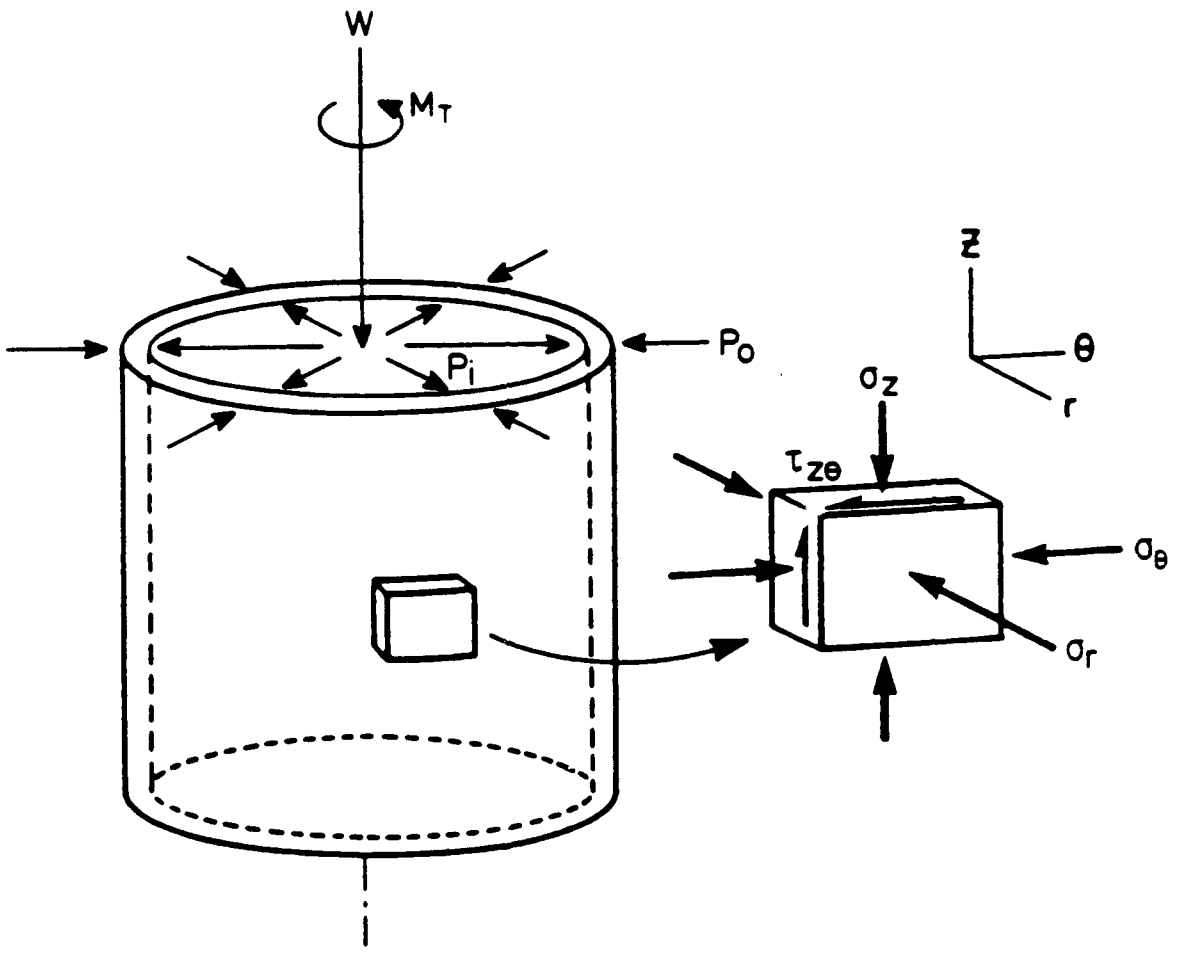

Figure 26. Loads and Stresses on a Hollow Cylinder.

Since there are no shear stresses acting in the radial direction of the hollow cylinder specimen, σ_r and the plane on which it acts (Figure 26) must be a principal stress and a principal plane, respectively. The directions on which the other two principal stresses act must then be normal to that of σ_r (ie. in the z-θ plane). The exact directions of these latter principal stresses which, again, must be normal to each other depend on the magnitude of the shear stresses acting on the z-θ plane and can be easily obtained by means of the Mohr's circle for stress (28).

Figure 27 illustrates the construction of a Mohr circle based on the condition that $\sigma_z > \sigma_\theta$ and $\tau_{\theta z}$ is positive and shows that the same condition can be represented by the two principal stresses and an angle of rotation α. Based on Figure 27, the following equations for the principal stresses and the angle of principal stress rotation can be established:-

$$\sigma_1 = \frac{\sigma_z + \sigma_\theta}{2} + \sqrt{\left(\frac{\sigma_z - \sigma_\theta}{2}\right)^2 + \tau_{\theta z}^2} \tag{15}$$

$$\sigma_2 = \sigma_r \tag{16}$$

$$\sigma_3 = \frac{\sigma_z + \sigma_\theta}{2} - \sqrt{\left(\frac{\sigma_z - \sigma_\theta}{2}\right)^2 + \tau_{\theta z}^2} \tag{17}$$

$$\alpha = \tan^{-1}\left(\frac{\tau_{\theta z}}{(\sigma_1 - \sigma_\theta)}\right) \tag{18}$$

Note that equations (15) to (18) are only true under the following conditions:-

1. $p_i \geq p_o$ (19)

2. $p_i - p_o \leq \frac{W}{\pi ab}$ (20)

Where W, P_i, P_o, a and b are as defined earlier.

The stress conditions in a hollow cylinder sample can also be expressed in the form of stress invariants such as the octahedral normal and octahedral shear stress. In terms of principal stresses, they are defined by:-

$$\sigma_{oct} = \frac{1}{3}(\sigma_1 + \sigma_2 + \sigma_3) \tag{21}$$

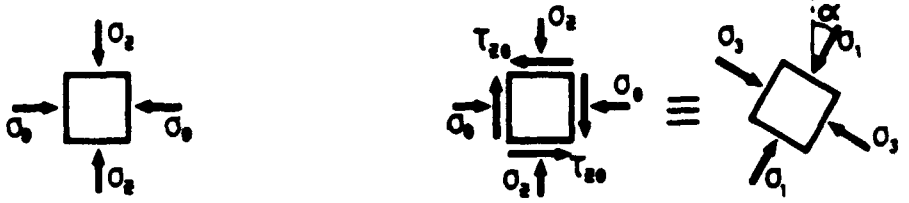

a. Condition with No Shear.

b. Condition with Shear.

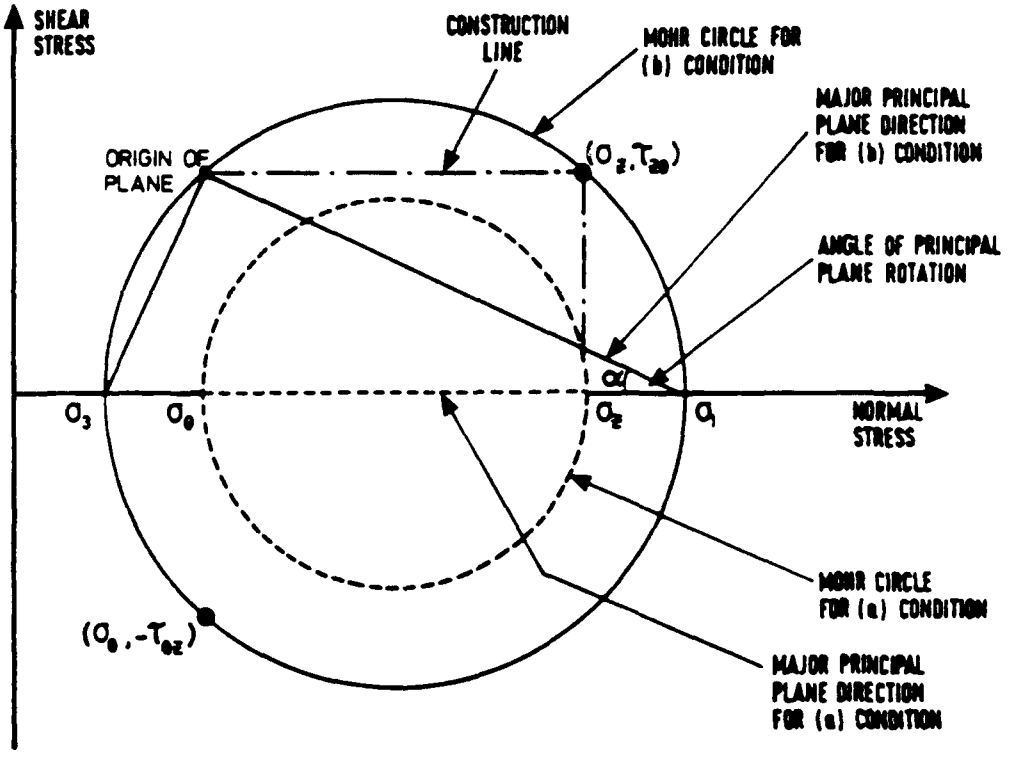

c. Mohr Circle showing Principal Plane Rotation.

Figure 27. Mohr Circle for Stress.

$$q_{oct} = \frac{1}{\sqrt{2}} \left[(\sigma_1 - \sigma_2)^2 + (\sigma_2 - \sigma_3)^2 + (\sigma_3 - \sigma_1)^2 \right]^{1/2} \quad (22)$$

Note that

$$p = \sigma_{oct} \quad (23)$$

According to Figure 27 and Equations (15) to (18), the rotation of principal planes in the hollow cylinder specimen can only occur within the σ_1 and σ_3 planes. Therefore, it appears to be possible to use the shear invariant q whenever shear stresses in the σ_1-σ_3 plane are considered. q is defined by:-

$$q = (\sigma_1 - \sigma_3) \quad (24)$$

However, in order to investigate the influence due to the intermediate principal stress, σ_2, it is also necessary to use the parameter, b, which is defined as:-

$$b = \frac{(\sigma_2 - \sigma_3)}{(\sigma_1 - \sigma_3)} \quad (25)$$

The parameter, b, can only be either 0 or 1 in triaxial test conditions. However, in a hollow cylinder test, this parameter can be varied continuously from 0 to 1.

D. STRAIN IN A HOLLOW CYLINDER

For the same reasons discussed for stress in a hollow cylinder, assumptions about the uniformity of strains have to be made. The average strains for a hollow cylinder are defined as follows:-

$$\varepsilon_z = \frac{\delta l}{L} \quad (26)$$

$$\varepsilon_\theta = \frac{\delta d}{(a + b)} \quad (27)$$

$$\varepsilon_r = \frac{\delta t}{(b - a)} \quad (28)$$

where ε_z, ε_θ and ε_r are the average axial, circumferential and radial strains respectively

δl = change in vertical displacement over the gauge length L

δd = Change in specimen diameter

δt = Change in thickness of specimen wall

a, b = interior and exterior radius of the specimen respectively

The shear strains in the z-θ plane can be deduced from the Mohr circle for strain if ε_z, ε_θ and the normal strain at a known direction within the plane can be obtained. A convenient method is to measure the strain at 45 degrees to the vertical axis. The Mohr circle to determine the shear strains is shown in Figure 28. It can be graphically shown that:-

$$\varepsilon_{z\theta} = \varepsilon_{45} - \frac{1}{2}(\varepsilon_\theta + \varepsilon_z) \tag{29}$$

where $\varepsilon_{z\theta}$ is the pure shear strain on the plane at an angle α_ϵ from the vertical

ε_{45} is the normal strain at 45 degrees to the vertical and

α_ϵ is the rotation of the major principal strain plane

Figure 28 also shows that:-

$$\varepsilon_1 = \frac{\varepsilon_z + \varepsilon_\theta}{2} + \sqrt{\left(\frac{(\varepsilon_z - \varepsilon_\theta)}{2}\right)^2 + \varepsilon_{z\theta}^2} \tag{30}$$

$$\varepsilon_3 = \frac{\varepsilon_z + \varepsilon_\theta}{2} - \sqrt{\left(\frac{(\varepsilon_z - \varepsilon_\theta)}{2}\right)^2 + \varepsilon_{z\theta}^2} \tag{31}$$

$$\alpha_\epsilon = \tan^{-1}\left(\frac{\varepsilon_{z\theta}}{\varepsilon_1 - \varepsilon_\theta}\right) \tag{32}$$

where ε_1 and ε_3 are the major and minor principal strains in the θ-z plane respectively.

Because there is no shear stress acting on the z-r and r-θ directions, it can be assumed that the shear strains ε_{rz} and $\varepsilon_{r\theta}$ are zero. Hence ε_r becomes the third principal strain and, in theory:-

$$\varepsilon_r = \varepsilon_2 \tag{33}$$

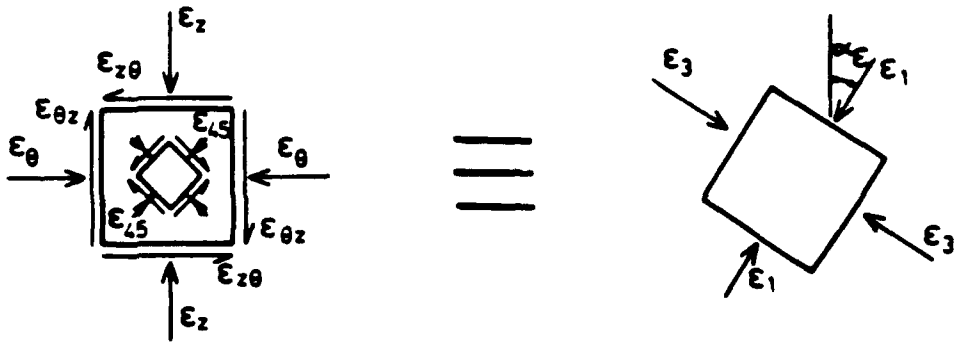

a. General Strains.

b. Principal Strains and Angle of Rotation.

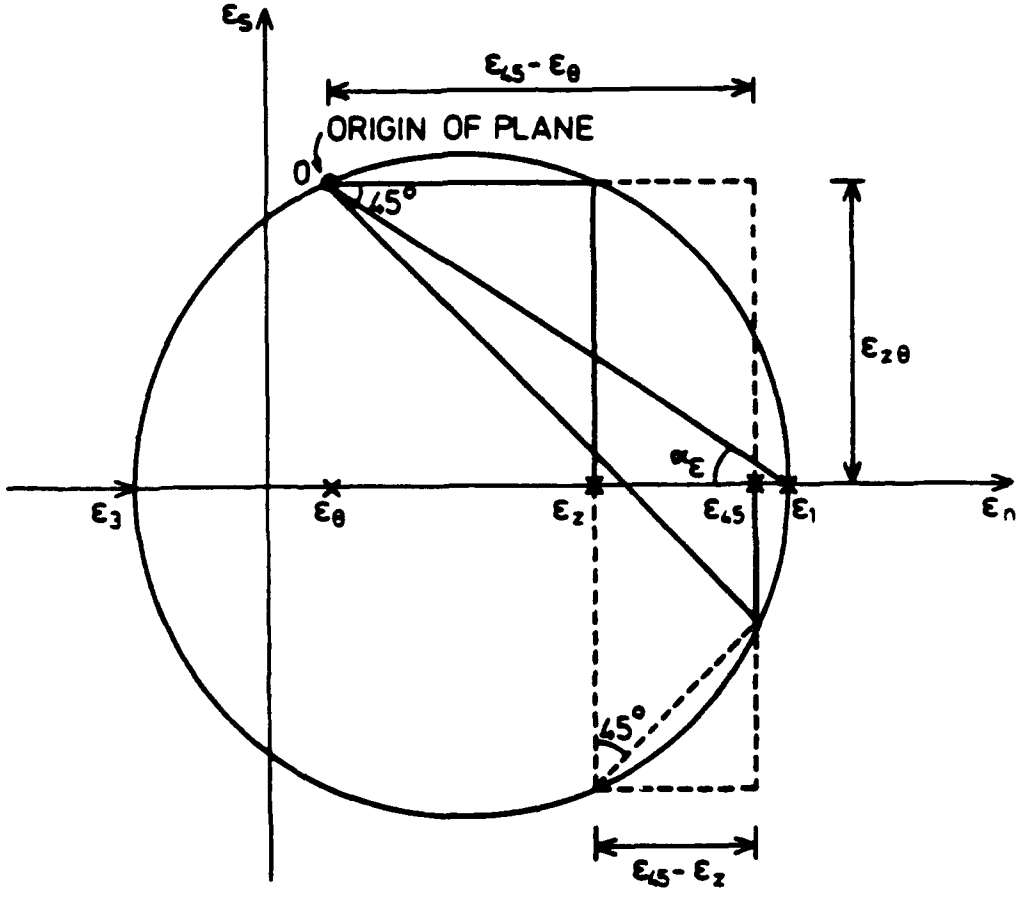

c. Mohr Circle Construction for Strain.

Figure 28. Mohr Circle for Strain

The maximum shear strain in the z-θ plane is defined as ε_{max} where:-

$$\varepsilon_{max} = \frac{1}{2}(\varepsilon_1 - \varepsilon_3) \tag{34}$$

The state of strain in the specimen can also be represented by strain invariants. However, the invariants should be selected such that they correspond to those used for stresses. The strain invariant for q (Equation (24)) is ε_{max} defined in equation 34. The invariants for p and q_{oct} (Equation (22)) are ε_v and ε_s, respectively, and they are defined as:-

$$\varepsilon_v = \varepsilon_1 + \varepsilon_2 + \varepsilon_3 \tag{35}$$

$$\varepsilon_s = \frac{\sqrt{2}}{3}\left[(\varepsilon_1 - \varepsilon_2)^2 + (\varepsilon_2 - \varepsilon_3)^2 + (\varepsilon_3 - \varepsilon_1)^2\right]^{1/2} \tag{36}$$

E. SPECIMEN PREPARATION

When carrying out destructive tests, such as those for the investigation of permanent deformation characteristics of granular material, the importance of using "identical" specimens is overwhelming. Therefore, a specimen preparation technique which is repeatable and capable of producing specimens with the same properties is needed. For the repeated-load hollow cylinder tests, a new method, based on the British Standard vibrating hammer test (BS5835) was developed. A sketch showing the basic principal of the method is presented in Figure 29.

To make a hollow cylindrical specimen, an inner and an outer mold are required. The inner mold consists of three articulated sections which can be extended and locked in its cylindrical shape by two internal connections. The outer mold is essentially a thin walled cylinder which is divided into three equal sections and held together by three Jubilee clips. Both molds rest under their own weight on top of the base which is placed on top of a vibrating table. Three spacers are used at the top of the mold to ensure that the required uniform wall thickness is achieved.

Two pieces of membranes are also required. The inner membrane fits the outside of the inner mold tightly, thereby forming the required cylindrical shape. A vacuum should be used at six locations to hold the outer membrane firmly against the inside of the outer mold.

The sample was built up in approximately seven layers with each consisting of three kilograms of dry material. After the material had been poured and evenly spread, an aluminium

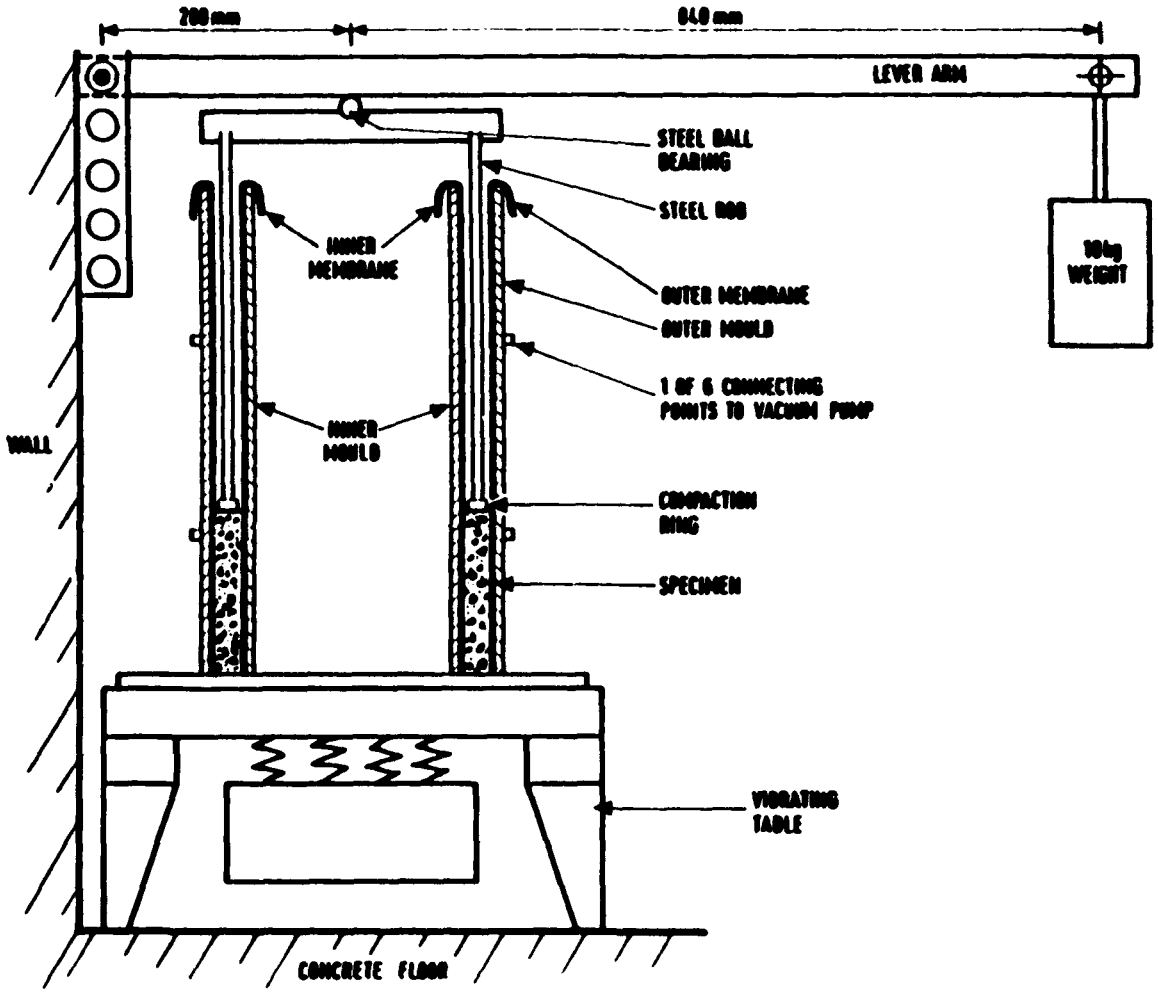

Figure 29. Details of Compaction Device for Hollow Cylinder Specimen.

compaction ring was placed on top. A surcharge load of approximately 40 kg was imposed on the ring through a lever system. While the surcharge is acting, 120 seconds of vibration, at 50 Hz frequency, were applied. The amplitude of vibration was allowed to decrease gradually from its maximum value to 0 during the last 30 seconds.

After each layer had been compacted, the vertical distance between the surface of the compacted material to the top of the mold was measured at eight locations. These measurements allowed calculation of the average thickness, and the density of each layer.

After the specimen was completely built and sealed (see Figure 23) an internal vacuum was applied prior to release of the molds. The inner mold was folded inward and removed while the outer mold was released simply by unfastening the Jubilee clips. A plan view of these molds during and after specimen construction is shown in Figure 30. Installation of the instrumentation followed, then the outer pressure chamber was placed and the top cap was fastened.

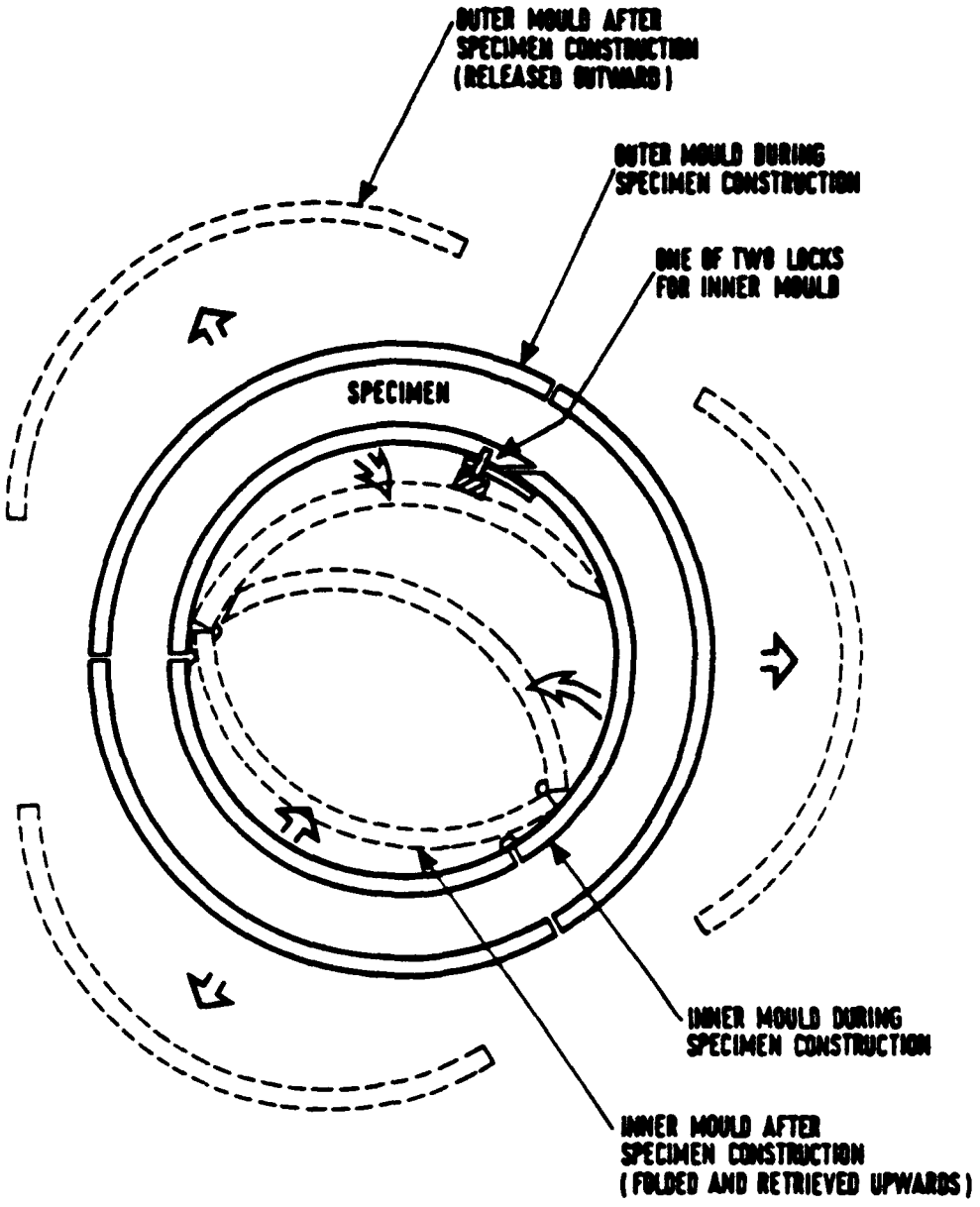

Figure 30. Plan View of Compaction Molds for Hollow Cylinder Specimen during and after Compaction.

SECTION V

TEST PROGRAM FOR REPEATED-LOAD HOLLOW CYLINDER TESTS

A. INTRODUCTION

One of the main objectives of carrying out repeated-load hollow cylinder tests for this project was to study the effect of reversed shear stresses on the permanent deformation behavior of granular material. For this part of the study, emphasis was placed on the difference between the with-shear and without-shear (or simply the triaxial) conditions. The tests also examined the difference in behavior under the laboratory simulated condition involving unidirectional and bidirectional shear reversal.

The test program also included tests to determine the resilient stress-strain behavior of the granular material concerned. An understanding of this behavior under the new stress regime available from the HCA is also essential as the stiffness of the material will affect the load spreading capability of the granular material.

Comparison of the behavior of granular material tested in the repeated-load HCA under triaxial conditions and that tested in the repeated-load triaxial test apparatus is also warranted. This comparison can be viewed as a means to "calibrate" both test devices, thereby, new interpretations may be made of the large amount of existing results from the repeated-load triaxial tests.

B. THE TEST MATERIAL

The material used for the repeated-load hollow cylinder tests was a crushed dolomitic limestone. Because of the small thickness of the specimen wall, the maximum particle size was limited to about 5 mm, giving a ratio of specimen thickness to maximum particle size of approximately 1:6. A representative grading envelope for the uncompacted "virgin" material is shown in Figure 31. The envelope indicates that the material was continuously graded with 95 and 18 percent of the material passing the 5 mm and 75 μm sieve respectively. The curves also follows closely Fuller's equation (Equation (1)) with maximum particle size of 5.6 mm and an "n" value of 0.4. A series of standard vibrating hammer tests (BS 5835) was carried out on the dry materials. The maximum dry density obtained from the test was 2216 kg/m^3 . The specific gravity of the material contained between the 5 mm and 2 mm sieves was found to be 2.7. The shape of the

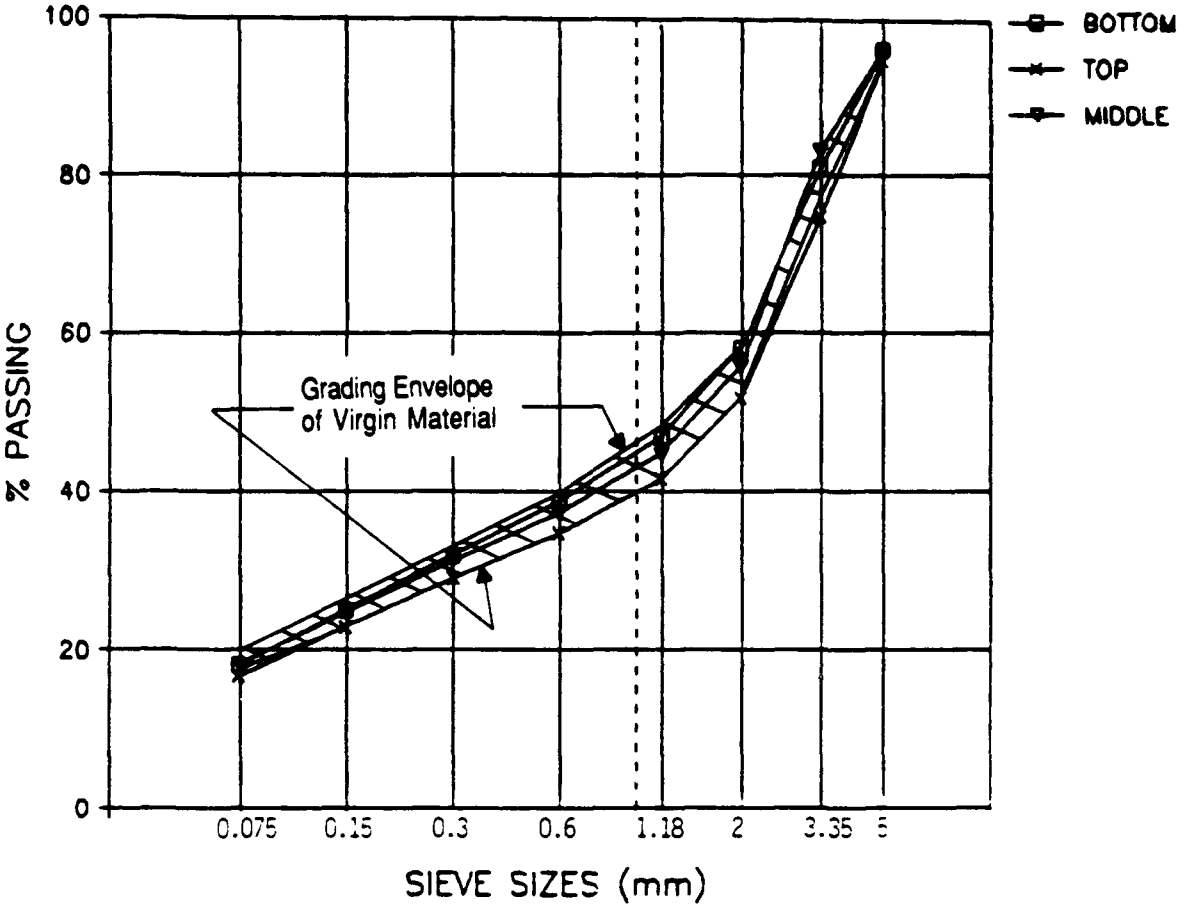

Figure 31. Grading Envelope of the Virgin Material and the Average Gradings of Samples obtained from Top, Middle and Bottom of tested Hollow Cylinder Specimens.

aggregate particles for this group of materials, when examined under a microscope, could be considered as flaky. Because there were no pore pressure or suction measuring devices available in the HCA, the material was tested dry. This ensured that all the stresses used and measured were effective stresses.

The method of specimen preparation described in the last chapter was found to be satisfactory and capable of producing relatively high density, despite the large height of the specimen. Segregation was found to be acceptable as shown also in Figure 31 by the average gradings of the materials retrieved from the top, middle and bottom of the tested specimen. Except for the last layer, the variation of density of the compacted material between different specimens was found to be small, as shown in Figure 32 for all the specimens prepared. Furthermore, if consideration was given only to the middle section of the specimen where deformations were measured, the difference became less significant.

C. PERMANENT STRAIN TESTS

A permanent strain test consisted of applying many cycles of the same stress conditions to a specimen and monitoring its permanent, nonrecoverable deformation at regular time intervals. Because the permanent strain behavior of granular material is dependent on its stress and strain history (i.e. the stresses and strains it has previously been subjected to), only one particular set of stress conditions could be used for each specimen.

A total of 9 tests belonging to this category, each involving at least 10,000 cycles of repeated loading, were carried out. These tests were divided into three series of three tests each as detailed in Table 4. The magnitude of the stresses chosen were based on the stress measurements obtained from the granular base in a full scale test carried out in the Nottingham PTF (23). Although the granular materials involved were different, it was believed that the stresses adopted here were realistic. In all nine tests, both the internal and external cell pressures were kept constant at 100 kPa.

The three specimens involved in each series were subjected to the same repeated vertical stress which varied sinusoidally at a frequency of 0.5 Hz. The only difference was the applied shear stress. The variations of shear stress in each test within one series were designed to allow comparison of results for the following three conditions:

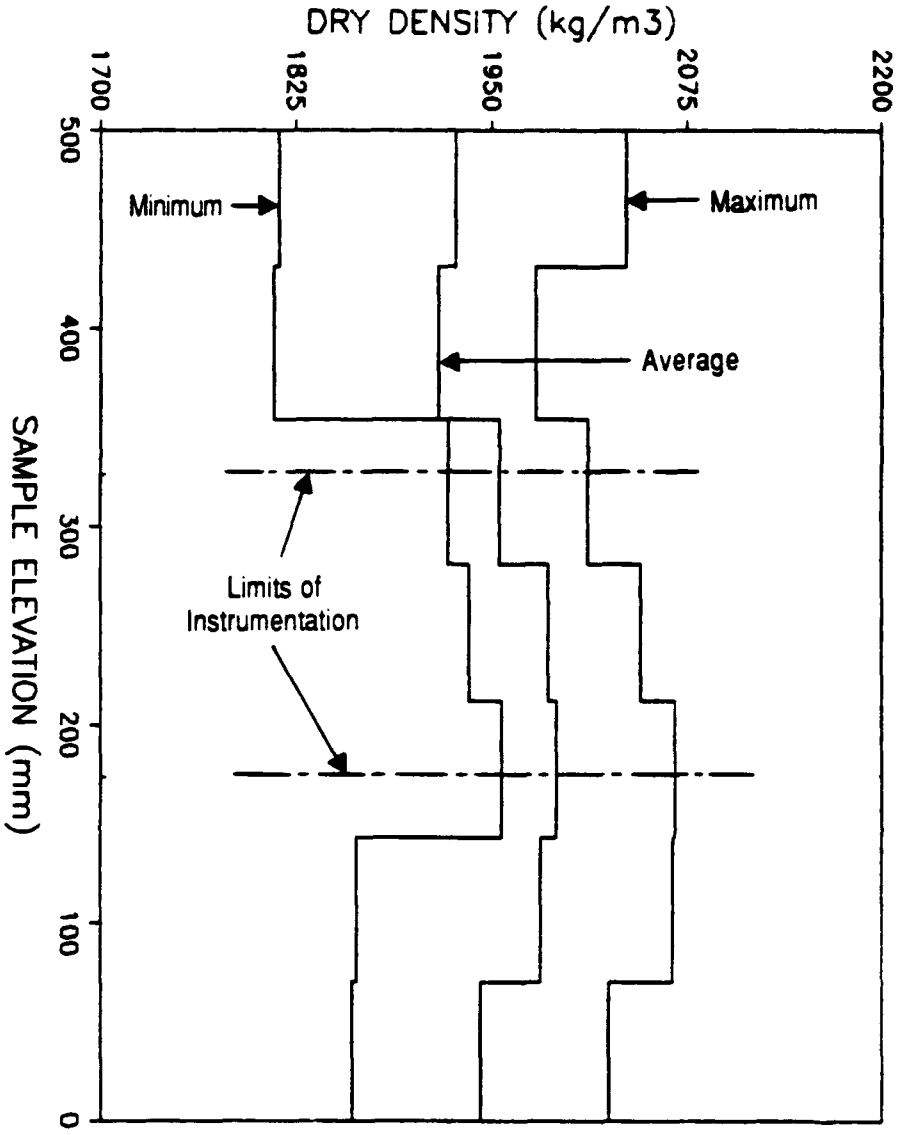

Figure 32. Variation of Dry Density with Depth of Hollow Cylinder Specimens

TABLE 4.

DETAILS OF PERMANENT STRAIN TESTS CARRIED OUT WITH THE REPEATED-LOAD HOLLOW CYLINDER TEST APPARATUS

Test Series	Test Number	Vertical Stress (kPa)	Torsional Shear Stress (kPa)	Phase Angle between Vertical & Torsional Stresses
1	1	0-150	0	0
	2	0-150	-20-+20	-90
	3	0-150	-20-+20	+90/-90
2	4	0-200	0	0
	5	0-200	-20-+20	-90
	6	0-200	-20-+20	+90/-90
3	7	0-200	0	0
	8	0-200	-30-+30	-90
	9	0-200	-30-+30	+90/-90

1. Triaxial Condition

In this case, no shear stress was applied. This provided the basis for comparison of results with those which involved shear stress reversals. It also allowed results obtained from the repeated-load triaxial test apparatus to be compared.

2. Condition under a wheel load moving in one direction (unidirectional shear reversal)

To simulate the stresses under this condition, the phase angle between the vertical and the shear stress (which also varied sinusoidally at the same frequency) waveforms was adjusted to 90 degrees, as shown in Figure 33. As a result, the variation of angle of principal plane rotation with time shown in Figure 34 was obtained. Because the HCA was not able to generate a variable cell pressure, the variation of horizontal stress (as shown in Figure 1 Section I) could not be simulated. Instead, a constant pressure was used.

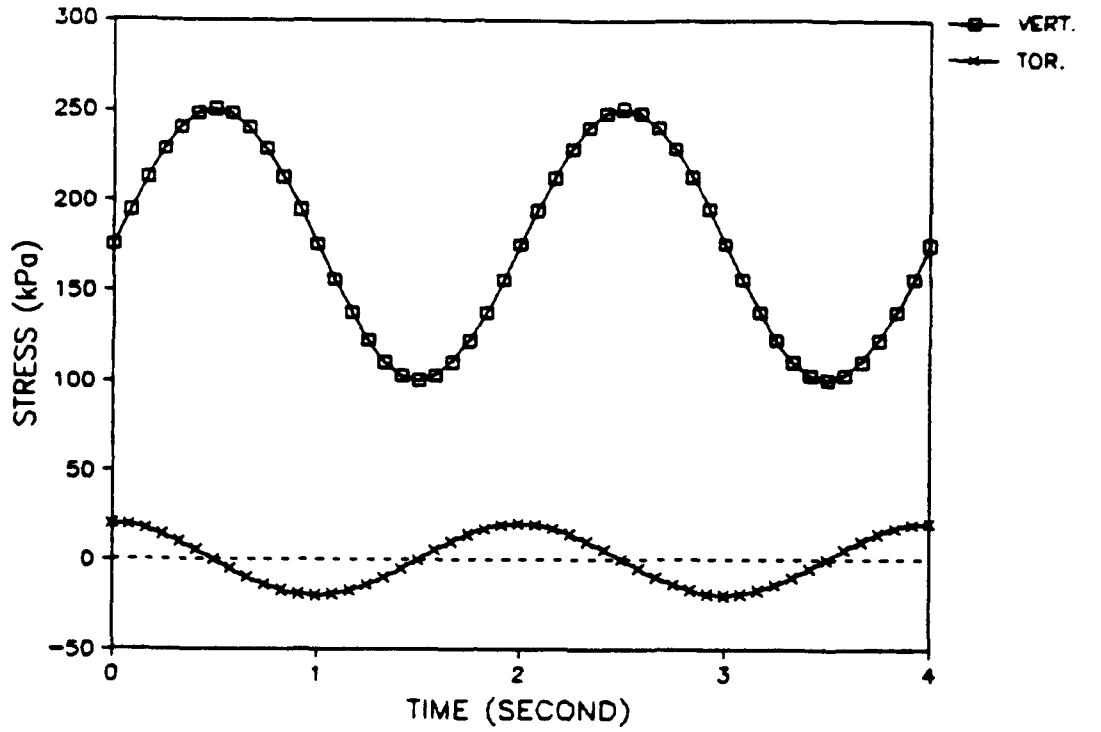

Figure 33. Waveforms for Vertical and Torsional Stresses in Tests with Unidirectional Shear Reversal.

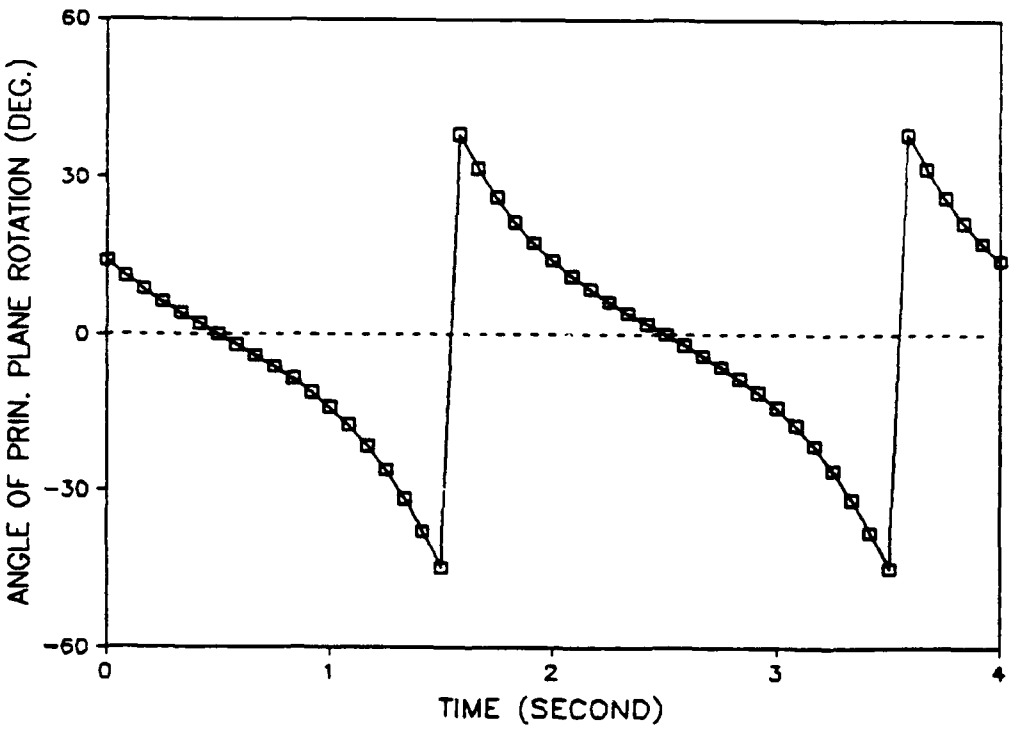

Figure 34. Variation of Angle of Principal Plane Rotation with Time in Tests with Unidirectional Shear Reversal.

3. Condition under a wheel load moving in both directions (bidirectional shear reversal)

This condition , as represented in Figures 35 and 36, was basically the same as that for the unidirectional shear reversal. The exception was that at regular preset interval during the test, the phase angle between the vertical and shear stress was switched from +90 to -90 degrees or visa versa. For the purpose of simulating laboratory bidirectional loading, it would be ideal if the switching of the phase angle were carried out in successive cycles. However, since the switching process was manually controlled, it became impractical, if not impossible for it to happen. Therefore a compromise for the sequence of changes of phase angle as shown in Figure 37 was adopted for this test.

The stress paths for the three series of tests are shown, in q-p stress space, in Figure 38. The paths for the two conditions with reversed shear stresses are practically identical and slightly curved. For the triaxial condition, a straight stress path is apparent. Despite this difference, the end points of the paths are identical for each series of tests.

D. 50-CYCLE TESTS

When the stress path used in a permanent deformation test approaches the static failure condition, both the magnitude and the rate of development of permanent strain will increase. As the resulting deformations are generally large, the effect due to stress or strain history will be very much reduced. Using this assumption, a series of permanent strain tests involving several stress paths, each of increasing severity, can be carried out on a single specimen of granular material. Because of the rapid build-up of permanent strain, only a limited number of cycles of each repeated stress condition could be allowed before the specimen was totally damaged.

In this project, the number of cycles used for each stress path was approximately 50, hence the name "50-cycle test." The main objective of the "50-cycle" test was to make use of a less time-consuming method to examine the effect of the reversed shear stresses on the rate of development of permanent strains. In order to achieve this, each test was divided into two parts, each part consisting of 25 cycles of the same stress condition. In one part, only the vertical stress was cycled while, in the other, an additional unidirectional reversed shear stress was applied. An example of the variation of the stress conditions recorded during a 50-cycle test is shown in Figure 39. In some tests, the "without-shear" condition was allowed to precede the "with-shear" (or triaxial) condition in order to counteract the possible strain history effect caused during the initial 25 cycles

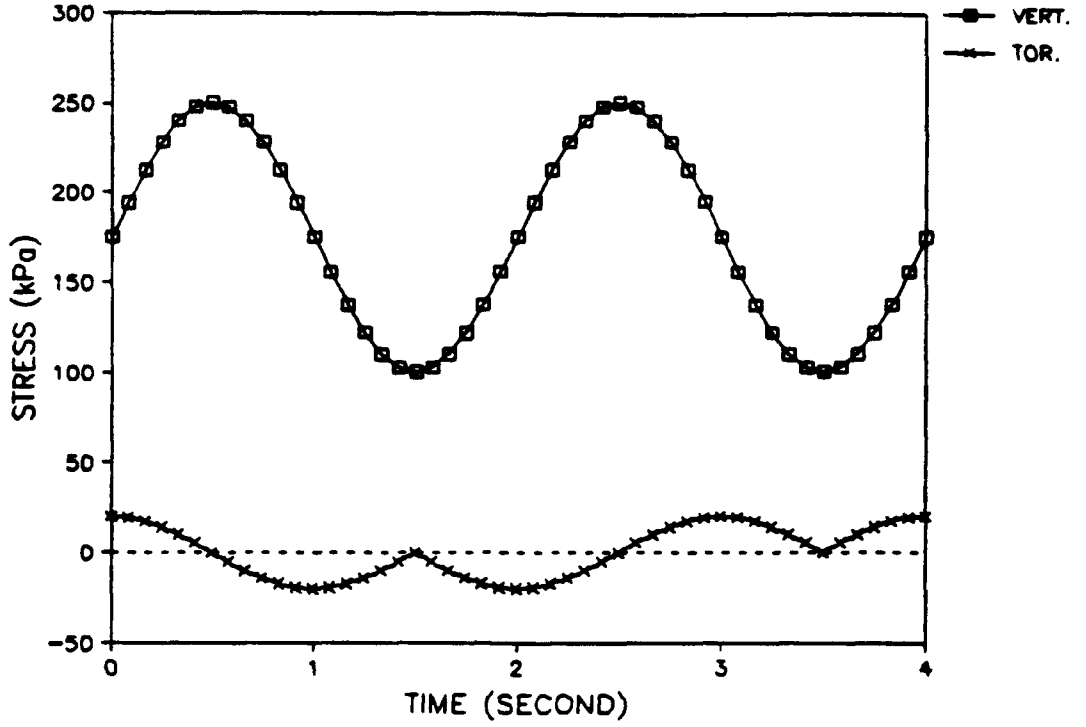

Figure 35. Waveforms for Vertical and Torsional Stresses in Tests with Bidirectional Shear Reversal.

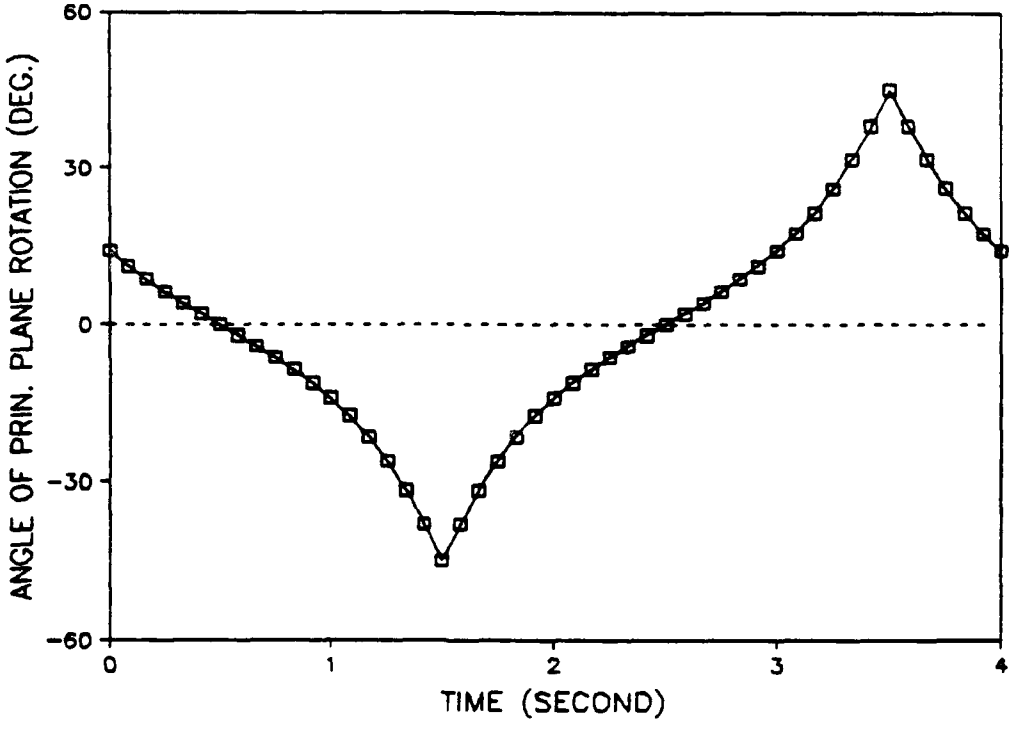

Figure 36. Variation of Angle of Principal Plane Rotation with Time in Tests with Bidirectional Shear Reversal.

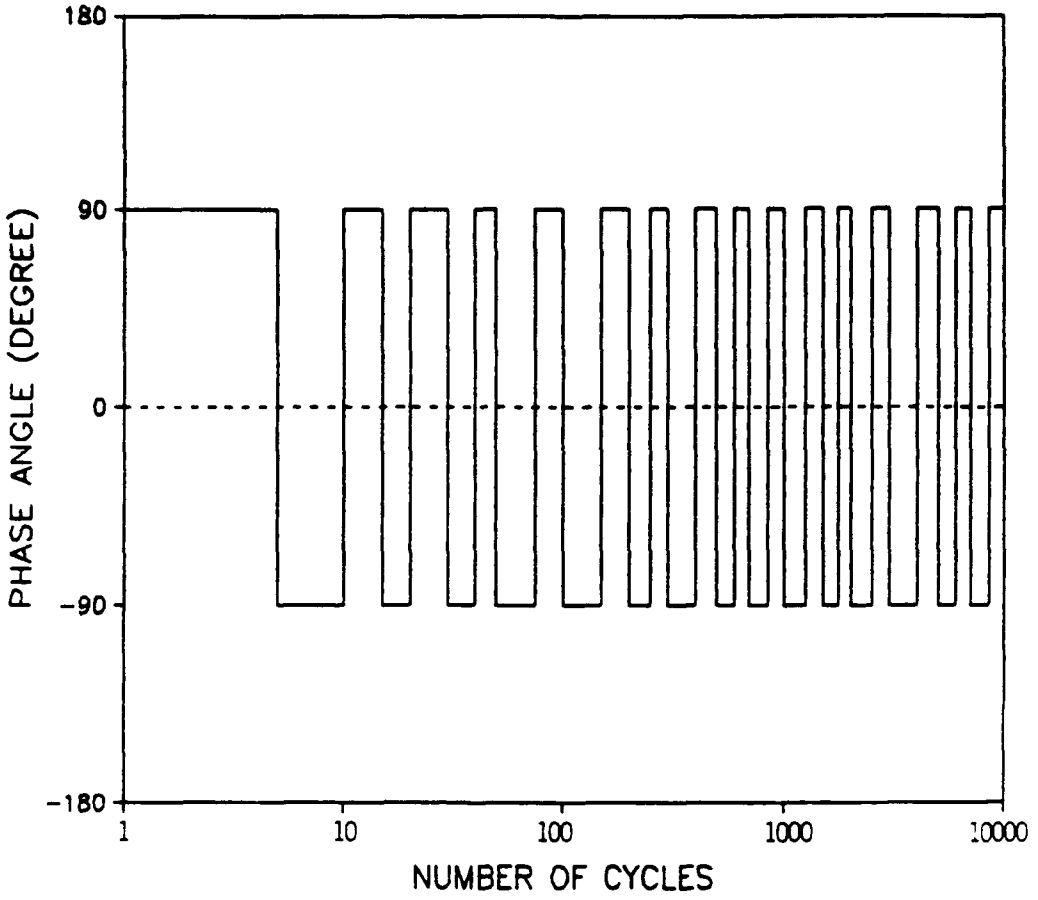

Figure 37. Variation of Phase Angle Shift between the Vertical and Torsional Stress Waveforms during Tests with Bidirectional Shear Reversal.

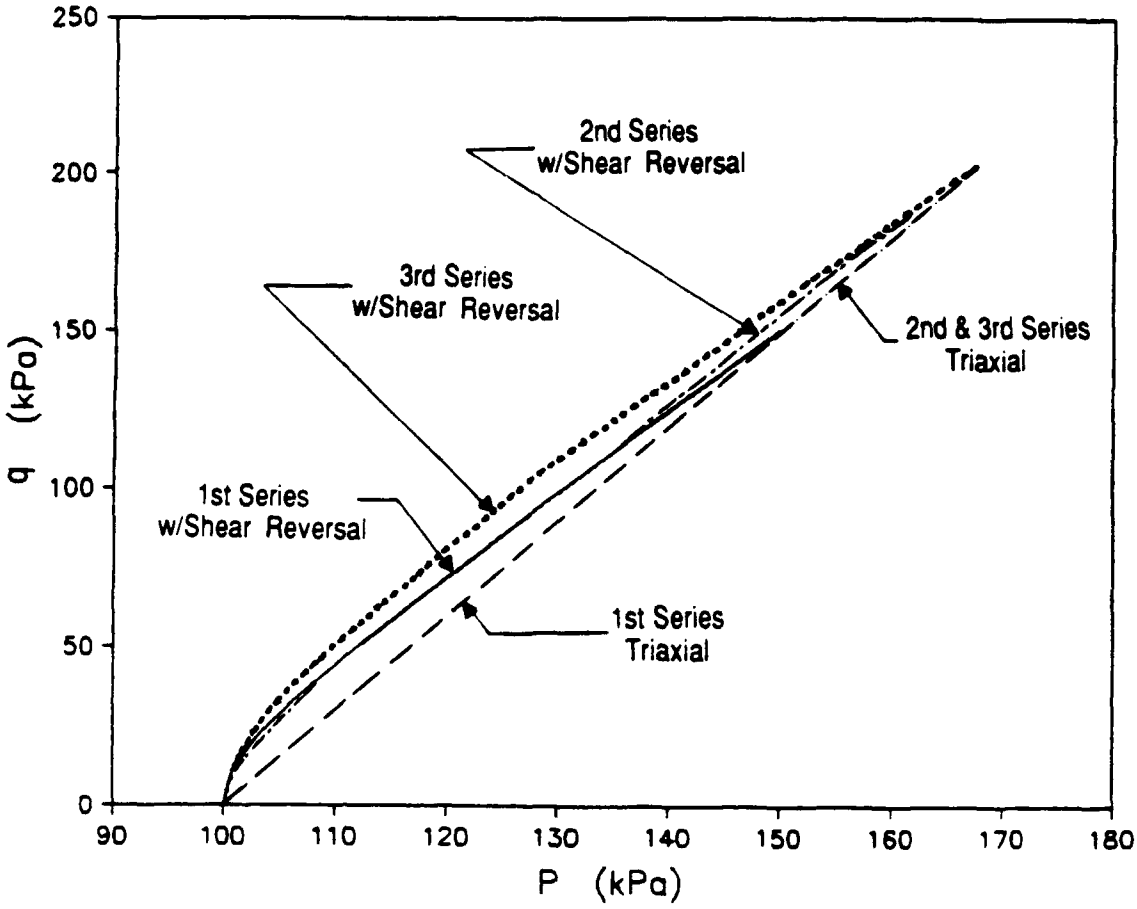

Figure 38. Stress Paths in q-p Space used in Permanent Strain Tests.

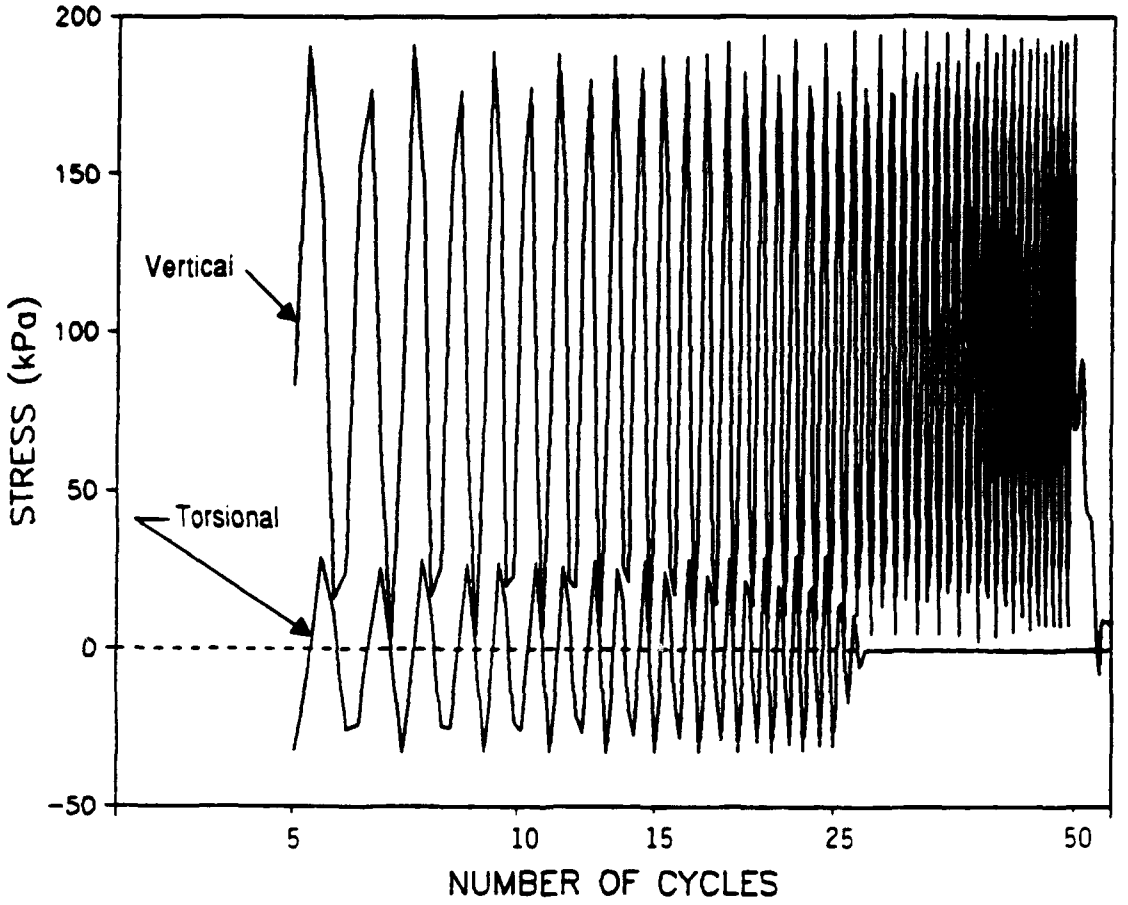

Figure 39. Variation of Stresses with Time in a 50-Cycle Test.

of stresses. All components of strain, both recoverable and the non-recoverable (permanent), were monitored continuously during the 50 cycles of stress, allowing their variations during the two parts of test to be compared.

Seven 50-cycle tests were carried out on one hollow cylinder specimen. Details of the stress conditions used are shown in Table 5. The stress paths in q-p stress space are shown in Figure 40. The solid lines represent the paths with reversed shear stresses. In order to allow more time to implement the stress changes (from "with-shear" to "without-shear"), a slower frequency of 0.4 Hz was used for the repeated stress waves.

TABLE 5

DETAILS OF 50-CYCLE TESTS

Test Number	Vertical Stress (kPa)	Torsional Shear Stress (kPa)	Cell[1] Pressure (kPa)	Maximum (q/p) Ratio	Test[2] Sequence
1	0-200	-30-+30	100	1.20	1
2	0-200	-30-+30	70	1.46	2
3	0-250	-30-+30	50	1.88	1
4	0-300	-30-+30	50	2.00	1
5	0-250	-30-+30	38	2.06	2
6	0-250	-30-+30	35	2.11	1
7	0-200	-30-+30	23	2.23	2

Note: 1. The pressure is for both the inner and outer cell chamber.
2. "1" means that the "without-shear" condition precedes the "with-shear" condition. "2" means the reverse.
3. Phase angle between the vertical and torsional stresses is 90 degree for all tests

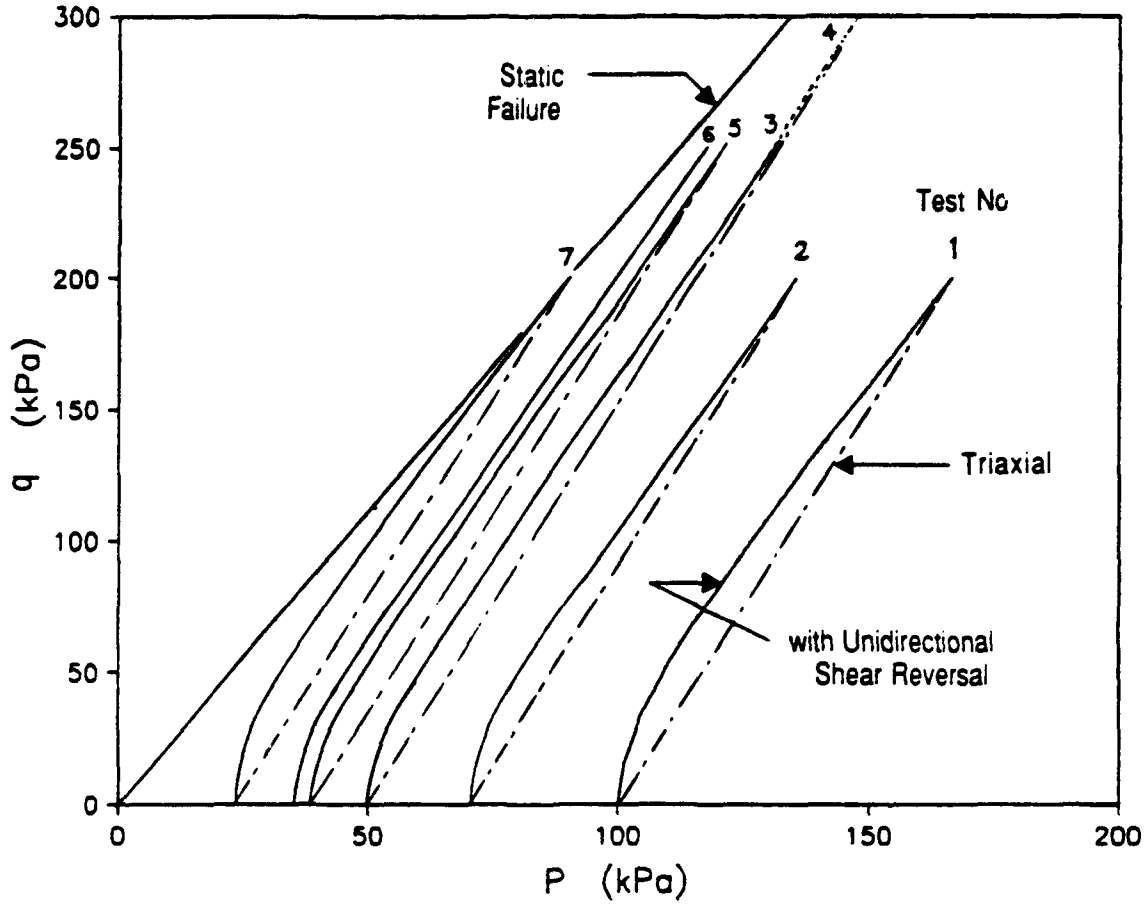

Figure 40. Stress Paths in q-p Space used in 50-Cycle Tests.

E. RESILIENT STRAIN TESTS

In a resilient strain test, the stress paths used are well away from the failure condition. As a result, it can be assumed that the specimen responds elastically and all the strain components essentially recover during unloading.

The resilient behavior of the specimen used in the permanent strain tests was regularly monitored during the tests. However, the resilient stress paths involved were only limited to the one used for that particular permanent strain test. This cautious procedure was adopted to minimize the risk of causing a stress or strain history effect on the result of the permanent strain tests. A new specimen, therefore, was constructed to allow a more thorough study of the resilient behavior of the granular material used. The specimen was subjected to a much wider range of stress conditions as detailed in Appendix C. The test program aimed at covering a range of intermediate principal stress and angle of principal plane rotation.

However, "Jump" rotation of 90 degrees can occur between the circumferential plane (on which σ_θ acts) and the axial (on which σ_z acts) or radial (on which σ_r acts) plane during repeated loading when σ_r becomes larger than σ_z and σ_θ or when σ_θ becomes larger than σ_r. In these cases, principal plane rotation will occur in both the z-r or θ-r directions. Therefore, in order to avoid complications caused by the three dimensional rotation, the conditions stated in equations 19 and 20 were followed at all times during the resilient tests. This ensured that σ_r was always the intermediate principal stress and rotation of principal stress plane was restricted to the θ-z plane. The frequency of the repeated stress wave used in these tests was 0.5 Hz.

F. REPEATED-LOAD TRIAXIAL TESTS

The repeated-load HCA is undoubtedly a complicated testing device which will remain as a research tool for some time. At the moment, results of tests from this device are scarce and, therefore, cannot be used immediately with confidence. As a result, it appears to be advantageous to make comparisons between the performance of the HCA and that of the more widely used repeated-load triaxial test apparatus.

Two cylindrical specimens of the same granular material used in the HCA tests, with diameters of 150 mm and heights of 300 mm were tested in a repeated-load triaxial test apparatus. In the first test, a series of resilient stress paths, as detailed in Appendix E, were applied. After the

resilient tests were completed, a permanent strain test, which used the same stress path as that for Tests 4 and 7 of the HCA test program, was carried out on the same specimen. For the second specimen, only the permanent strain test was performed. The permanent strain test involved at least 10,000 cycles of repeated load at a frequency of 0.5 Hz.

The triaxial specimens were manufactured, using the same vibrating table and surcharge as for the HCA specimens. As a result, the densities obtained for the triaxial specimens TX1 and TX2, which were 1950 and 1909 kg/m^3 respectively, were similar to those of the hollow cylinder specimens.

SECTION VI

RESULTS FROM REPEATED-LOAD HOLLOW CYLINDER TESTS

A. INTRODUCTION

The results of the tests described in Section V are presented in the following sections. A total of 11 hollow cylinder and 2 triaxial specimens were tested for this part of the investigation. In the permanent strain tests, because the number of specimens was limited, it was not possible to perform replicate tests for each stress path. However, for the resilient strain tests, duplicate tests were carried out. The emphasis of the presentation of the results from the permanent strain tests is placed mainly on the trend of permanent strain development rather than the absolute values of strains. This approach is considered to be applicable, particularly for programs involving small numbers of tests. In general, more information was available from resilient strain tests, despite the use of much fewer specimens. As a result, a more detailed analysis of the results was possible.

B. PERMANENT STRAIN TESTS

In a permanent strain test, the electronic signals from all the instrumentation were monitored without interruption during the first 30 cycles. Typical plots of the relationship between stresses and one of the strain components with time are shown in Figures 41 and 42, respectively. A few cycles of time are normally required at the start of the test for the stresses to reach their target values. The average number of data points captured per cycle during the first 30 cycles was about eight. To collect data for subsequent numbers of cycle, the test was stopped and the nonrecoverable or permanent strain components were then individually recorded.

1. Comparison between Triaxial, Uni- and Bidirectional Shear Reversal Conditions

The variations of permanent strain with number of stress cycles, for the nine specimens used in the three series of repeated-load HCA tests, are shown in Figures 43 to 46. Four types of strains were included for comparison. They were the permanent axial strain, $(\varepsilon_a)_p$ (Figure 43), the permanent horizontal strain, $(\varepsilon_h)_p$ (Figure 44), defined here as the sum of the radial and circumferential strains , the permanent volumetric strain, $(\varepsilon_v)_p$ (Figure 45) and the permanent maximum shear strain in the θ-z plane, $(\varepsilon_{max})_p$, as defined in equation 34 (Figure 46).

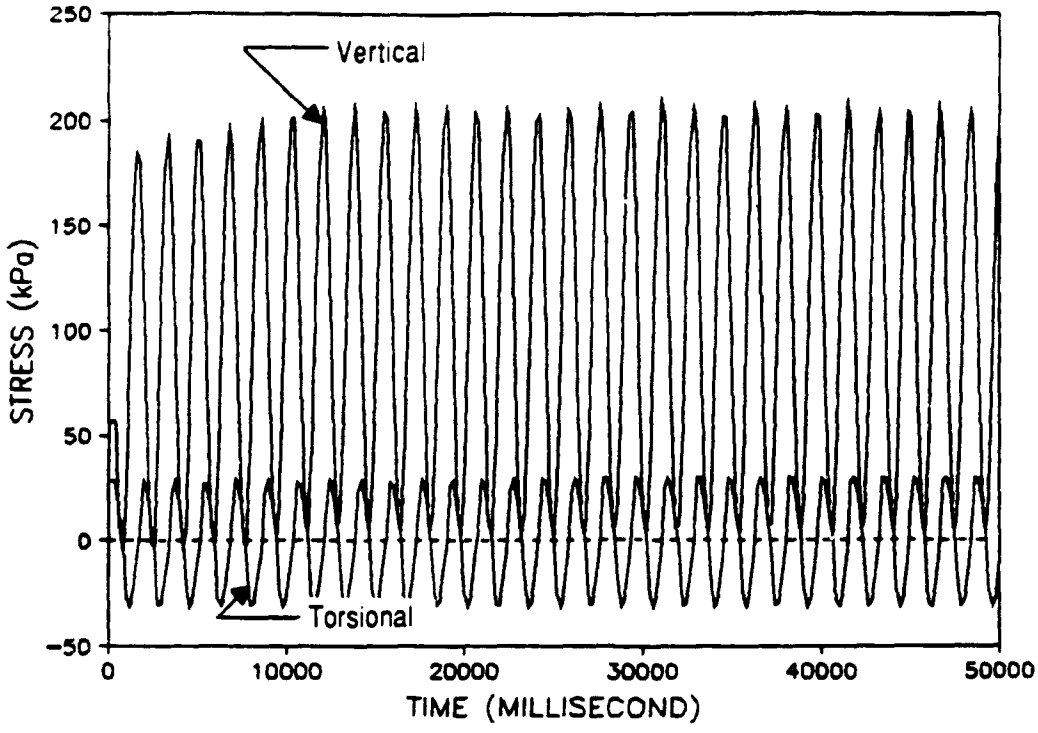

Figure 41. Variation of Stresses with Time during the first 30 Cycles of a Permanent Strain Test.

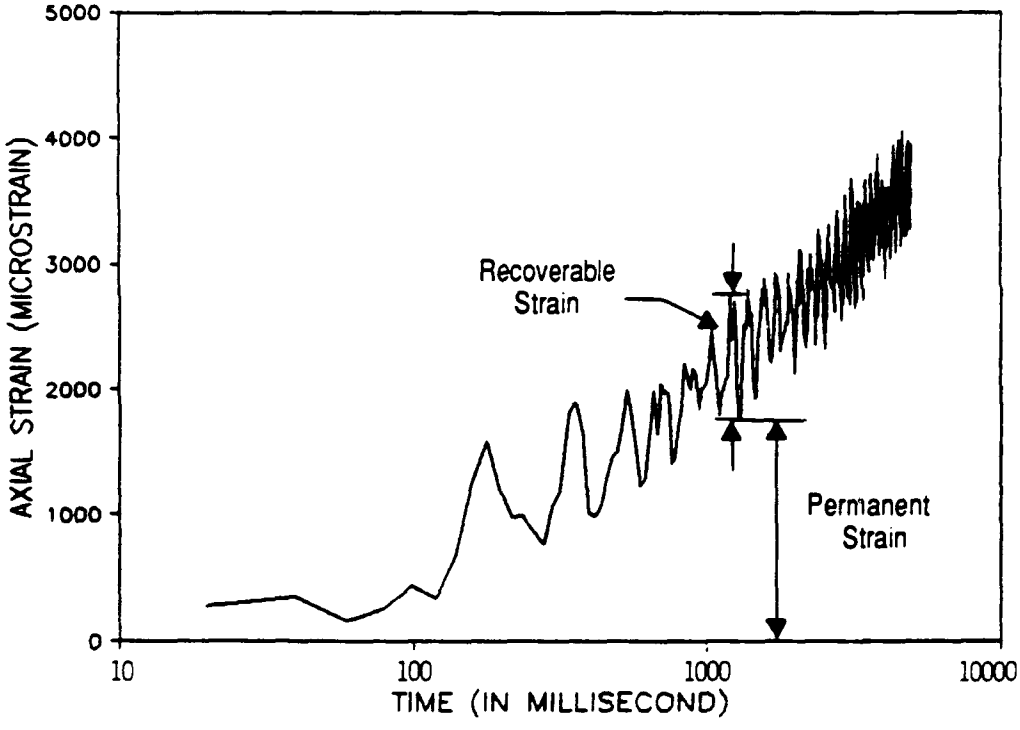

Figure 42. Variation of Axial Strain with Time during the first 30 cycles of a Permanent Strain Test.

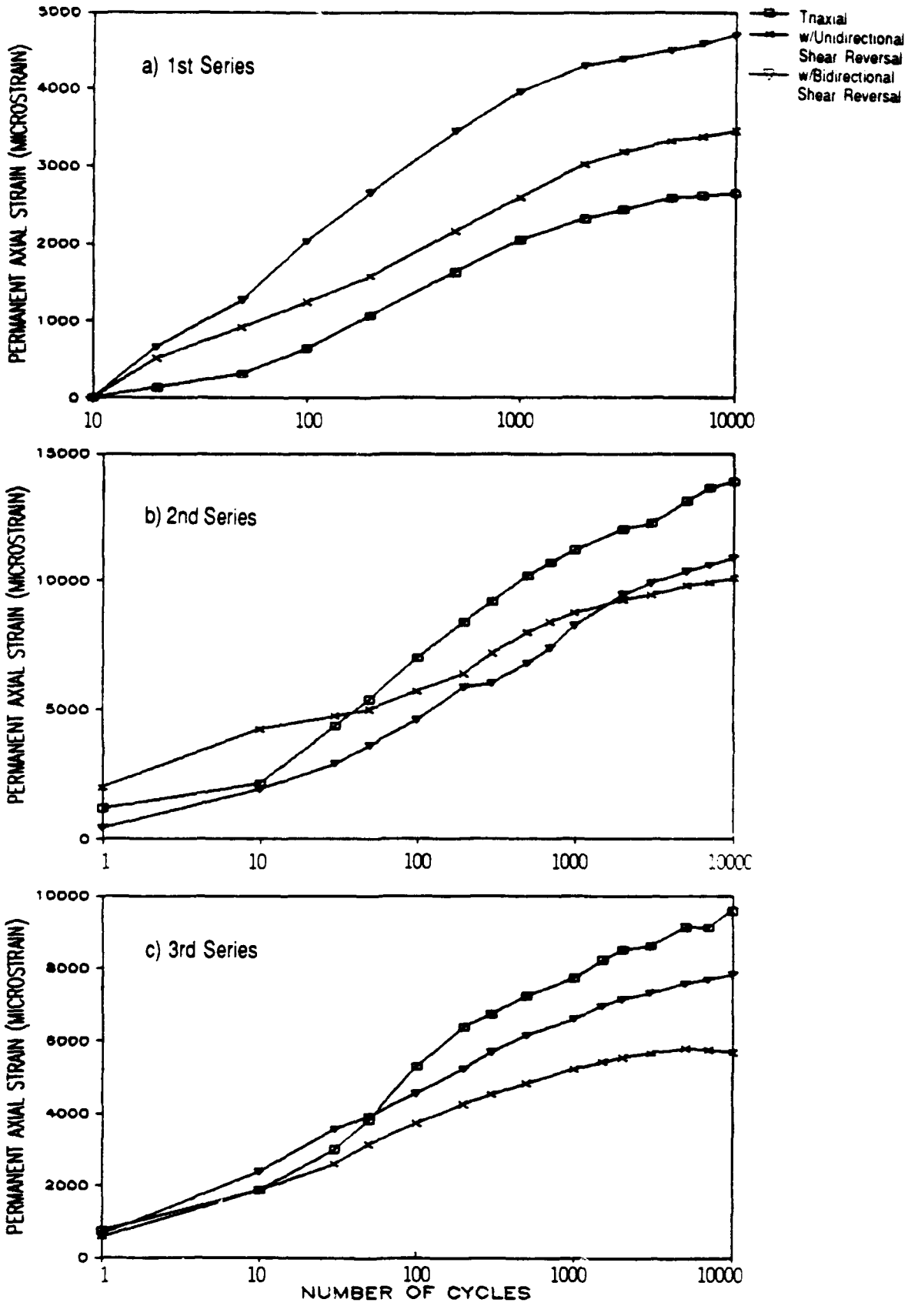

Figure 43. Variation of Permanent Axial Strains with Number of Stress Cycles for all Series of Permanent Strain Tests.

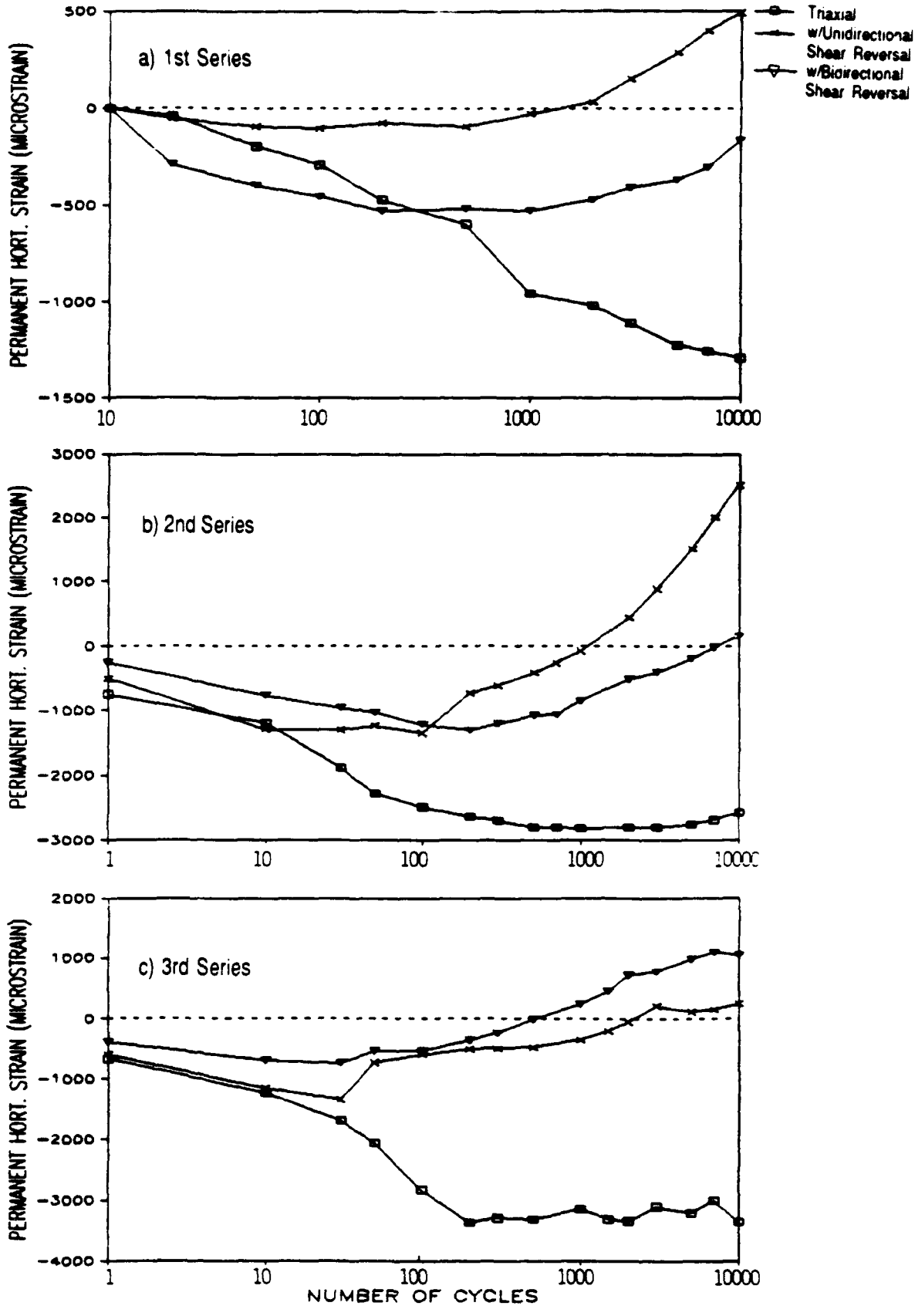

Figure 44. Variation of Permanent Horizontal (Sum of Radial and Circumferential) Strains with Number of Stress Cycles for all Series of Permanent Strain Tests.

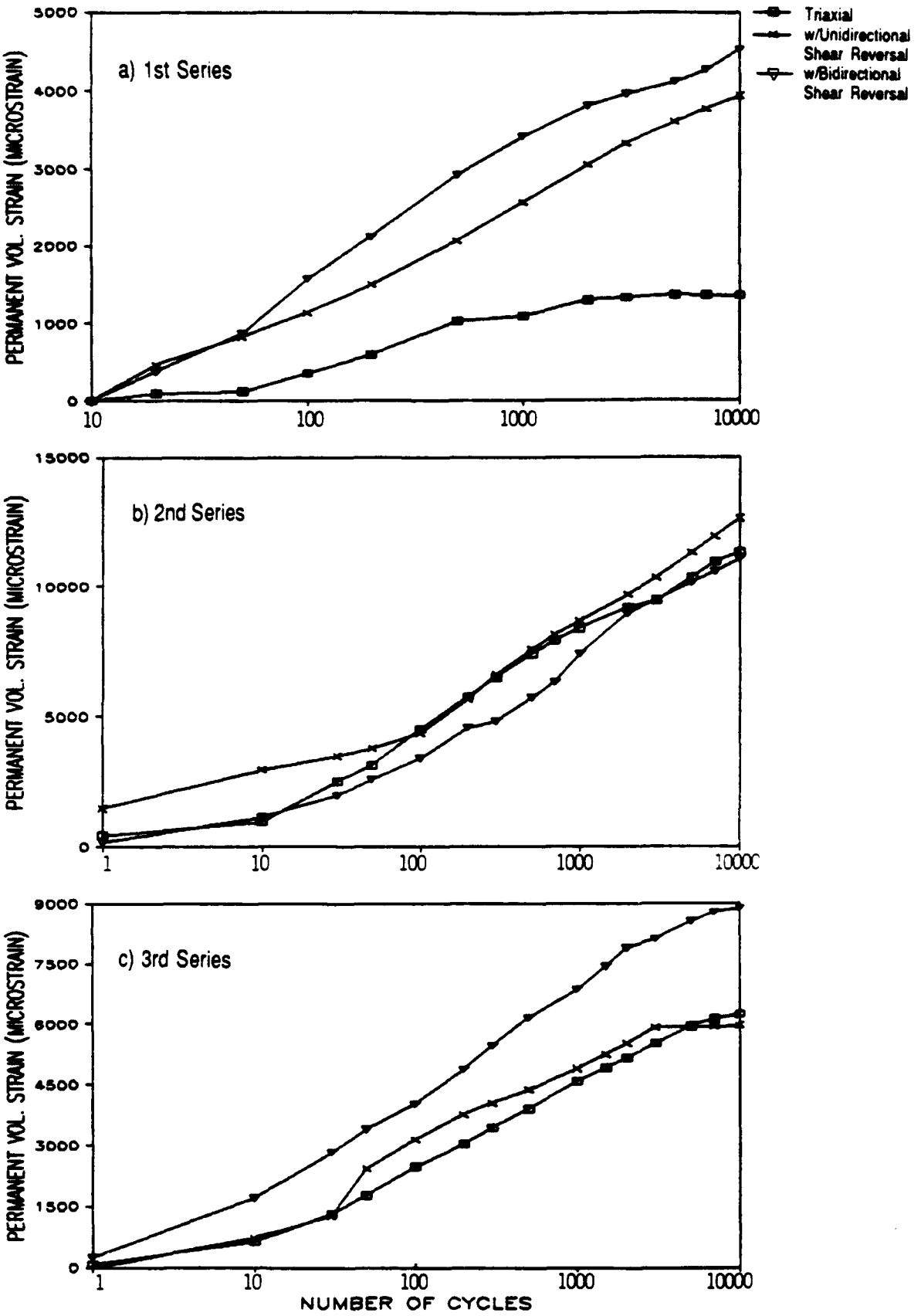

Figure 45. Variation of Permanent Volumetric Strains with Number of Stress Cycles for all Series of Permanent Strain Tests.

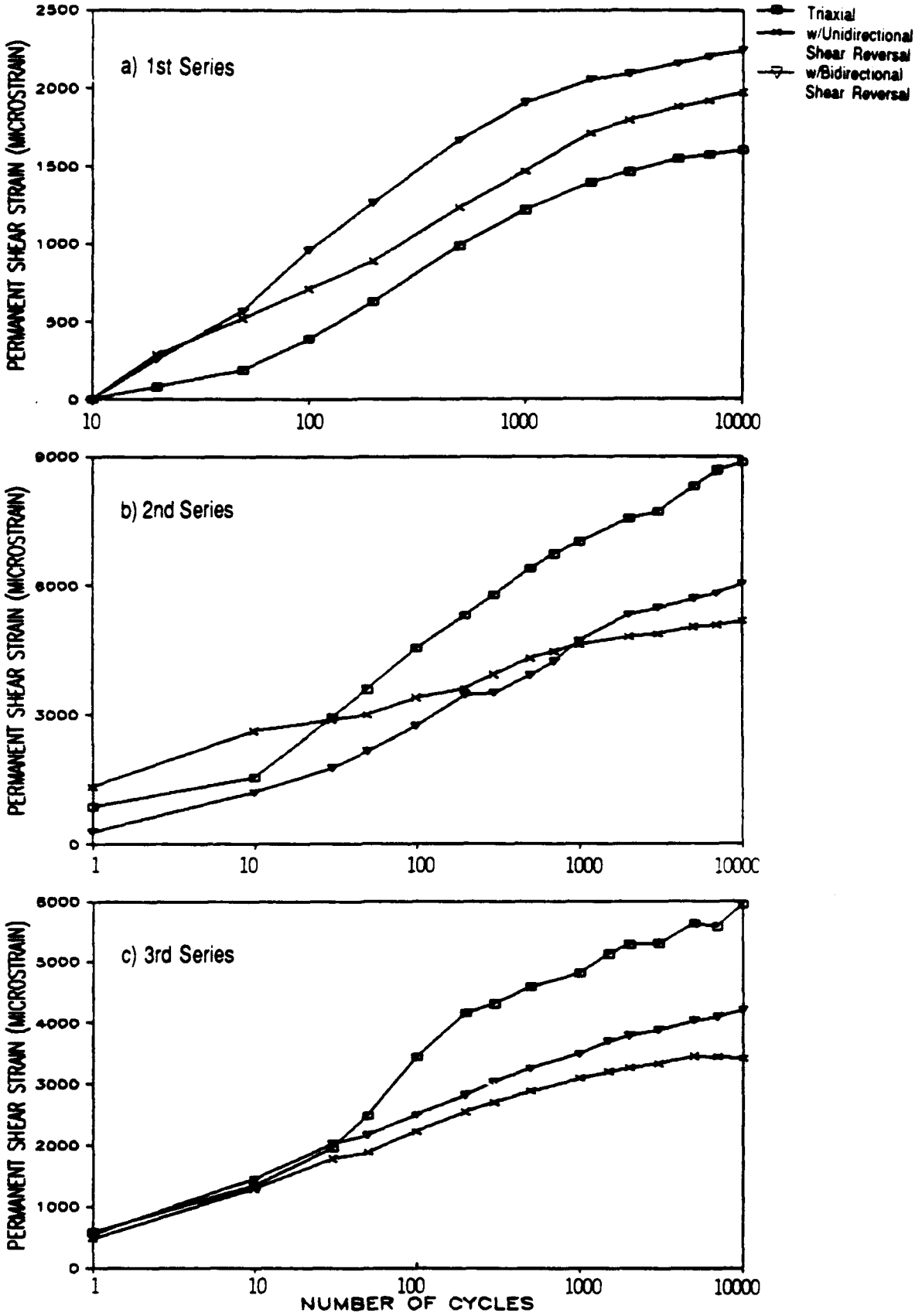

Figure 46. Variation of Permanent Maximum Shear Strains with Number of Stress Cycles for all Series of Permanent Strain Tests.

The use of the sum of the radial and circumferential instead of their individual values was justifiable as they both had broadly the same magnitude and sign and varied in similar manner with the number of cycles.

Figures 43 to 46 are largely self-explanatory. However, some description may be required to highlight the important features:

a. In the first series of tests, while the skill of operating the newly modified test apparatus was still being perfected, the stresses which were applied to the specimens during the first 10 cycles were rather variable. As a result, it was decided that the permanent strains occurring during this early period should be discarded. Hence, zero permanent strains were assumed at cycle 10 for all the tests in this series. In subsequent test series, all strains were presented from the first cycle.

b. The magnitude of all strain components is quite small, even after 10,000 cycles of stress. In the first test series, the maximum strain remained less than 0.5 percent. With the shear stress ratio, $(q/p)_{max}$ increased from 1 (in the first test series) to 1.2, the maximum strain in the second and third series reached about 1.5 percent. In general, $(\varepsilon_v)_p$ is about 2 times $(\varepsilon_{max})_p$. In all tests, $(\varepsilon_a)_p$ are positive (compressive) while most $(\varepsilon_h)_p$ values are negative (dilatant). However, because of the predominantly high magnitude of the axial strains, the resulting volumetric strains are all positive, indicating contraction. The permanent maximum shear strains, on the other hand, are all positive by definition.

c. Most components of strains, with the exception of $(\varepsilon_h)_p$, increase gradually and, broadly linearly, with the logarithm of the number of cycles. In the first test series, after about 2000 cycles, the permanent strains tended to stabilize. In subsequent series, signs of stabilization of strain were observed for some but not all tests.

d. The most obvious difference in permanent strain behavior among the three investigated stress conditions is found in the development of permanent horizontal strain (Figure 44). Under triaxial condition, $(\varepsilon_h)_p$ was dilatant and remained so throughout the test. It also tended to stabilize rather rapidly at a terminal value. However, when reversed shear stresses were applied, the initial permanent strain was dilatant but then after 100 to 300 cycles of stress, it started to move towards the compressive end. In the two cases with unidirectional shear reversal in Series 1 and 2, the change from negative to positive permanent strain occurred rather rapidly and tended to accelerate towards the end of the tests.

e. It appears that higher permanent contractive volumetric strains occurred when reversed shear stresses were applied (see Figure 45). In the first test series, $(\varepsilon_v)_p$ under triaxial stress conditions was only one third to one fourth of that with shear reversal. However, with the ratio of the torsional shear to vertical stress reduced, there seemed to be less difference between the strains for the three conditions. Figure 45 may also suggest that when the stress ratio mentioned above is high, conditions with bidirectional shear reversal are likely to result in more permanent volumetric strain.

f. The behavior of $(\varepsilon_a)_p$ and $(\varepsilon_{max})_p$ is very similar. In the first test series, the specimen under triaxial stress conditions (which incidentally was the very first specimen to be tested in the test program) developed the smallest permanent strain. However, in both subsequent test series, specimens under triaxial stress conditions were found to develop the highest strains. The results from these latter test series led to the belief that the first specimen may have suffered from some disturbance or strain history during the "setup" of the test. This may also explain the much smaller permanent volumetric strains which occurred in this specimen.

g. Taking into account of the possible error mentioned in paragraph f above and based on Figure 46b and 46c, it appears that when reversed shear stresses are applied, a reduction in the build-up of permanent maximum shear strain is likely to occur. Figure 46 also indicates consistently that higher $(\varepsilon_{max})_p$ occurs under the bidirectional than unidirectional shear stress reversal.

2. Comparison between Results from Tests carried out in Repeated-load HCA and Triaxial Apparatus

A comparison of the permanent strains from the HCA Tests 4 and 7 under triaxial stress conditions and the two tests carried out in the repeated-load triaxial test apparatus involving the use of an identical set of stresses are shown in Figures 47 to 50.

The scatter of results shown in the figures were considered acceptable when compared with others (18) which involved up to five replicate tests using one piece of test apparatus. More consistent results were obtained for permanent axial strain than for horizontal strain which, for tests carried out in the triaxial test apparatus, is defined as twice the permanent radial strain. For the latter strain, although the pattern of strain development in tests carried out in both apparatus was very much the same, the strain magnitudes obtained from the HCA were found to be much higher.

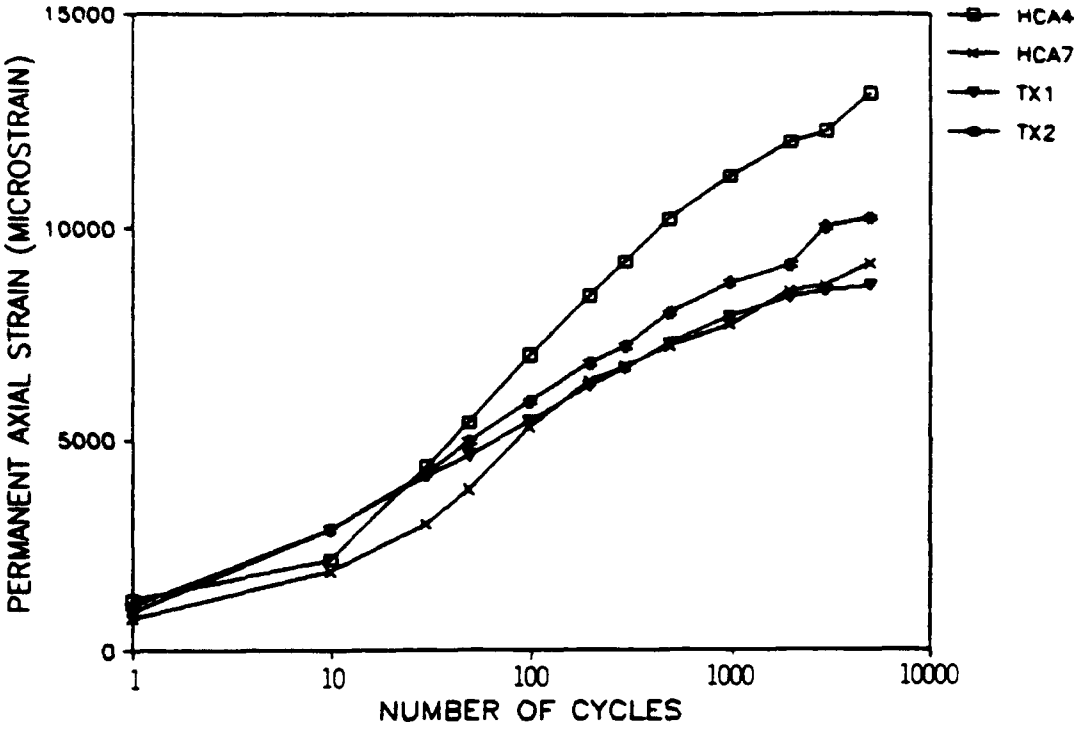

Figure 47. Comparison between Permanent Axial Strains obtained under identical Stress Conditions from the Repeated-Load Triaxial and Hollow Cylinder Test Apparatus.

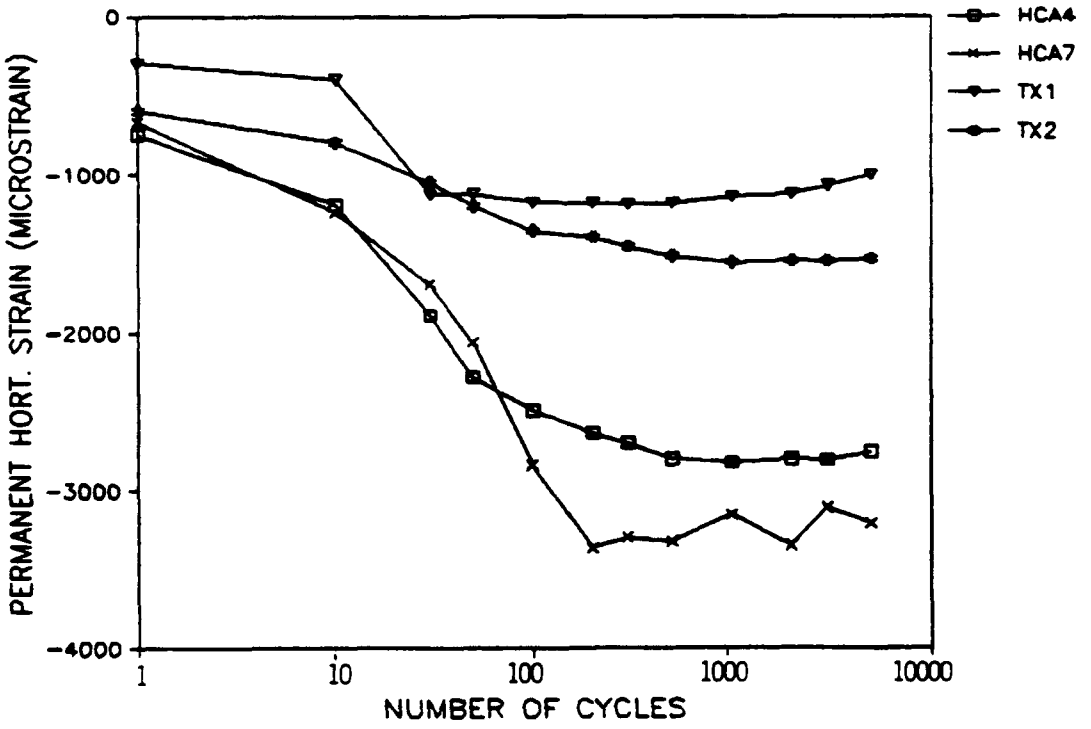

Figure 48. Comparison between Permanent Horizontal (Sum of Radial and Circumferential) Strains obtained under identical Stress Conditions from the Repeated-Load Triaxial and Hollow Cylinder Test Apparatus.

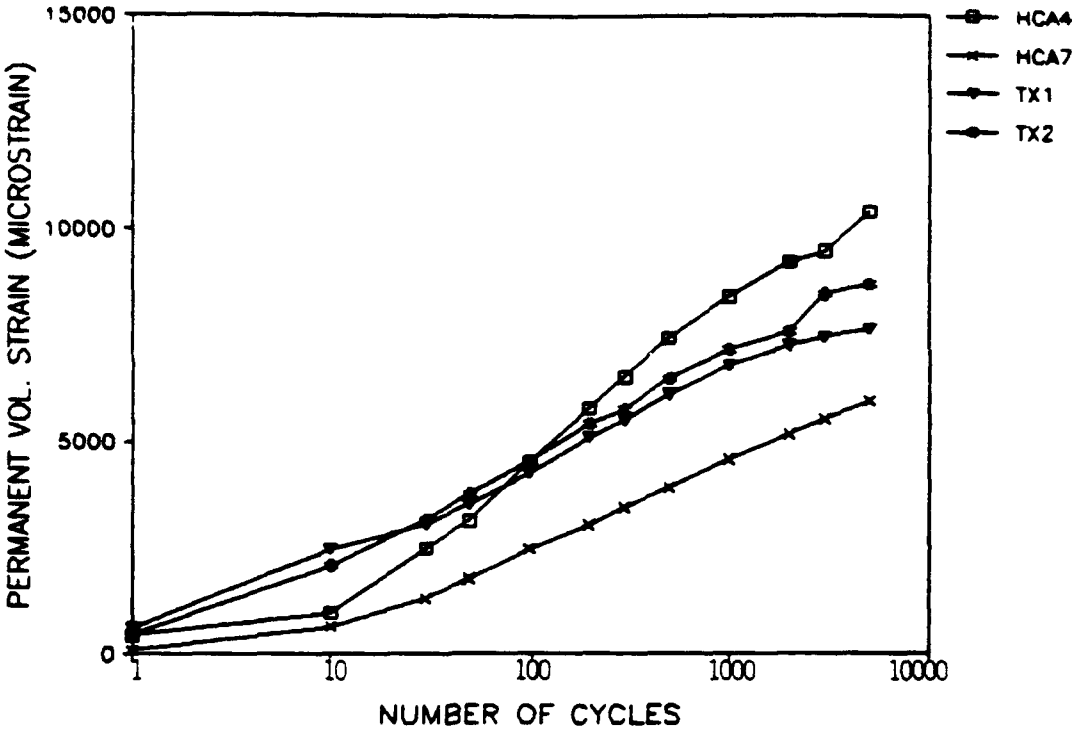

Figure 49. Comparison between Permanent Volumetric Strains obtained under the identical Conditions from the Repeated-Load Triaxial and Hollow Cylinder Test Apparatus.

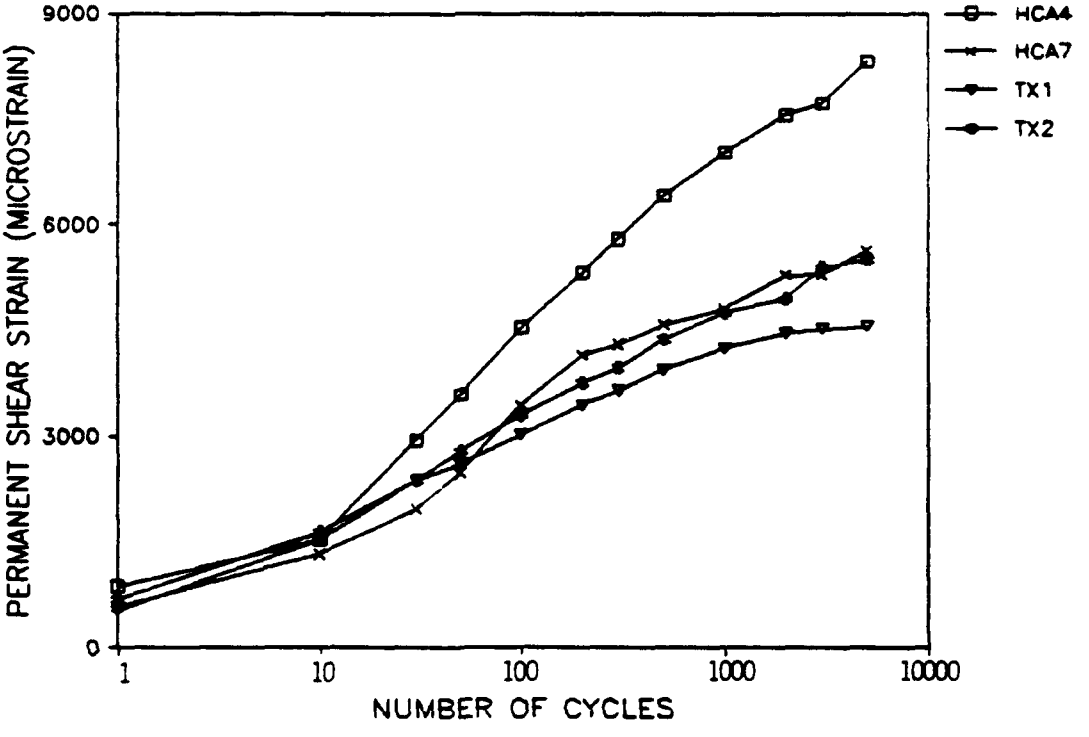

Figure 50. Comparison between Permanent Shear Strains obtained under identical Stress Conditions from the Repeated-Load Triaxial and Hollow Cylinder Test Apparatus.

A comparison of $(\varepsilon_v)_p$ and $(\varepsilon_{max})_p$ from the HCA Tests 5 and 8 and the two tests performed with the repeated-load triaxial test apparatus are shown in Figure 51 and 52 respectively. Both the HCA tests were performed under the condition with unidirectional shear reversal and both repeated-load triaxial tests involved an identical $(q/p)_{max}$ value as those used in the HCA tests.The comparison indicates that the permanent strain behavior of the granular material under the condition simulated by the HCA with the particular magnitude of reversed shear stresses is, by and large, similar to that obtained by the repeated-load triaxial test apparatus.

C. 50 - CYCLE TESTS

Since the stress-strain behavior of the hollow cylinder specimen was continuously monitored during the 50-cycle tests, the average number of data points recorded per cycle was reduced to five. As a result, some peaks and troughs of the stress and strain waveforms could not be captured. However, it was believed that the overall rate of permanent strain development during the two parts of each test was satisfactorily obtained for comparison purpose.

Figures 53 and 54 illustrate one of the results obtained from a 50-cycle test. In these figures, the variation of strain, including both the recoverable and non-recoverable components, with the logarithm of the number of cycles for the two parts of the test is shown. Figure 53 indicates that the accumulated permanent axial strain varies approximately linearly with the logarithm of the number of cycles within both parts of the test but at different rates under the two different stress conditions. This behavior was also observed for the permanent horizontal strain, as shown in Figure 54, although the behavior was generally dilatant. Simplified plots to illustrate these results are shown in Figure 55 in which the vertical axis represents only permanent strain and the slopes for the two parts of the test are highlighted. Similarly, the slopes for the permanent volumetric and maximum shear strain could be calculated.

A summary of these slopes, or rate of permanent strain development for the seven 50-cycle tests is shown in Table 6. All positive rate values represent a tendency to develop compressive strain while the negative ones indicate dilatancy. When these results were analyzed, emphasis was placed on the comparison of strain rates obtained within one test. The use of an individual strain rate for general comparison purposes may be misleading because of the likely strain history effect

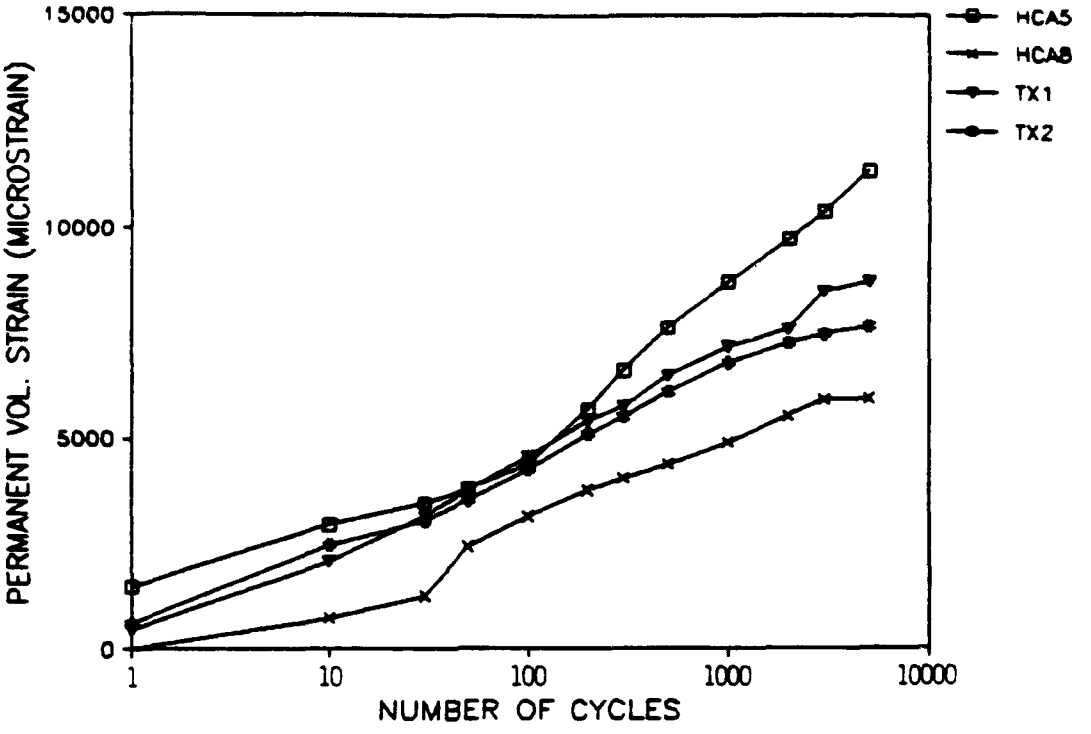

Figure 51. Comparison between Permanent Volumetric Strains obtained under identical $(q/p)_{max}$ from Repeated-load Triaxial Tests and Repeated-Load Hollow Cylinder Tests with Unidirectional Shear Reversal.

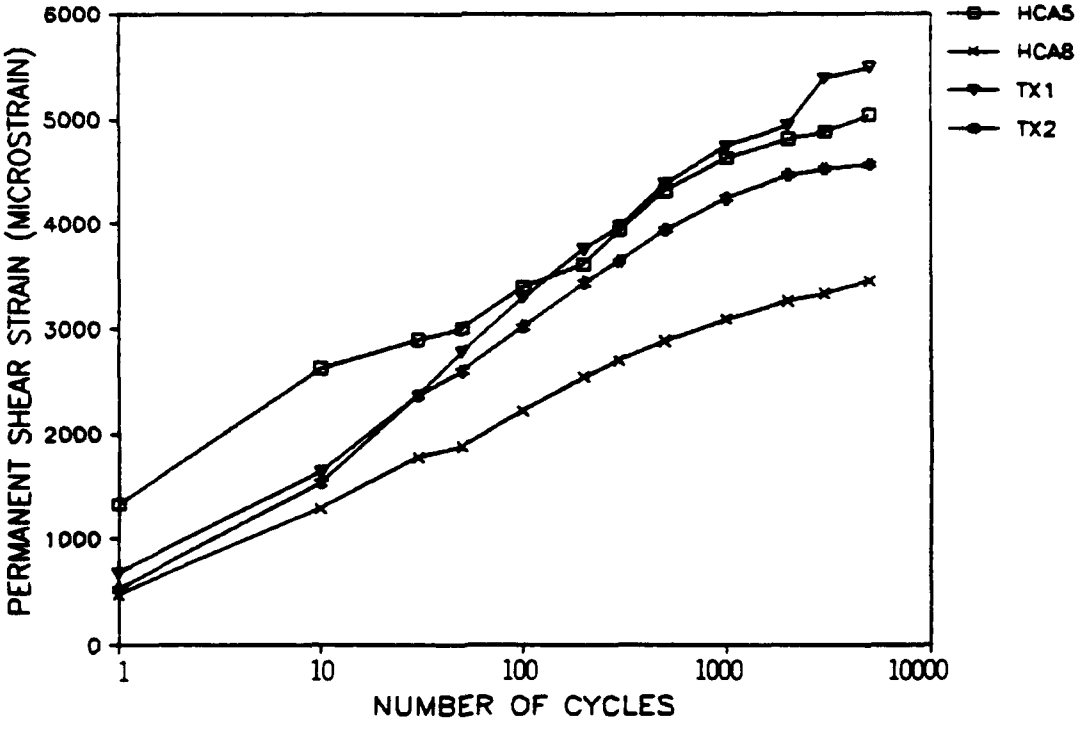

Figure 52. Comparison between Permanent Shear Strains obtained under identical $(q/p)_{max}$ from Repeated-load Triaxial Tests and Repeated-load Hollow Cylinder Tests with Unidirectional Shear Reversal.

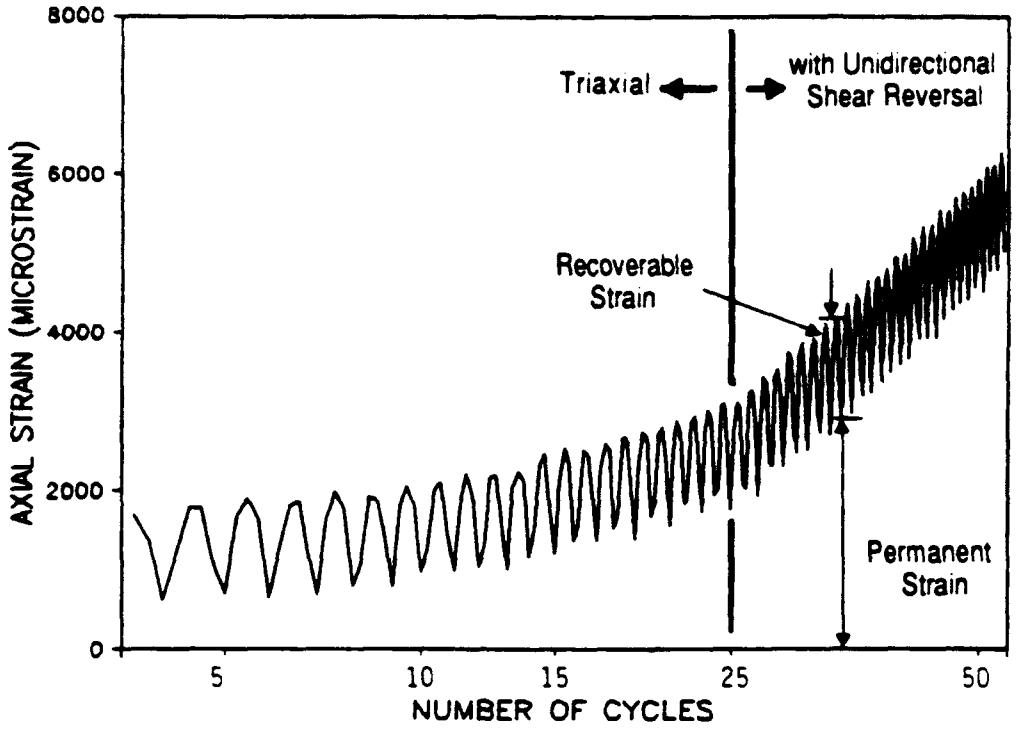

Figure 53. Variation of Axial Strain with Number of Stress Cycles in a 50-Cycle Test with Reversed Shear Stresses applied at the 25th Cycle.

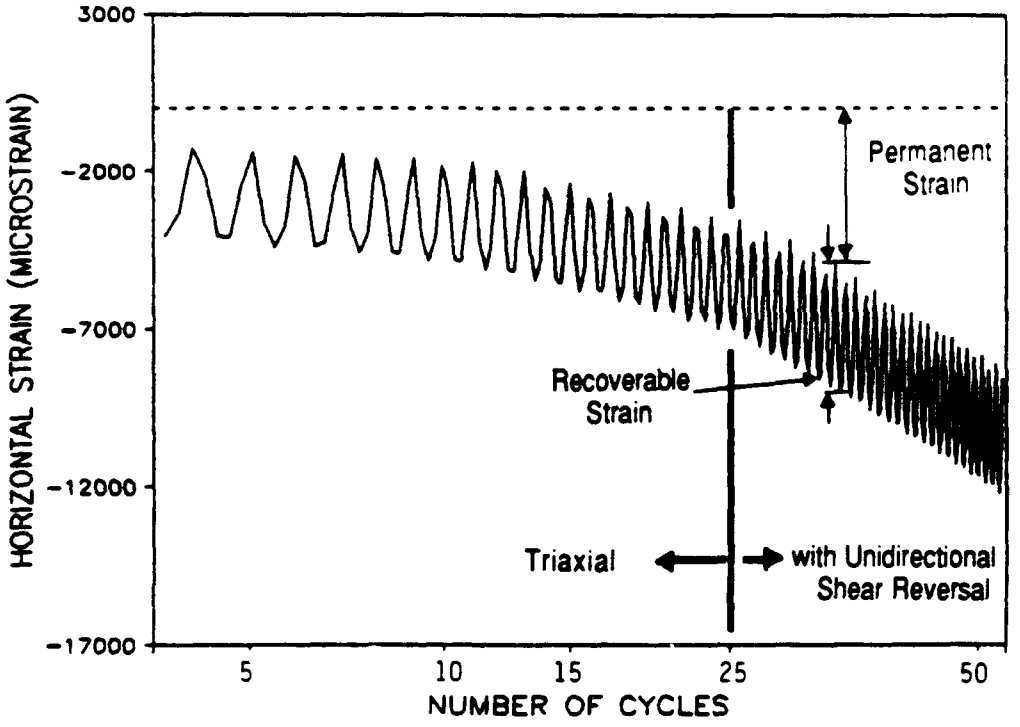

Figure 54. Variation of Horizontal (Sum of Radial and Circumferential) Strain with Number of Stress Cycles in a 50-Cycle Test with Reversed Shear Stresses applied at the 25th Cycle.

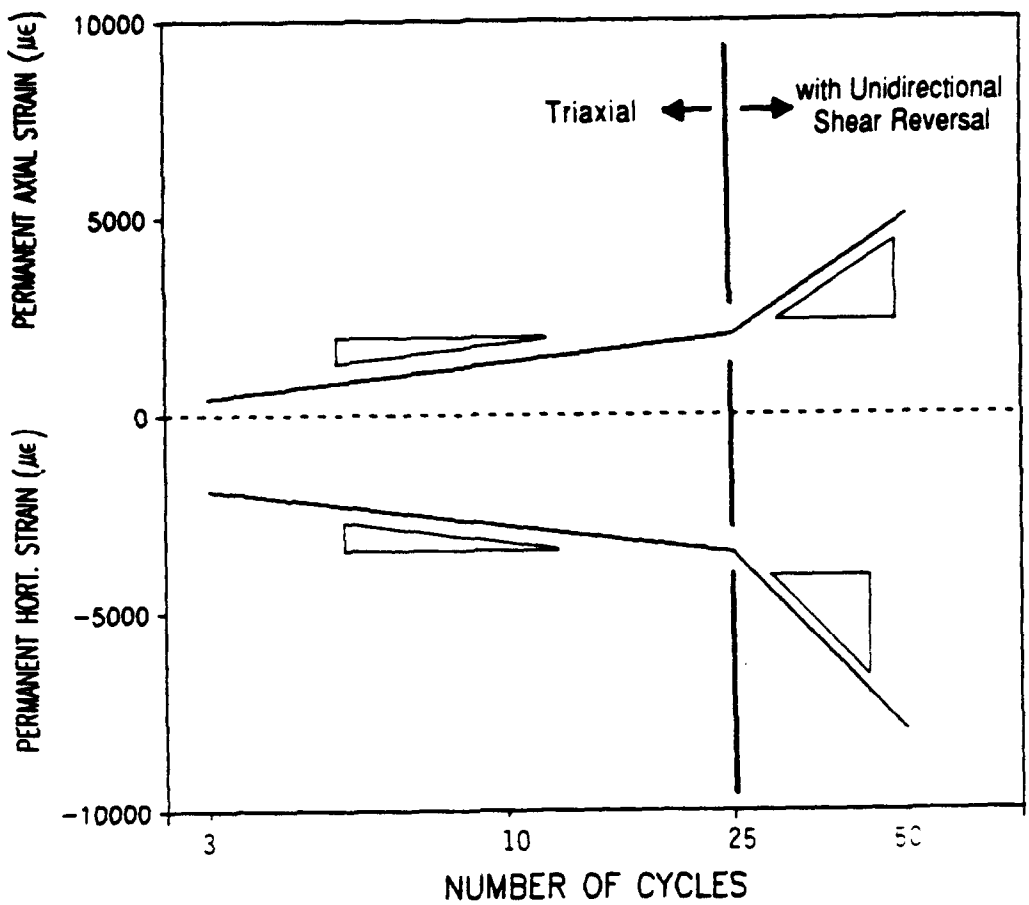

Figure 55. Simplified Plot of Variation of Permanent Strains with Number of Cycles showing the corresponding Strain Rates.

TABLE 6.

SUMMARY OF PERMANENT STRAIN RATES IN 50-CYCLE TESTS

Test Number	Axial Strain		Horizontal Strain		Volumetric Strain		Shear Strain	
	w/Shear	No/Shear	w/Shear	No/Shear	w/Shear	No/Shear	w/Shear	No/Shear
1	2600	2352	-300	-600	2100	1520	1100	1071
2	264	220	-76	-50	190	100	150	165
3	2530	334	-2616	-630	-346	-134	2375	289
4	5964	1832	-3737	-1532	1667	-209	4198	1443
5	10740	1471	-15226	-4712	-3924	-2513	8537	2242
6	1975	1859	-667	-860	325	-50	715	689
7	7291	3388	-14176	-9956	-2480	-2400	6501	3580

on the particular rate value. Examples can be found from the results for Tests 2 and 6. The strain rates obtained in these tests were generally very low despite an increased stress ratio $(q/p)_{max}$ (see Table 5).

A plot of the permanent strain rates obtained from stress conditions with unidirectional shear reversal against those from triaxial (no shear) conditions is shown in Figure 56. The plot contains values from the four strain components.

Figure 56 indicates that most data points lie well within the region where the absolute value of the permanent strain rate obtained under the condition with shear reversal is higher than that under triaxial condition. Note that the data points include results involving the two test sequences described in Table 5. Therefore, any possible strain history caused by the first 25 cycles of stress are considered in the comparison.

In Figure 56, the horizontal distance between the data points and the line of equality represents the difference between the two strain rates. Generally, large differences were obtained for both the permanent axial and horizontal strain rates. The change in strain rate for the permanent shear strain is somewhat smaller. The least difference in strain rate between the "with-" and

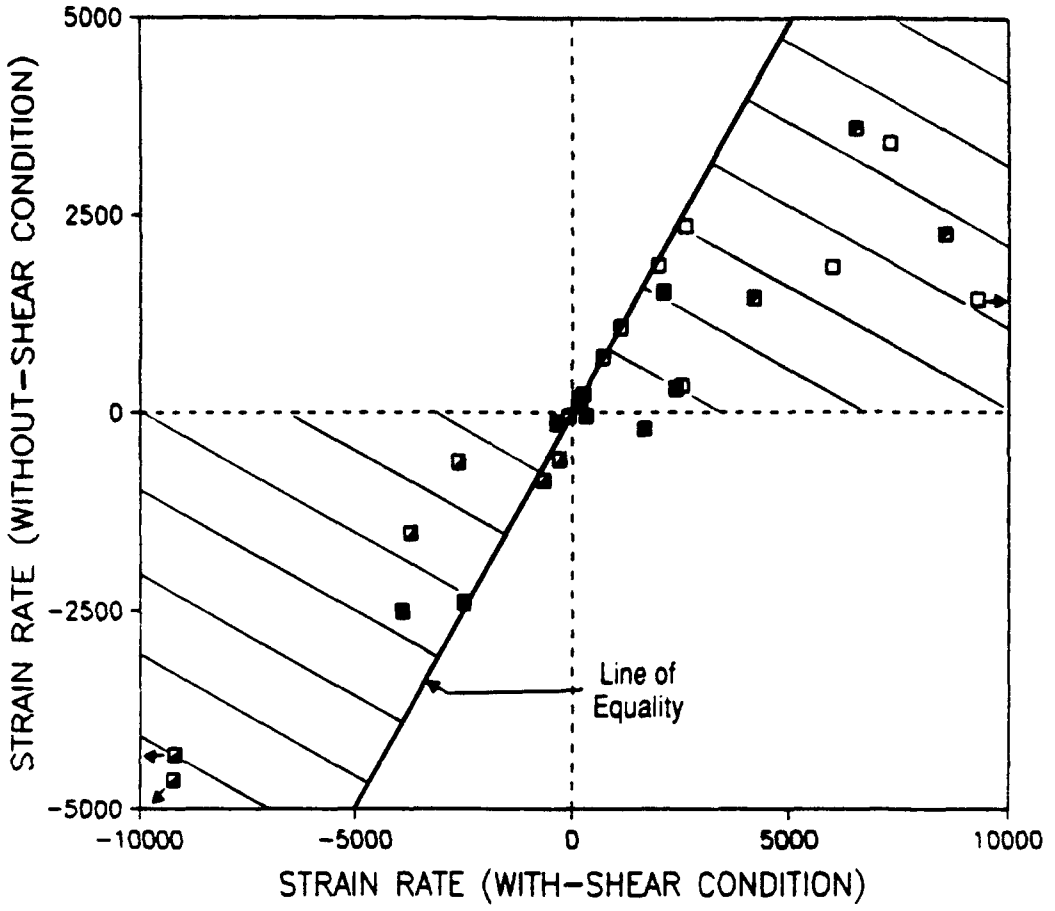

Symbol	Component of Strain
□	Axial
◪	Horizontal
■	Volumetric
◪	Maximum Shear
▨	Region where (strain rate) $_{\text{with shear}}$ > (strain rate)$_{\text{without shear}}$

Figure 56. *Comparison of Rates of Permanent Strain.*

"without-" reversed shear condition was that for the permanent volumetric strain. This is due largely to the fact that the signs for the permanent axial and horizontal strains are opposite. Hence, when their summation was performed to obtain the permanent volumetric strain, the effect due to the reversed shear stresses was significantly reduced. None the less, it is worth noting that in tests number 4 and 6, the permanent volumetric strain changed from dilatant when under triaxial condition to compressive when reversed shear stresses were applied (see Table 6).

D. RESILIENT STRAIN TESTS

1. Resilient Behavior during Permanent Strain Tests

The resilient behavior of the granular material during the permanent strain tests was continuously monitored. Comparisons of the resilient volumetric and maximum shear strains obtained during the nine tests are shown in Figures 57 and 58, respectively. All the strains were caused by the same stress conditions which were used for the particular permanent strain test. The comparisons generally indicate that the application of a reversed shear stress, either uni- or bidirectional, does not result in significant changes in the resilient behavior of the material. The only exception occurred, again, in the resilient volumetric strain of the first specimen of the first series (Figure 57a) which may have undergone some degree of strengthening due to previous straining. However, the overall results also indicate a gradual decrease in resilient strains as permanent strains build up.

2. Resilient Behavior under Wide Range of Stress Conditions

While Figures 57 and 58 only show the influence due to reversed shear stresses, more results were obtained from resilient strain tests performed on a separate hollow cylinder and one triaxial specimen. These tests covered a large number of stress paths which included variations in the angle of principle plane rotation and the intermediate principal stress. A summary of the results of these tests are presented in Appendix D.

For each stress path used in a resilient strain test, at least 50 cycles of stress were applied before the first set of strain responses was recorded. A duplicate set of results was taken after another 20 to 30 cycles (time required for the first set of data to be processed). The average of the two sets of results was then used for analysis. Since only one cycle of stresses and strains

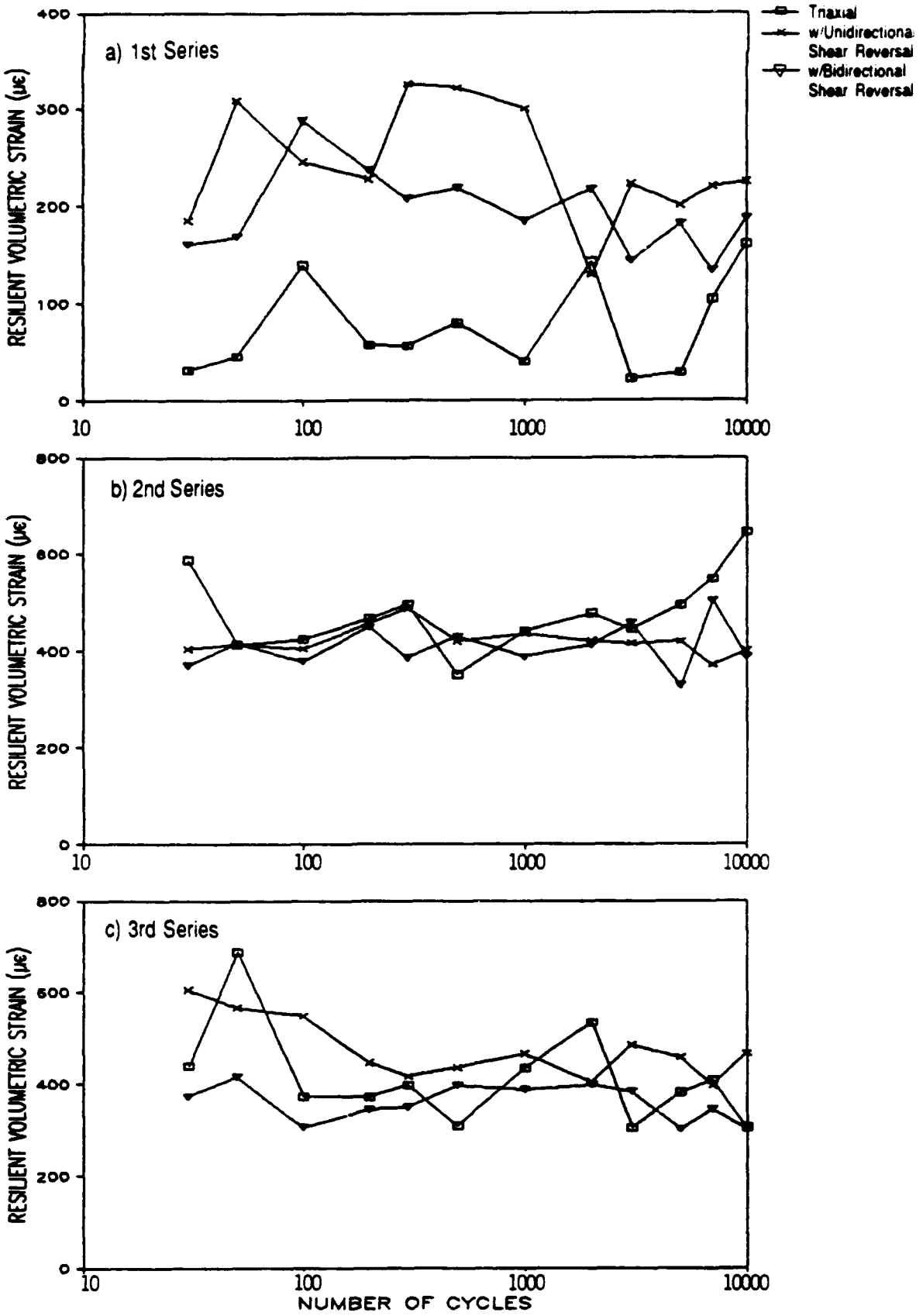

Figure 57. Variation of Resilient Volumetric Strains with Number of Stress Cycles in all Series of Permanent Strain Tests.

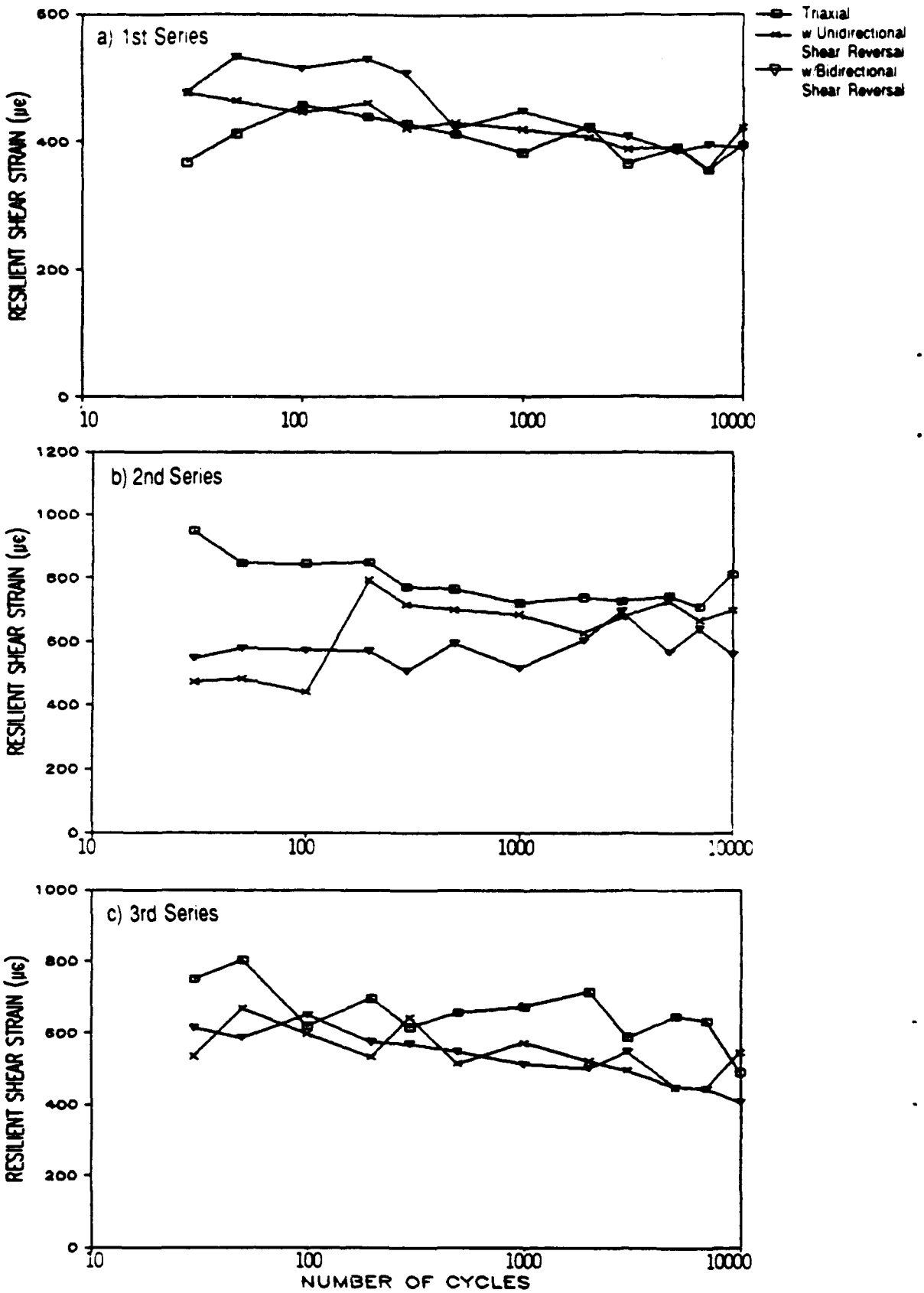

Figure 58. Variation of Resilient Maximum Shear Strains with Number of Stress Cycles in all Series of Permanent Strain Tests.

was normally recorded for each stress path used in a resilient strain test, it was possible to record 50 data points for each component of stress and strain.

a. Results of Tests carried out in the Repeated-load Triaxial Test Apparatus

Both the average resilient axial and radial strains were measured during the tests which involved the use of 19 stress paths. The stress-strain relationships of the granular materials was again summarized by the mathematical contour model described in Section IIC.

A multiple regression analysis was carried out to determine the coefficients used in Equations (7) and (9). The best fit values thus obtained are shown as follows:

G1= 1282	m= 0.20	
K1= 1596	n= 0.33	β= 0.08

where G1 and K1 are in kPa and the strains calculated are in fractions.

Plots of the resilient volumetric and shear strains calculated using the above coefficients against their measured values are shown in Figures 59 and 60 respectively. For the resilient shear strain, a correlation coefficient, R^2, of 0.96 was obtained. For the resilient volumetric strain, R^2, was 0.95. The overall high R^2 values confirmed that the contour model was able to predict the resilient behavior of the granular material tested by the repeated-load triaxial apparatus.

b. Results of Repeated-load Hollow Cylinder Tests

(1) Triaxial Stress Paths

Before analysis of the cases involving principal plane rotation, it appeared to be appropriate to consider the stress-strain behavior of the hollow cylinder specimens tested under triaxial stress conditions. To do this, the same contour model described in the last section was used. In order to allow direct comparison of the coefficients which governed the resilient shear modulus, the shear strain as defined in Equation (2) was used. The principal values involved in the equation were in turn calculated using Equations (30) and (31). For the evaluation of bulk modulus, the volumetric strain as defined in Equation (35) was used.

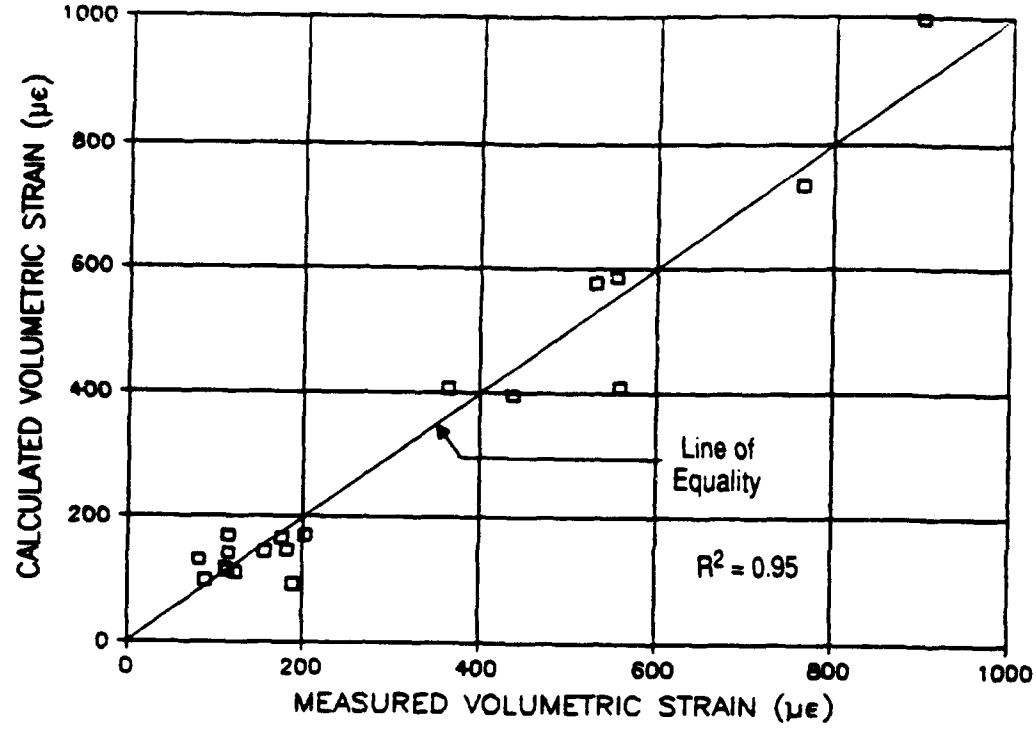

Figure 59. Comparison of Predicted and Measured Resilient Volumetric Strain from Repeated-Load Triaxial Tests.

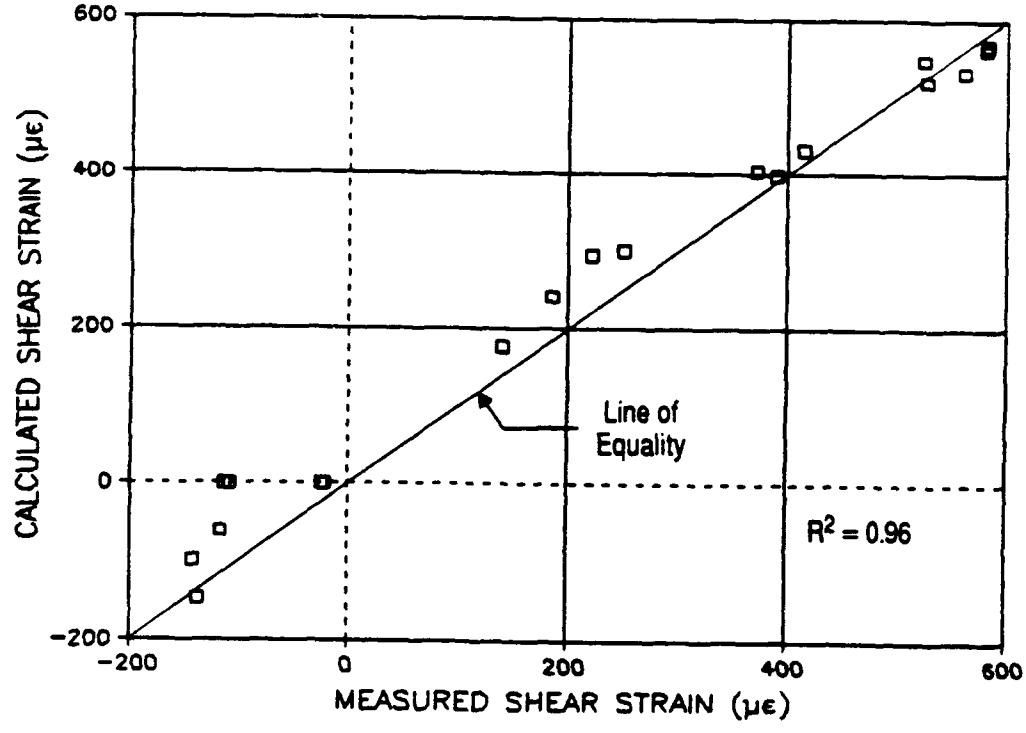

Figure 60. Comparison of Predicted and Measured Resilient Shear Strain from Repeated-Load Triaxial Tests.

A total of 23 triaxial stress paths were used in the resilient strain tests performed by means of the HCA. A multiple regression analysis performed on the results of these tests yielded the following results:

G1 = 994	m = 0.20	
K1 = 809	n = 0.33	β = 0.08

where G1 and K1 are in kPa and the strains calculated are in fraction.

Plot of the calculated resilient volumetric and shear strains against their measured values are shown in Figure 61 and 62 respectively. The R^2 value for the resilient shear strain is again very high but that for the volumetric strain is very much reduced. However, the best fit values for the coefficients m,n and β, obtained independently by multiple regression analysis, are the same as those obtained from tests using the repeated-load triaxial apparatus. This indicates that both laboratory devices are consistent in determining the non-linear and stress-dependent components of the behavior model used. However, for the remaining constants, K1 and G1, they were found to be respectively 97 percent and 29 percent less than their counterparts obtained from the triaxial test apparatus.

(2) Stress Paths involving Principle Plane Rotation

To model the behavior of granular material under rotating principal stresses, it is vital to know the directions of the strain change. In traditional material science theories, the general assumption is that during elastic behavior, the directions of principal stress and strain coincide. In this project, this assumption was examined first.

Figures 63 to 66 show the variation in the angles of major principal stress and strain (from the vertical direction) with time during one cycle of loading. The figures embrace the results from four different stress paths involving different modes of stress and strain rotation. The data shown in the figures were calculated from measured responses which were not electronically or mathematically filtered. As a result, they are subjected to errors due to electrical "noise" and other interference in the measuring system. Despite this, they indicate that the rotations of major principal stress and strain are generally coincident.

This finding is particularly encouraging as it suggests that there is no need for a stress-strain model to consider the additional relationship between the direction of stress

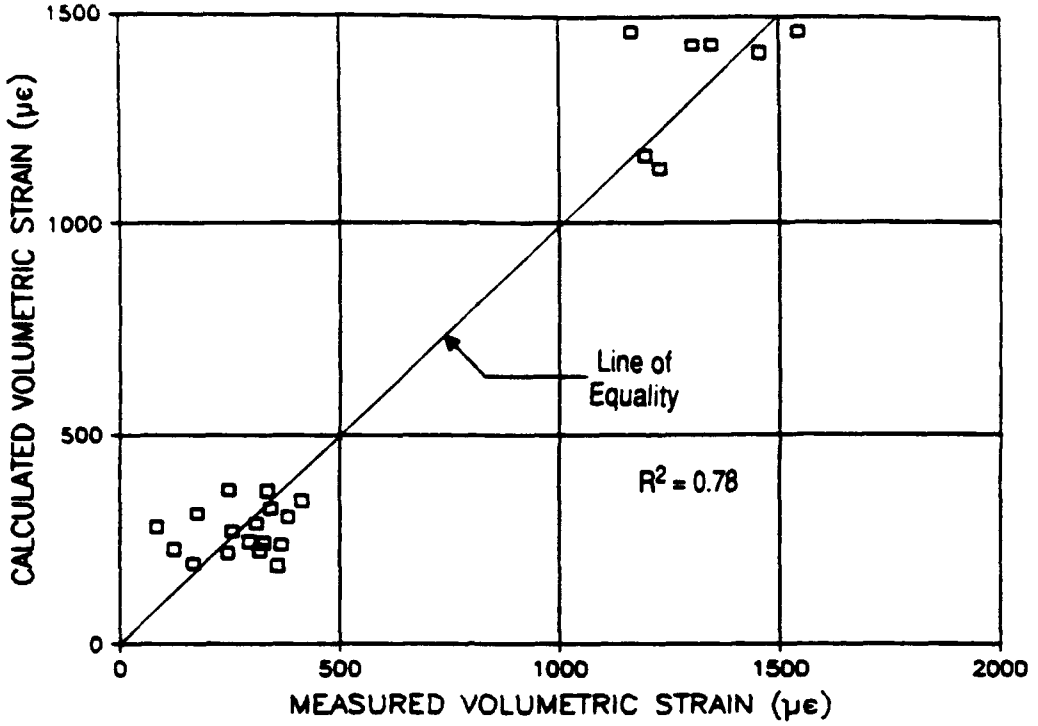

Figure 61. Comparison of Predicted and Measured Resilient Volumetric Strain from Repeated-Load Hollow Cylinder Tests under Triaxial Stress Conditions.

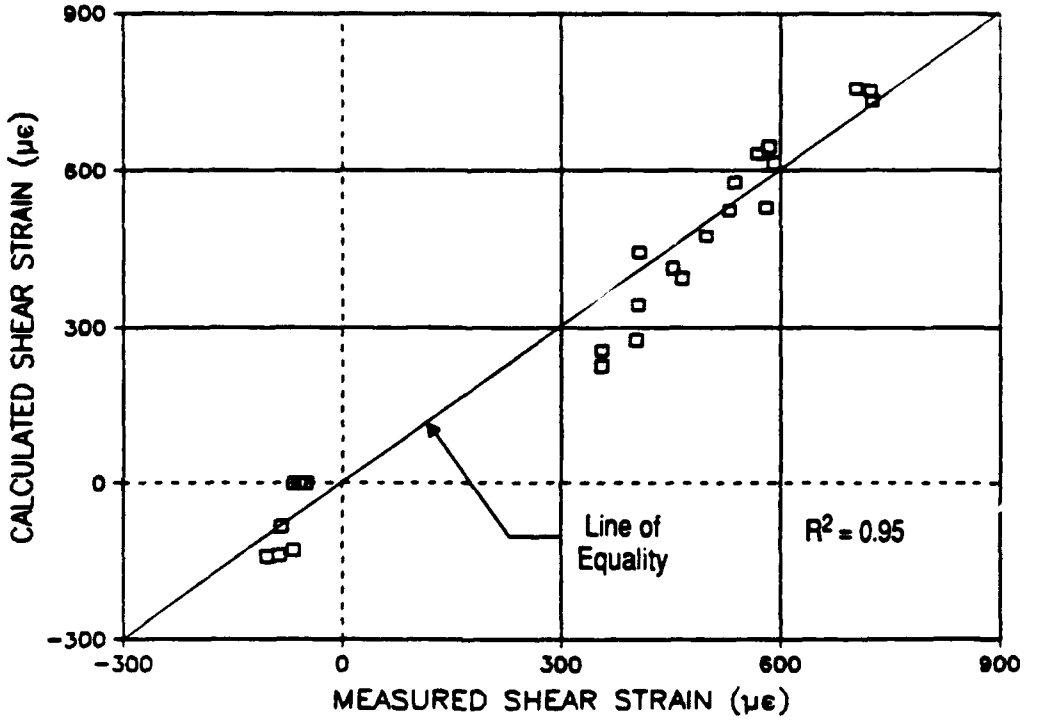

Figure 62. Comparison of Predicted and Measured Resilient Shear Strain from Repeated-Load Hollow Cylinder Tests under Triaxial Stress Conditions.

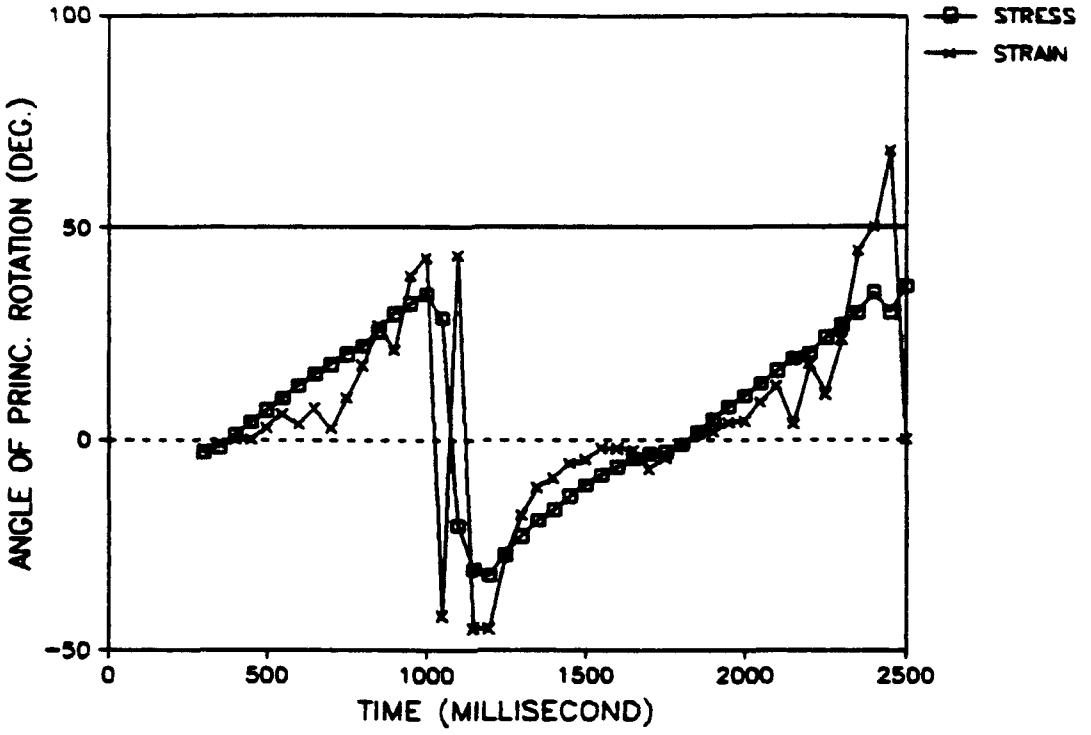

Figure 63. Relationship between Rotation of Principal Stress and Strain Planes (when Pi =Po= 100 kPa; σ_z varies from 100 to 250 kPa; $\tau_{z\theta}$ varies from -22 to 22 kPa and the phase angle shift between σ_z and $\tau_{z\theta}$ is +90°).

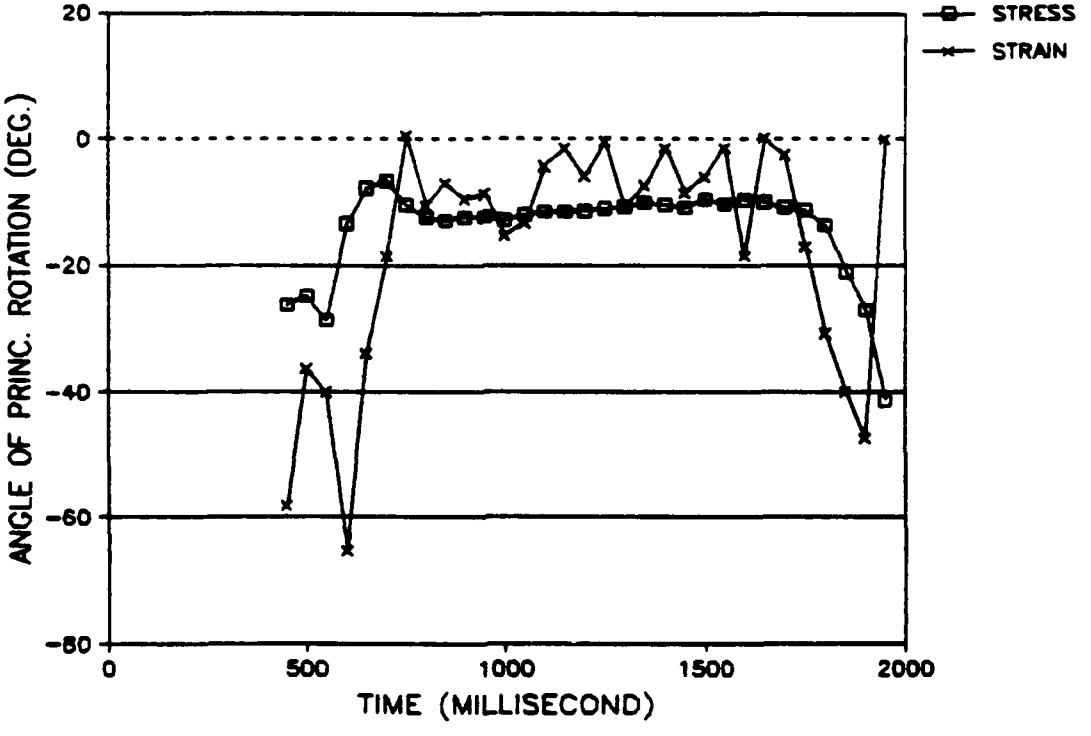

Figure 64. Relationship between Rotation of Principal Stress and Strain Planes (when Pi =Po= 100 kPa; σ_z varies from 100 to 200 kPa; $\tau_{z\theta}$ varies from 0 to 20 kPa and the phase angle shift between σ_z and $\tau_{z\theta}$ is 0°).

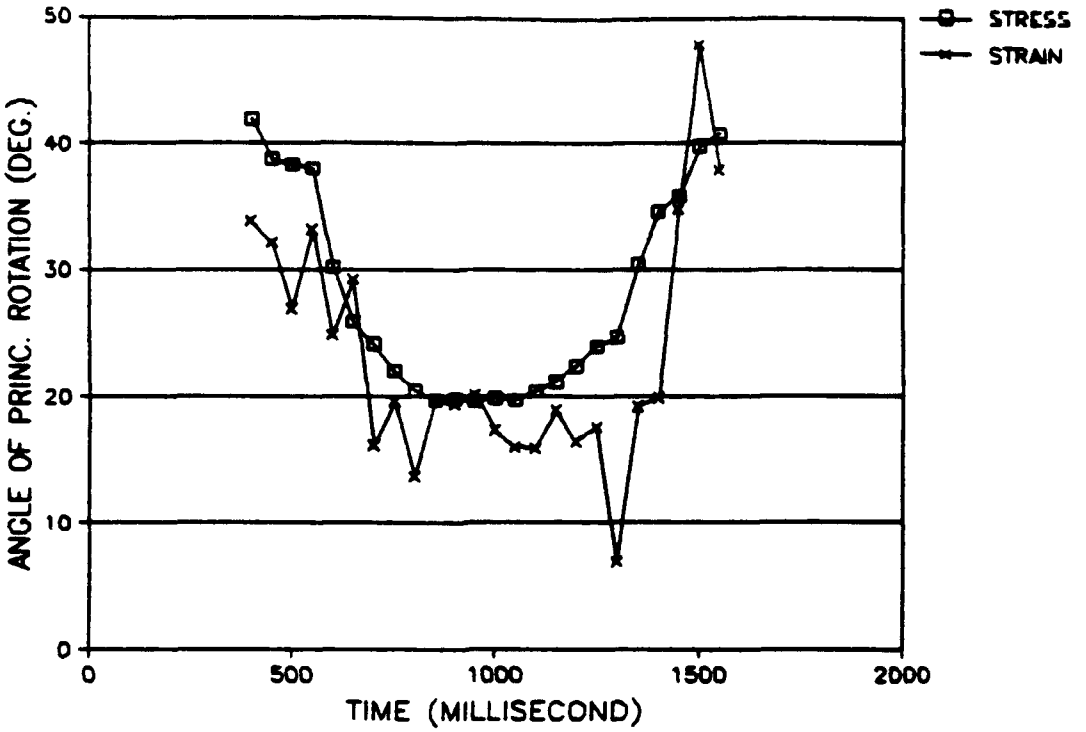

Figure 65. Relationship between Rotation of Principal Stress and Strain Planes(when Pi =Po= 100 kPa; σ_z varies from 100 to 150 kPa; $\tau_{z\theta}$ = 20 kPa)

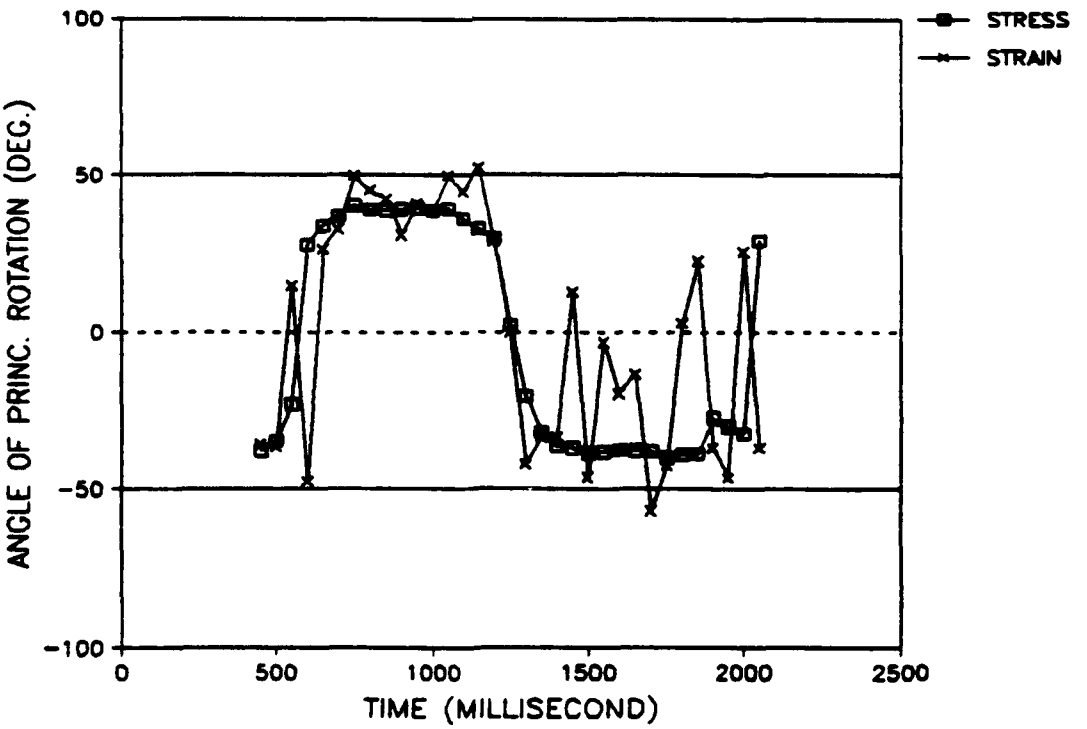

Figure 66. Relationship between Rotation of Principal Stress and Strain Planes(when Pi =Po= 100 kPa; σ_z =100 kPa; $\tau_{z\theta}$ varies from +20 to -20 kPa)

and strain. As a result, the use of an invariant approach, such as the contour model, to represent the general stress and strain conditions may still be considered appropriate. However, in doing so, the angle of principal plane rotation, α and possibly, the b-value which is used to characterize the intermediate principal stress, may need to be included.

The development of a resilient stress-strain models under general stress conditions is beyond the scope of this project. Therefore, the investigation performed here is only limited. The analysis consisted of using the contour model and the coefficients established earlier for the triaxial conditions to predict the resilient strains under the new and more complex stress conditions which involved principal plane rotation. In the prediction calculation, only principal stresses and strains were used. The applicability of the model was then evaluated by determining how well strains could be predicted.

As shown in Figure 67, the correlation between the predicted and measured resilient shear strains for the 133 stress paths which were used is generally very good with R^2 equal to 0.93. This indicates that principal plane rotation, which is not represented in the stress-strain model does not have much influence on the shear behavior. The results also show that, for the stress conditions analyzed which cover a wide range of b values (see Figure D-1,Appendix D), the effect of the intermediate principal stress, σ_2, can be satisfactorily represented by the stress invariant p. It is worth noting that better correlation is generally obtained when the strain is positive than negative.

To calculate resilient volumetric strain, the invariant for shear stress, q in equation 9 was replaced, more appropriately, by the octahedral value, q_{oct}. This also necessitates the correction of the β value in the equation. A plot of the calculated and measured strains is shown in Figure 68. Although a general trend towards equality was observed, considerable scatter of results and a marked drop in the degree of correlation were obtained. In order to investigate the discrepancy, the value, $\delta\epsilon_v$ defined as:

$$\delta\epsilon_v = \epsilon_{v_{(measured)}} - \epsilon_{v_{(predicted)}} \qquad (37)$$

was singled out for further analysis.

Figure 69 shows a plot of $\delta\epsilon_v$ against $\delta\tau/p_m$ which represents the change of torsional shear stress normalized by the mean p value, p_m. A similar plot of $\delta\epsilon_v$ against $\delta b/\eta_m$ which represents the cnange in b value normalized by the mean shear stress ratio, $(q_{oct})_m/p_m$, is shown in Figure 70. These normalized parameters were chosen simply because they

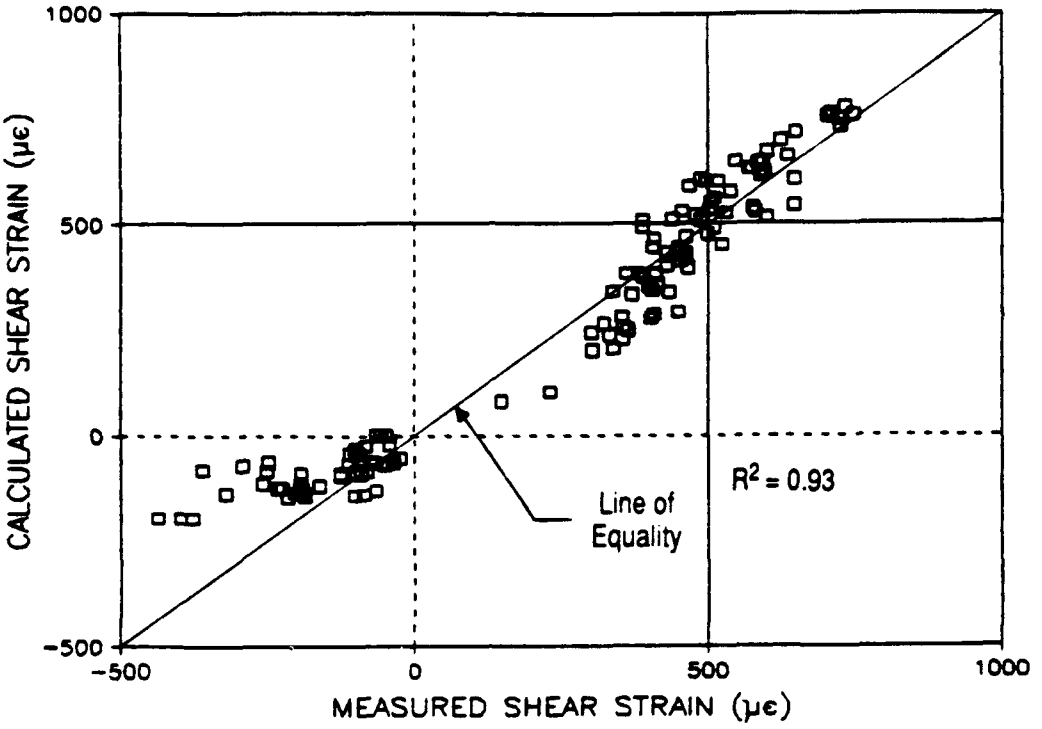

Figure 67. Comparison of Predicted and Measured Resilient Shear Strain from Repeated-Load Hollow Cylinder Tests under General Stress Conditions.

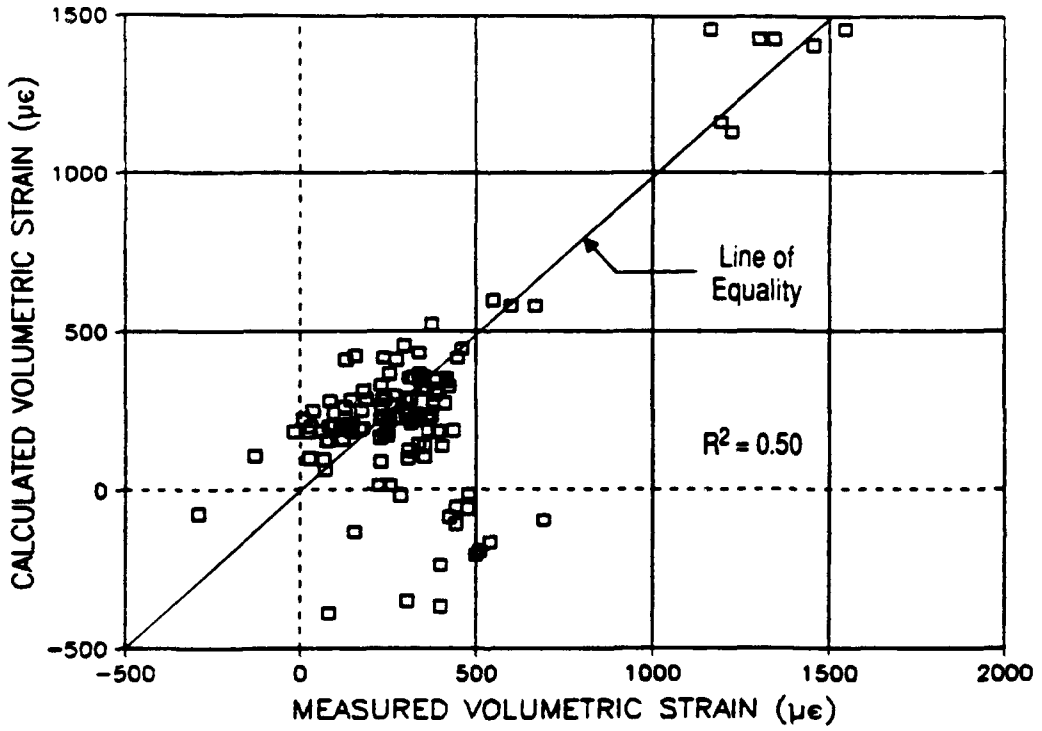

Figure 68. Comparison of Predicted and Measured Resilient Volumetric Strain from Repeated-Load Hollow Cylinder Tests under General Stress Conditions.

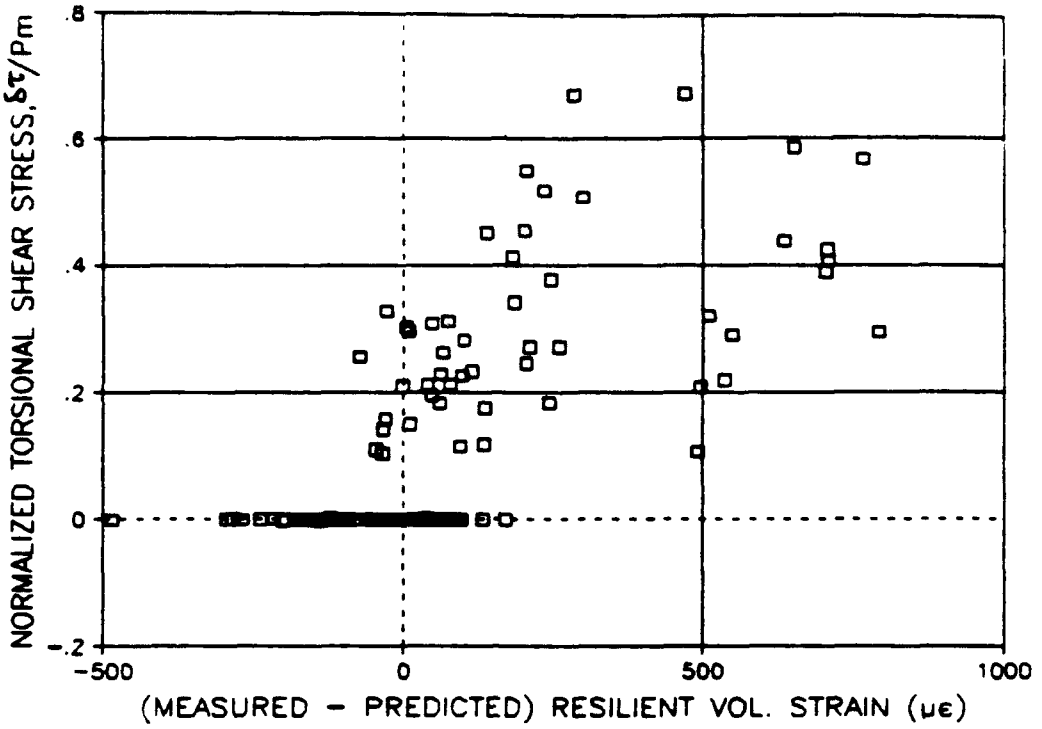

Figure 69. Variation of Normalized Torsional Shear Stress with Errors in Predicted Resilient Volumetric Strains in Repeated-Load Hollow Cylinder Tests.

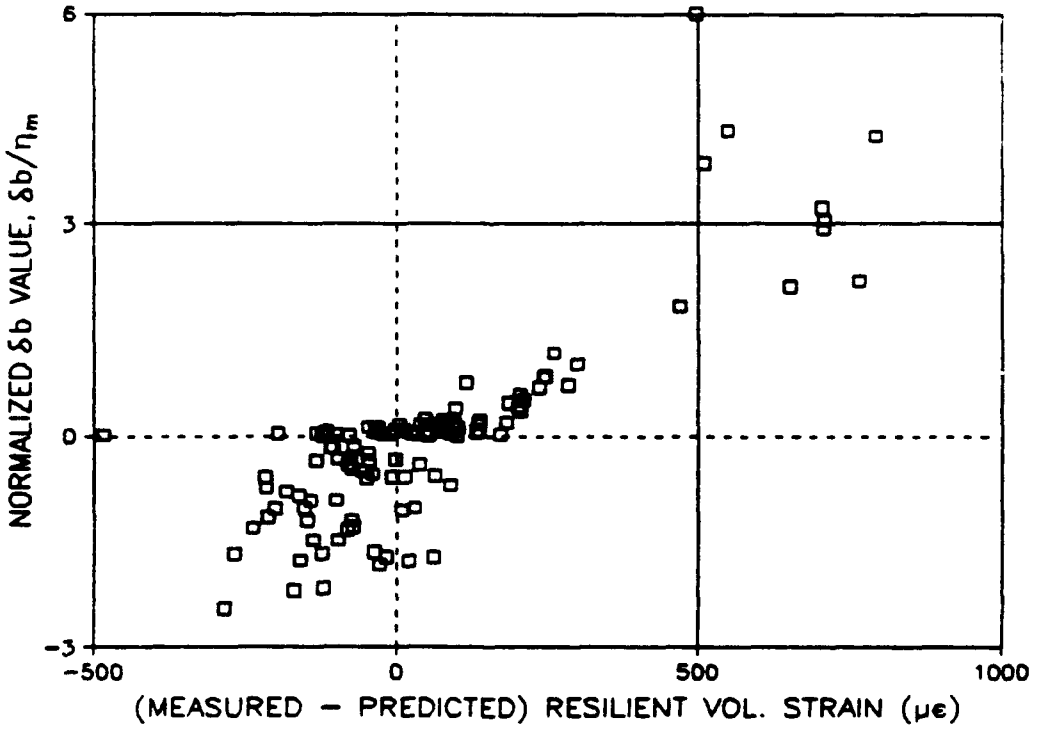

Figure 70. Variation of Normalized δb-value with Errors in Predicted Resilient Volumetric Strains in Repeated-Load Hollow Cylinder Tests.

fulfilled the vital requirement of being dimensionless and were able to represent respectively, the effect of principal plane rotation and the variation in intermediate principal stress. Furthermore, both parameters include the mean normal stress value, p and shear stresses, in the form of either τ or q_{oct}, which are of fundamental importance in the strain behavior of granular materials. Hence, they both have good potential to be included in the development of an improved stress-strain model.

Despite the widespread scatter of results in both figures, Figure 69 shows a tendency for higher change of torsional shear stress to cause more compressive volumetric strain than predicted. This finding is in apparent agreement with those of the permanent strain tests regarding the effect of the torsional shear stresses.

Figure 70 suggests that, for those stress paths which involved a decrease of b-value (i.e. $+\delta b$), the contour model tends to underpredict the compressive volumetric strain. However, when δb is negative, higher strain is predicted. Very little consideration has been given to the effect of the b-value on resilient behavior of granular material. One set of test results which has close relevance to the data presented here is from the triaxial extention-compression tests performed by Pappin (18). In those tests, b changed from 1 during extention to 0 when under compression. Hence δb equal to +1. He found that most of his calculated resilient volumetric strains were also underpredicted.

E. DISCUSSION OF RESULTS

1. Permanent Strain Behavior

Results of the hollow cylinder tests indicate that the permanent strain behavior of granular material is affected by the reversed shear stresses. However, because of the limited number of tests and stress conditions involved, it is difficult to draw any definite conclusion about their influence. The tests revealed that, when stress conditions are approaching failure, the rate of development of permanent strain may be significantly increased due to the additional reversed shear stresses. In conditions where $(q/p)_{max}$ is low and when the magnitude of the reversed shear stress is small, compared with other normal stresses, the difference between the strain response under the "with-shear" and triaxial conditions may be small. Under these low stress conditions, results of tests performed by the less complicated repeated-load triaxial test apparatus were found to be sufficiently accurate.

Results of the permanent strain tests consistently suggest that higher permanent strains, both volumetric and maximum shear, are obtained due to bidirectional reversed shear stresses. This finding appears to conform with the results of the large-scale rutting tests carried out in the Pavement Test Facility.

2 Resilient Strain Behavior

Although the scale of effort invested in the study of the resilient strain behavior was not as large as that for the permanent strain, a few interesting findings were obtained. One which may be considered important is the observation that rotation of principal stress and strain planes were coincident during resilient tests. This provides support for the continuing use of a relatively simple invariant approach to model the resilient behavior even under the more complex stress conditions. The investigation showed that the resilient shear strain in the plane where the torsional shear stress was acting was independent of the rotation of the principal plane caused by the shear stress. It further indicated that the contour model and its coefficients, obtained from tests under triaxial conditions, could be used to provide reasonably good predictions of the shear strain under a much wider range of complex stress conditions.

The volumetric behavior, however, was difficult to model correctly; nonetheless, an indication of behavior relating to the applied torsional shear stress and the variation of the intermediate principal stresses was obtained. This should provide some insight for future improvement of models for resilient volumetric strain.

Tests carried out in the repeated-load triaxial apparatus and the HCA yielded similar coefficients for the contour model. However, under identical stress conditions, the volumetric strains obtained from the HCA were found to be higher. One possible reason for the discrepancies could be due to the small gauge length in the radial direction of the hollow cylinder specimen. Compared with that in the circumferential direction of the same specimen and the radial direction of a triaxial specimen, it was respectively 8 and 5.4 times less. As a result, any possible error will be magnified by the same order. As the calculation of the resilient maximum shear strain in the hollow cylinder is independent of the radial strain, the discrepancy between the results obtained from the two pieces of apparatus was found to be very much reduced.

SECTION VII

VALIDATION OF REPEATED-LOAD HOLLOW CYLINDER TESTS

A. INTRODUCTION

The potential of the HCA to simulate moving traffic in laboratory element tests was demonstrated in the last section. The results of the tests indicated that the permanent deformation behavior, in particular, of granular material was very much influenced by the characteristic reversed shear stresses from a moving wheel load. In order to ensure that the HCA will continue to serve as an important and useful laboratory device for the study of granular material behavior for pavement applications, validation of the current test data by means of wheel tracking experiments in the Pavement Test Facility appeared to be desirable.

Emphasis of these validation tests was placed on the permanent deformation behavior of the granular material. This was because the latter behavior is generally difficult to model theoretically and, hence, its incorporation in any analytical design method will depend directly on the results of individual laboratory tests, such as those performed in this project.

B. APPROACH TO THE VALIDATION EXPERIMENT

The objective of the experiment was to reproduce the same stress conditions in the granular base of the PTF tests under a moving wheel as those imposed on the specimen in the earlier hollow cylinder tests which involved reversed shear stresses. Comparison of the permanent deformation response of the granular base was then made with that of the hollow cylinder specimen. The main comparison was limited to the permanent vertical strain which is closely related to the rut formation in the pavement.

Unlike the uniform stresses experienced by the hollow cylinder specimen, the magnitudes of the stress components within the granular base layer varied with the depth below the pavement surface. Furthermore, the magnitudes of the longitudinal (i.e. parallel to the direction of traffic) and lateral stresses in the pavement were not only different, but also were believed to be influenced by residual stresses resulting from the compaction process. These stresses are very difficult to measure. As a result, it became clear that only part of the granular base would experience similar

stresses to those used in the HCA tests and that matching of all components of stress at a general depth within the layer would be difficult, if not impossible.

Nevertheless, to identify an appropriate part of the granular base for comparison of response, a comprehensive instrumentation program was designed so that the stresses and the corresponding strains, both resilient and permanent, could be captured. However, matching the stresses would be hampered by the limited number of stress measuring device that could be installed in the granular layer. Therefore, it appeared advantageous to use the measured resilient vertical strain, which, in turn, depended on the overall stress changes, as the primary matching criterion for the validation experiment. The limited number of stress measurements, on the other hand, would be used in an analytical evaluation procedure to aid the determination of a more complete stress pattern throughout the granular layer.

Efforts were also made to ensure that other test condition, with the exception of the means of loading, were similar. These conditions included:

1. Materials

Both the granular materials used in the HCA and PTF tests were produced by the same quarry with maximum particle size of 5 mm and Fuller's "n" value of approximately 0.4. As the material was formed by only one bin size of aggregates, variations of grading were found to be negligible. Whilst approximately 21 kg of materials was needed for each HCA test. over 3000 kg of material was used in the large-scale experiment. The granular base was overlain by a British Standard (29) gap graded bituminous wearing course and underlain by a stiff silty clay subgrade with CBR of about 5 percent.

2. Means of Compaction

Both materials were subjected to a vibratory type of compaction. The granular base was compacted by a vibrating roller, while the granular material in the HCA tests was compacted by a vibrating table. The similarity in method of specimen preparation may help to reduce the influence on behavior due to the possibly different fabric caused by different means of compaction.

3. Dry Density and Moisture Content

The dry density of the granular base was continuously monitored during compaction by means of a nuclear density meter. The average dry density of the base was 1953 kg/m^3, which compared with 2000 kg/m^3 for Specimens 5 and 8 of the HCA tests. Moisture content of the granular base was about 2 percent after a limited period of air drying. In the HCA tests, however, dry materials were used.

C. PAVEMENT DESIGN

The thickness of the granular base was dictated by the number of instruments that needed to be accomodated. As a result, the minimum thickness of 225 mm was used. The existing subgrade condition was considered acceptable. Therefore, the only design variable was the thickness of the bituminous layer. The computer program, BISTRO (30), which is based on linear elastic layer theory, was used to guide the preliminary design. The elastic moduli for the bituminous and subgrade materials were estimated on the basis of past research. However, test results presented in the last section were used to obtain moduli for the granular base. The design also took into consideration the range of contact stresses provided by the PTF. The final designed thickness of the bituminous layer was 60 mm. With this value, it was estimated that the vertical stress and strain at the middle of the granular base due to a 8 kN wheel load would be similar to that used in the HCA tests.

Due to the crudeness of the design method and recognizing the complex stress-strain behavior of pavement materials, it was decided that two identical pavement sections, both fully instrumented, should be constructed and tested. The first pavement was used in a series of trials in which the moving wheel load was progressively increased and the stresses and strains in the granular base were continuously monitored. The final wheel load was selected when the target stress conditions in the granular base were achieved. This wheel load was then used from the beginning of the test performed on the second pavement section. Both pavement tests involved over 10,000 passes of the wheel which was loaded unidirectionally along a single track. Wheel speed was about 3.6 km/hr and the test temperature was 20 to 25 °C. A photograph of the two tracks used in the experiment is shown in Figure 11 (Page 25).

D. INSTRUMENTATION

The pavement sections were instrumented using diaphragm pressure cells, developed at Nottingham, and Bison inductance strain coils. Details of instrument characteristics and method of calibration are reported elsewhere (31). Details of the arrangement of instruments in one pavement section are shown in Figure 71. The use of two columns of strain coils allowed vertical strains at five locations along the depth of the granular base to be captured. Despite the need for detailed stress distribution, the number of pressure cells had to be limited in order to prevent the relatively thick cable and large cells from interfering with the stress field. A pressure cell inclined at 45 degrees to the vertical was included to allow calculation of shear stress in the material. A photograph of the arrangement of the pressure cells is shown in Figure 72. Other pertinent data, such as the tensile strain at the bottom of the bituminous layer and the vertical strain at the top of the subgrade were also covered by the instrumentation program.

In addition to the instrumentation installed within the pavement materials, a profilometer (Figure 73), consisting of a linear potentiometer mounted on a roller carriage, was used. It was connected to an X-Y plotter which provided hard copies of the measured transverse surface profile.

E. RESULTS OF THE VALIDATION EXPERIMENT

The final wheel load used for the experiment was 10kN. A plot of the variation of wheel load and position with time is shown in Figure 74. It indicates that a rather uniform load is achieved when the wheel moves in the forward direction and no loading is imposed on the pavement when the wheel is in reverse. The slope of the line for the wheel position indicates that a uniform velocity is achieved.

Recording of the resilient strains, transient stresses, wheel load and wheel position was made by means of a data acquisition system which comprised a personal computer and a 12-channel, fast A/D converter. Permanent strains were measured at appropriate intervals when the wheel was stopped and unloaded.

1. Resilient Strain

Plots of typical recorded strain pulses at various locations in the pavement are shown in Figure 75 to 80. The pulse time due to the moving wheel varied from about 0.4 second at

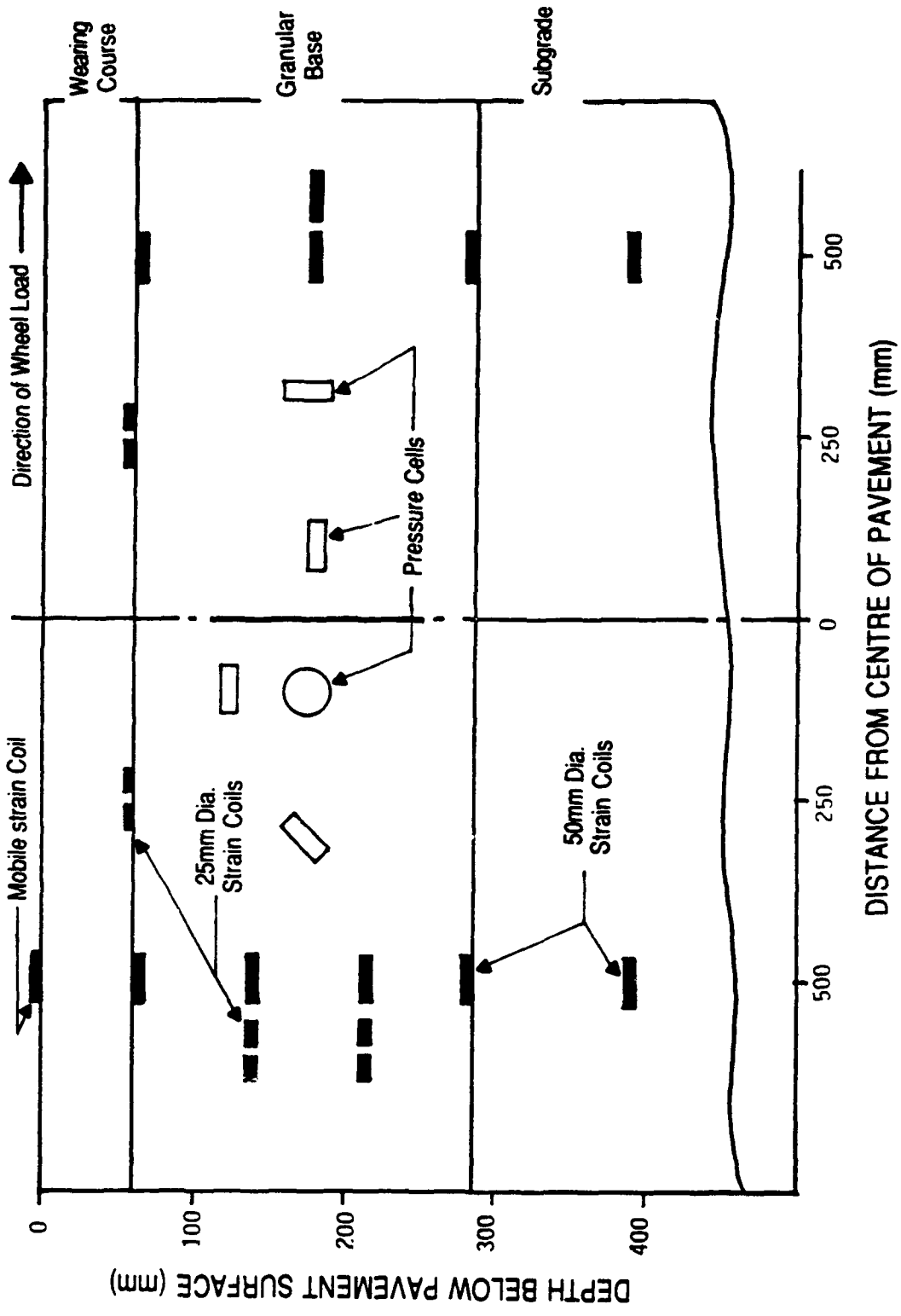

Figure 71. Side View of Layout of Instrumentation used in the Validation Experiment.

Figure 72. Arrangement of Pressure Cells installed in Granular Base.

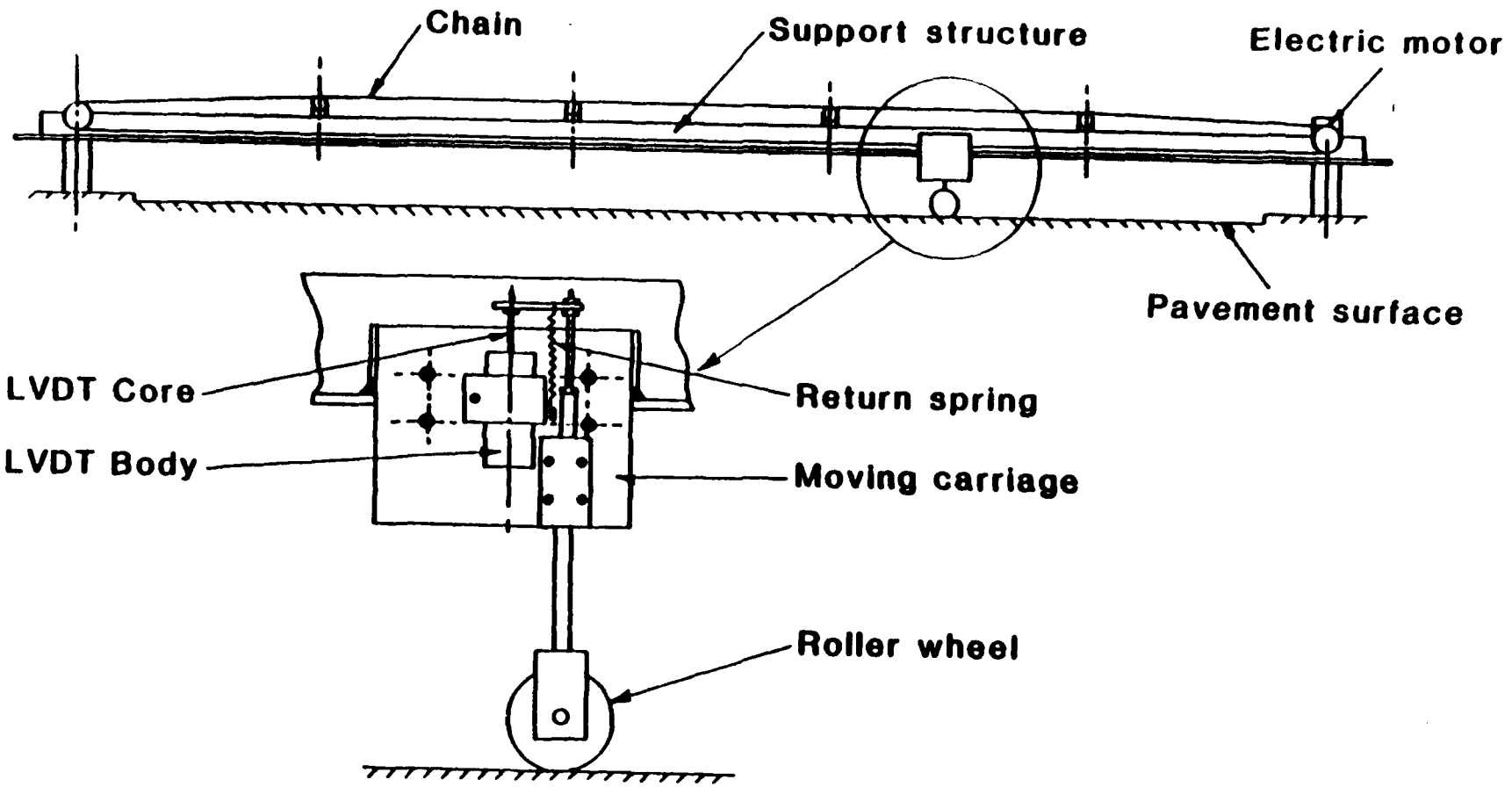

Figure 73. Profilometer used for Measurement of Transverse Profile of Pavement Sections.

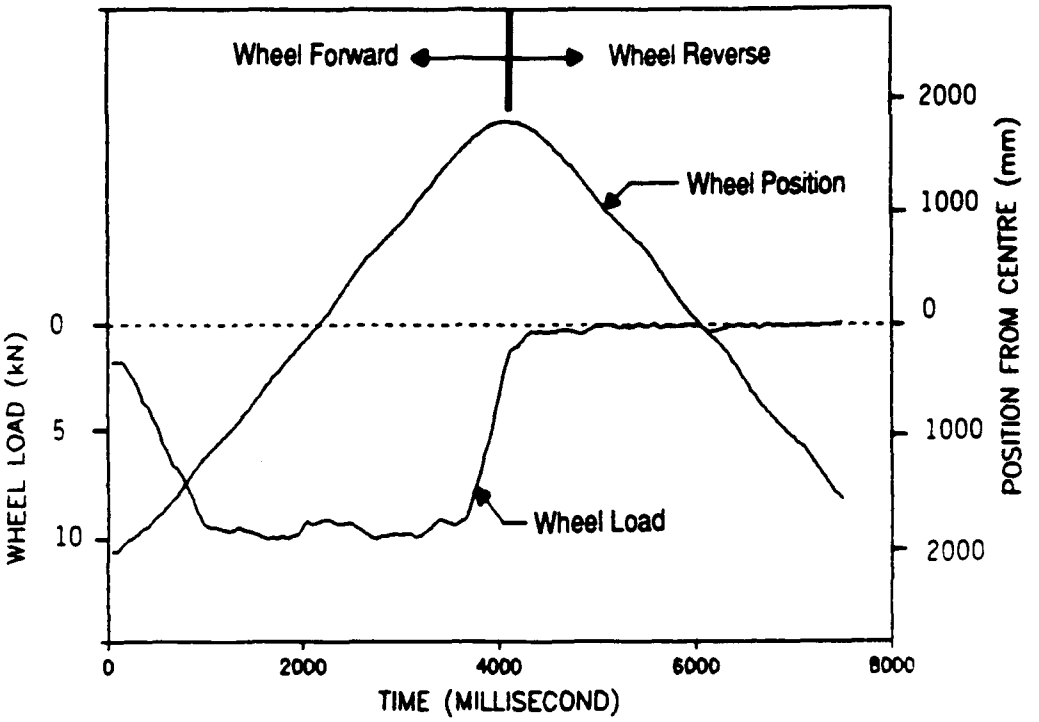

Figure 74. Variation of Wheel Load and Position from Center of Section with Time.

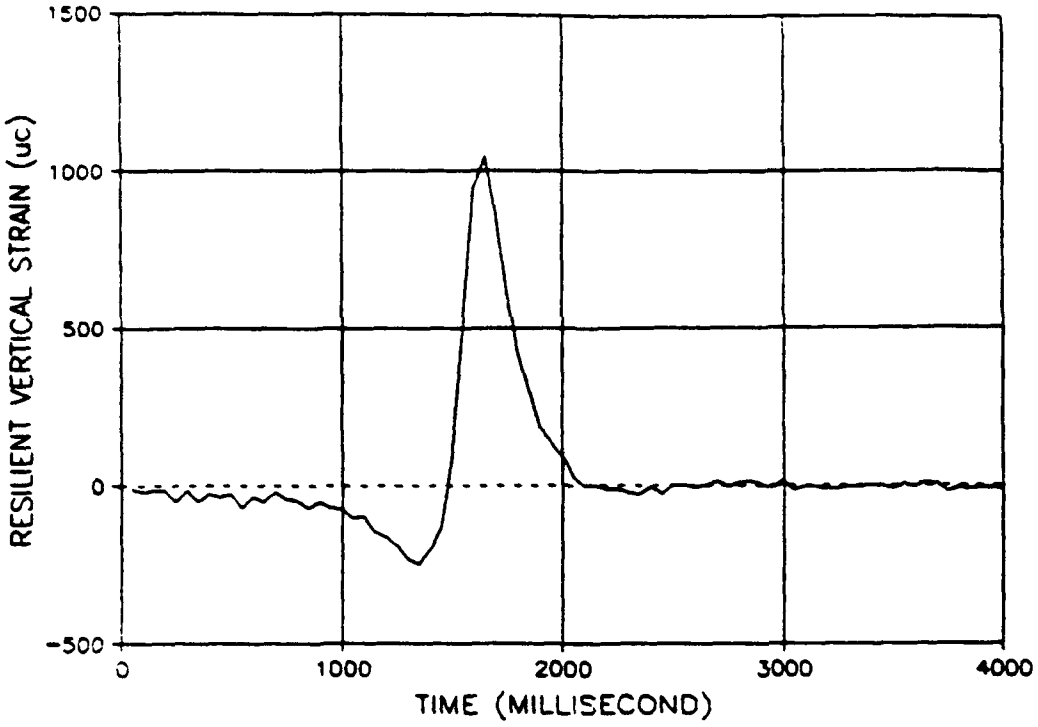

Figure 75. Variation of Vertical Strain with Time at Upper Granular Base due to a 10kN Moving Wheel Load travelled at 3.6 km/hr.

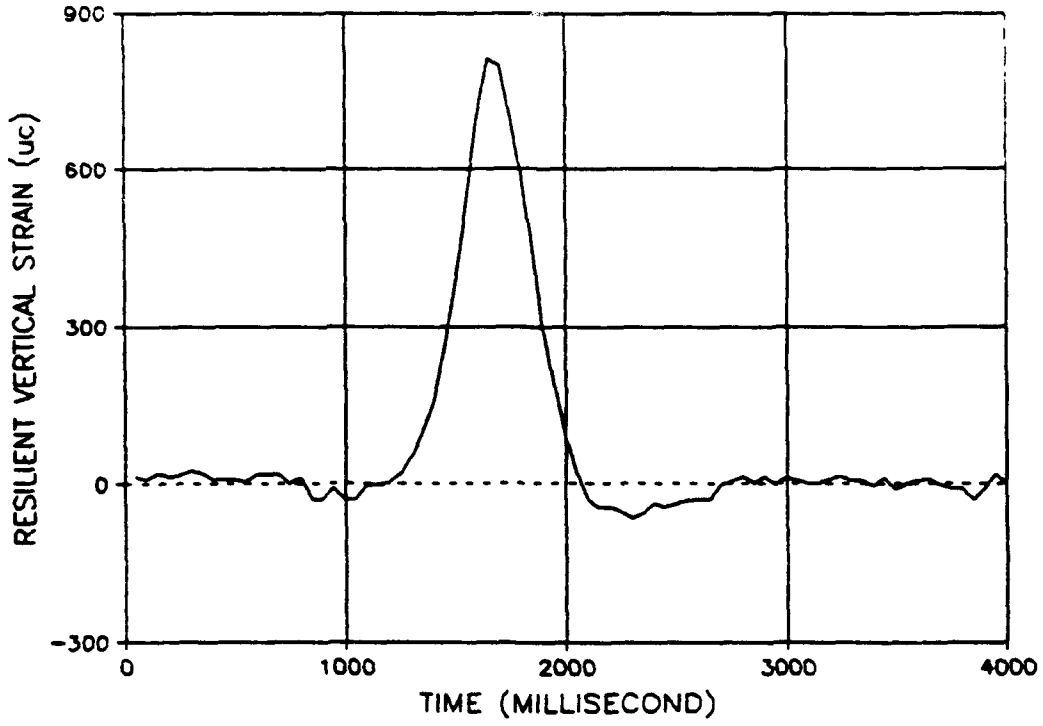

Figure 76. Variation of Vertical Strain with Time at Lower Granular Base due to a 10kN Moving Wheel Load travelled at 3.6 km/hr.

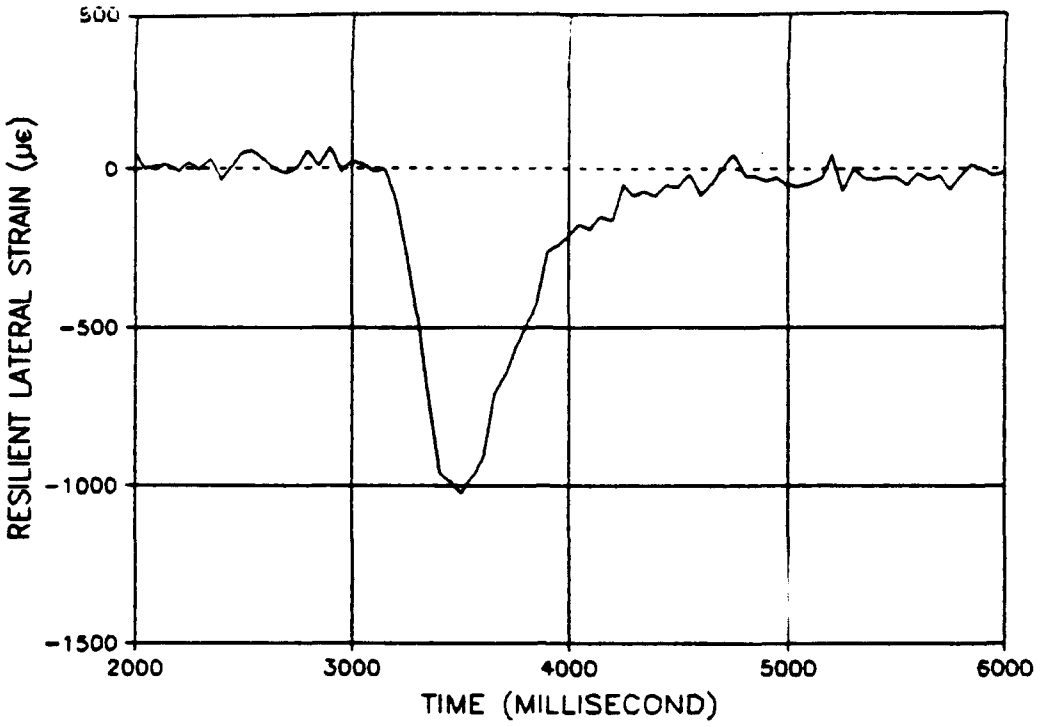

Figure 77. Variation of Lateral Strain with Time at Upper one third of Granular Base due to a 10kN Moving Wheel Load travelled at 3.6 km/hr.

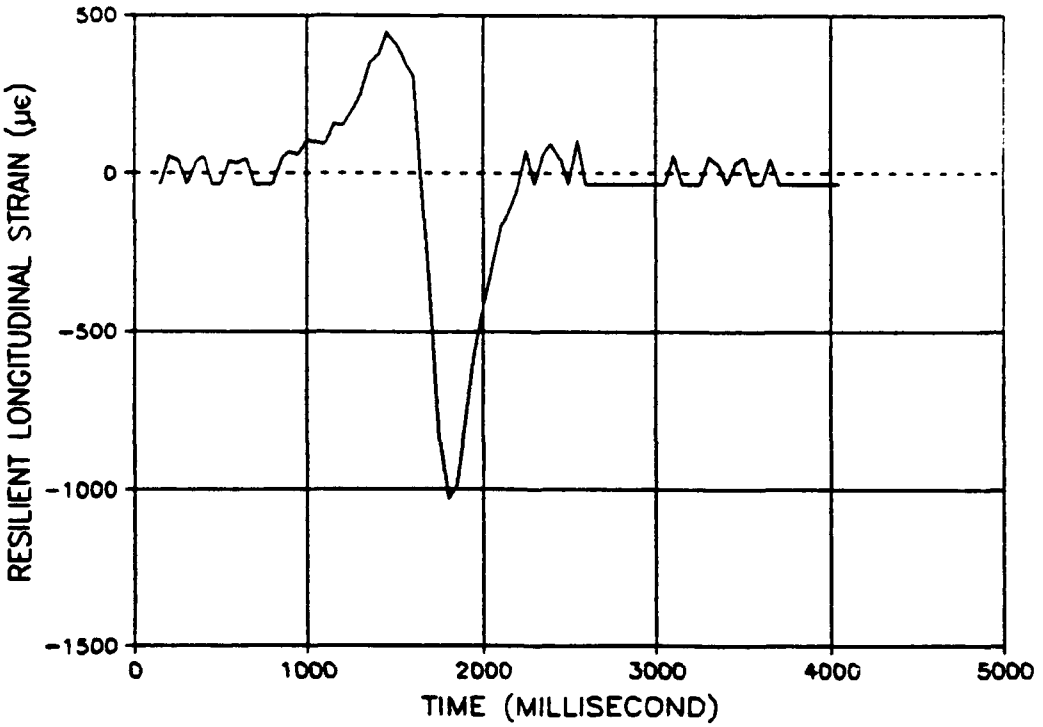

Figure 78. Variation of Longitudinal Strain with Time at Upper one third of Granular Base due to a 10kN Moving Wheel Load travelled at 3.6 km/hr.

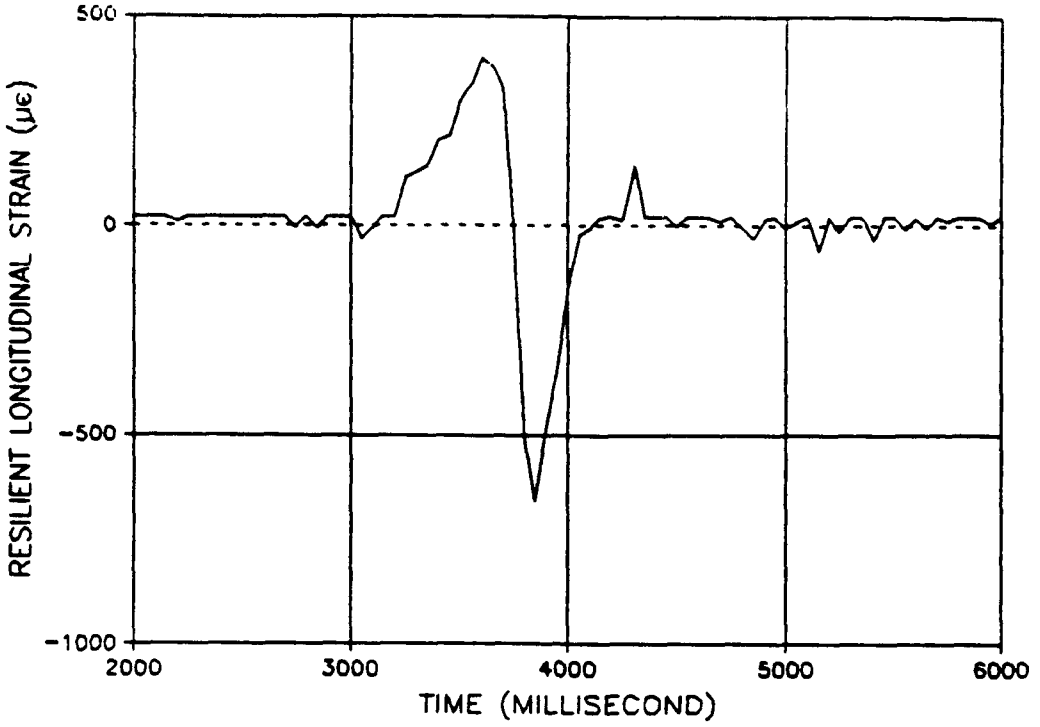

Figure 79. Variation of Longitudinal Strain with Time at the Bottom of Bituminous Wearing Course due to a 10kN Moving Wheel Load travelled at 3.6 km/hr.

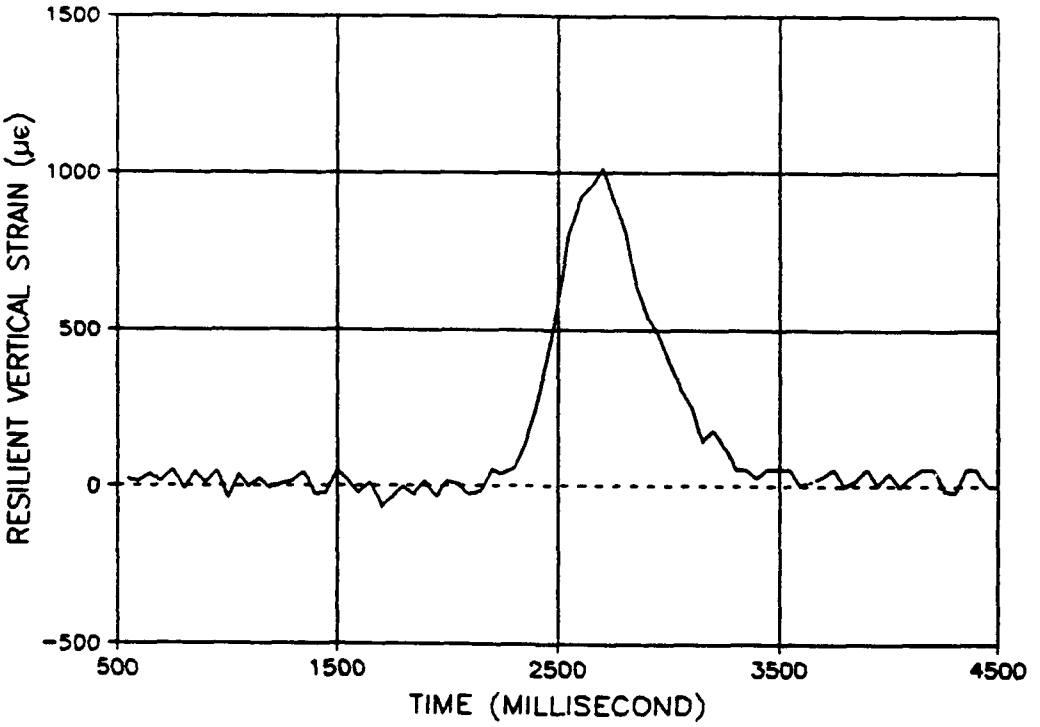

Figure 80. Variation of Vertical Strain with Time at the Top of Subgrade due to a 10kN Moving Wheel Load travelled at 3.6 km/hr.

the bottom of the bituminous layer to 1.2 seconds at the top of the subgrade. The plots also indicate that all vertical strains are compressive and the longitudinal and lateral strains are tensile.

The variations of resilient vertical strain with depth below pavement surface for the two pavement tests are shown in Figure 81. The values are plotted at the mid-distance between the two strain coils which measure the corresponding vertical movement. Figure 81 shows that strain decreases with depth until it reaches the layer boundary where a discontinuity occurs. Superimposed on the figure are the limits of the resilient vertical strain measured during HCA Tests 5 and 8 which involved the use of reversed shear stresses. When the two vertical lines representing the limits intersected with the two strain profiles from the pavement tests, two sublayers within the granular base were obtained. These sublayers represented the zones where there was a high probability that the strain, and possibly the stress conditions, would match those used in the HCA tests.

2. Permanent Strain

The variations of permanent vertical strain with depth at selected stages during the two pavement tests are shown in Figures 82 and 83. The figures indicate that most of the permanent strain developed in the top 100 mm of the layer and then decreased rapidly with depth towards the subgrade. The two sublayers identified by the resilient vertical strain are also highlighted in the figures.

3. Comparison of Permanent Strains

Figures 84 and 85 show a comparison of the permanent vertical strain obtained from the HCA tests with those from the sublayers of the granular base in the pavement tests. The figures indicate that, generally, both the rate of development and the magnitude of strain are very similar. The permanent strain from the first pavement tests (Figure 84) indicated that the granular material might have suffered from some strain history effect as a result of the trial tests performed prior to the main test, since, very little permanent strain occurred during the first 100 load cycles .

4. Transient Stresses

A plot of the stress pulses measured within the granular base is shown in Figure 86. As the pressure cells were located at different positions, the peak stresses were recorded at

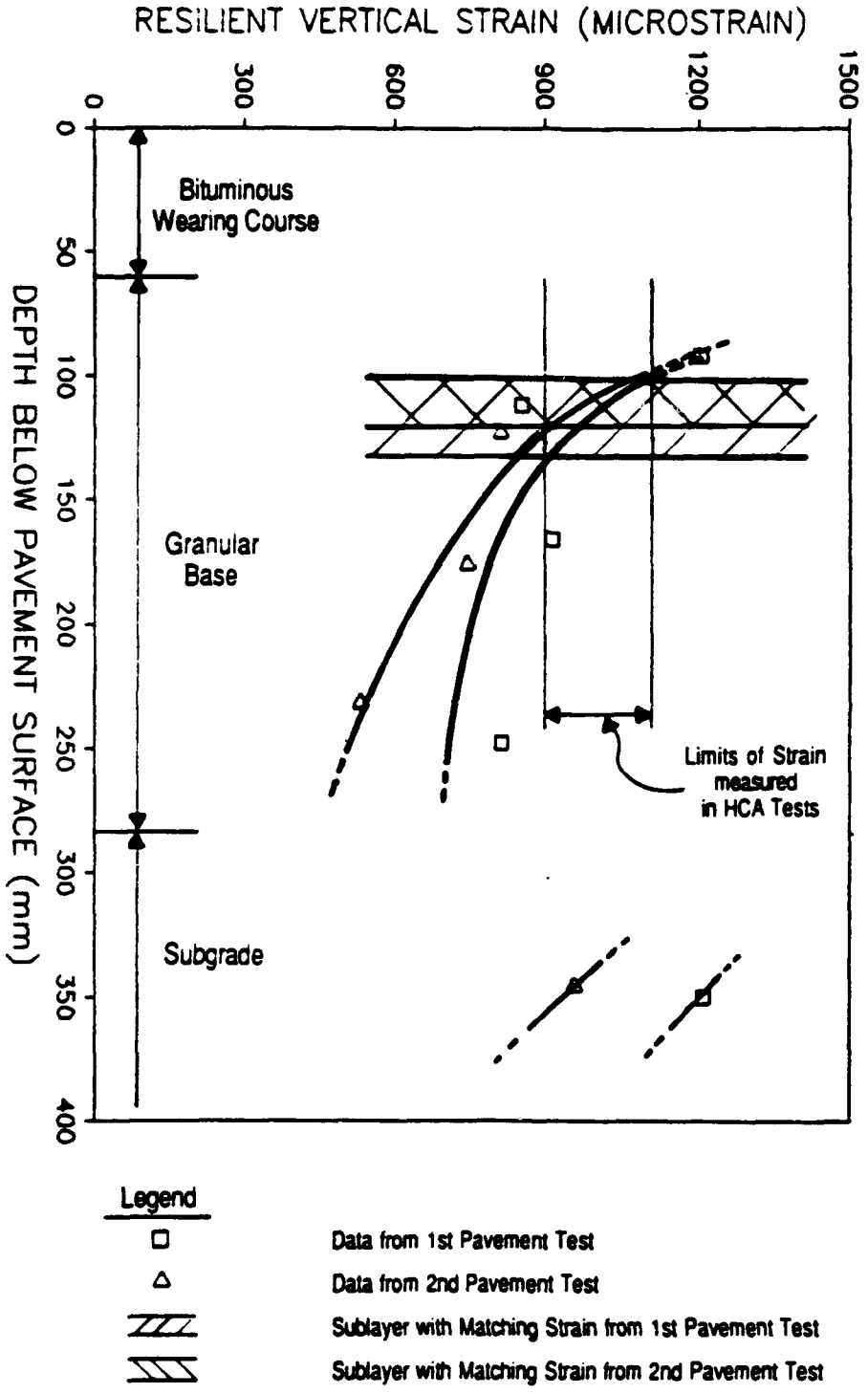

Figure 81. Variation of Resilient Vertical Strain with Depth below Pavement Surface during the Validation Tests performed in the Pavement Test Facility.

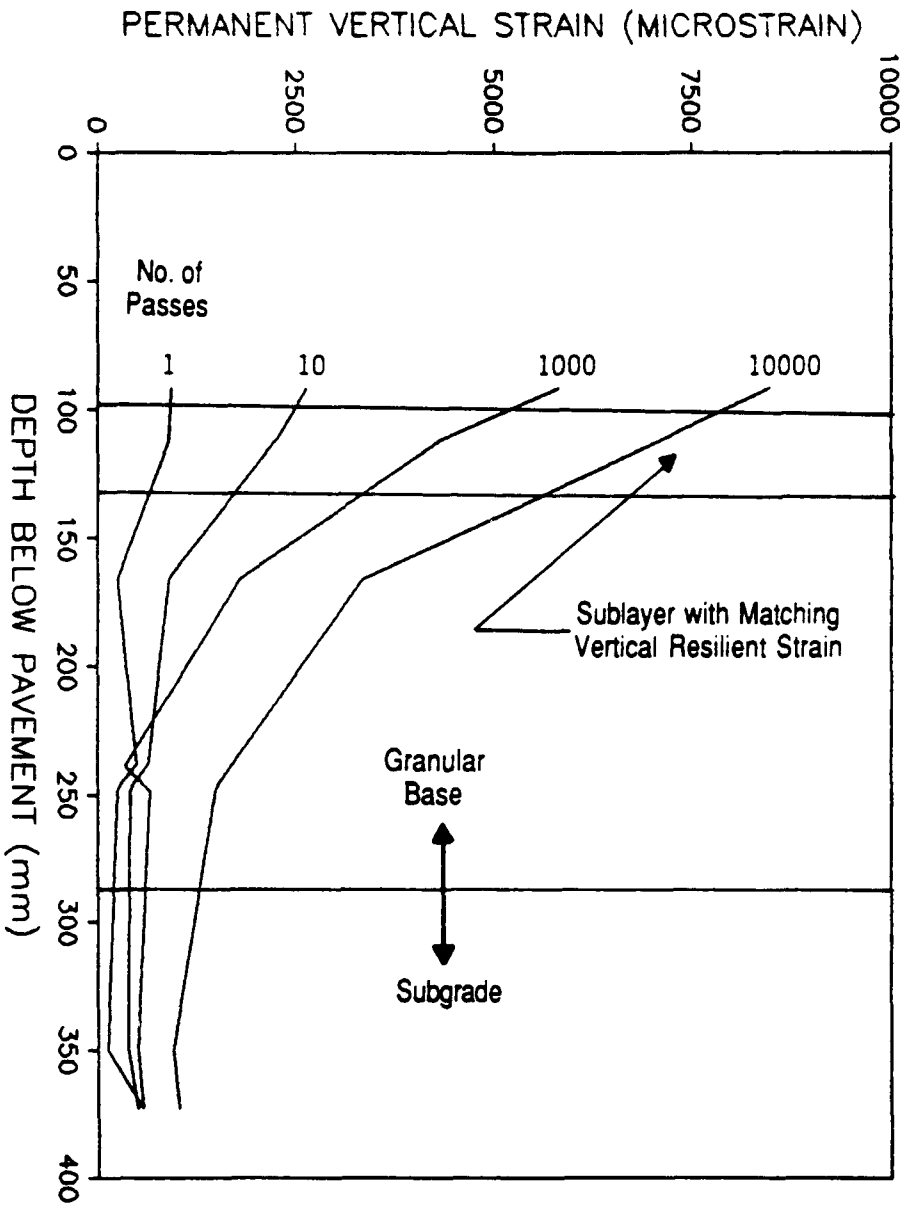

Figure 82. Variation of Permanent Vertical Strain with Depth below Pavement Surface at various Number of Passes of a 10kN Moving Wheel Load on the First Pavement Section.

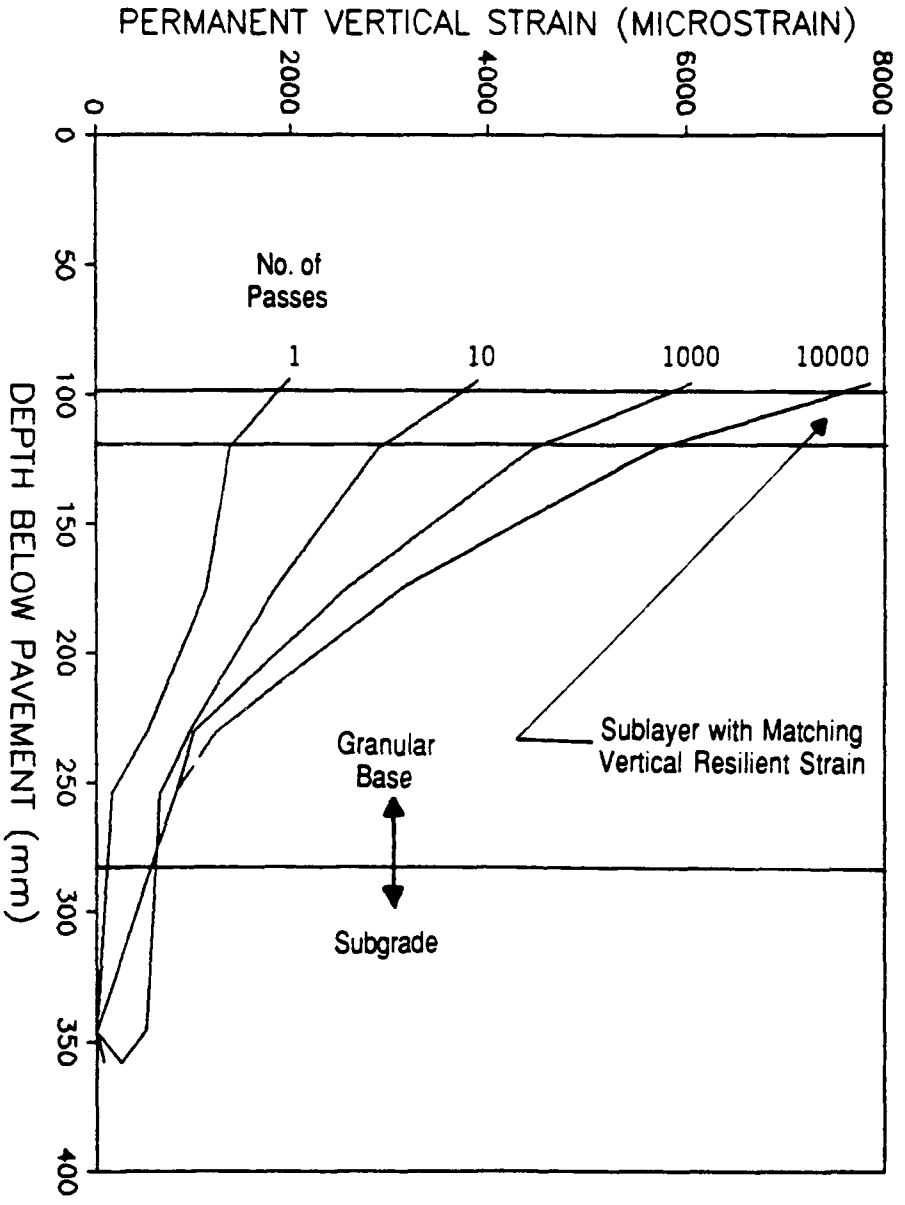

Figure 83. Variation of Permanent Vertical Strain with Depth below Pavement Surface at various Number of Passes of a 10kN Moving Wheel Load on the Second Pavement Section.

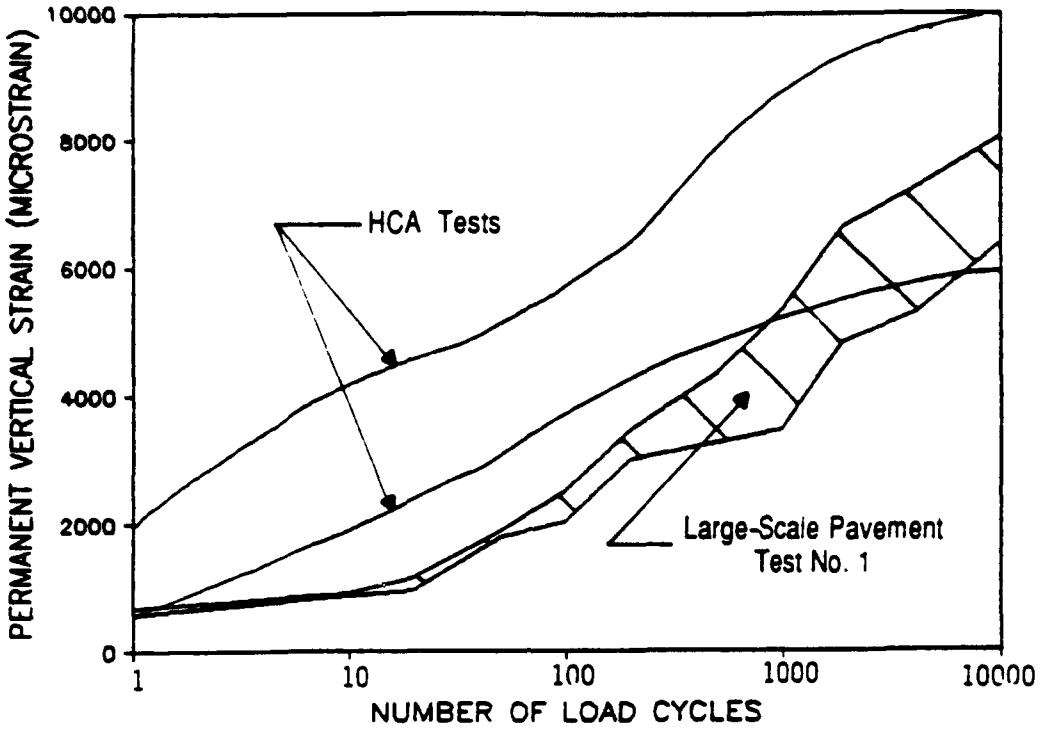

Figure 84. Variation of Permanent Vertical Strain with Number of Load Cycles for the HCA and the First Large-Scale Pavement Test.

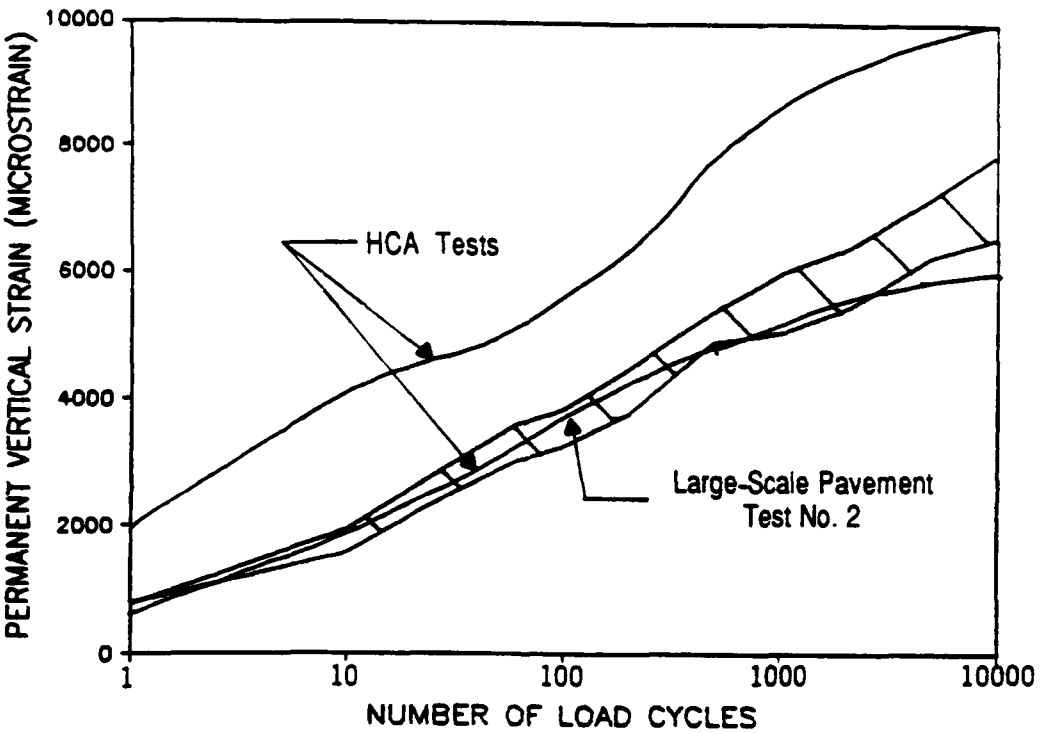

Figure 85. Variation of Permanent Vertical Strain with Number of Load Cycles for the HCA and the Second Large-Scale Pavement Test.

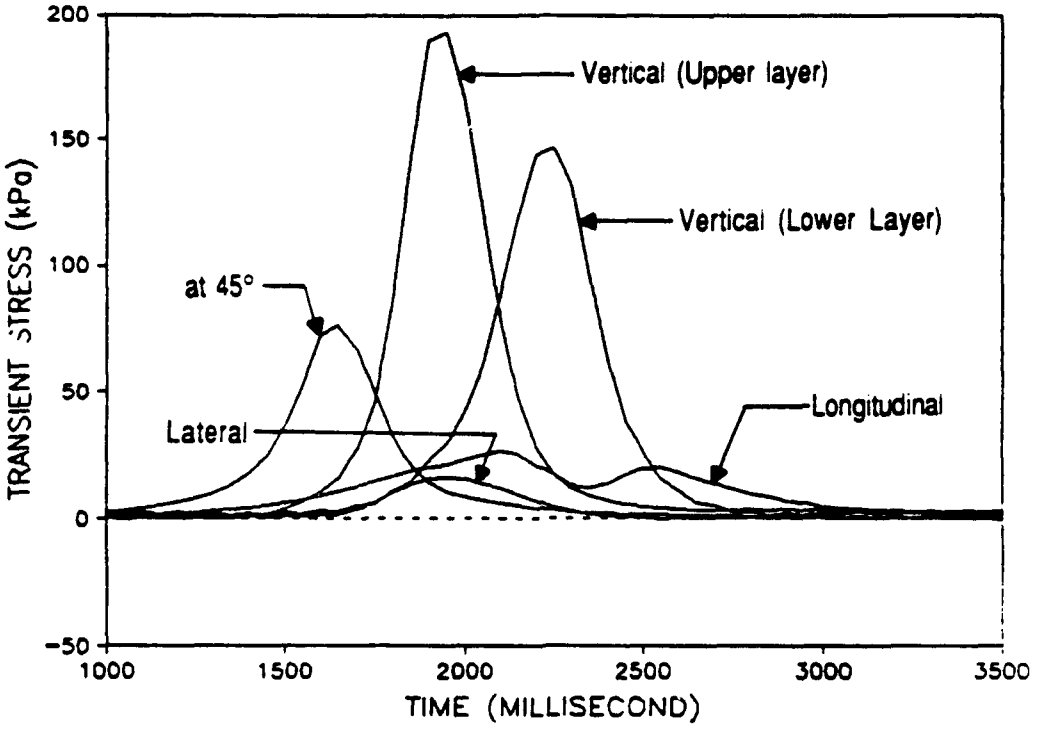

Figure 86. Variation of Stresses at various Orientations with Time in the Granular Base due to a 10kN Moving Wheel Load travelled at 3.6 km/hr.

different times. The plots indicate that pulse time varies with both the distance below pavement surface and orientation. The measured vertical transient stress at a depth of about 125 mm from the surface of the pavement , or approximately at the bottom of the identified sublayers, was 180 to 195 kPa. This compares well with the 200 kPa vertical stress used in the HCA tests. No pressure cells were installed at the vicinity of the sublayer to measure the transient lateral, longitudinal and shear stresses. However, based on a structural evaluation procedure developed at Nottingham which ultilizes a finite element analytical approach (32), the shear stress close to the bottom of the sublayer was found to be 26 kPa. This, again, compares well with the 20 and 30 kPa values used in the HCA tests. The calculated values of the two horizontal stresses, assuming no residual stresses, was generally unsatisfactory and indicated much lower stresses existing in the pavement, compared with those used in the HCA element tests. However, previous research (33) has indicated the presence of residual stresses in granular bases caused by compaction during construction and subsequent trafficking. These stresses are difficult to measure but their existence is likely to reduce the difference in horizontal stresses used in the large-scale pavement and the HCA element tests.

F. DISCUSSION

The main objective of the experiment was to validate the HCA test results. Therefore, the approach and methods adopted to obtain permanent deformation data in the granular base were planned accordingly. The experiment demonstrated the difficulties of accurate prediction for total permanent deformation in a granular base caused by a moving wheel load. To carry out the prediction, not only would a large number of laboratory tests be required but the appropriate stress conditions used in the tests would also need to be determined before the test results could be of any use. As a result, high percentage errors in the prediction due to the use of simplified or averaged conditions are often acceptable. However, these errors may also mask the influence of various factors or mechanism which contribute to the permanent deformation.

The experiment reported in this section clearly shows that the stresses in the granular base under the action of a moving wheel are complex and that the stress-permanent strain-time relationship of the granular base is complicated. These two factors undoubtedly imposed very severe limitations on the objectives of the validation exercise. Nevertheless, the results indicate that the HCA would have provided a very good prediction of both the rate of development and magnitude of the permanent vertical strain in a sublayer of the granular base subjected to a moving wheel load. This has provided strong support for the continuous use of the modified HCA to carry out future research on the behavior of granular materials.

The results of the experiment may also be used to check predictions of permanent strain obtained from repeated-load triaxial tests. Comparison of the predictions from this and the HCA tests could then be made. However, such comparison would only be meaningful for results from a sublayer of the granular base where the magnitude of the shear stress is insignificant relative to the normal stresses. Results shown in Figures 13 and 56 indicate that when shear stresses are high, both the magnitude and the rate of development of permanent strain would be underestimated by the triaxial test simulation .

SECTION VIII

CONCLUSIONS

Research has been carried out to improve knowledge on the behavior of granular bases for pavements. To this end, a repeated-load Hollow Cylinder Apparatus was developed to model the stress and strain conditions imposed by a moving wheel load.Tests using the repeated-load triaxial test apparatus and two wheel tracking facilities were also carried out. The main conclusions of the investigations performed are listed below.

A. GRADING / DENSITY AND MECHANICAL PROPERTIES

1. A grading design procedure which is based on the use of Fuller's grading curves and the British standard vibrating hammer test was proposed. This procedure allows convenient characterization of continuous gradings and offers a simple and repeatable means of carrying out design for high density gradings.

2. For a crushed dolomitic limestone with maximum particle size of 38 mm, the optimum grading which produced the highest density when the material was dry had a Fuller's "n" value of about 0.4.

3. For dry or partially saturated granular material, higher density generally leads to a slight improvement in resilient properties but a large improvement in permanent deformation resistance under repeated-load.

B. PERMANENT DEFORMATION BEHAVIOR OF GRANULAR MATERIAL IN LARGE-SCALE RUTTING TESTS

Results of the large-scale rutting tests carried out in the Slab and Pavement Test Facilities led to the following conclusions.

1. The permanent vertical deformation of the granular base subjected to a moving wheel load was at least three times higher than that subjected to a repeated vertical load with the same magnitude of contact stress.

2. The magnitude of a moving wheel load had greater influence on the permanent deformation of the granular base than that of a repeated vertical load.

3. In two out of three pairs of pavement sections, higher permanent deformations were obtained from a bidirectional than unidirectional wheel load. The exceptional pavement sections were less well compacted and, hence, the trend caused by the different modes of loading was probably masked by the generally high level of permanent deformation.

C. REPEATED-LOAD HOLLOW CYLINDER TESTS

The Nottingham repeated-load Hollow Cylinder Test Apparatus was successfully modified to include an outer cell, an upgraded electronic control system and a data acquisition system. Eleven hollow cylinder specimens were tested by means of the modified device. To complement these experiments, two tests on the same material used in the HCA tests were carried out using the repeated-load triaxial apparatus. The conclusions from these tests were:

1. Permanent Strain Behavior

a. Reversed shear stresses were found to cause more contractive permanent strains in both the radial and circumferential direction when results were compared with those obtained under triaxial conditions.

b. When stress conditions were approaching failure, the rate of development of all components of permanent strain was found to be significantly increased due to the additional reversed shear stresses.

c When the maximum shear stress ratio, $(q/p)_{max}$ used in the stress path was low and when the magnitude of the reversed shear stress was small compared with the normal stresses, the difference between the strain response under the condition with reversed shear stresses and the triaxial condition was less clear. Nonetheless, it appeared that under these

circumstances, reversed shear stresses would cause higher permanent contractive volumetric strains but less permanent maximum shear strains.

d. Higher permanent volumetric and maximum shear strains were obtained due to bidirectional than unidirectional shear reversal.

e. Under identical stress conditions, permanent axial strains obtained from both the HCA and the repeated-load triaxial apparatus were similar but the permanent horizontal strain obtained from the HCA was much higher.

2. Resilient Strain Behavior

a. Rotation of the principal stress and strain planes were coincident during resilient tests.

b. The coefficients m, n and β used in the resilient strain contour models, which were obtained by means of a multiple regression analysis from results of repeated-load triaxial tests, were found to be identical to those obtained from HCA tests. The constants K1 and G1, however, were found to be respectively 97 and 29 percent less for results from HCA tests, indicating that lower stiffnesses were obtained during the tests.

c. The contour model and its coefficients, which were obtained from tests under triaxial conditions, could be used to provide reasonably good predictions of the resilient maximum shear strain under stress conditions which involve principal plane rotation and variation in the intermediate principal stress.

d. Resilient volumetric strain was generally underpredicted by the contour model under stress conditions which involved the application of torsional shear stress.

e. The difference between the measured and predicted resilient volumetric strain using the contour model appeared to bear a curvilinear relationship with the normalised value, $\delta b/\eta_m$ which is defined as the change in the intermediate principal stress parameter divided by the mean shear stress ratio, $(q_{oct})/p_m$.

D. VALIDATION OF REPEATED-LOAD HCA TESTS

In order to provide validation for the findings from the HCA tests, a pilot-scale experiment involving two fully-instrumented flexible pavement sections was performed in the Nottingham Pavement Test Facility. The validation was limited to the permanent vertical strain which is closely related to the rut formation. The conclusions were:

1. The stresses and strains in the granular base of a flexible pavement due to a moving wheel load varied with the depth below the pavement surface. Therefore, comparison of results is meaningful only within a sublayer where the conditions are similar to those used in the HCA tests.

2. A sublayer within the granular base where the resilient vertical strains matched those obtained from the HCA tests was identified. The measured transient vertical stress and the calculated shear stress near the sublayer were also found to matched those used in the HCA tests. However, because of the difficulty in accounting for residual stresses, both the calculated and measured horizontal stresses indicated much lower stresses existing in the pavement.

3. Results of the two pavement tests indicated that the permanent strain tests performed in the HCA would have provided a good prediction for both the magnitude and rate of development of the vertical permanent strain in the sublayer of the granular base.

4. The results of the validation experiment provide strong support for further use of the modified repeated-load HCA as a research tool.

SECTION IX

RECOMMENDATIONS

A. GENERAL

Work carried out during this project has indicated that the permanent deformation behavior of granular material is complicated and yet less understood than the resilient behavior. Nevertheless, for pavements with heavily loaded granular bases, an understanding of the accumulation of permanent strains would be essential. Therefore, the more fundamental aspects of the behavior, including the deformation mechanism under repeated load and effects due to stress variations should be studied. Methods which can improve the permanent deformation resistance, such as the use of high density grading or, perhaps, some form of reinforcement, which may provide more immediate and practical results should receive equally important attention.

To bridge the gap between laboratory simulated and in situ conditions, the use of a sophisticated device, such as the repeated-load hollow cylinder apparatus has proved to be very valuable and able to produce some important data. The potential of this laboratory device as a research tool should be further explored and effort to expand its capability should be considered.

B. TESTINGS WITH THE HOLLOW CYLINDER APPARATUS

1. Further Work on the Same Material used in Current Investigations

A much improved HCA is now available and some test results have been validated by means of large-scale experiments. Therefore, further research which makes use of this apparatus is desirable. Tests carried out for the current project have established the influence of the reversed shear stresses, both uni- and bidirectional, on the permanent strain behavior. Although more tests involving other stress paths with reversed shear stresses are warranted, it may be useful to investigate the effect of the intermediate principal stress, σ_2. This can be achieved by using various differences in inner and outer cell pressures to create a range of anisotropic conditions. Stress conditions existing off the centre of a moving single wheel and along the centre line of dual or tandem wheels may involve different magnitudes of shear stress and modes of stress reversal. It seems likely that these complex stress regimes could be modelled in the HCA with further improvements to the control system.

To achieve high density and high strength for the material used in the current investigation, a continuous grading with high fines content was used. It would be of interest to investigate the permanent strain behavior of an open-graded specimen which may be expected to have much better drainage properties. The requirement for both good strength and good permeability for granular bases is inevitably contradictory. Hence, it would be useful to compare the performance of specimens having these two different gradings and subjected to realistic stress conditions involving shear stress reversals.

2. Work on Other Materials

A great degree of realism was attached to the choice of the type and grading of the material used in this project. As a result, a material widely used in the highway industry, a scaled down version of a realistic grading and a correspondingly high density were selected. However, these choices may not be ideal in the theoretical study of the various fundamental mechanisms of granular material behavior. Furthermore, comparison of results with those from other research organizations would be difficult if different categories of materials were tested. Hence, it would be useful if future test programs could incorporate testing of some model materials such as the well researched Leighton Buzzard sand and other similarly "well-known" materials. Testing of single sized material should also generate useful results for comparison.

C. FURTHER DEVELOPMENT OF THE HCA

The improvement to the HCA carried out in this project has eliminated a large area of restrictions on the possible stress regimes that can be applied to an element of granular material in the laboratory. This has undoubtedly allowed better simulation of in situ stress conditions. Despite these achievements, in order to fully make use of this torsion-triaxial system, the capability of providing cyclic internal and external cell pressures is highly desirable. More sensors to measure the response of the cell or possibly pore pressures will be needed. The control of such a system will be more complicated and will most certainly require the aid of a computer. However, with the advance of modern electronics and computer programming, such a system can be incorporated to the existing facility at a reasonable cost.

REFERENCES

1. Crockford, W W, Chua, K M, Yang, W S, Rhee, S K and Senadheera, S P , "Response and Performance of Thick Granular Layers," Final Technical Report submitted to the US Air Force, 1988.

2. Brown, S F and Pappin J W, "The Modeling of Granular Materials in Pavements," Transportation Research Record 1022, 1985, pp 45-51.

3. Sweere, G T H, Penning, A and Vos, E, "Development of a Structural Design Procedure for Asphalt Pavements with Crushed Rubble Base Courses," Proc. 6th Int. Conf. on the Structural Design of Asphalt Pavements, Ann Arbor, Michigan, 1987, pp 35-49.

4. Ansell, P and Brown, S F, "Cyclic Simple Shear Apparatus for Dry Granular Materials," Geotechnical Testing Journal, Vol. 1, No. 2, June 1978, pp 82-92.

5. Arthur, J R F, Chua, K S and Dunstan, T, "Induced Anisotropy in a Sand," Geotechnique 27, No. 1, 1977, pp 13-30.

6. Groth, P J, " The Use of High Density Granular Layers in Road Pavements." Proc. 2nd Symp. on Unbound Aggregates in Roads, Part 1, 1985, pp 99-107.

7. Robinson, R.G., "Measurement of the Elastic Properties of Granular Materials using a Resonance Method," Transport and Road Research Laboratory Supplementary Report, 111UC, 1974.

8. Hick, R.G. and Monismith, C.L., "Factors influencing the Resilient Response of Granular Materials," Highway Research Record No. 345, 1971, pp. 15-31.

9. Rada, G. and Witczak, M.W., "Comprehensive Evaluation of Laboratory Resilient Moduli Results for Granular Materials," Transportation Research Record 810, 1981, pp 23-33.

10. Barksdale, R D, "Laboratory Evaluation of Rutting in Basecourse Materials," Proc. of 3rd Int. Conf. on the Structural Design of Asphalt Pavements, London, 1972,pp 161-174.

11. Thom, N H and Brown, S F, "The Effect of Grading and Density on the Mechanical Properties of a Crushed Dolomitic Limestone," Internal Report, University of Nottingham, 1988.

12. Chan W K F, Dawson A R and Brown S F, "Granular Bases for Heavily Loaded Pavements," First Annual Research Report submitted to the US Air Force, October, 1988.

13. Lees G, "The Rational Design of Aggregate Gradings for Dense Asphaltic Compositions," Proceedings of Association of Asphalt Paving Technologists, Vol. 39, pp 60-97, 1972.

14. British Standard Institution, "Recommendations for Testing of Aggregates," BS 5835, Part 1, 1980.

15. Fuller W B and Thompson S E, "The Laws of Proportioning Concrete," Transaction of the American Society of Civil Engineering, Vol. 59, pp 67-172, 1907.

16. Department of Transport, Specifications for Highway Works, Part 3, 1986.

17. Chan W K F and Brown S F, "Granular Bases for Heavily Loaded Pavements", Second Annual Research Report submitted to the US Air Force, December, 1989.

18. Pappin J W, "Characteristics of a Granular Material for Pavement Analysis," PhD Thesis, University of Nottingham, 1979.

19. Jouve P, Martinez J, Paute J S and Ragneau E, "Rational Model for the Flexible Pavements Deformations," Proceedings of the 6th International Conference on the Structural Design of Asphalt Pavements, pp 50-64, Ann Arbor, August 1987.

20 Brown, S F, "Repeated Load Testing of a Granular Material," Journal of Technical Engineering Division, ASCE, Vol. 100, No. GT7, July, 1974, pp 825-841.

21. Thom, N H,"Design of Road Foundation," PhD Thesis, University of Nottingham, 1988.

22. Brown S F and Brodrick B V, "Nottingham Pavement Test Facility," Transportation Research Record 810, pp 67-72, 1981.

23. Brown, S F, Brodrick, B V and Pappin, J W, "Permanent Deformation of Flexible Pavements," Final Technical Report submitted to the US Army, University of Nottingham, 1980.

24. O'Reilly, M P, "Mechanical Properties of Granular Materials for use in Thermal Energy Stores," PhD Thesis, University of Nottingham, 1985.

25. Hight D W, Gens A And Symes M J, "The Development of a New Hollow Cylinder Apparatus for Investigating Effects of Principal Stress Rotation in Soils," Geotechnique 33, 1983.

26. Wright D K, Gilbert P A and Saada A S, "Shear Devices for Determining Dynamic Soil Properties," Proceedings of American Society of Civil Engineers Speciality Conference on Earthquake Engineering and Soil Dynamics, Vol. 2, pp 1056-1075, CA, Pasadena, 1978.

27. Boyce J R and Brown S F, "Measurement of Elastic Strain in Granular Material," Geotechnique, 26/4, pp 637-640, 1976.

28. Atkinson J H and Bransby D L, "The Mechanics of Soils: An Introduction to Critical State Soil Mechanics," McGraw Hill, 1978.

29 British Standard Institution, "British Standard 4987: Coated Macadams for Roads and other Paved Areas," London, 1988.

30 Peutz, M.G.F., Van Kempen, H.P.M. and Jones, A.,"Layered System under Normal Surface Loads - Computer Program BISTRO," Koninklijke/ Shell Laboratorium, Amsterdam, 1968.

31 Brown, S F and Brodrick, B V, "Stress and Strain Measurements in Flexible Pavements," Proc. Conf. on Measurements in Civil Engineering, Newcastle, England, 1977.

32. Almeida, J.R., Brunton, J.M. and Brown, S.F.,"Structural Evaluation of Pavements," 2nd Research Progress Report submitted to Transport and Road Research Laboratory, 1991 (in preparation).

33. Uzan, J.,"Characterization of Granular Material," Transportation Research Record 1022, pp.52-58, 1985.

APPENDIX A

REPEATED LOAD TRIAXIAL TEST APPARATUS

Details of the repeated-load triaxial test apparatus which can accommodate test specimen with diameter of 150 mm are shown in Figures A-1 and A-2. The axial load is applied to the specimen by a servo-hydraulic actuator and monitored by a strain gauged load cell located at the bottom section of the loading ram. The confining pressure which is also servo-hydraulically controlled is applied through a nonconducting medium of silicone oil and is monitored by a thin wall pressure cell.

For repeated loading, a waveform generator, capable of providing sinusoidal, square or triangular waveforms was used to generated the required command signals. During testing, the feedback signals from the two monitoring devices are compared with the command signal. An error message is then relayed to the servo-valves so that the necessary adjustment may be made. This arrangement ensures that the required loading conditions are achieved.

To measure deformation of the specimen, an on-sample instrumentation technique is used. This involves using four brass studs which are embedded in the sides of the specimen during sample preparation. The studs allow threaded rods to be attached to the specimen. The rods, in turn, enable the mounting of instruments. Two LVDTs mounted between the two pairs of rods are used to measured axial deformations. For radial deformations, two epoxy hoops incorporating strain gauges are used.

All the stress and strain data are recorded by the new data acquisition system described in Chapter Six. Dedicated software for the repeated-load triaxial tests was developed. They are similar to those which are presented in Appendix C for the repeated HCA tests .

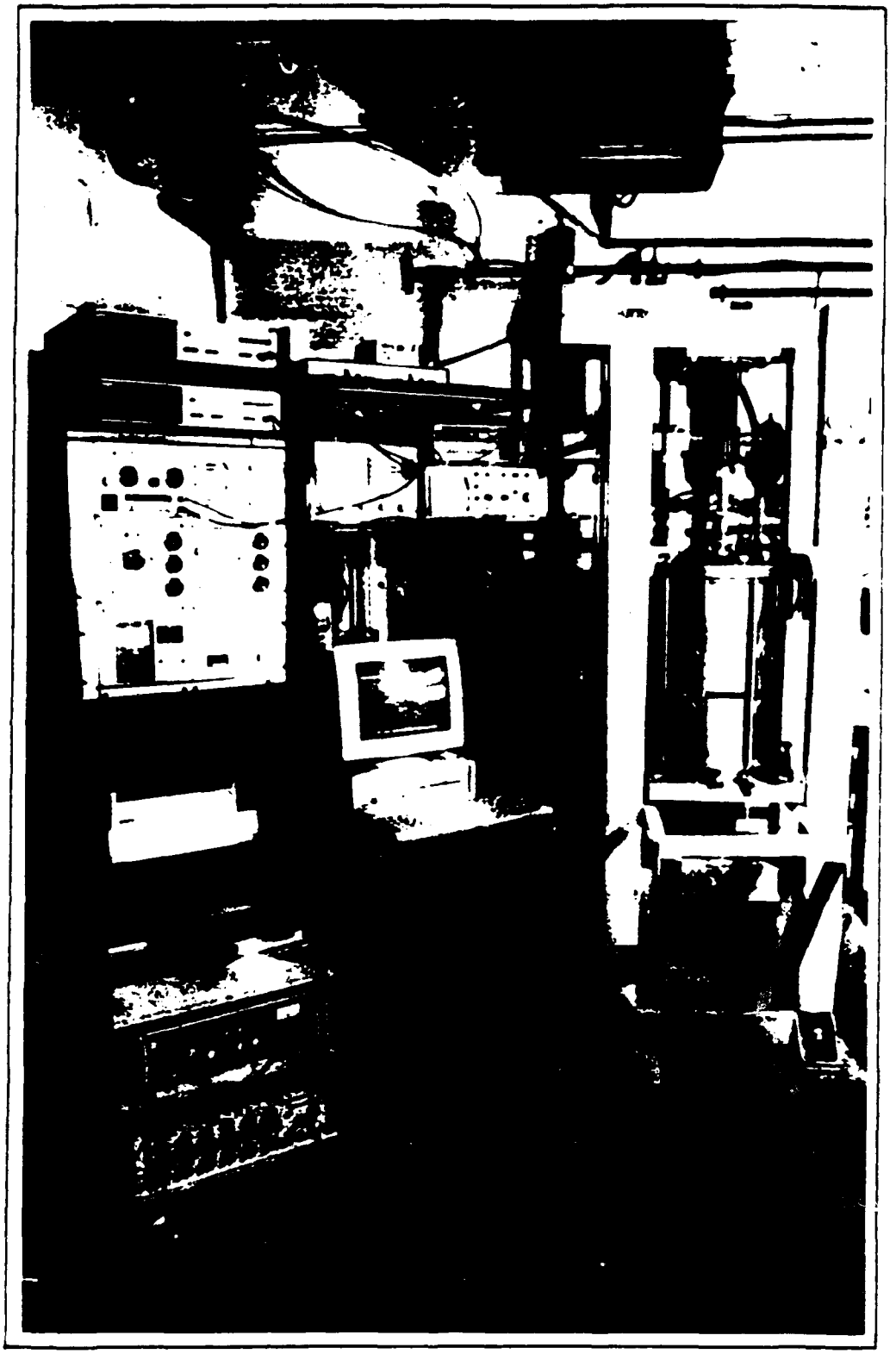

Figure A-1. Laboratory Set-up of the Repeated-Load Triaxial Test Apparatus.

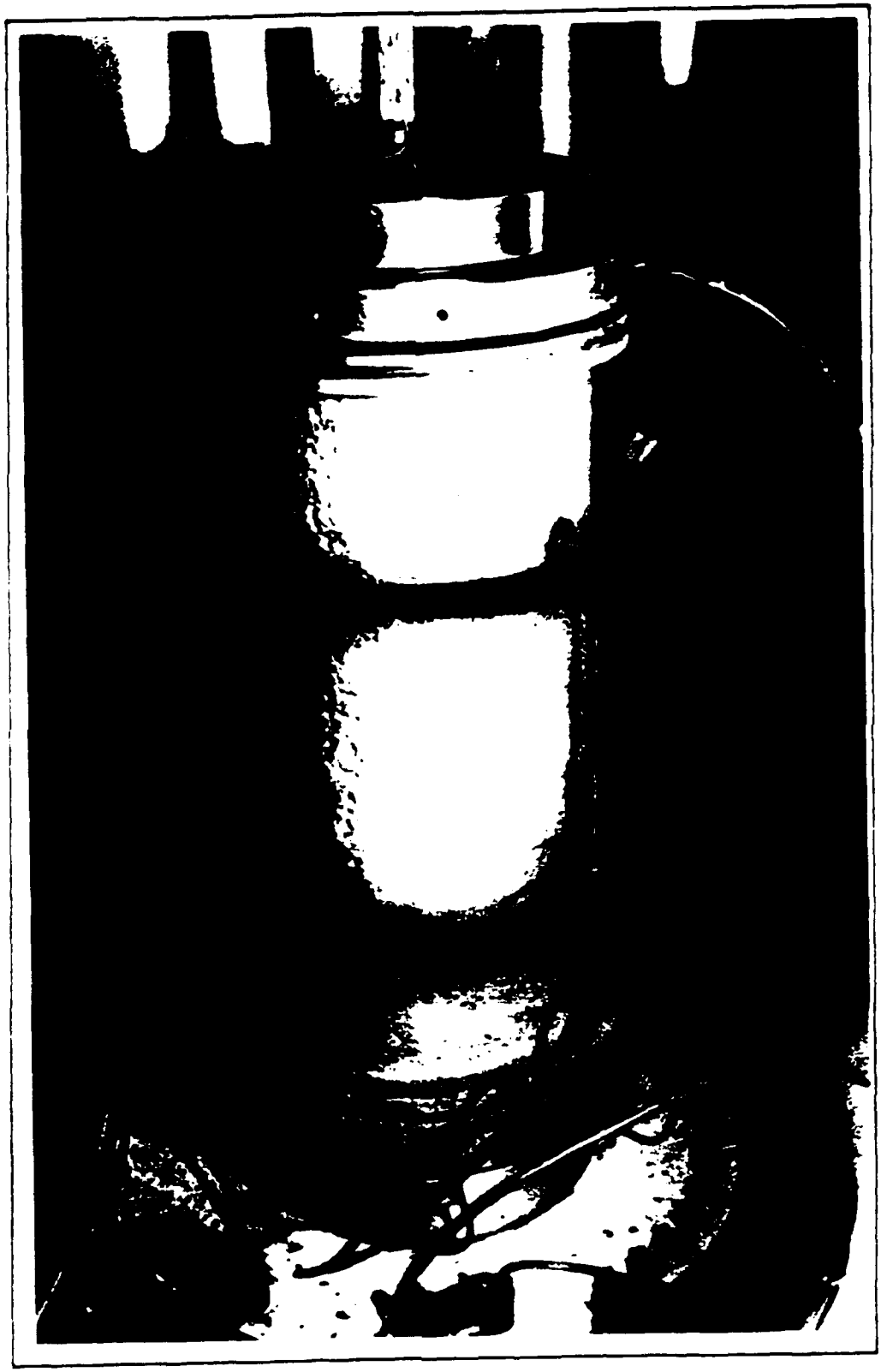

Figure A-2 150mm diameter Triaxial Specimen with Instrumentations.

APPENDIX B

CALIBRATION OF TRANSDUCERS USED IN REPEATED-LOAD HOLLOW CYLINDER APPARATUS

Calibration of the transducers used in repeated-load HCA tests was carried out approximately once every two tests. A brief description of the methods used is presented as follows and the results are shown in Table B.1.

B.1. Vertical Load Cell

The vertical load cell was calibrated by means of a standard proving ring with maximum capacity of 14 kN and load per division value of approximately 0.011 kN. The vertical compressive load was provided by a standard hydraulic jack and the response of the load cell at regular values of deflection of the proving ring was monitored by a voltmeter. Maximum load of 12 kN, equivalent to approximately 350 kPa in axial stress was used. Linearity between the output voltage and the proving ring deflection was generally observed with coefficient of correlation, R^2, in the region of 0.999.

B.2 Torsional Load Cell

The best method of calibrating the torsional load cell was by means of a pair of hangers and weights connected, via a pulley system to a set of extended steel arms bolted to the load cell. Calibration was carried out in steps of 1 or 2 kg on each hanger, which is equivalent to 1.4 or 2.8 kPa respectively in torsional shear stress. This continued until a total of 35 kg or approximately 50 kPa was reached. Both clockwise and anti-clockwise loading were performed. It was noted that linearity between the applied moment and the output from the load cell during the initial 30 to 35 kPa in shear stress was generally good. However, beyond this magnitude, some hysteretic effect was observed. Despite this, R^2 of 0.993 to 0.998 were achieved.

B.3 LVDTs

The LVDTs were individually calibrated by means of a micrometer capable of providing reading to 0.0025 mm which was equivalent to 17 $\mu\varepsilon$ for a gauge length of 150 mm. The gain

TABLE B-1

RESULTS OF CALIBRATIONS FOR THE TRANSDUCER USED IN REPEATED-LOAD HCA TESTS

Date	LVDTs (mm/volt)				Strain Hoops (mm/volt)		Strain Coil (mm/volt)		Torsional Load Cell (kPa/Volt)	Vertical Load Cell (kPa/Volt)
	1	2	3	4	1	2	1	2		
14.08.89	0.4717	0.4027	0.3534	0.3639	1.146	1.263	0.120	0.112	14.30	169.2
14.09.89	0.4075	0.4139	0.3531	0.4035	1.195	1.329	/	/	13.44	171.5
17.10.89	0.4050	0.4014	0.3550	0.4030	1.225	1.325	0.107	0.111	13.60	172.3
02.01.90	1.1869	1.244	1.3955	1.1584	1.139	1.285	0.112	0.109	13.20	172.0
29.01.90	1.1732	1.2423	1.4311	1.1623	1.170	1.293	/	/	14.08	172.0

Note: "/" means not available.

setting of the strain gauge amplifier was set initially for a full scale deflection of about 2.5 percent strain. However, subsequent tests required this to be increased to 4 percent. Linearity was generally very good for the LVDTs.

B.4 Strain Hoops

Calibration of the two strain hoops was performed simultaneously by means of a specially assembled device consisting of a micrometer and three sets of mounting units. Both compressive and tensile deformations of the strain hoops were calibrated. Good linearity within the range of ±2 percent strains was obtained.

B.5 Bison Strain Coils

Calibration of the strain coils was carried out according to the instruction manual published by Bison Instruments. It involved the use of the Bison Recorder and a special mounting unit which incorporated a micrometer. Because of the small wall thickness of the hollow cylinder specimen and in general, small change in thickness, it is not possible to rely on the amplitude value to determine the spacing between coils. Instead, the voltage produced by the small differential movement at a particular balanced position was used. A "CALIBRATION" setting of 500 was chosen. Although the micrometer can resolve movement down to 0.0025 mm, due to the small gauge length involved (28 to 30 mm), it only represents a strain value of 89 $\mu\varepsilon$. However, since the relationships between output voltage and the small differential movement is linear, interpolation can be carried out to determine smaller strain value. This method required that calibration be carried out at a few balanced positions corresponding to the anticipated gauge lengths.

APPENDIX C

SOFTWARE PROGRAMS FOR THE REPEATED-LOAD HCA TEST

The main program for the data acquisition of the repeated-load HCA tests is called HCA. The primary functions of the program are:

1. Retrieve data from the specified channels (maximum 8) at specified intervals (2 to 510 milliseconds) for a specified number of times.

2. Based on the input calibration value for each channel, calculate the corresponding stresses and strains. It also calculate all the relevant invariant parameters.

3. Store the raw and/or processed data onto disks.

4. Output test information and key results onto printer.

The total number of scans that can be performed during one run of the program depends on the number of channels selected and cannot be larger than the quotient obtained by dividing 2048 by the number of channels. For each new run, a new data file name in sequential order will be generated. Further analysis or plotting of the data is found to be more efficiently performed by using existing commercially available softwares. To facilitate this, all data files are created such that they can be "imported" by most popular softwares.

The program was written in BASIC language and a listing is presented as follows:

```
10 '                    DATA ACQUISITION FOR THE REPEATED LOAD
20 '                        HOLLOW CYLINDER TEST APPARATUS
30 '                    ******************************************
40 '
50 '
60 'Startup
70 '
80 DEF SEG=0
90 DRIVER1=PEEK(&H4F0)+256*PEEK(&H4F1)
100 DRIVER2=PEEK(&H4F4)+256*PEEK(&H4F5)
110 DEF SEG=DRIVER1 : REM SELECT CARD £1
120 INIT=3 : ABORTIO=6 : DEVCLEAR=9 : LOCAL=12
130 LOCALLOCKOUT=15 : REMOTE=18 : IRESUME=21 : TRIGGER=24
140 OUTPUT=27 : ENTER=30 : STATUS=33 : SETTERMINATOR=36
150 SETTIMEOUT=39 : SERIALPOLL=42 : SRQCHECK=45 : ERRCHECK=48
160 SETEOI=51 : SETTERM=54 : PARALLELPOLL=57 : SRVREQ=60
170 NCINIT=63 : BLOCKOUT=66 : BLOCKIN=69 : BYTESWAP=72
180 TRANSFER=75 : TALK=78 : UNTALK=81 : LISTEN=84
190 UNLISTEN=87 : ATTN=90 : MTA=93 : MLA=96
200 '
210 CALL INIT                                          'initialize driver
220 AD%=9                                              'device address
230 V$=SPACE$(56)                                      'reserve space for data *
240 DIM R(8,256)                                       'data array             *
250 DIM AXSS(256) : DIM TORSS(256) : DIM P(256) : DIM Q(256)
260 DIM OCTASS(256) : DIM ANGSS(256) : DIM AXST(256) : DIM CIRST(256)
270 DIM OBST(256) : DIM RADST(256) : DIM VOLST(256) : DIM SHEARST(256)
280 DIM OCTAST(256) : DIM ANGST (256) : DIM TORST(256):DIM TORP(256)
290 DIM SS1(256) : DIM SS3(256)
300 CHAN=8 : CHAN$="8"                                 '                       *
310 '
320 GOSUB 1170                                          'erase old data files
330 GOSUB 1300                                         'user options
340 GOSUB 460                                          'set device parameters
350 GOSUB 580                                          'retrieve readings
360 GOSUB 2160                                          'read initial data
370 GOSUB 2330                                         'cal stresses
380 GOSUB 2760                                         'cal strains
390 GOSUB 3390                                         'output to printer
400 GOSUB 1520                                         'transfer to disc
410 GOSUB 760                                          'print readings
420 GOSUB 1870                                         'repeat option
430 END
440 '
450 '
460 'Set device parameters
470 '
480 CMD$="A,PA6144,G0,I0,I1,I2,I3,I4,I5,I6,I7,G5"+SCAN$+","+"GD"+DELAY$        '
    *
490 CALL OUTPUT(CMD$,AD%)                              'output command string to device
500 CMD$="GE"                                          'trigger command
```

```
510 LOCATE 23,1 : INPUT "RETURN TO TRIGGER  ",DUM$      'RETURN to trigger
520 CALL OUTPUT(CMD$,AD%)
530 LOCATE 23,1 : PRINT "TAKING READINGS                "
540 GOSUB 1110                                           'wait for SRQ=1
550 SOUND 150,2                                          'beep !
560 RETURN
570 '
580 'Retrieve data
590 '
600 CMD$="PA6144,QI"                                    'reset pointers
610 CALL OUTPUT(CMD$,AD%)
620 '
630 FOR I=1 TO SCAN
640 CALL ENTER(V$,AD%)                                   'get data from A-D
650 R(1,I)=VAL(MID$(V$,1,6))/3277                        'split into channels &
660 R(2,I)=VAL(MID$(V$,8,13))/3277                       'and convert to
670 R(3,I)=VAL(MID$(V$,15,20))/3277                      'voltage
680 R(4,I)=VAL(MID$(V$,22,27))/3277
690 R(5,I)=VAL(MID$(V$,29,34))/3277
700 R(6,I)=VAL(MID$(V$,36,41))/3277
710 R(7,I)=VAL(MID$(V$,43,48))/3277
720 R(8,I)=VAL(MID$(V$,50,55))/3277
730 NEXT
740 RETURN
750 '
760 'Print Results
770 '
780 LOCATE 6,1 : PRINT STRING$(72,45)                    '------
790 LOCATE 7,2 : PRINT "TIME"
800 '
810 FOR J=1 TO 8
820 LOCATE 7,(8+8*(J-1)) :PRINT "CHANNEL"
830 LOCATE 8,(10+8*(J-1)) :PRINT J-1
840 NEXT
850 LOCATE 9,1 : PRINT STRING$(72,45)                    '------
860 '
870 B=0 : I=1
880 LOCATE (10+B),1 : PRINT (I*DELAY*2)                    'time
890 '
900 FOR J=1 TO CHAN
910 LOCATE (10+B),(8+8*(J-1)) : PRINT USING"£.£££"; R(J,I)          'result
920 NEXT
930 '
940 B=B+1 : I=I+1                                        'next
950 IF B<>14 THEN 1040                                    'check if screen full
960 LOCATE 23,1 : PRINT"RETURN to CONTINUE / ESC to SKIP / ANY OTHER KEY to SCRO
LL BACK"
970 Q$=INKEY$ : IF LEN(Q$)=0 THEN 970                    'wait for input
980 IF ASC(Q$)=27 THEN RETURN                            'IF ESC .....
990 IF ASC(Q$)=13 THEN 1020                               'IF RETURN ....
1000 '
```

```
1010 IF I=15 THEN I=1 ELSE I=I-28                          'scroll back
1020 B=0
1030 VIEW PRINT 9 TO 23 : CLS : VIEW PRINT 1 TO 24         'clear data
1040 IF I=SCAN THEN 1050 ELSE GOTO 880                     'end of results ?
1050 LOCATE 23,1 : PRINT"Press RETURN to CONTINUE - ANY OTHER KEY to SCROLL BACK
"
1060 Q$=INKEY$ : IF LEN(Q$)=0 THEN 1060
1070 IF ASC(Q$)=13 THEN RETURN
1080 IF I<15 THEN I=1 ELSE I=I-14-B
1090 GOTO 1020
1100 '
1110 'SRQ Check
1120 '
1130 CALL SRQCHECK(SRQ)                                    'test SRQ
1140 IF SRQ<>1 THEN 1130
1150 RETURN
1160 '
1170 'Erase Old Data Files
1180 '
1190 '
1200 OPEN "A:TESTX" AS #1 LEN=3                  'holds last result file no.
1210 IF LOF(1)=0 THEN CLOSE :GOTO 1250           'IF does not exist ..
1220 FIELD #1, 3 AS X$                           'define field
1230 GET#1,1 : CLOSE                             'get record
1240 '
1250 CLS
1260 LOCATE 1,25 : PRINT "DATA FILE ";(VAL(X$)+1)
1270 LOCATE 2,25 : PRINT "**************"
1280 RETURN
1290 '
1300 'User Inputs
1310 '
1320 VIEW PRINT 5 TO 23 : CLS : VIEW PRINT 1 TO 24         'clear screen
1330 '
1340 LOCATE 3,1 : PRINT" ZERO STRAIN CRITERIA (A or T) =   "
1350 LOCATE 3,40 : INPUT ZEROCR$
1360 LOCATE 4,1 : PRINT "Interscan Delay  =    "
1370 LOCATE 4,50 : PRINT"MAX = 255"
1380 LOCATE 4,21 : INPUT"",DELAY$
1390 DELAY=VAL(DELAY$)
1400 VIEW PRINT 23 TO 23 : CLS : VIEW PRINT 1 TO 24
1410 IF DELAY > 255 THEN LOCATE 23,1 : PRINT "Delay is too long " : GOTO 1360
1420 '
1430 '
1440 LOCATE 5,1 : PRINT "Scans  =    "
1450 LOCATE 5,50 : PRINT "MAX = 256"                       '       *
1460 LOCATE 5,12,0,7 : INPUT"",SCAN$
1470 SCAN=VAL(SCAN$)
1480 IF SCAN>256 THEN LOCATE 23,1 : PRINT "Too many scans " : GOTO 1440 '*
1490 VIEW PRINT 23 TO 23 : CLS : VIEW PRINT 1 TO 24
1500 RETURN
```

```
1510 '
1520 'Transfer Data to Disc
1530 '
1540 OPEN "A:TESTX" AS #1 LEN=3
1550 FIELD #1,3 AS X$
1560 GET #1,1
1570 Y$=STR$(VAL(X$)+1) : L=LEN(Y$) : Y$=RIGHT$(Y$,L-1)
1580 '
1590 OPEN "A:RES"+Y$+".PRN" FOR OUTPUT AS #2            'open data file
1600 PRINT #2,CHR$(34);"DATA FILE =";CHR$(34);(VAL(X$)+1)
1610 PRINT #2,CHR$(34);"No.Scans = ";CHR$(34);SCAN$
1620 PRINT #2,CHR$(34);"Delay = ";CHR$(34);DELAY$
1630 '
1640 GOSUB 2050                                        'experimental conditions
1650 '
1660 PRINT #2,CHR$(34);"   TIME     AXSS    TORSS      P         Q       TORP
OCTASS";CHR$(34)
1670 FOR I=LOW TO HIGH
1680 PRINT #2,(I*DELAY*2),AXSS(I),TORSS(I),P(I),Q(I),TORP(I),OCTASS(I),ANGSS(I),
AXST(I),CIRST(I),OBST(I),TORST(I),RADST(I),VOLST(I),SHEARST(I),OCTAST(I),ANGST(I
),SS1(I),SS3(I),RADSS 'store result #
1690 NEXT
1700 '
1710 OPEN "A:DAT"+Y$+".PRN" FOR OUTPUT AS #3
1720 PRINT #3,CHR$(34);"DATA FILE =";CHR$(34);(VAL(X$)+1)
1730 PRINT #3,CHR$(34);"No.Scans = ";CHR$(34);SCAN$
1740 PRINT #3,CHR$(34);"Delay = ";CHR$(34);DELAY$
1750 FOR J=1 TO 5
1760 PRINT #3,CHR$(34),C$(J),CHR$(34)                  'save on disc
1770 NEXT
1780 PRINT #3,CHR$(34);"   TIME   CHAN 0   CHAN 1   CHAN 2   CHAN 3   CHAN 4   C
HAN 5   CHAN 6   CHAN 7  ";CHR$(34)
1790 FOR I=1 TO SCAN
1800 PRINT #3,(I*DELAY*2),R(1,I),R(2,I),R(3,I),R(4,I),R(5,I),R(6,I),R(7,I),R(8,I
)
1810 NEXT
1820 LSET X$=Y$                                        'store latest file no.
1830 PUT #1,1                                          'record on disc
1840 CLOSE                                             'close all files
1850 RETURN
1860 '
1870 'Repeat Data Collection
1880 '
1890 LOCATE 23,1 : PRINT "Press ANY KEY to use same settings - RETURN otherwise
                  "
1900 Q$=INKEY$
1910 IF LEN(Q$)=0 THEN 1900
1920 IF ASC(Q$)=13 THEN 1970
1930 VIEW PRINT 5 TO 23 : CLS : VIEW PRINT 1 TO 24
1940 LOCATE 1,35 : PRINT (VAL(Y$)+1) : GOTO 340        'print new file no.
1950 '
1960 '
1970 VIEW PRINT 5 TO 23 : CLS : VIEW PRINT 1 TO 24
1980 LOCATE 23,1 : PRINT " Press RETURN to END - ANY KEY otherwise"
1990 Q$=INKEY$
2000 IF LEN(Q$)=0 THEN 1990
```

```
2010 VIEW PRINT 5 TO 23 : CLS : VIEW PRINT 1 TO 24
2020 IF ASC(Q$)<>13 THEN LOCATE 1,35 : PRINT (VAL(Y$)+1) : GOTO 330
2030 RETURN
2040 '
2050 'Record Exprimental Conditions
2060 '
2070 VIEW PRINT 6 TO 23 : CLS : VIEW PRINT 1 TO 24
2080 FOR J=1 TO 5
2090 LOCATE (6+J*2),1 : PRINT "Condition  ";J            'user prompt
2100 LOCATE (6+2*J),16 : INPUT"",C$(J)
2110 PRINT £2,CHR$(34),C$(J),CHR$(34)                   'save on disc
2120 NEXT
2130 VIEW PRINT 6 TO 23 : CLS : VIEW PRINT 1 TO 24
2140 RETURN
2150 '
2160 '
2170 ' READ INITIAL DATA
2180 '
2190 DAY$ ="19TH JANUARY 1990 "
2200 SAMPLE$="SAMPLE NUMBER 6 (PERMANENT STRAIN TEST)"
2210 AXZERO= -1.000001E-02
2220 TORZERO=-0!
2230 POUT= 100 :PIN=100
2240 CAL1=172 : CAL2=-13: CAL5=-9346:CAL6=8294:CAL7=9429:CAL8=8840
2250 CAL4=-4790: CAL3=3620
2260 COIL=.52
2270 HOOP=-1.529
2280 LVDT1=1.989
2290 LVDT2=-2.084
2300 LVDT3=-2.909
2310 LVDT4=-2.305
2320 RETURN
2330 'CALCULATE STRESSES AND FIND MAX.AND MIN. STRESSES
2340 RADSS=3.96825*(POUT*.14+PIN*.112)
2350 CIRSS=35.71429*(POUT*.14-PIN*.112)
2360 FOR I=1 TO SCAN
2370 AXSS(I)=(R(1,I)-AXZERO)*CAL1+141.72*(.0196*POUT-.01254*PIN)
2380 TORSS(I)=(R(2,I)-TORZERO)*CAL2
2390 MOHRRA= SQR(((AXSS(I)-CIRSS)/2)^2+TORSS(I)^2)
2400 MOHRCE= (AXSS(I)+CIRSS)/2
2410 P(I)= (AXSS(I)+RADSS+CIRSS)/3
2420 Q(I)=MOHRRA
2430 SS1(I)=MOHRRA+MOHRCE
2440 SS3(I)=MOHRCE-MOHRRA
2450 OCTASS(I)=SQR((SS1(I)-RADSS)^2+(RADSS-SS3(I))^2+(SS1(I)-SS3(I))^2)*.7071
2460 ANGSS(I)=ATN(TORSS(I)/(SS1(I)-CIRSS))*57.296
2470 NEXT I
2480 '
2490 'FIND MAX AND MIN STRESSES
2500 '
```

```
2510 MAX1=-99999! : MIN1=99999!:MINI1=99999! 'FOR AXIAL STRESS
2520 MAX2=-99999! : MIN2=99999!:MINI2=99999!      'FOR TORSIONAL STRESS
2530 MAX11=-99999! : MIN11= 99999!      'FOR STRESS ANGLE
2540 '
2550 FOR I=1 TO SCAN
2560 IF ABS(AXSS(I))<=MIN1 THEN MIN1=ABS(AXSS(I)): MINSS= I
2570 IF ABS(TORSS(I))<=MIN2 THEN MIN2=ABS(TORSS(I)): MINTOR= I
2580 NEXT I
2590 IF (ZEROOR$ = "A") THEN KK=MINSS
2600 IF (ZEROOR$ = "T") THEN KK=MINTOR
2610 HIGH=KK+16
2620 LOW=KK-16
2630 IF LOW<1 THEN LOW=1:HIGH=32:GOTO 2650
2640 IF HIGH>SCAN THEN LOW=SCAN-32:HIGH=SCAN
2650 FOR I=LOW TO HIGH
2660 IF AXSS(I)>MAX1 THEN MAX1=AXSS(I) : MAXSS= I
2670 IF AXSS(I)<MINI1 THEN MINI1=AXSS(I):MSS=I
2680 IF TORSS(I)>MAX2 THEN MAX2=TORSS(I):MAXTOR= I
2690 IF TORSS(I)<MINI2 THEN MINI2=TORSS(I):MTOR=I
2700 IF ANGSS(I)>MAX11 THEN MAX11=ANGSS(I)
2710 IF ANGSS(I)<MIN11 THEN MIN11=ANGSS(I)
2720 NEXT I
2730 IF (ZEROOR$ = "A") THEN LL=MAXSS: MM=MSS
2740 IF (ZEROOR$ = "T") THEN LL=MAXTOR:MM=MTOR
2750 RETURN
2760 '
2770 'CALCULATE RESILIENT STRAINS
2780 '
2790 FOR I=LOW TO HIGH
2800 TORP(I)=2*TORSS(I)/(P(I)+P(KK))
2810 AXST(I)=((R(6,I)-R(6,KK))*CAL6+(R(7,I)-R(7,KK))*CAL7)/2
2820 CIRST(I)=(R(4,I)-R(4,KK))*CAL4
2830 OBST(I)=((R(5,I)-R(5,KK))*CAL5+(R(8,I)-R(8,KK))*CAL8)/2
2840 RADST(I)=(R(3,I)-R(3,KK))*CAL3
2850 TORST(I)=-1*(2*OBST(I)-AXST(I)-CIRST(I))/2
2860 MOHRR=SQR(((AXST(I)-CIRST(I))/2)^2+TORST(I)^2)
2870 MOHRC=(AXST(I)+CIRST(I))/2
2880 VOLST(I)=AXST(I)+CIRST(I)+RADST(I)
2890 SHEARST(I)=MOHRR
2900 ST1=MOHRR+MOHRC
2910 ST3=MOHRC-MOHRR
2920 OCTAST(I)=SQR((ST1-ST3)^2+(ST1-RADST(I))^2+(RADST(I)-ST3)^2)*.4714
2930 ANGST(I)=ATN(TORST(I)/(ST1-CIRST(I)+1))*57.296
2940 NEXT I
2950 '
2960 'CALCULATE STRAIN and STRESS INVARIANTS AT MAXIMUM STRESS
2970 '
2980 P1=P(KK): P2=P(LL): Q1=Q(KK): Q2=Q(LL)
2990 QP1=Q1/P1 : QP2=Q2/P2
3000 DQP=QP2-QP1:  QPM=(Q2+Q1)/(P1+P2)
```

```
3010 L2MX=(R(6,LL)-R(6,KK))*CAL6
3020 L3MX=(R(7,LL)-R(7,KK))*CAL7
3030 AXSTMX=((R(6,LL)-R(6,KK))*CAL6+(R(7,LL)-R(7,KK))*CAL7)/2
3040 CIRSTMX=(R(4,LL)-R(4,KK))*CAL4
3050 L1MX=(R(5,LL)-R(5,KK))*CAL5
3060 L4MX=(R(8,LL)-R(8,KK))*CAL8
3070 OBSTMX=((R(5,LL)-R(5,KK))*CAL5+(R(8,LL)-R(8,KK))*CAL8)/2
3080 RADSTMX=(R(3,LL)-R(3,KK))*CAL3
3090 TORSTMX=-1*(2*OBSTMX-AXSTMX-CIRSTMX)/2
3100 MOHRR=SQR(((AXSTMX-CIRSTMX)/2)^2+TORSTMX^2)
3110 MOHRC=(AXSTMX+CIRSTMX)/2
3120 VOLSTMX=AXSTMX+CIRSTMX+RADSTMX
3130 SHEARMX=MOHRR
3140 ST1=MOHRR+MOHRC
3150 ST3=MOHRC-MOHRR
3160 OCTASTMX=SQR((ST1-ST3)^2+(ST1-RADSTMX)^2+(RADSTMX-ST3)^2)*.4714
3170 ANGSTMX=ATN(TORSTMX/(ST1-CIRSTMX))*57.296
3180 '
3190 'CALCULATE PERMANENT STRAIN AT CURRENT MINIMUM STRESS LEVEL
3200 '
3210 PL2=(R(6,KK)-LVDT2)*CAL6
3220 PL3=(R(7,KK)-LVDT3)*CAL7
3230 AXSTPX=((R(6,KK)-LVDT2)*CAL6+(R(7,KK)-LVDT3)*CAL7)/2
3240 CIRSTPX=(R(4,KK)-HOOP)*CAL4
3250 PL1=(R(5,KK)-LVDT1)*CAL5
3260 PL4=(R(8,KK)-LVDT4)*CAL8
3270 OBSTPX=((R(5,KK)-LVDT1)*CAL5+(R(8,KK)-LVDT4)*CAL8)/2
3280 RADSTPX=(R(3,KK)-COIL)*CAL3
3290 TORSTPX=-1*(2*OBSTPX-AXSTPX-CIRSTPX)/2
3300 MOHRR=SQR(((AXSTPX-CIRSTPX)/2)^2+TORSTPX^2)
3310 MOHRC=(AXSTPX+CIRSTPX)/2
3320 VOLSTPX=AXSTPX+CIRSTPX+RADSTPX
3330 SHEARPX=MOHRR
3340 ST1=MOHRR+MOHRC
3350 ST3=MOHRC-MOHRR
3360 OCTASTPX=SQR((ST1-ST3)^2+(ST1-RADSTPX)^2+(RADSTPX-ST3)^2)*.4714
3370 ANGSTPX=ATN(TORSTPX/(ST1-CIRSTPX))*57.296
3380 RETURN
3390 '
3400 'SEND RESULTS AND DATA TO PRINT
3410 '
3420 LPRINT "*********** DATA FILE ";(VAL(X$)+1)
3430 LPRINT
3440 LPRINT "DATE :"; DAY$
3450 LPRINT "SAMPLE DESCRIPTION :"; SAMPLE$
3460 LPRINT
3470 LPRINT "************************** SET-UP DATA **************************"
3480 LPRINT
3490 LPRINT
3500 LPRINT "CAL FACTOR & IN.VOLTAGE FOR AXIAL STRESS       =";CAL1,AXZERO
3510 LPRINT "CAL FACTOR & IN.VOLTAGE FOR TORSIONAL STRESS   =";CAL2,TORZERO
3520 LPRINT "CAL FACTOR & IN.VOL FOR AXIAL STRAIN (LVDT2)   =";CAL6,LVDT2
```

```
3530 LPRINT "CAL FACTOR & IN.VOL FOR AXIAL STRAIN (LVDT3)   =";CAL7,LVDT3
3540 LPRINT "CAL FACTOR & IN.VOL FOR CIRCUM. STRAIN (HOOP)  =";CAL4,HOOP
3550 LPRINT "CAL FACTOR & IN.VOL FOR 45-DEG STRAIN (LVDT1)  =";CAL5,LVDT1
3560 LPRINT "CAL FACTOR & IN.VOL FOR 45-DEG STRAIN (LVDT4)  =";CAL8,LVDT4
3570 LPRINT "CAL FACTOR & IN.VOL FOR RADIAL STRAIN (COIL)   =";CAL3,COIL
3580 LPRINT
3590 LPRINT "*********************  LOAD DATA  **************************"
3600 LPRINT
3610 LPRINT "INNER CELL PRESSURE(kPa)                       =";PIN
3620 LPRINT "OUTER CELL PRESSURE (kPa)                      =";POUT
3630 LPRINT "MAXIMUM AXIAL STRESS (kPa)                     =";MAX1
3640 LPRINT "MINIMUM AXIAL STRESS (kPa)                     =";MINI1
3650 LPRINT "MAXIMUM TORSIONAL STRESS (kPa)                 =";MAX2
3660 LPRINT "MINIMUM TORSIONAL STRESS (kPa)                 =";MINI2
3670 LPRINT "P one      (kPa)                               =";P1
3680 LPRINT "P two      (kPa)                               =";P2
3690 LPRINT "Q one      (kPa)                               =";Q1
3700 LPRINT "Q two      (kPa)                               =";Q2
3710 LPRINT "(Q/P) one   &  (Q/P) two                       =";QP1,QP2
3720 LPRINT "CHANGE  &  MEAN (Q/P)                          =";DQP,QPM
3730 LPRINT
3740 LPRINT "MAXIMUM PRINCIPAL STRESS ROTATION (DEGREE)     =";MAX11
3750 LPRINT "MINIMUM PRINCIPAL STRESS ROTATION (DEGREE)     =";MIN11
3760 LPRINT
3770 LPRINT "*************************  STRAIN DATA  ************************"
3780 LPRINT
3790 IF(ZEROCR$="A") THEN LPRINT"ZERO STRAINS ASSUMED AT ZERO or ABSOLUTE MINIMU
M AXIAL STRESS"
3800 IF(ZEROCR$="T") THEN LPRINT"ZERO STRAINS ASSUMED AT ZERO or ABSOLUTE MINIMU
M TORSIONAL STRESS"
3810 LPRINT
3820 LPRINT "MAXIMUM STRESS OBTAINED AT SCAN NUMBER"; LL
3830 LPRINT "MINIMUM STRESS OBTAINED AT SCAN NUMBER"; MM
3840 LPRINT "ZERO STRAIN OBTAINED AT SCAN NUMBER";KK
3850 LPRINT
3860 LPRINT "RESILIENT STRAINS AT MAXIMUM STRESS ARE AS FOLLOWS:"
3870 LPRINT "RESILIENT AX STRAIN (MICROSTRAIN) (AV/L2/L3)   =";AXSTMX,L2MX,L3MX
3880 LPRINT "RESILIENT CIRCUMFERENTIAL STRAIN (MICROSTRAIN) =";CIRSTMX
3890 LPRINT "RESILIENT RADIAL STRAIN (MICROSTRAIN)          =";RADSTMX
3900 LPRINT "RESILIENT 45 STRAIN (MICROSTRAIN) (AV/L1/L4)   =";OBSTMX,L1MX,L4MX
3910 LPRINT "RESILIENT TORSIONAL STRAIN (MICROSTRAIN)       =";TORSTMX
3920 LPRINT "RESILIENT VOLUMATRIC STRAIN (MICROSTRAIN)      =";VOLSTMX
3930 LPRINT "RESILIENT MAX.SHEAR STRAIN (MICROSTRAIN)       =";SHEARMX
3940 LPRINT "ANGLE OF STRAIN INCREMENT ROTATION             =";ANGSTMX
3950 LPRINT
3960 LPRINT "ACCUM. PERMANENT STRAINS AT CURRENT MINIMUM STRESS ARE AS FOLLOWS:"
3970 LPRINT
3980 LPRINT "PERMANENT AX STRAIN (MICROSTRAIN) (AV/L2/L3)   =";AXSTPX,PL2,PL3
3990 LPRINT "PERMANENT CIRCUMFERENTIAL STRAIN (MICROSTRAIN) =";CIRSTPX
4000 LPRINT "PERMANENT 45 STRAIN (MICROSTRAIN) (AV/L1/L4)   =";OBSTPX,PL1,PL4
4010 LPRINT "PERMANENT RADIAL STRAIN (MICROSTRAIN)          =";RADSTPX
4020 LPRINT "PERMANENT SHEAR STRAIN (MICROSTRAIN)           =";SHEARPX
4030 LPRINT "PERMANENT VOLUMATRIC STRAIN (MICROSTRAIN)      =";VOLSTPX
4040 RETURN
```

APPENDIX D

MEASURED STRESSES AND STRAINS FROM RESILIENT STRAIN TESTS

D.1 Results from Repeated-Load Triaxial Tests

FILE NUMBER	INITIAL DEVIATOR STRESS (kPa)	FINAL DEVIATOR STRESS (kPa)	INITIAL CELL PRESSURE (kPa)	FINAL CELL PRESSURE (kPa)	RADIAL STRAIN (με)	AXIAL STRAIN (με)
1	.0	55.0	150.0	150.0	-41.0	170.0
2	.0	101.0	150.0	150.0	-87.0	290.0
3	.0	158.5	150.0	150.0	-149.0	474.0
4	.0	210.0	150.0	150.0	-213.0	628.0
5	.0	54.5	100.0	100.0	-52.0	227.0
6	.0	102.4	100.0	100.0	-134.0	425.0
7	.0	154.8	100.0	100.0	-201.0	585.0
8	.0	50.5	70.0	70.0	-73.0	260.0
9	.0	106.0	70.0	70.0	-236.0	554.0
10	.0	55.0	50.0	50.0	-158.0	428.0
11	.0	58.6	30.0	30.0	-228.0	645.0
12	.0	.0	30.0	80.0	266.3	232.2
13	.0	.0	50.0	100.0	240.9	72.4
14	.0	.0	100.0	150.0	240.1	78.8
15	.0	.0	50.0	150.0	309.8	278.2
16	50.0	50.0	100.0	150.0	204.0	29.6
17	50.0	50.0	50.0	100.0	245.4	39.8
18	100.0	100.0	100.0	150.0	192.5	-20.2
19	.0	227.0	150.0	150.0	-252.0	619.0

D.2 Results from Repeated-Load Hollow Cylinder Tests

FILE NUMBER	INITIAL VERTICAL STRESS (kPa)	FINAL VERTICAL STRESS (kPa)	INITIAL TORSIONAL STRESS (kPa)	FINAL TORSIONAL STRESS (kPa)	INITIAL INNER PRESSURE (kPa)	FINAL INNER PRESSURE (kPa)	INITIAL OUTER PRESSURE (kPa)	FINAL OUTER PRESSURE (kPa)	AVERAGE RADIAL STRAIN (με)	AVERAGE CIRCUM. STRAIN (με)	AVERAGE AXIAL STRAIN (με)	AVERAGE 45 DEGREE STRAIN (με)
1	.0	.0	.0	.0	100.0	200.0	100.0	200.0	480.7	-15.3	700.0	-2.9
2	49.6	49.2	.0	.0	100.0	200.0	100.0	200.0	758.0	-12.4	710.0	-59.0
3	101.0	100.1	.0	.0	100.0	200.0	100.0	200.0	677.0	20.0	650.0	-110.0
4	99.8	99.3	.0	.0	100.0	200.0	100.0	200.0	503.3	149.2	650.0	36.0
5	.0	.0	-19.9	-19.9	105.0	100.0	100.0	100.0	-40.7	70.7	.4	61.0
6	.0	.0	20.1	19.9	105.0	100.0	100.0	100.0	-58.5	131.8	6.7	14.3
7	50.7	49.6	-20.1	-19.9	105.0	100.0	100.0	100.0	-58.6	108.2	-66.1	10.3
8	49.7	50.3	.0	.0	110.0	100.0	100.0	100.0	-98.2	286.5	-61.5	9.9
9	.0	.0	.0	-10.6	100.0	100.0	100.0	100.0	-138.6	34.0	482.0	321.0
10	.0	.0	.0	-20.8	100.0	100.0	100.0	100.0	-137.5	39.0	539.1	461.7
11	.0	53.7	.0	.0	100.0	100.0	100.0	100.0	-170.7	-60.8	552.0	426.2
12	.0	54.6	.0	-20.0	100.0	100.0	100.0	100.0	-172.3	-50.5	654.9	506.3
13	.0	.0	.0	-29.0	100.0	100.0	100.0	100.0	-167.4	40.0	567.9	539.5
14	.0	53.7	.0	-29.5	100.0	100.0	100.0	100.0	-164.7	-43.9	608.8	568.0
15	.0	103.6	.0	.0	100.0	100.0	100.0	100.0	-231.0	-125.0	739.2	480.7
16	.0	.0	.0	-38.8	100.0	100.0	100.0	100.0	-154.9	52.0	612.6	603.6
17	49.2	50.9	.0	.0	105.0	100.0	100.0	100.0	17.5	93.7	-49.9	-38.8
18	49.3	49.5	-20.1	-20.0	110.0	100.0	100.0	100.0	-93.4	274.5	-25.8	7.8
19	.0	.0	-39.9	-40.0	105.0	100.0	100.0	100.0	-58.5	125.4	-58.7	71.8
20	99.7	99.2	.0	.0	105.0	100.0	100.0	100.0	-45.8	92.2	98.0	-16.6
21	49.7	50.1	-39.9	-40.0	105.0	100.0	100.0	100.0	-43.8	120.0	71.0	96.6
22	99.3	99.8	-19.9	-19.9	105.0	100.0	100.0	100.0	-42.7	89.6	67.7	14.0
23	.0	152.7	.0	.0	100.0	100.0	100.0	100.0	-310.3	-227.7	883.8	496.9
24	.0	.0	-20.0	-19.9	75.0	70.0	70.0	70.0	-65.3	139.3	90.7	23.4
25	.0	.0	20.0	19.9	75.0	70.0	70.0	70.0	-85.8	217.9	53.2	63.8
26	49.8	50.4	.0	.0	75.0	70.0	70.0	70.0	-102.5	163.3	33.9	23.0
27	51.4	49.9	-19.9	-20.0	75.0	70.0	70.0	70.0	-57.2	132.7	-40.0	70.1
28	.0	.0	.0	-20.5	70.0	70.0	70.0	70.0	100.0	39.0	553.1	493.4
29	.0	51.4	.0	.0	70.0	70.0	70.0	70.0	-186.4	-88.7	643.6	445.3
30	.0	54.4	.0	-19.3	70.0	70.0	70.0	70.0	-169.0	-63.0	620.8	513.9
31	.0	.0	.0	-29.7	70.0	70.0	70.0	70.0	-144.0	39.0	584.9	571.2
32	.0	54.9	.0	-29.8	70.0	70.0	70.0	70.0	-211.4	-47.6	609.2	557.4
33	.0	101.4	.0	.0	70.0	70.0	70.0	70.0	-253.8	-177.9	743.8	473.1
34	.0	102.9	.0	-10.2	70.0	70.0	70.0	70.0	-233.7	-153.0	796.8	509.4
35	.0	.0	.0	.0	30.0	100.0	30.0	100.0	396.5	98.9	700.0	22.8
36	50.4	48.1	.0	.0	30.0	100.0	30.0	100.0	448.5	128.9	650.0	51.4
37	.0	51.8	.0	.0	30.0	30.0	30.0	30.0	-172.8	-98.5	601.2	455.3
38	.0	58.1	.0	-10.4	30.0	30.0	30.0	30.0	-205.4	-81.1	645.7	511.0
39	.0	54.4	.0	-20.1	30.0	30.0	30.0	30.0	-220.7	-47.7	601.3	589.6
40	.0	.0	.0	-20.2	30.0	30.0	30.0	30.0	-153.3	80.0	612.0	556.7
41	.0	.0	.0	.0	30.0	80.0	30.0	80.0	615.0	129.0	800.0	38.0
42	.0	24.6	.0	.0	30.0	30.0	30.0	30.0	-153.3	-62.7	575.6	416.5
43	.0	26.4	.0	-9.3	30.0	30.0	30.0	30.0	-158.2	-47.3	556.0	470.8
44	.0	.0	.0	-9.6	30.0	30.0	30.0	30.0	-131.0	39.0	513.6	464.6
45	.0	102.8	.0	-39.0	150.0	150.0	150.0	150.0	-193.5	-60.0	590.3	466.8

FILE NUMBER	INITIAL VERTICAL STRESS (kPa)	FINAL VERTICAL STRESS (kPa)	INITIAL TORSIONAL STRESS (kPa)	FINAL TORSIONAL STRESS (kPa)	INITIAL INNER PRESSURE (kPa)	FINAL INNER PRESSURE (kPa)	INITIAL OUTER PRESSURE (kPa)	FINAL OUTER PRESSURE (kPa)	AVERAGE RADIAL STRAIN (με)	AVERAGE CIRCUM. STRAIN (με)	AVERAGE AXIAL STRAIN (με)	AVERAGE 45 DEGREE STRAIN (με)
46	.0	148.9	.0	.0	150.0	150.0	150.0	150.0	-179.9	-136.4	730.5	426.7
47	.0	150.4	.0	-20.1	150.0	150.0	150.0	150.0	-225.0	-112.1	759.3	478.4
48	.0	149.4	.0	-39.6	150.0	150.0	150.0	150.0	-241.9	-98.3	717.5	525.0
49	.0	202.4	.0	.0	150.0	150.0	150.0	150.0	-264.1	-212.9	814.8	436.0
50	.0	201.8	.0	-20.0	150.0	150.0	150.0	150.0	-271.7	-179.5	757.1	469.8
51	.0	201.9	.0	-39.0	150.0	150.0	150.0	150.0	-243.5	-157.8	791.6	505.9
52	.0	251.0	.0	.0	150.0	150.0	150.0	150.0	-343.5	-274.3	869.8	446.2
53	.0	253.1	.0	-19.8	150.0	150.0	150.0	150.0	-339.7	-243.7	903.3	497.8
54	.0	254.1	.0	-40.5	150.0	150.0	150.0	150.0	-323.9	-224.7	904.6	521.2
55	.0	.0	-39.8	-39.8	110.0	100.0	100.0	100.0	-143.3	535.1	-21.1	29.5
56	98.6	100.2	.0	.0	110.0	100.0	100.0	100.0	-102.0	342.7	29.1	86.9
57	50.7	49.7	-39.7	-39.8	110.0	100.0	100.0	100.0	-93.5	389.0	-2.8	82.2
58	100.2	100.9	-39.7	-39.7	105.0	100.0	100.0	100.0	-46.8	114.4	55.5	64.2
59	100.5	98.9	-19.9	-19.9	110.0	100.0	100.0	100.0	-79.9	304.4	10.6	45.9
60	99.0	98.9	-39.9	-39.8	110.0	100.0	100.0	100.0	-149.3	589.1	18.2	161.8
61	.0	154.6	.0	-19.8	100.0	100.0	100.0	100.0	-253.3	-187.9	708.6	489.4
62	.0	156.4	.0	-38.8	100.0	100.0	100.0	100.0	-277.7	-178.3	729.4	525.6
63	.0	201.8	.0	.0	100.0	100.0	100.0	100.0	-332.1	-309.4	820.5	409.0
64	.0	204.2	.0	-20.1	100.0	100.0	100.0	100.0	-332.6	-300.8	931.9	471.5
65	.0	203.9	.0	-40.4	100.0	100.0	100.0	100.0	-359.2	-283.9	869.0	532.5
66	48.9	49.7	.0	.0	80.0	70.0	70.0	70.0	-202.6	766.1	35.3	246.4
67	100.5	99.2	.0	.0	75.0	70.0	70.0	70.0	-82.7	223.9	30.6	49.3
68	100.2	101.0	-19.8	-19.9	75.0	70.0	70.0	70.0	-88.6	267.1	-52.5	1.2
69	50.8	49.3	-39.7	-39.8	75.0	70.0	70.0	70.0	-80.2	347.1	-28.0	-6.3
70	.0	104.9	.0	-20.0	70.0	70.0	70.0	70.0	-242.4	-154.3	697.6	490.0
71	.0	51.6	.0	-39.9	70.0	70.0	70.0	70.0	-169.0	-61.9	512.1	557.4
72	.0	.0	.0	-39.7	70.0	70.0	70.0	70.0	-137.0	100.0	433.4	617.8
73	.0	101.9	.0	-39.5	70.0	70.0	70.0	70.0	-266.9	-119.9	689.2	573.5
74	.0	152.5	.0	.0	70.0	70.0	70.0	70.0	-306.5	-276.2	841.6	394.3
75	.0	151.3	.0	-19.9	70.0	70.0	70.0	70.0	-291.9	-234.9	757.7	491.7
76	.0	.0	-20.0	-20.0	55.0	50.0	50.0	50.0	-108.9	530.6	23.9	134.3
77	49.6	50.9	.0	.0	55.0	50.0	50.0	50.0	-68.9	313.3	-15.8	48.7
78	49.7	51.3	-19.8	-19.9	55.0	50.0	50.0	50.0	-115.6	417.5	47.1	54.2
79	50.9	49.5	19.9	19.8	55.0	50.0	50.0	50.0	-154.9	510.2	58.1	238.6
80	.0	52.8	.0	-30.4	50.0	50.0	50.0	50.0	-222.8	-74.3	549.2	568.9
81	.0	.0	.0	-29.3	50.0	50.0	50.0	50.0	-157.1	105.0	352.8	597.0
82	.0	105.2	.0	.0	50.0	50.0	50.0	50.0	-295.1	-232.7	825.1	396.7
83	.0	100.6	.0	-20.8	50.0	50.0	50.0	50.0	-287.0	-167.5	700.7	488.5
84	.0	50.0	.0	.0	30.0	30.0	30.0	30.0	-231.0	-137.1	617.1	392.7
85	.0	47.9	.0	-9.9	30.0	30.0	30.0	30.0	-204.3	-110.7	550.6	460.0
86	.0	52.2	.0	-21.2	30.0	30.0	30.0	30.0	-248.4	-111.6	580.7	548.8
87	199.1	198.8	.0	.0	105.0	100.0	100.0	100.0	-31.9	108.4	50.8	36.5
88	200.0	198.2	-19.9	-19.9	105.0	100.0	100.0	100.0	-43.8	98.3	40.4	28.7
89	198.3	199.5	-39.7	-39.9	105.0	100.0	100.0	100.0	-77.7	159.8	14.6	76.6
90	199.0	199.7	39.9	39.9	105.0	100.0	100.0	100.0	-29.6	175.4	-8.7	62.9
91	201.5	197.1	.0	.0	110.0	100.0	100.0	100.0	-104.7	424.0	16.1	156.0
92	.0	254.4	.0	.0	100.0	100.0	100.0	100.0	-442.9	-445.2	972.6	401.2
93	.0	253.7	.0	-20.1	100.0	100.0	100.0	100.0	-434.2	-404.6	1,066.9	454.7
94	.0	248.6	.0	-39.9	100.0	100.0	100.0	100.0	-406.5	-348.0	1,064.9	551.1
95	.0	.0	-39.8	-40.0	75.0	70.0	70.0	70.0	-83.5	463.5	5.0	141.0

FILE NUMBER	INITIAL VERTICAL STRESS (kPa)	FINAL VERTICAL STRESS (kPa)	INITIAL TORSIONAL STRESS (kPa)	FINAL TORSIONAL STRESS (kPa)	INITIAL INNER PRESSURE (kPa)	FINAL INNER PRESSURE (kPa)	INITIAL OUTER PRESSURE (kPa)	FINAL OUTER PRESSURE (kPa)	AVERAGE RADIAL STRAIN (με)	AVERAGE CIRCUM. STRAIN (με)	AVERAGE AXIAL STRAIN (με)	AVERAGE 45 DEGREE STRAIN (με)
96	99.5	99.5	-39.8	-39.8	75.0	70.0	70.0	70.0	-112.2	217.7	129.9	57.1
97	98.8	99.6	.0	.0	80.0	70.0	70.0	70.0	-200.7	826.5	42.5	244.0
98	99.7	99.8	-20.0	-20.0	80.0	70.0	70.0	70.0	-186.4	703.4	.3	219.2
99	.0	154.8	.0	-39.5	70.0	70.0	70.0	70.0	-367.9	-265.0	938.6	380.2
100	.0	202.3	.0	.0	70.0	70.0	70.0	70.0	-441.3	-406.8	973.8	415.8
101	.0	198.9	.0	-20.1	70.0	70.0	70.0	70.0	-430.4	-351.7	1,028.2	497.7
102	98.8	99.3	.0	.0	55.0	50.0	50.0	50.0	-70.4	344.9	64.0	127.0
103	.0	106.9	.0	-30.5	50.0	50.0	50.0	50.0	-380.4	-229.1	856.0	583.6
104	.0	55.4	.0	-39.6	50.0	50.0	50.0	50.0	-238.6	-132.6	523.6	666.9
105	.0	153.3	.0	.0	50.0	50.0	50.0	50.0	-407.1	-428.2	1,004.6	397.4
106	.0	.0	.0	-20.1	30.0	30.0	30.0	30.0	-153.8	-114.7	349.5	546.5
107	20.0	20.0	.0	-19.5	110.0	110.0	100.0	100.0	132.6	25.0	318.8	458.4
108	24.0	76.0	.0	.0	110.0	110.0	100.0	100.0	-171.7	-74.2	365.7	405.0
109	24.0	24.0	.0	-39.5	110.0	110.0	100.0	100.0	121.0	-70.3	346.0	630.5
110	25.0	125.0	.0	.0	110.0	110.0	100.0	100.0	-222.3	-157.5	554.7	381.2
111	24.0	126.0	.0	-19.5	110.0	110.0	100.0	100.0	-202.2	-137.2	562.8	428.2
112	23.0	198.0	.0	.0	110.0	110.0	100.0	100.0	-305.4	-360.7	689.6	403.4
113	20.0	202.0	.0	-39.1	110.0	110.0	100.0	100.0	-337.5	-371.9	776.0	501.6
114	23.0	75.0	.0	.0	80.0	80.0	70.0	70.0	-223.9	-110.3	413.1	404.3
115	25.0	77.0	.0	-20.5	80.0	80.0	70.0	70.0	-207.1	-122.2	398.7	504.1
116	23.0	125.0	.0	.0	80.0	80.0	70.0	70.0	-250.0	-238.2	561.6	392.1
117	23.0	127.0	.0	-19.7	80.0	80.0	70.0	70.0	-280.4	-247.4	553.7	491.7
118	24.0	126.0	.0	-39.7	80.0	80.0	70.0	70.0	-267.2	-524.1	503.1	641.7
119	24.0	175.0	.0	.0	80.0	80.0	70.0	70.0	-338.6	-449.9	659.4	436.8
120	.0	.0	-19.9	-20.0	100.0	200.0	100.0	200.0	532.9	-103.7	-175.4	-284.4
121	.0	.0	19.9	19.9	100.0	200.0	100.0	200.0	550.7	24.8	44.6	69.1
122	54.1	49.8	-20.0	-20.0	100.0	200.0	100.0	200.0	529.6	26.1	111.2	-47.1
123	.0	.0	-40.1	-39.9	100.0	200.0	100.0	200.0	541.1	-173.9	-23.2	-133.1
124	49.2	51.0	-40.0	-40.0	100.0	200.0	100.0	200.0	495.5	57.3	-20.3	-37.3
125	99.4	100.0	-19.9	-19.9	100.0	200.0	100.0	200.0	492.5	106.7	49.0	-59.7
126	99.8	98.3	-39.9	-39.9	100.0	200.0	100.0	200.0	532.6	129.2	76.6	-28.2
127	.0	.0	-19.9	-19.8	50.0	100.0	50.0	100.0	396.8	98.1	24.4	-25.8
128	50.4	48.8	-19.9	-20.0	50.0	100.0	50.0	100.0	427.3	138.2	57.9	33.8
129	50.8	49.6	19.9	20.0	50.0	100.0	50.0	100.0	444.7	213.4	49.2	99.8
130	.0	.0	-40.0	-39.8	50.0	100.0	50.0	100.0	411.6	65.2	130.1	-132.0
131	50.9	49.5	-40.0	-39.9	50.0	100.0	50.0	100.0	458.4	152.9	-69.8	11.9
132	49.6	49.6	39.8	40.0	50.0	100.0	50.0	100.0	449.1	270.7	4.5	160.3
133	.0	.0	-20.0	-20.0	30.0	80.0	30.0	80.0	388.4	189.0	30.0	-73.6

The range of b-values and angles of principal plane rotation are summarized in Figures D- 1 and D- 2 respectively.

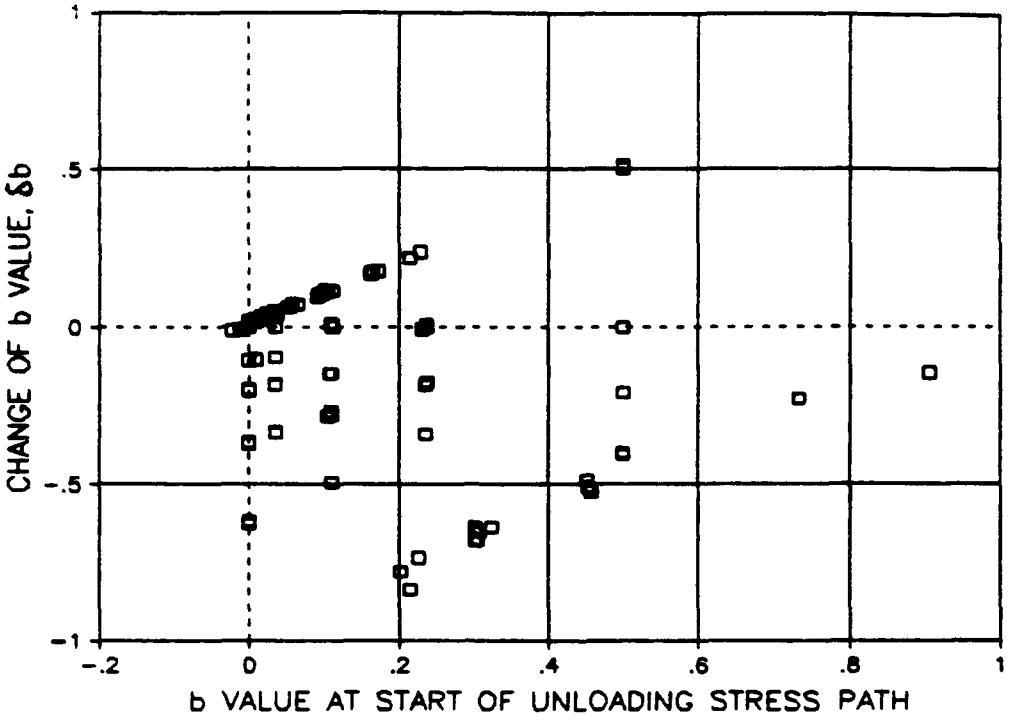

Figure D-1. Range of b-Values used in Resilient Strain Tests carried out with the Repeated-Load Hollow Cylinder Test Apparatus.

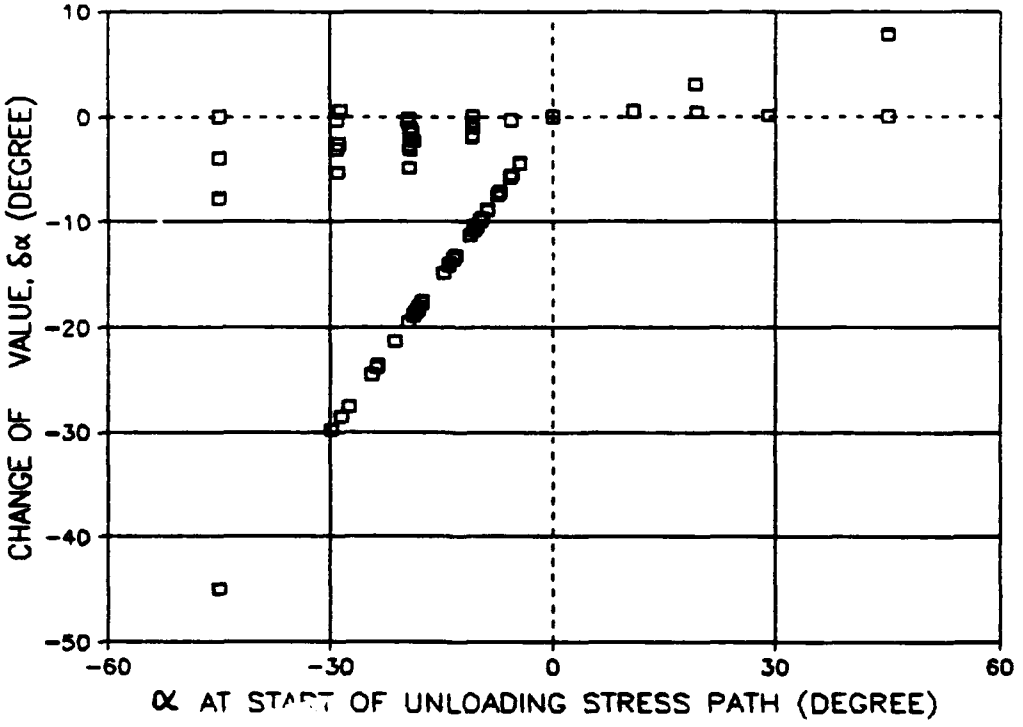

Figure D-2. Range of Angles of Principal Plane Rotation used in Resilient Strain Tests carried out with the Repeated-Load Hollow Cylinder Test Apparatus.